NATIONAL AKADEMY OF SCIENCES OF UKRAINE
INSTITUTE FOR SINGLE CRYSTALS

Vol.2, No.1 1995

FUNCTIONAL MATERIALS

Kharkov

National Academy of Sciences of Ukraine
Department of Physical and Technical Problems of Materials Science

Institute for Single Crystals

Functional Materials

Founded in September 1993
(4 numbers per year)

Address:

60, Lenin Ave., 310001, Kharkov, Ukraine
Phone: +380 (572) 307 411, +380 (572) 307 960;
Fax: +380 (572) 320 273
E-mail: shcherbina@isc.kharkov.ua

Reports

from Summer School on Chemistry and Physics of Surfaces

CPS'94

September 4 – 10, 1994, Kiev, Ukraine

Part I

Works presented by CPS'94 International Program Commitee

Contents

Letter to the Editor

UKRAINE-USA SUMMER SCHOOL ON CHEMISTRY AND PHYSICS OF SURFACES

4-10 September 1994 Kiev, Ukraine

CPS'94

On behalf of the International Organizing Committee and the Program Committee it is our pleasure to introduce the first Ukrainian–USA Summer School on Chemistry and Physics of Surfaces (CPS-94). It was organized by National Kiev University and Ukraine Physical Society and continues a series of schools jointly established by Ukrainian and American Physical Societies in 1993 sponsored by International Science Foundation (USA) and the Army Research Office (USA).

The scientific program of the CPS-94 was organized by an International Program Committee: V.V.Skopenko (T.Shevchenko University, Kiev, Ukraine), B.S.Hudson (University of Oregon, Eugene, OR, USA), A.A.Chuiko (Institute for Surface Chemistry, Kiev, Ukraine), A.I.Khizhnyak (Institute of Physics, Kiev, Ukraine), Yu.G.Ptushinsky (Institute of Physics, Kiev, Ukraine), V.V.Soukhan (T.Shevchenko University, Kiev, Ukraine), V.V.Strelko (ISEP, Kiev, Ukraine). Organizing Committee of the school was included V.N.Zaitsev (National University, Kiev, Ukraine), D.E.Bergbreiter (Texas A&M University, USA), V.O.Andreev (Ukrainian Physical Society, Ukraine), L.V.Poperenko (Kiev University, Ukraine), V.Yu.Reshetniak (Institute for Surface Chemistry, Ukraine), V.A.Tertych (Institute for Surface Chemistry, Ukraine). It was designed so as to combine interests of chemists and physicists and the following topics were addressed by participants: Surface modification; Applications of modified surfaces for HPLC phases, adsorbents, catalysts, sensors etc.; Surface induced properties of systems; Chemical and physical processes on surfaces; Modern methods for surface analysis and characterization; Self assembly on solid materials.

The scientific program consisted of lectures and poster presentations. The CPS-94 included special sessions with introductory lectures discussing fundamental problems and techniques in surface characterization, in surface modification and in studies of reactions at gas/solid and liquid/solid interfaces.

In order to involve maximum graduate student participation, the organizing committee offered graduate students free admission. Moreover, all participants from CIS countries received grants that covered all expenses connected with the meeting: organizing fee, travel, accommodation and per diem cost. These expenses were covered by a grant from the International Science Foundation (USA). The School was also sponsored by US Army Research Office (American and European divisions). These funds allowed us to invite advanced scientists to Kiev and to publish the CPS-94 materials. The Organizing committee also offered 15 awards for poster contributors to recognize the best presentation.

The school program consisted 45–60 minute lectures:

Begrambekov L.B. (Moscow Physical Engineering Institute Plasma Phys.Dept.) Surface interaction in model thermonuclear set-up.

Bergbreiter D.E. (Dept.of Chem., Texas A&M University, College station) Synthesis and characterization at functionalized polymer–solvent interfaces.

Ferguson Gregory (Department of Chemistry, Lihigh University) Mosaic tiling in molecular dimensions: chemical approaches to nanostructural thin films.

Golub A.A. (Shevchenko University, Kiev) Quantum chemical methods for prediction of immobilised molecules interactions.

Gritsyna V.T. (Kharkov State University) Ion beam modification of complex oxide surfaces.

Kalibabchuk V.A. (Kiev Medical University) Polymers for medical application

Kamalov G.L. (Physico-Chemical Institute, Odessa) Interaction of macrocyclic Shiff bases with silica.

KartelN.T.(Institute for Sorption & Endoecology, Kiev) Physico-chemical properties of synthetic carbons and their medical application.

Kholin Yu.V. (Kharkov State University) Quantitative physico-chemical analysis of chemisorption on complexing silicas.

Korobov A.I. (Kharkov State University) The rate of a surface reaction in terms of Dirichlet domains.

Loshkaryov Yu.M. (Dniepropetrovsk State University) The role of adsorption phenomena in the metals electrodeposition process.

Mardezjov A.S. (Inst. of Semiconductors Physics) The condition of ellipsometry in situ at deposition of solid solution film of CdHgTe by molecular beam epitaxy method.

Milhofer Helga (The Hebrew University of Jerusalem) Interaction of macromolecules and molecular assembling at crystal/solution interfaces.

Paradies H. Henrich (Markische Fachhochschule Biotechnology and Physical Chemistry) Internal chain dynamics in polymer-like distearyldimethyl ammonium hydroxide (DSDMA OH) chains and their interaction with surfaces.

Pidzyraylo M.S. (Lviv State University, Physics Dept.) Using of the modified substrate surfaces for obtaining high-resolution cathodoluminescent screens.

Pinkevich I.P. (Kiev University Physics Dept.) Interaction with surface and structure of director field in liquid crystal cells containing disclinations or spherical particles. Influence on optical properties.

Podlipenets A.N. (Department of Electroelasticity, Institute of Mechanics, Kiev) Long-wavelength phonons in superlattices: Hamiltonian system formalism.

Poperenko L.V. (Kiev University Physics Dept.) Evolution of the near-surface structure in amorphous metalic alloys.

Reznikov Yu.A. (Institute of Physics, Kiev) Electrical control of light scattering in suspension of liquid crystal-silica.

Rustichelli F. (Instituto di Scienze Fiziche) Structural properties of monolayers and multilayers of bipolar lipids from thermophilic bacteria.

Shaikevich I.A. (Kiev University Phys.Dept.) Electronic properties investigation of metals by spectro ellipsometry with surface polariton excitation.

Sheka E.F. (Russian University of Peoples Friendship, Moscow) Surface of disperse silica: reality and computer simulation.

Strelko V.V. (Institute of Sorption and Endoecology problems) Surface chemistry and affinity of inorganic ionites to cations and anions.

Styrov V.V. (Priazovsky State Technical University) The phonon, electron and atomic emission from the surfaces of solids during adsorption and heterogeneous chemical reactions.

Tertych V.A. (Institute for Surface Chemistry, Kiev) Chemical reactions on a silica surface.

Voytsenja V.S. (Physical-Technical institute, Kharkov) The change of optical properties of metallic mirrors at ion bombardment.

White John M. (Dept.of Chemistry University of Texas at Austin) Photon and electron driven reactions on single crystal metals.

Yashchuk V.N. (Kiev University) The catch of triplet exitons by molecular oxygen on surface of aromatic polymers.

Yates John T.Jr. (Surface Science Center, Dept.of Chemistry University of Pittsburgh) Reactions on semiconductor surfaces — studies at the atomic level.

Yatsimirsky K.B. (Institute of Physical chemistry, Kiev) Determinated chaos in chemistry.

Yatsimirsky V.K. (Shevchenko University, Kiev) Adsorbents and catalysts investigation by means of termoprogrammimg desorption.

More then 140 participants was registrated and more then a hundred posters were presented. As is evident from the list of participants, the school was truly international in scope. Participants came not only from the USA and Ukraine but also from Israel, Italy, Germany and Russia. This is evidence of the international recognition of Kiev as a center for advance research in surface chemistry and physics.

We believe that CPS-94 expanded international scientific collaboration for Ukrainian research organisations and participants and promoted integration of the Ukraine into the international scientific community.

Organizing committee chairmen,
Prof. David E.Bergbreiter,
Prof. Vladimir N.Zaitsev

Functional Materials 2, No.1 (1995)

Organic chemistry at functionalized polymer/surface interfaces

D.E.Bergbreiter, H.N.Gray and B.Srinivas

Department of Chemistry, Texas A&M University,
College Station, Texas 77843-3255 U.S.A.

The chemistry of surface-modified polymers is discussed. General analytical problems, general synthetic strategies for polymer surface modification are discussed along with specific analytical and synthetic approaches for surface modification of polyolefins. Chemistry leading to surface grafting of polyethylene films is emplasized along with some discussion of fluorescence probes of solvation and reactivity at the functionalized and later suface-grafted polyethylene film surfaces.

Обговорюються проблеми хімії полімерів з модифікованими поверхнями. Розглянуто загальні проблеми аналізу і синтезу стосовно до модифікування поверхні полімерів, а також специфічні аналітичні та синтетичні питання, які стосуються поверхневої модифікації поліолефінів. Особливу увагу приділено хімічним процесам прищеплення різних функціональних груп до поверхні поліетиленових плівок та розгляду застосування флуоресцентних зондів для сольватації і реакційної здатності плівок, оброблених з метою створення на них функціональних груп з наступним прищепленням модифікаторів.

Polymers are macromolecules that find applications in varied technologis such as plastics, coatings, packaging, textiles and medicine. Polymers typically have good mechanical, electrical, thermal, optical and chemical properties. However, these properties mainly derive from a polymer's bulk properties. In polymer applications involving wettability, adhesion, permeability, friction, dyeing, and biocompatibility, a polymer's surface chemistry is more important. This has led to increasing interest in surface modification of polymers [1—3].

While the technological importance of surface chemistry is clear, what constitutes a polymer's "surface" is less clear. This is especially true when considering polymer/solvent interfaces [5]. Polymers unlike metals or amorphous glasses interact with a second condensed phase. Thus, the definition of what constitutes the "surface" of a polymer depends both on what phenomena one chooses. Furthermore, the techniques used to characterize a polymer's surface sample deal with various depths of the polymer (Fig.1). Thus, how one carries out a study and the techniques used also affect one's definition of a polymer's "surface".

The techniques most commonly used in surface analysis of polymers include contact angle analysis, XPS spectroscopy and ATR-IR spectroscopy. As shown in Fig.1, each of these tech-

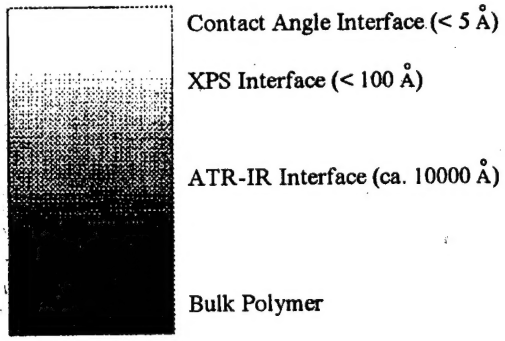

Fig.1. Schematic diagram illustrating the interfacial nature of a surface-functionalized polymer and the nominal depth assayed by various analytical techniques.

niques analyzes a different depth of a surface functionalized polymer.

A number of problems are encountered in the analysis of modified surfaces. Characterization of surface functionality is difficult due to the low concentration of functional groups. It is equally problematic to distinguish the surface from bulk polymer. The 3-dimensional spatial distribution of the functional groups in the surface is an important consideration in surface analysis. One has to also be cautious about sample contamination. Sample roughness and surface stability (e.g. reconstruction) complicate analyses of surface modifications. Relatively few techniques exist that can be used to analyze the 2-dimensional distribution or morphology of functionalized surfaces. This is especially true for surfaces in contact with a second liquid phase.

One of the most surface-sensitive and simplest analytical instruments is the contact angle goniometer. Contact angle analyses probe the top few Å of a surface. In this technique, a drop of a liquid is placed on a solid surface to measure the contact angle of the surface with respect to that liquid. A schematic representation of a sessile drop on a solid surface is shown below in Fig.2 [2]. Contact angles are related to interfacial free energy and therefore provide qualitative information about a surface [4]. For example, a low energy surface is hydrophobic and has a high contact angle with water while a high energy surface has a low contact angle water and is hydrophilic. The situation of complete wetting is not often met with polymers because their surface tensions are small (between 10 and 50 dynes/cm^2). The contact angle data are complicated in polymer samples by the presence of multiple species present in the surface, each of which contribute to the energy of the surface. An additional problem is surface roughness, encountered with all non ideal surfaces.

X-ray photoelectron spectroscopy (XPS) is another versatile tool to determine the atomic composition of the top 50 Å of the surface [5]. In XPS the sample surface is illuminated with a source of X-rays. Photoionization of a core level electron from surface atoms then occurs. The photoelectrons formed have a kinetic energy E which is related to the X-ray energy ($h\nu$) by the Einstein relation (equation 1)

$$E = h\nu - E_B - \phi \qquad (1)$$

where E_B is the binding energy of the electron in the material and is characteristic of the individual atom and ϕ is the work function of the instrument

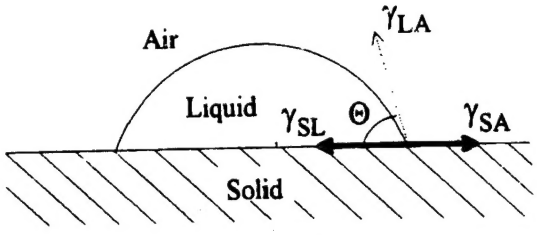

Fig.2. Sessile drop showing surface tensions acting in all three phases present.

[6]. Information about the binding energies of electrons within a sample thus allows direct elemental analysis. Chemical shifts also provide information about the chemical environment of specific atoms.

XPS can also be used in determining the concentration profile of a species over the top 50 Å of the surface. In angular dependent studies, the takeoff angle between the sample surface and the electron analyzer is varied. Since electron mean free paths are short, a grazing exit angle enhances surface features compared with a takeoff angle normal to the surface as shown in Fig.3. In most commercial spectrometers, the angle between the X-ray source and the analyzer is fixed. Therefore provisions are made for the sample holder to be tilted to facilitate depth profile studies. An alternative destructive method of depth profiling is to use ion sputtering, which physically etches away the surface before analysis by XPS spectroscopy.

Infrared spectroscopy (IR) is one of the most informative techniques in the study of the physical and chemical nature of polymers. Surface IR, also known as attenuated total reflectance (ATR) spectroscopy, has become an indispensable tool for surface analysis. Though the sampling depth of ATR-IR spectroscopy is much deeper than XPS (~1 μm), it is a convenient technique to study functional groups at depth greater than 100 Å.

Other techniques like ellipsometry, electron microscopy, Auger electron spectroscopy, and Rutherford back scattering are also available for surface analysis. Indeed, more than one technique is usually used to probe a modified surface. Complementary data obtained from more than one technique give a better picture of the system under study. The choice of a particular technique for analysis is dictated by several factors such as the sensitivity of the technique, the presence of identifiable functional groups, the depth of analysis, the stability of the surface to the analytical technique and the availability of proper instrumentation.

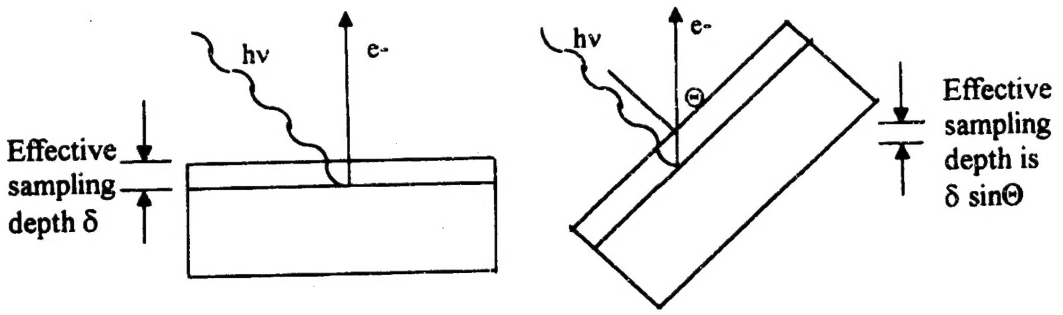

Fig.3. Angular dependent studies for samples in which spectra are studied as a function of the electron takeoff angle Θ with respect to the sample surface.

In our work, we have also found that analytical techniques such as fluorescence and ESR spectroscopy are also very useful. Though neither of these techniques are surface selective, their use in cojunction with appropriate chemistry in polymer suspensions provides insightful information. The information obtained by these spectroscopies provides data about modified polymer surfaces in contact with solvents and reagents. Examples of such approaches are discussed below.

Chemical modification of polymer surfaces has an extensive literature [8-13]. Substrates for this chemistry can be divided into two groups. One group includes reactive polymers with reactive functionality in their backbone. This includes polymers like polyesters, polyamides and polyamides and polyanhydredes. The second group would include unreactive polymers like polyolefins or PTFE. The lack of reactive functionality makes modification of these polymers more difficult and challenging and it is this type of chemistry and the issues involved that will be the focus of the following discussion.

The most common approaches to modification of polyolefins involve gas phase chemistry [12]. This is most convenient industrially. However, such approaches are best suited for simple mofifications. Synthetically more elaborate procedures or those designed to introduce spectroscopic labels to study surface chemistry and surface—solvent interactions often require a more sophisticated organic synthesis like liquid phase chemical treatments.

The classical approach to liquid phase modification of a polyolefin is oxidative etching. For example, oxidation of LDPE with CrO_3/H_2SO_4 at 70 °C introduces ketone and carboxyl groups onto polyethylene surface [13]. Synthetic conversions of carboxylic acids are well established in organic chemistry and have been employed to further derivatize these oxidized surfaces. Although this functionalization procedure is effective, the main drawback is that extensive pitting and chain scission are observed under such vigorous conditions [14]. Nonetheless, this chemistry has proven very useful in carrying out fundamental molecular level studies. Many of these studies were performed on the derivatized surface by measuring water contact angles. These studies include some of the most detailed works on the chemistry of functional groups at polymer-solvent interfaces. For example, the effects of pH on ionizable functional groups and the distinct differences between acid-base chemistry at surfaces versus solution have been elegantly examined.

Various alternatives to this harsh etching chemistry have been explored. For example, our group examined models of biooxidants as an alternative reagent for polyolefin surface functionalization [16]. This work used the Gif system initially developed by Barton as a model of methane monooxygenase chemistry [17]. We used two systems. In the first one, a polyethylene or polypropylene film was suspended in pyridine containing the iron catalyst $[Fe_3O(OCOCH_3)_6]$, zinc powder, acetic acid and a small amount of water. The reaction suspension was stirred and aerated. Zinc powder was used as a heterogeneous agent to reduce oxidized iron species. The second system used ferric chloride-picolinic acid-hydrogen peroxide in pyridine. Modest amounts of oxidation were reflected by small changes in the water contact angle for the product polyolefin films. Further confirmation of surface oxidation was obtained by chemical derivatization. Earlier oxidation studies on using the Gif system had shown that this oxidation yielded ketones from saturated hydrocarbons [17]. Therefore, function-

alized films were reduced with BH_3-Me_2S and then treated with trifluoroacetic anhydride to test for the presence of hydroxyl groups from carbonyl reduction. Surface analysis by X-ray photoelectron spectroscopy confirmed the incorporation of fluorine on the modified surface. The reduced films were also treated with pyrene butyric acid chloride. Fluorescence spectroscopy of the product film showed that pyrene ester groups had been incorporated onto the films' surface and supported the conslusions from XPS studies. Together, these labeling experiments strongly supported the contact angle evidence for oxidation by the Gif system. Overall, these studies show that organometallic C—H bond activating agents can be employed to functionalize both polyethylene and polypropylene surfaces though the extent of functionalization was disappointedly low.

A surface modified with hydrophilic groups has a high surface energy. Reorganization of functional groups at the surface move into the nonpolar polymer matrix will result in lowering of surface energy and a loss in wettability [18]. This possibly transient and history dependent nature of a functionalized surface can be a problem in surface modification. Such reorganization can be minimized by having longer hydrophilic grafts which have a lesser probability of diffusing into the bulk polymer. However, such surface graft polymerization requires initiation sites on the polymer surface. Chemistry to generate such sites has been a theme in both our work and that of others as is discussed below.

When high energy radiation impinges on a polymeric material, free radicals are generated on the surface which form peroxides in the presence of oxygene. This methodology has been used by Suzuki and others to graft acrylamide onto a polyethylene film [19]. Polyethylene film in air can also be irradiated with γ-rays from ^{60}Co to yeild surface bound peroxides. The resulting peroxide groups can then be used in surface grafting chemistry.

A more selective approach to surface grafting developed by Ranby uses UV light and an intitiator to selectively generate surface radicals from polyolefins by a C—H bond scission [20]. In this chemistry, benzophenone was used to absorb light and to form a triplet excited state. The excited triplet so formed then abstracts hydrogens from a polyolefin substrate forming radical sites for graft polymerization (equation 2).

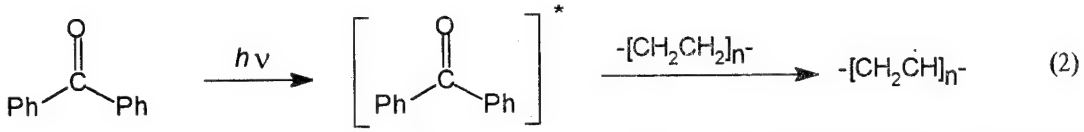

(2)

A final example of the use of established synthetic methodology to initate grafting onto polymeric substrates is our work using thiohydroxamic acid esters as initiators (equation 3) [21]. This work showed that photolysis of these esters generated surface bound methylene radicals which initiated graft polymerizations using vinyl monomers. A semi-quantitative estimate of the polymerization degree was obtained from IR analyses of the residual carbonyl intensity to the intensity of IR bands from the graft polymer. Monomers like acrylonitrile, styrene, ethyl acrylate, glycidyl acrylate and methacrylonitrile were all successfully grafted onto polyethylene in this way.

While chemical derivatization of preformed films has proven to be a useful method to functionalization and grafting, most of our work has emphasized a physical blending approach we call entrapment functionalization [22]. In this process (Sheme I), a low molecular weight functionalized polyethylene and a high molecular weight commercial polyethylene are dissolved and co-precipi-

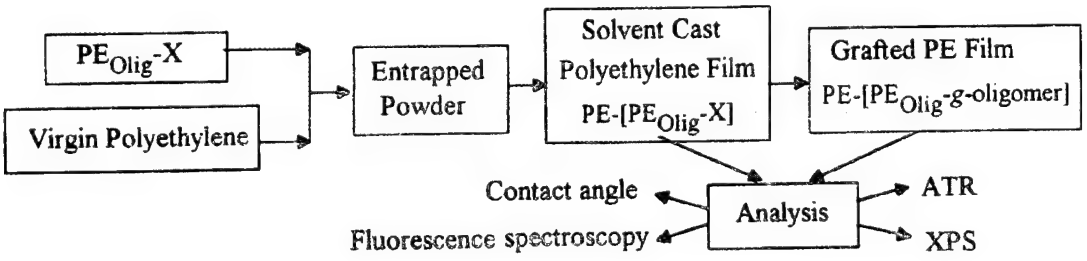

Scheme I. Entrapment functionalization of polyethylene by PEOlig derivatives.

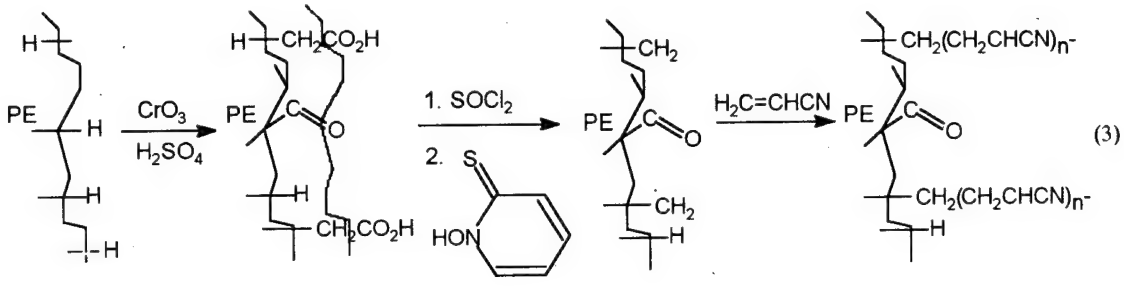

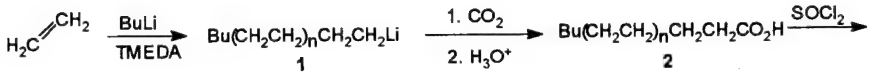

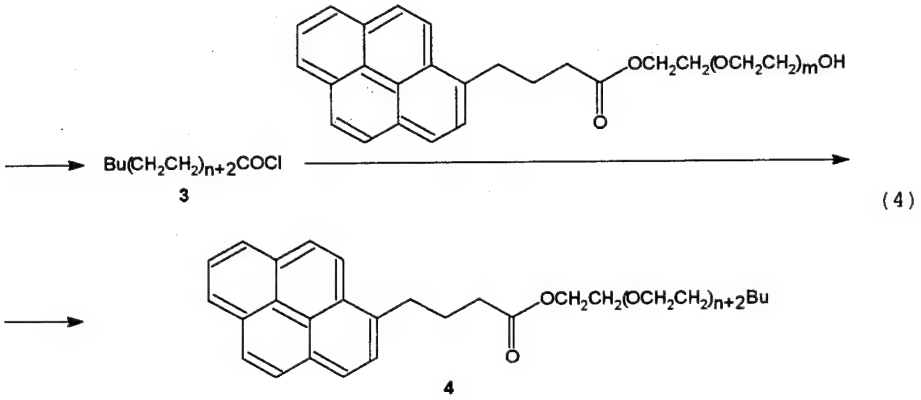

tated from hot toluene. The low molecular weight oligomer is synthesized by anionic oligomerization and can contain a wide range of functional groups, spectroscopic labels or block cooligomers at its terminus. Surface segregation of this low molecular weight additive during blending leads to the desired surface-functionalized polymer, as spectroscopic and reactivity studies showed.

Block cooligomers of ethylene and ethylene glycol prepared according to equation 4 [23] can be blended into virgin polyethylene to produce a surface functionalized film. The surface selectivity of the process with respect to varying size of poly(ethylene glycol) blocks and varying amounts of the block cooligomer used, have been studied using contact angle measurements, variable angle XPS, and variable angle ATR-IR spectroscopy [24]. Studies incorporating a fluorescent pyrene label at the terminus of the poly(ethylene glycol) block of a diblock polyethylene-poly(ethylene glycol) copolymer (equation 4) successfully used this pyrene group to probe the solvent dependent environment of the termini of the poly(ethylene glycol) grafts at the surface of entrapment functionalized polyethylene films [25]. These studies showed that the entrapped films prepared using **4** (PE/PE_{Olig}-**4**) had a variety of fluorescent properties that differed from that expected for a typical terminally functionalized polymer chain. For example, as is shown in Fig.4, the extent of excimer formation in a 2.5 wt.% loaded PE-[(PE_{Olig}-PEG_{1000}-pyrene] film was greatest in polar solvents that solvated the surface well. This is in contrast to the known effects of solvent variation on fluorescence of polymers in solution that have been end-labeled with pyrene groups. In solution, poorer solvents lead to more excimer because the polymer chains collapse and aggregate. Good solvents decrease the amount of excimer. At least at these surfaces, this effect is reversed. The entropic constraints faced by a pyrene groups randomly immolbilized in a surface or interfacial layer preclude the diffusion and the necessary face-to-face interaction needed to generate excimer fluorescence. Better solvents facilitate swelling of this surface layer and permit pyrene groups to interact.

Another example of a functionalized surface is the pyrene labeled surface prepared as shown in Scheme II. In this case, anionic oligomerization of ethylene was followed by quenching with an electrophilic pyrene-containing alkene [27]. The resulting pyrene oligomer was then entrapped in polyethylene to give a functionalized polyethylene containing weakly acidic C—H bonds. Subsequent deprotonation and addition of an

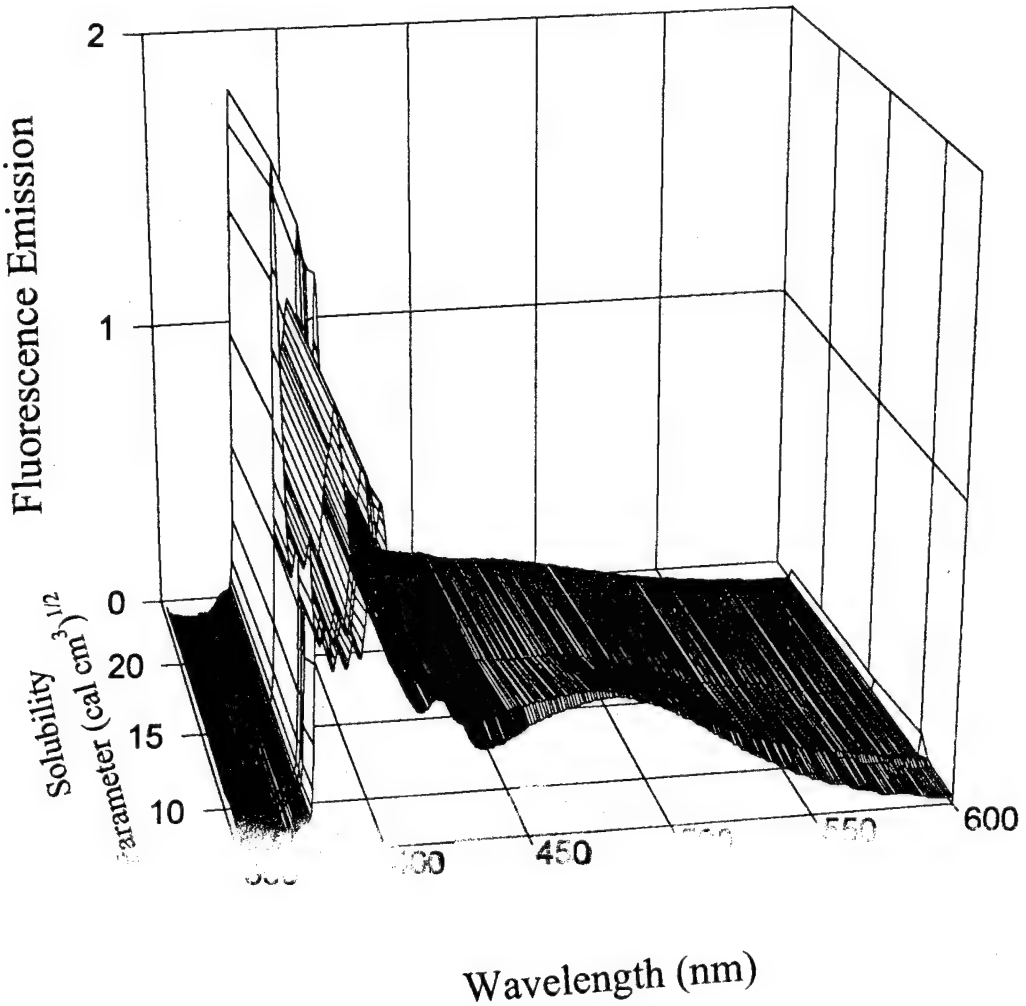

Fig.4. 3*D* plot of emission spectra of polyethylene films functionalized with 2.5 weight percent pyrene (PE-(PE_{Olig}-PEG_{1000}-pyrene)) suspended in different solvents showing a decrease in the excimer fluorescence for poorer solvents (solvents with higher solubility parameters).

appropriate monomer led to anionic grafting as shown in equation 5. Further studies of such surface-grafted materials are now ongoing in our laboratories but have already revealed a wealth of details about polymer-solvent interactions and the effects of surface grafts on such interactions.

Contact angle analysis, XPS spectroscopy and ATR IR spectroscopy all provide useful information about this surface and its derivatives before and after grafting. However, fluorescence spectroscopy again provided unique sorts of information. In this case, we were able to use both

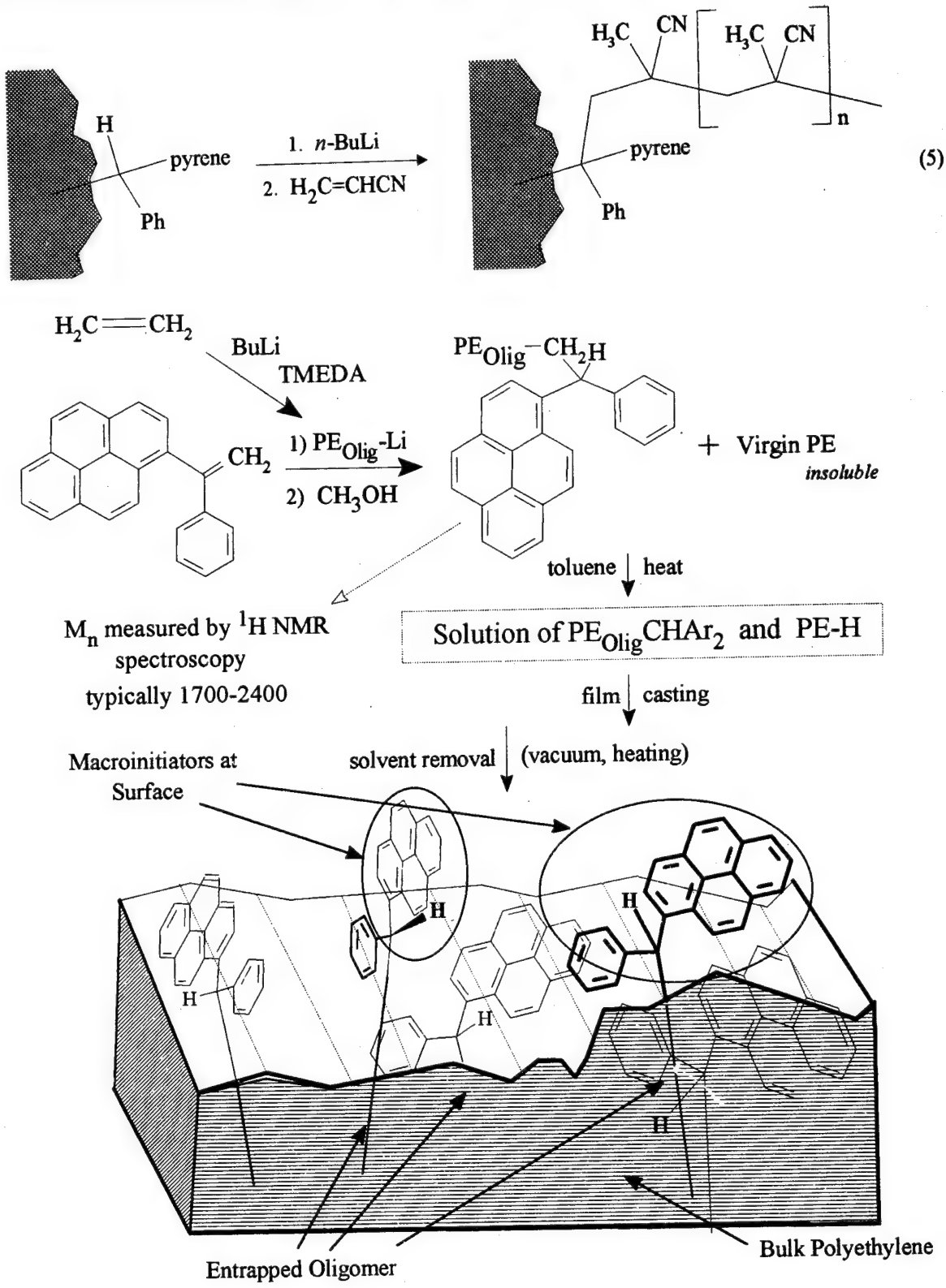

Scheme II. Diarylmethyl-functionalized polyethylene surfaces containing pyrene fluorescence labels can be prepared by entrapment functionalization. The product films contain pyrene-containing macroinitiator groups throughout the polymer/solvent interface.

solvation of the pyrene fluorophore and its reactivity with polyethylene-incompatible quenching agents to probe the 3-dimensional nature of the functionalized polyethylene surfaces produced by entrapment functionalization both before and after grafting.

In our work, static quenching was used to study the accessibility of pyrenes to N,N-dimethylethanolamine (DMEA). DMEA is reportedly a very surface selective reagent in that it selectively quenches pyrenes at the surface of polyethylene versus pyrene groups in bulk polyethylene [29]. Thus, when a PE-[PE$_{Olig}$-CH(Ph)pyrene] film was treated with N,N-dimethylethanol amine in various solvents, a portion of the pyrene fluorescence was quenched. The amount of fluorescence quenched varied depending on solvent. In THF, ca. 70% of the pyrene fluorescence was quenched. In methanol, only about 50% of the fluorescence was quenched. The difference was ascribed to the difference in the accessibility of pyrene in these two suspensions and to the different nature of the functionalized polymer surface/solvent interface in these two situations.

Fluorescence also provided a way to study the microenvironment of entrapped pyrene-tagged macroinitiators. These experiments relied on the known effect of solvents on the I_1/I_3 value of pyrene by solvents of varying polarity. The general effect is that the I_1/I_3 value decreases as solvent polarity decreases. In the case of a PE-[PE$_{Olig}$-CH(Ph)pyrene] film, the I_1/I_3 value increased with increasing solvent polarity to a plateau around I_1/I_3=1.95. Much smaller solvent effects were observed for grafted PE-[PE$_{Olig}$-CH(Ph)pyrene] film. Specifically, when a PE-[PE$_{Olig}$-CH(Ph)pyrene] film was deprotonated with BuLi and then treated with a THF solution of methacrylonitrile, a PE-[PE$_{Olig}$-C(Ph)pyrene-*g*-PMAN] film was formed. This film showed in the same solvents little or no solvent effect on the entrapped pyrene's I_1/I_3 values. This suggests that the PMAN grafts are present at the polyethylene-solvent interface and that they block solvation of the pyrenyl moieties at their attachment sites.

The effects of surface grafting on pyrene quenching was also studied. These effects which are shown in Fig.5 are in general accord with the effects on I_1/I_3 seen before and after grafting. As shown in Fig.5, the extent of quenching uniformly decreased in all four solvents studied. For example, for films suspended in ethanol, ca. 50% of the bound pyrenes were quenched before grafting and only about 20% were quenched after introduction of a poly(methacrylonitrile) graft onto

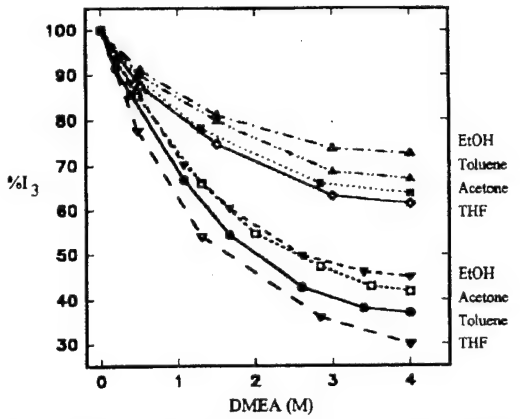

Fig.5. Effect of different solvents on quenching of PE-H/PE$_{Olig}$-CH(Ph)pyrene or PE-H/PE$_{Olig}$-C(Ph)pyrene-*g*-polymethacrylonitrile by N,N-dimethylethanol amine.

the pyrene initiator groups. Further evidence that this change reflected surface solvation of a brush overlayer is the change in order of extent of quenching with different solvents. Specifically, the relative extent of quenching in different solvents changed with acetone (a good solvent for PMAN) becoming a relatively better solvent for quenching after introduction of the PMAN graft.

Summary

Surface funtionalization of polymers is a technologically useful and important process that can be accomplished by both simple practical techniques and by more sophisticated chemical procedures. When spectroscopic probes are incorporated into the product polymer surface and when that surface is, in turn, synthetically elaborated, a variety of information about polymer-solvent interactions is forthcoming. Such studies show that solvents can differentially solvate the outermost interface of such functionalized polymers and that entropic effects and microenvironment effects can significantly alter known low molecular weight and conventional soluble polymer chemistry.

Acknowledgments

Support of this work by the National Science Foundation is gratefully acknowledged.

References

1. W.J.Eeast, H.S.Munro, Eds., Polymer Surfaces and Interfaces, John Wiley and Sons: Chichester, (1987); W.J.Feast, H.S.Munro, R.W.Richards, Eds., Polymer

Surfaces and Interfaces II; John Wiley and Sons: Chichester, (1993).
2. A.W.Adamson, Physical Chemistry of Surfaces, Wiley-Interscience publications: 5th Ed., New York, (1990).
3. W.T.Ford, Chemically Modified Surfaces, H.A.Mottola, J.R.Steinmetz, Eds. Elsevier Science Publishers, New York (1992).
4. M.K.Chaudhury, G.M.Whitesides, *Science*, **255**, 1230 (1992).
5. C.D.Bain, G.M.Whitesides, *J.Phys.Chem.*, **93**, 1670 (19889).
6. D.T.Clark, *Adv.Polym.Sci.*, **24**, 125 (1977).
7. N.J.Harrick, Internal Reflectance Spectroscopy, Wiley-Interscience publications: New York (1967).
8. M.Aglietto, R.Alterio, R.Bertani et al., *Polymer*, **4**, 1240 (1992).
9. K.W.Lee, S.P.Kowalczyk, J.M.Shaw, *Macromolecules*, **23**,2097 (1990).
10. G.F.Xu, D.E.Bergbreiter, A.Letton, *Chemistry of Materials*, **4**, 1240 (1992).
11. K.W.Lee, S.P.Kowalczuk, J.M.Shaw, *Macromolecules*, **23**, 2097 (1990).
12. D.E.Bergbreiter, *Prog.Polym.Sci.* in press, (1994).
13. S.R.Holmes-Farley, R.H.Reamey, T.J.McCarthy et al., *Langmuir*, **1**, 725 (1985).
14. J.R.Rasmusen, E.R.Stredonsky, G.M.Whitesides, *J.Am.Chem.Soc.*, **99**, 4736 (1977).
15. S.R.Holmes-Farlay, C.D.Bain, G.M.Whitesides, *Langmuir*, **4**, 921 (1988).
16. D.E.Bergbreiter, N.White, J.Zhou, *J.Poly.Sci.:Part A; Poly.Chem.*, **30**, 389 (1992).
17. D.H.R.Barton, D.Doller, *Acc.Chem.Soc.*, **25**, 504 (1992).
18. D.E.Bergbreiter, K.Kabza, *J.Am.Chem.Soc.*, **113**, 1447 (1991).
19. M.Suzuki, Y.Tamada, H.Iwata, Y.Ikada, Physicochemical aspects of polymer surfaces, Vol.2; K.L.Mital Ed., Plenum Press (1981).
20. K.Allmer, A.Hult, B.Ranby, *J.Poly.Sci.:Part A; Poly.Chem.*, **26**, 2099 (1988); K.Allmer, A.Hult, B.Ranby, *J.Poly.Sci.:Part A; Poly.Chem.*, **27**, 3405 (1989).
21. D.E.Bergbreiter, J.Zhou, *J.Poly.Sci.:Part A; Poly.Chem.*, **30**, 2049 (1992).
22. D.E.Bergbreiter, Z.Chen, H.P.Hu, *Macromolecules*, **17**, 2111 (1984), D.E.Bergbreiter, H.P.Hu, M.D.Hein, *Macromolecules*, **22**, 654 (1989).
23. D.E.Bergbreiter, J.R.Blanton, R.Chandran et al., *J.Poly.Sci.:Part A; Poly.Chem.*, **27**, 4205-26 (1989).
24. D.E.Bergbreiter, B.Srinivas, *Macromolecules*, **25**, 624 (1992).
25. D.E.Bergbreiter, H.N.Gray, B.Srinivas, *Macromolecules*, **27**, (1994) in press,.
26. S.Boileau, F.Mechin, J.M.G.Martinho, M.A.Winnik, *Macromolecules*, **22**, 215 (1989).
27. R.N.Young, R.P.Quirk, L.J.Fetters, *Adv.Polym.Sci.*, **56**, 1 (1984).
28. D.E.Bergbreiter, H.N.Gray, B.Srinivas, *Macromolecules*, **26**, 3245 (1993).
29. J.Naciri, R.G.Weiss, *Macromolecules*, **22**, 3928 (1989).
30. K.Kalyanasundaram, Photochemistry in Microheterogeneous Systems; Academic Press: New York, 1987 and references therein.

Органическая химия границ раздела функционализированных полимеров с поверхностями

David E. Bergbreiter*, H. Neil Gray and B.Srinivas

Обсуждаются проблемы химии полимеров с модифицированными поверхностями. Рассматриваются общие проблемы анализа и синтеза в применении к модифицированию поверхностей полимеров, а также специфические и синтетические задачи, относящиеся к поверхностной модификации полиолефинов. Особое внимание уделено химическим процессам прививки различных функциональных групп к поверхности полиэтиленовых пленок и рассмотрению применения флуоресцентных зондов для исследования сольватации и реакционной способности пленок, подвергнутых обработке с целью создания на них функциональных групп с последующей прививкой модификаторов.

Functional Materials **2**, No.1 (1995)

Polymer materials for medical purposes

V.A.Kalibabchuk and V.N.Zaitsev*

A.Bogomolets Ukrainian State Medical University,
13 Shevchenko Boul., 252004 Kiev, Ukraine

*T.Shevchenko Kiev University,
64 Vladimirskaja St., 252017 Kiev, Ukraine

Three types of bio-medical polymer materials have been surveyed. These are: natural; synthetic inert and biocompatible polymers; natural and synthetic polymers with favourable biological properties. Most attention is payed for biocompatible sorbents on cellulose (CS) base, for methods of cellulose modification that introduce ion-exchange groups, for properties of modified CS and it medical applications. The prospectives of sorptionally-active materials in views of third generation medical polymers development has been shown.

Розглянуто три типи медико-біологічних полімерних матеріалів: природні, синтетичні інертні та біосумісні полімери, що мають корисну біологічну дію. Особливу увагу приділено біосумісним волокнистим сорбентам на основі целюлози (ЦЗ): методам модифікації ЦЗ для надання їй іонообмінних властивостей, використанню в медицині та інших суміжних галузях. Показано перспективність розвитку методів модифікації сорбційно-активних волокнистих матеріалів з метою створення медичних полімерів третього покоління.

The origination of new scientific lines and areas is one of remarkables phenomena in the natural sciences development during the last quarter of our century. A prominent example is, especially, the creation and dramatical progress of the biomedical polymers chemistry [1] which has been originated at the interfaces of organic chemistry, high-molecular compounds physics and chemistry, biochemistry, molecular biology, pharmacology, and medicine. The vivid interest to this area is due to two circumstances: the fundamental natural science aspect — the living and inanimate nature interaction — and practical results of a wide variety of polymers uses for medical and public health care purposes.

At present, three types of biomedical polymers can be distinguished, somewhat arbitrarily [2]. First, there are natural polymers (especially, polysaccharides, e.g. soluble and insoluble dextrane, cellulose, or starch derivatives, some polypeptides — albumine and others). Second, it is to point to synthetic inert and bio-compatible, soluble or insoluble polymers, containing (desirably) biodegradable bonds in the main chain or in a side one, between the polymer itself and a medicinal compound linked to it. Third, finally, natural or synthetic polymers must be mentioned which have an useful biological effect or can enhance such effect of a medicinal substance linked to them (heparine, specific sulphonated polymers, etc.).

The first generation consisted of so-called «inert» polymers. They were associated with the first stage of synthetic polymers use, when no polymeric materials were yet created specially for medical uses, but appropriate polymers were chosen among the known engineering-designed ones. Investigators have found presently, however, that such «inert» polymers can cause sometimes even such phenomena as tissues necrosis, etc., due to impermeability of materials studied, substances migration blockage and, accordingly, the intercellular exchange inhibition.

Therefore, nowadays, ever-increasing attention is given to the development of polymer materials whose biocompatibility is determined not by

inertness, but by their interaction with organism, yet such one at which neither polymers themselves nor their degradation products would effect the organism undesirably.

This allowed to come immediately to a next step of a principial and practical importance, namely, to begin with the «third generation» creation of medical polymers. Such materials are not only biocompatible, but can also be included into biochemical processes, interacting with biological medium to cause a required useful effect on this medium or on whole organism. On the impressionable background of polymers materials, such polymer possessed, until recently, a rather modest place.

The fibrous sorption-active materials comply most full with the requirements to «third-generation» polymers [3]. The advantage of these materials over other ion-exchange resins consists in that they have more developed specific surface, possess a plethora of channels and pores which remain conserved after chemical modification, thus assuring a high volume capacity, selectivity and swellability of such sorbents.

The biocompatible fibrous sorbents on the cellulose (CS) basis are especially promising in this regard [4]. The cellulose macromolecule does not contain structural elements causing undesirable chemical effects on the human organism. It is easily modifiable, what allows to obtain a wide variety of its derivatives having predetermined composition and properties.

A great number of various methods can be used to modify cellulose for conferring ion-exchanging properties on cellulose. The main ones are:

1) selective oxidation of cellulose alcoholic groups to carboxyls;

2) etherification of cellulose by compounds containing additional acid or basic groups;

3) grafting of various polymers containing functional groups to cellulose macromolecules;

4) esterification by polycarboxylic acids;

5) alkylation.

Using the methods mentioned above, one can obtain cellulose-based ion exchangers containing any groups both cationic and anionic type.

Let us consider the main methods of cellulose-based cation-exchangers synthesis in more detail.

1. Ion-exchangers synthesis by cellulose oxidation

The best oxidizers for the cellulose are periodic acid and nitrogen oxides which allow to perform the oxidation more selectively than known oxidizing agents [5].

Periodic acid oxidizes secondary alcoholic groups of cellulose under breaking the pyranic ring and formation of dialdehyde cellulose which, by the further oxidation with sodium chlorite, gives dicarboxy cellulose:

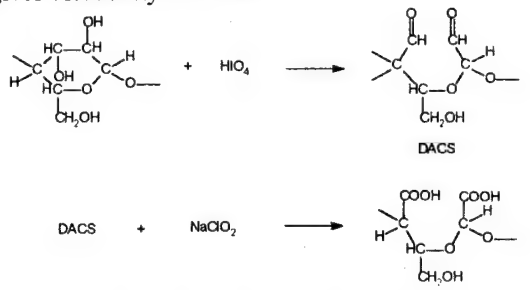

In parallel with these main reactions, side processes take place resulting in the formation of products containing various functional groups.

The main reaction of cellulose oxidation by nitrogen dioxide N_2O_4 resulting in the monocarboxycellulose occurs according to scheme:

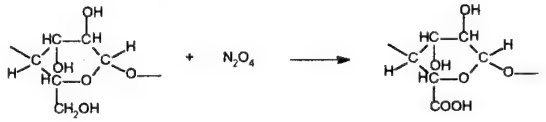

The oxidized cellulose, however, has a series of specific properties limiting its use for some medical purposes: such are thermal instability in air, strength drop during storage, etc. Besides, the material losses its features of an insoluble sorbent when certain critical value of carboxy group content is exceeded. Therefore, at the preparation of ion-exchanging celluloses, two important factors must be taken into account: on the one hand, a sufficient exchange capacity must be achieved, and on the other, the sorbent must be insoluble, chemically resistant and have satisfactory physical and chemical properties.

2. Ion-exchangers synthesis by etherification

Cellulose ethers possessing the ion-exchanging properties are obtained usually by the action of alkyl sulphates or alkyl halides on the basic cellulose:

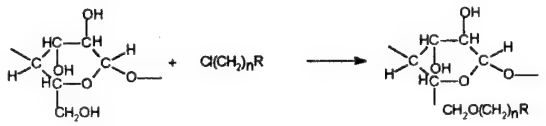

3. Ion-exchangers synthesis by esterification

Cellulose esters having ion-exchanging properties have been obtained, with phtalic, succinic, maleic, glutaric, and citric acids, the esterification being performed by acid anhydrides in the glacial acetic acid medium, in the presence of anhydrous sodium acetate.

As cellulose-based cation-cxchangers, the cellulose phosphates are most popular. They have found a wide use in the analytical chemistry and biochemistry for the polypeptides and vitamins separation, at chemical analyses for ion-exchange chromatography, solutions concentration, etc.

4. Ion-exchangers synthesis by polymers grafting to cellulose

Using the grafting of polymers to cellulose, ion-exchangers containing various types of functional groups can be obtained. The grafting is performed usually by following techniques:

1) Using preliminary introduction of groups forming macroradicals at the degradation. By such a means, the copolymers of cellulose with polyacrylic and polymethacrylic acids are obtained.

2) Radiation-chemical synthesis. By γ irradiation, the graft-polymers of cellulose with acrylic and methacrylic acids are developed.

3) Grafting to an oxidized cellulose. So, the copolymers of oxidized cellulose and cellulose phosphate with polyacrylonitrile are obtained.

The last-mentioned method has some disadvantages, namely, the low sorbents stability against aggressive media and the composition unhomogeneity due to the presence, in copolymer, of some homopolymer amount which undergoes extraction in the course of sorption. The troubles mentioned restrict the use of such polymer in the medical practice. To extend the service life of cellulose-based chemisorbents and to impart the insolubility to them, additional treatments by bifunctional and structurizing compounds are used, e.g. by hydrazine hydrate, peroxides, epichlorohydrine.

Using methods discussed above, a number of cellulose derivatives having ion-exchanging properties has been obtained, including carboxy cellulose, cellulose ethers and esters, copolymers of cellulose with various macromolecules, aminocellulose, sulphocelluloses. In all these syntheses, ionogenic groups can be introduced into cellulose macromolecule in an amount no more than one group for 20 to 30 structural glucose links. That is the limit of the ion-exchanging capacity for such products; when the number of ionogenic groups is increased, cellulose undergoes a destruction.

The composition and properties of some cellulose-based ion-exchangers are given in Table 1.

Cellulose phosphate

Cellulose phosphates are the inorganic cellulose esters most often used in medicine (Table 1). The phosphorylation of cellulose is performed by the action of derivatives of P(III) and P(V) acids. Phosphorous acid is the most effective phosphorylating agent among derivatives of phosphorus (III) acids. it should be noted, however, that products of cellulose phosphorylation by derivatives of P(III) acids are destructurized profoundly and instable to hydrolising action. These circumstances as well as the inevitable use of toxic substances to obtain such products, exclude their use for medical purposes.

One of popular techniques of the phosphorylation with derivatives of phosphorus (V) acids is the cellulose esterification by orthophosphoric acid and its chlorides:

$$CS\text{–}OH + H_3PO_4 \rightarrow CS\text{–}O\text{–}P(OH)_2 + H_2O$$

By its nature, cellulose phosphate is a polyfunctional cation-exchanger containing both strong and weak acid groups. As a polymeric acid, cellulose phosphate binds, by ion-exchange mechanism, inorganic and organic cations under formation of corresponding salts and strong phosphatic complexes. The high sorption capacity of phosphorylated cellulose is noted toward Cu(II), Fe(II), alkali, alkali-earth, and rare-earth metals ions as well as toward aliphatic amines and antibiotics (kenalicin, streptomycin, linkomycin, monomycin) [6].

For inorganic and organic ions sorption by cellulose phosphate, the form of phosphoric acid groups (H- or Na-form) is of primary importance. For example, in the case of exchange of Ca(II) ions on the H-form of cellulose phosphate, the strong acid groups are primarily involved in the reaction. On the other hand, in the course of Ca(II) sorption by the Na-form of cellulose phosphate, NaCl is given off into solution what results in the increase of its sorption capacity toward Ca(II) ions.

On this phenomenon, the medical use of cellulose phosphate is based as the sorbent for the donor blood stabilization [7] and for the Ca(II) ions binding at the kidneystone disease treatment (see Table 2).

Table 1. Ion-exchanging celluloses

No.	Name	Ionogenic group	Properties	Complete absorption capacity, mg-equiv./g
1.	Sulphoethyl cellulose	$—OC_2H_4SO_3H$	strong acid	0.4-0.5
2.	Sulphomethyl cellulose	$—OCH_2SO_3H$	strong acid	0.4-0.5
3.	Cellulose phosphate	$—OPO_3H_2$	strong acid	0.8
4.	Monocarboxy cellulose (oxycellulose)	—COOH	strong acid	0.7
5.	Carboxymethyl cellulose	$—OCH_2COOH$	weak acid	0.7
6.	Carboxyethyl cellulose	$—OC_2H_4COOH$	moderate acid	0.7
7.	Cellulose citrate	$—OOC—OH—(CH_2COOH)_2$		1.2-2.4
8.	Cellulose succinate	$—OOCC_2H_4—COOH$		3.15
9.	Cellulose maleinate	$—OOC—C_2H_2—COOH$		1.13
10.	Cellulose glutarate	$—OOC—C_6H_4—COOH$		0.80
11.	Cellulose phtalate	$—OOC—C_6H_4—COOH$		1.70
12.	*Para*-amino benzyl cellulose	$—CH_2—C_6H_4—NH_2$	weak basic	0.6
13.	Product of ethyl chlorohydrine, triethylamine reaction with cellulose	ionogenic group structure is not determined	weak basic	0.5
14.	Aminoethyl cellulose	$—C_2H_4NH_2$	weak basic	0.7
15.	Product of ethyl bromide reaction with DEAE cellulose	ionogenic group structure is not established	moderate basic	1.0
16.	Diethylamino ethyl cellulose	$—C_2H_4N(C_2H_5)_2$	moderate basic	1.0
17.	Guanido ethyl cellulose	$—C_2H_4NHC(NH)NH_2$	moderate basic	0.7

EDTA celluloses

From the viewpoint of fibrous sorbents use in the hematology, they are desirable to be similar, in their action, to known blood stabilizers being introduced into it for conservation, but, in the same time, to retain the advantages inherent in the sorptional method. In that relation, the sorbent similar, by its selectivity, to ethylendiamine tetraacetic acid sodium salt (Na-EDTA) may be very promising (see Table 2).

Acid salts of cellulose esters with antiseptic

The use, as sorbents, of salts of cellulose acid esters in which cation is an antiseptic [6], e.g. laevomycetin, synthomycin, trilaphlavin, offers a possibility to avoid the antiseptics introduction in conservants compositions and, in so doing, to prevent any action, even temporary, of elevated antiseptics concentration on the blood components capable to case their damage (Table 2).

A salt of cellulose phosphate with antiseptic is forming according the scheme

$$CS–O–P(O)(OH)ONa + K_aCl \rightarrow$$
$$\rightarrow CS–O–P(O)(OH)OK_a + NaCl$$

where K_a is an antiseptic cation.

Acetyl cellulose

Cellulose, as a polyhydric alcohol, undergoes an easy esterification with various acids or their anhydrides forming corresponding esters. By esterification of cellulose with acetic acid or its anhydride, the acetyl cellulose is obtained:

$$[C_6H_7O_2(OH)_3]_n + CH_3COOH \rightarrow$$
$$\rightarrow [C_6H_7O_2(OCOCH_3)_3]_n + nH_2O$$

Table 2. Cellulose-based sorbents and their clinical applications

Sorbent	Ionogenic group	CEC*	OEC**	SD***	Applications
Cellulose phosphate	—$OP(O)(OH)_2$	3.2	0.76	60	Haemostatic means; stomach ulcer treatment; biologically inert suture material; in the milk treatment for children and dietic nourishment; for ammonia vapours removing from air; filters for air and liquids sterilization; as a substrate for plants growing; for the protection from «soft» X-rays
Cellulose citrate	—CH_2—COOH	1.70	0.47	50	For donor blood stabilization
EDTA-cellulose	—$N(CH_2COOH)_2$	1.03	0.30	50	Blood purification when prompt and massive transfusions are required
Acid salts of cellulose esters with an antiseptic	-	-	-	-	For antiseptic bandage of prolonged effect
Acetyl cellulose	—$OOCCH_3$	-	-	-	For microbiological, biological, and physico-chemical analyses; for drug solutions purification from microorganisms and mechanical impurities; for sterilizing filtrations; for the electrophoretic separation of blood serum albumens
Acetyl phtalyl cellulose	—C_6H_4COOH	-	-	-	As the tablet envelope; to prepare the intestinal-soluble tablets (naphtamon, aspirin); in tuberculosis therapy complex; at the introduction of tetracyclin with laevorin to assure the prolonged effect of those substances
Methyl cellulose	—OCH_3	-	-	-	As the protecting envelope of drug preparations for enteric or local introductions; to introduce the pancreatin into the duodenum; as a binder in gypsum suspensions; for ointments and wet bandages; in protecting ointments for operating with organic solvents and aggressive media; as a eye-ointments base; for the treatment of skin diseases, burns, and for local anaesthesia; for the X-ray investigation of gastro-intestinal way
Ethyl cellulose	—OC_2H_5	-	-	-	As a graining agent for medicinal substances; in slow-dissolvable tablets for oral administration; for microcapsulation and protecting envelopes obtaining; in the hypertension and cardiovascular diseases treatment
Carboxymethyl cellulose	—CH_2COOH	-	-	-	A marked stimulation of reparative processes in infected skin wounds, acceleration of granulated tissue arising, etc.
Oxypropylene methyl cellulose	—$OCH_2CH_2OCH_3$	-	-	-	As a cellular coating material for gastrosoluble solid drugs forms; in the atophan, analgin, amidopyrin tablets technology
Monocarboxy cellulose	—COOH	-	-	-	An efficient haemostatic material: to stop the capillary and parenchimatous haemorrages from lunge wounds, caverns, cellular tissues surrounding blood vessels and gullet, operative wounds; in purulent surgery, etc.; a suture material

* Complete exchange capacity for NaOH, mg-equiv./g.
** Operating exchange capacity for $CaCl_2$, mg-equiv./g.
*** Substitution degree for N, per cent.

Acetyl cellulose possesses a characteristic ability to form elastic permeable films, membranes, etc., what motivates its widespread medical use. Nowadays, enzymes immobilized in microcapsules are obtained. The enzyme immobilization by microcapsulation retains the enzyme essentially in solution, i.e. in the native state. A polymeric envelope, being impermeable for both ferment contained in the capsule and high-molecular substances from the external medium, allows, in the same time, for the free passage of low-molecular compounds — substrates and products of enzymatic reaction.

Methyl cellulose

Methyl cellulose became firmly established in the drugs production area. It is soluble in cold water. In solution, the methyl cellulose macromolecules are covered by hydrated envelopes bonded with cellulose by hydrogen bonds. When temperature rises, the hydrogen bonds break, and methyl cellulose dehydration occurs. Cations and anions are also able to cause the dehydration; according to their ability to depress the solution gelation temperature, they can be arranged in series:

Pb (II), Zn (II), Cu (II), Fe (III), NH_4^+, Ca (II), Ba (II), K^+, Mg (II), Na^+, Al (III);

I^-, CNS^-, BO_3^{3-}, NO_3^-, CO_3^{2-}, Cl^-, $CH3COO^-$, SO_4^{2-}, PO_4^{3-}.

Water solutions of methyl cellulose are stable in a wide pH range (from 2 to 12), have good surface-active properties; after drying, a high-strength, colorless, odourless and tasteless film is obtained, resistant against bacteria, mould, and organic solvent action.

The use of methyl cellulose for medical purposes is based on its good binding, film-forming, and gel-forming properties.

Carboxymethyl cellulose

The treatment of carboxymethyl cellulose (CMC), obtained through the action of monochloroacetic acid on cellulose, by cross-linking agents like formaldehyde, epichlorohydrine, or diglycidyl ether, gives the highly hydrophilic, water-insoluble Na-CMC which can be used for sanitary and hygienic articles production.

On the CMC basis, a polymeric anaesthetic for local use is developed, called celcovocaine, which is effective in the therapeutic blockades performing, treatments of stomach and lungs malignant neoplasms, chronic cholecystopancreatitis, and also of acute and chronic pancreatitis.

Monocarboxy cellulose (MCC)

Among modified celluloses, the MCC finds the most widespread medical use, what is due to its successful combination of favourable physico-chemical and medico-biological properties.

The MCC is insoluble in water, organic solvents, as well as in diluted inorganic and organic acids.

Similar to some other cellulose derivatives, e.g. cellulose phosphate, carboxymethyl cellulose and acetic phtalyl cellulose, MCC is a polyelectrolyte and has ability to exchange reactions, being a more strong cation-exchanger than synthetic carboxyl-containing ones.

There are two main lines in MCC medical use development. First, it is the use of MCC itself, secondary, the use of its modification products.

The sorption-active cellulose-based materials can have, in addition to ion-exchanging properties, complexing ones, i.e. they can be modified by complex biometals compounds to obtain new textile species designated for medico-biological purposes.

Cellulose dialdehyde (DACS), the product of cellulose oxidation by periodic acid (see Scheme 1), is the most convenient source material for obtaining of physiologically active cellulose derivatives of the third generation. Dialdehyde cellulose contains the reactive aldehyde groups which allow to extend substantially the range of cellulose chemical modifications.

One of most typical reactions of aldehyde group is the interaction with primary amines resulting in azomethines, i.e. compounds including the C=N- group. This group is labile enough to split out, in a weak acid medium, the physiologically active molecular fragment, thus assuring the prolonged action of a preparation. Using this property, a number of chemical changes of DACS was performed through its condensation with various primary amines, including aromatic and heterocyclic ones. The grafted compounds obtained show strong complexing abilities what allows to prepare metal complexes.

Metal chelates grafted to a textile surface can provide the basis to obtain preparation of combined effect. The matrix containing metal complexes with tripsine are of special interest in this context.

Cellulose may be also modified by acting of previously prepared metal complexes on its oxidized surface. Using this scheme, the cobalt (III) — monoethanol amine and copper (II) — trioxymethylamine (TRIS) complexes has been grafted to a polysaccharide matrix.

The immobilization of physiologically active substances has been performed on the DACS modified by the above-mentioned complexes; a

high bactericidic activity has been found for a number of samples containing silver, cobalt, and copper ions.

The DACS oximes containing, in addition to alcoholic and aldehydic groups, oximidic fragments which are the potential metal-binding centers, are capable to form complexes with substances being sorbed.

An oxyl-containing cellulose matrix has been obtained by covalent bonding of the hydroxyl amine to a polymeric textile support. In this matrix, the azomethine bonds are formed according to scheme:

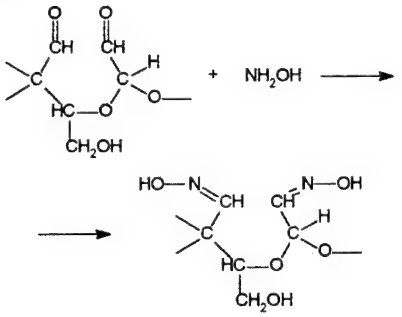

The study of the sorbtional properties of DACS oximes in relation to 3*d*-transitional metals had shown that DACS oximes preparations provide the features of polymer complexing agents. The capability of cellulose oximide reactions to bind metallic ions is determined mainly by the possibility of polydentate binding complexing ion resulting in stable chelate cycles, by metal nature, and by the chelatic links number. The most favourable condition of metal coordination is created by its positioning in the 2,3-dioximino cellulose unit.

The textile metal chelates on the basis of cobalt, nickel, and copper oxaminates provide the most strong antimicrobic efficience. The information described above shows that the development of modifying methods of sorption-active fibrous materials is highly promising for the creation of «third-generation» medical polymers.

References

1. S.Manabu, Polymers for Medical Applications, Medicina, Moscow (1982) [cited by Russian Ed.; orig. in Japan].
2. M.T.Alyushin, Synthetic and Biological Polymers in Pharmacy [in Russian], Medicina, Moscow (1990).
3. I.N.Ermolenko, I.P.Buglov, I.P.Lubmener, New Fibrous Sorbents for Medical Purposes [in Russian], Nauka i tekhnika, Minsk (1978).
4. F.N.Kazhutsky, T.L.Yurkshtovich, Drug Preparations on the Basis of Cellulose Derivatives [in Russian], Universitetskoe, Minsk (1989).
5. E.G.Davydova, V.V.Rachinsky, *Usp.Khimii*, **34**, 252 (1965).
6. A.D.Virnik, *Zh.Vsesoyuzn.Khim.Obshch.*, **30**, 447 (1985).
7. A.D.Virnik, in: Results in Sci.and Techn.: Chem.and Technol.of High-Molecular Comp. [in Russian], **21**, 35 (1986).
8. E.E.Kriss, I.I.Volchenskova, A.S.Grigorieva, et al., Metal Coordination Compounds in Medicina, Naukova Dumka, Kiev (1986).

Полимерные материалы медицинского назначения

В.А.Калибабчук, В.Н.Зайцев

Рассмотрены три типа медико-биологических полимерных материалов: природные, синтетические инертные и биосовместимые полимеры, обладающие полезным биологическим действием. Особое внимание уделено биосовместимым волокнистым сорбентам на основе целлюлозы (ЦЗ): методам модификации ЦЗ для придания ей ионообменных свойств, применению в медицине и других смежных областях. Показана перспективность развития методов модифицирования сорбционно-активных волокнистых материалов с целью создания медицинских полимеров третьего поколения.

Functional Materials **2**, No.1 (1995)

Quantitative physico-chemical analysis of chemisorption on complexing silicas

Yu.V.Kholin

Kharkov State University,
4 Svobody Sq., 310077 Kharkov, Ukraine

One of the most commonly used methods for investigating complex compounds forming silicas (a quantitative physico-chemical analysis, QPCA) has been considered in the paper. It was subjected to some analysis in what way the procedures of the QPCA, proposed for studying the complex formation in solutions, have to be changed to take into account the features of chemisorption on the complex compounds forming silicas. The overview of the meaningful physico-chemical models which are in use to interpret primary data of QPCA has been presented. The methods to establish the structure of the models and to find their parameters have been discussed. The thermodynamical justifications of the models have been presented and the connections between their parameters have been found. The paper contains the proposed hierarchical system of the models and the recommendations for their use in practice.

В статті розглянуто один з найпоширеніших методів дослідження комплексоутворюючих хімічно модифікованих кремнеземів — кількісний фізико-хімічний аналіз (КФХА). Проаналізовано, яким чином слід змінити методики КФХА, запропоновані для вивчення комплексоутворення в розчинах, щоб коректно врахувати особливості комплексоутворюючих кремнеземів. Представлено огляд змістовних фізико-хімічних моделей, що їх вживають для інтерпретації первинних даних КФХА. Розглянуто методи структурної параметричної ідентифікації моделей. Обговорена термодинамічна обгрунтованість моделей, знайдені зв'язки між їх параметрами. Запропонована ієрархічна система моделей і надані рекомендації з їх використання.

Since the late 70s, investigations on synthesis and use of silicas with N, O, P, S-containing electron-donor groups covalently fixed on their surfaces are intensively progressing [1,2]. Sorbents of this type (complexing chemically modified silicas, CCMS) are used to separate and concentrate metal ions, in the development of heterogeneous metal-complex catalysts, etc. [1,3]. One of methods to study CCMS, quantitative physico-chemical analysis (QPCA), is the division of a physico-chemical analysis. It deals with the determination of stoichiometric composition and stability constants of reagents on the basis of relationships between the composition of a system and a certain its property in equilibrium conditions [4]. The objective of a quantitative physico-chemical analysis as applied to the study of metal ions chemisorption on CCMS is to obtain such information concerning the composition and thermodynamic stability of complex compounds grafted to the SiO_2 surface, which information could be compared with similar data characterizing complexes in solutions. The accumulation and analysis of great arrays of the QPCA results will make possible the quantitative characterization of factors causing the changes of reactants properties at fixation and, on this basis, the application of a vast information relating to complex formation equilibria in solutions [5,6]. The methodology of the QPCA was elaborated to study the chemical equilibria in solutions, systems containing bottom phases, extraction equilibria [8,9]. It cannot be extended mechanically to the investigation of equilibria involving objects which are new for chemistry, namely, complexing silicas. Physico-chemical meaningful models [10] designated to account for the CCMS specific features, are the tools of QPCA. In this work, such models and their practical applications are reviewed, the thermodynamic validity of models is discussed and,

on the basis of these considerations, the unified system of model is formed instead of odd ones.

QPCA features in systems under consideration

Let a functional group Q be fixed on a silica surface, a group concentration is $t(Q)$ mol per kg of CCMS. A weighed CCMS sample with the mass a, kg, is brought into contact with a known initial volume (V, dm^3) of a salt M solution (besides of M, other reactants, X, may also present in the solution). Under varying a, V, total reactant concentrations in solution $t(M)$, $t(X)$ (mol/dm^3), a certain property (g) of the equilibrium system is measured, e.g. pH of solution, light absorption, amount of M remained in solution in the equilibrium conditions, etc. The array of measurement results offers the initial data for QPCA, a "composition-property" dependence

$$g_k = f(t(Q), t_k(M), t_k(X), ..., a_k, V_k), \qquad (1)$$

where k is the number of experimental point, f, a function. In the special case, when adsorption of M on a complexing silica is measured at a constant temperature, Eq.(1) is defined as the adsorption isotherm. Dependence (1) is specified by a table on a finite set of points; therewith, both arguments $t(Q)$, $t(M)$ and responses g values are determined with certain errors, and the form of function f is unknown a priori. The problem of QPCA is to determine, on the basis of dependence (1), the number of species, stoichiometric composition, and thermodynamic stability of complex compounds M_mQ_q on the CCMS surface. To solve this problem, meaningful (physico-chemical) models are applicated. These are constructed in two stages. First, the structural identification is carried out, i.e. such a form of function f is specified, at which parameters, having a physical sense (e.g. stability constants of complexes), are fitting parameters for the model. On the second stage, the parametric identification of the model is accomplished, i.e. from the condition of "the best" approximation of dependence (1) by the model, the numerical values of fitting parameters are determined. The particular form of function f does not follow from thermodynamics, but any form of f cannot be in contradiction to the general thermodynamic principles. First, the fact must be taken into account that the true thermodynamic components (i.e. substances which can be introduced into the system independently of each other) are not the solvent, salt (M), ligands (Q), and carrier (SiO_2), but the solvent, salt M, and supermolecule [11] of complexing silica, each such supermolecule containing a certain amount of SiO_2 and some number, s, of grafted Q groups.Second, complex formation takes place on the solution-solid interface, therefore, in constructing models, the thermodynamic language is to be used which has been approved for the surface phenomena description: Gibbs method or the finite-thickness layer method [12,13].

The choice of thermodynamic language

Recently, a work was published [14] where authors have attempted to avoid the choice between the Gibbs method and the finite-thickness layer method and, at a minimum of assumptions, have considered an adsorption system using the fundamental Gibbs equation for adsorption. It is impossible to use that approach to justify the QPCA practice, because, when the fundamental equation alone is used, the expression for chemical potentials of reactions, μ_i, are not specified and, consequently, the form of the mass action law is undetermined. Having established expressions for μ_i, the authors [14] were going to the finite-thickness layer method without stating this fact explicitly. Such an "implicit" character of the transition may create the illusion that the QCPA of chemisorption can be strictly substantiated directly by the fundamental Gibbs equation, without account for approximations and restrictions associated with the adsorption determination used in the finite-thickness layer method.

According to Gibbs, adsorption, Γ, is an excessive quantity. Due to this, Γ cannot characterize the near-surface layer composition, and, in the Gibbs method, concentrations became senseless. Since the QPCA involves the evaluation of stability constants and, therefore, the use of concentrations, the Gibbs' method is unsuitable to justify the QPCA.

In terms of the finite-thickness layer method, an adsorption system is considered as that consisting of three phases: an inner sorbent volume whose properties remain unchanged at adsorption, a homogeneous liquid phase, and an unhomogeneous adsorption layer (AL) [12,13]. Let us consider the relationship between the experimentally measured value of adsorption, g, and the adsorption definition as the total sorbate content in the adsorption layer. In the first case,

$$g = V \cdot \{t(M) - [M]\}/a, \qquad (2)$$

where V is the initial volume of solution; for the second, the expression

$$X = (1/a)\int_{z_1}^{z_2} c(z)\,dz, \qquad (3)$$

is valid, where $c(z)$ is the M concentration in the adsorption layer varying along the normal (z) to CCMS surface; z_1, z_2 are the positions of the layer boundaries. It is obvious that X depends on the choice of AL boundaries. The farther the outer boundary is drawed from the surface, the greater are the AS volume and X value. Such an incertainty is a essential disadvantage of the method complicating its application. In the same time, the X gives a quantitative estimation of the near-surface layer composition. The difference between g and X can be easily found as

$$g - X = (V^p - V) \cdot [\mathrm{M}]/a, \qquad (4)$$

where V^p is the equilibrium volume of homogeneous solution minus volume included in the AL. Since volume of diluted solution varies insignificantly at reactions, the difference between g and X is small, too. Therefore, it is allowable to interprete the measured quantity g as the thermodynamically rigorous X one, bearing in mind that such approach is somewhat approximative.

Two methods to express concentrations of grafted species

In the initial stage of the simulating complex formation equilibria, the concentrations of grafted species were related to the volume of liquid phase and measured in mol/dm^3 ("the homogeneous approach"). Later, the "heterogeneous" approach was believed to be more justified, according to which, the species concentrations were related to a sample mass or to CCMS surface area [15,16]. If, however, we understand adsorption to be a total content of sorbate in a finite thickness layer, the conclusion about approximative character of both appoaches can be drawn. That approximativeness is the price which must be paid for the uncertaintities in the establishing of adsorption layer boundaries and for the absence of aprioric information about its inhomogeneity. Indeed, the relation of the grafted species concentrations to the CCMS mass or to the solution volume is equivalent to the assumption that the phase interfaces are so established that the actual AL is "compressed" up to a monolayer formed by anchored ligands and complexes. Therewith, the liquid phase is believed to be homogeneous, as before, and the influence of carrier on the complex formation is not taken into account explicitly. In fact, the concentrations of species are related to an area of that model monolayer. The value of that area is unknown. It can be assumed to be proportional (perhaps equal) to the surface area (A) of CCMS as determined by the physical adsorption of nitrogen, phenol, etc. Then, the concentration of grafted species must be related to A and expressed in mol/m^2. Since

$$A = a \cdot A_{sp}, \qquad (5)$$

where A_{sp} is the specific surface area, m^2/kg, there exists an equivalent way to express the concentrations. One can relate the concentrations to the mass of sorbent (a) and express as mol per kg of CCMS. Formally, the decision to relate concentration of grafted species to a surface area or a mass of CCMS corresponds to description of the system as two-phase heterogeneous one (solution + adsorbent). Another assumption, namely that the area of a "model" monolayer is proportional to the liquid phase volume. In this case, concentrations of species must be related to the volume V and expressed in mol/dm^3. Then the chemisorptional system is considered as a homogeneous one.

If the adsorption isotherm for M is measured under condition of constant a/V ratio for all experimental points, the "homogeneous" and"heterogeneous" approaches are equivalent to each other: for reaction

$$m\mathrm{M} + q\mathrm{Q} = \mathrm{M_mQ_q}, \qquad (6)$$

where m, q are stoichiometric indexes and coefficients, the concentrational stability constant for a fixed complex $\mathrm{M_mQ_q}$ in the "homogeneous" concept is determined as

$$\beta_{qm} = [\mathrm{M_mQ_q}]/[\mathrm{M}]^m[\mathrm{Q}]^q, \qquad (7)$$

where quantities in brackets are the equilibrium concentrations. The value of constant in the "heterogeneous" approach (β^*_{qm}) differs only by a constant factor [17]: $\beta^*_{qm} = \beta_{qm} \cdot (a/V)^{q-1}$. In other cases, it is possible to determine which of concepts is more close to truth through comparing a quality of approximation of dependence (1) with both approaches. Special experiments have shown that adsorption isotherms are described somewhat better in terms of "homogeneous" approach [17,18].

General requirements to meaningful models of chemisorption on CCMS

Whatever the structure of a meaningful physico-chemical model may be, it must contain equations of three types: 1) equations describing

the relationships between the property being measured and the equilibrium composition; 2) material balance equations; 3) equations of the mass action law (MAL). The property under measurement can be essentially always expressed as a linear combination of equilibrium concentrations

$$g = \sum_{i=1}^{Z} a_i [L_i] \ , \qquad (8)$$

where L_i are species; Z, their number; a_i, coefficients (known or to be determined, called sometimes "intensity factors" [19]); quantities in brackets, the equilibrium concentrations. To write the material balance conditions, let use the canonic form of reaction description [20]

$$\sum_{j=1}^{p} \nu_{ij} B_j = L_i, \qquad (9)$$

where B_j is a subset of reactants called independent components; γ_{ij}, stoichiometric coefficients. The number of independent components, p, is equal to the number of species (Z) minus the number of reactions between them (r): $p = Z - r$. The invariants of the system are total concentrations of components:

$$t_j = \sum_{i=1}^{Z} \nu_{ij} \cdot c(L_i) = \sum_{i=1}^{Z} \nu_{ij} \cdot [L_i], \ j = 1,2,...,p, \quad (10)$$

where $c(L_i)$ are initial L_i concentrations, known from the conditions of reactants blending. Equations (10) specify the material balance conditions. MAL equations for the complex formation in solution have the form

$$[L_i] = \exp\{\ln \beta_i + \sum_{j=1}^{p} \nu_{ij} \ln [B_j]\}, i = 1,2,...,Z, \quad (11)$$

where β_i is a concentrational stability constant of L_i,

$$\ln \beta_i = \ln \beta_i^T + \sum_{j=1}^{p} \nu_{ij} \ln \gamma_j - \ln \gamma_i, \qquad (12)$$

where β_i^T is a thermodynamic constant; γ_i, γ_j, activity coefficients. Since, in complex formation studies, the method of constant ionic strength is used, γ_i, γ_j do not vary at reactions, and the use of concentrational constants β_i^T instead of thermodynamic ones (β_i) does not provoke objections [8].

Extending the experience of the equilibrium simulation in solutions to equilibria in adsorption layers of CCMS, we cannot change two first groups of equations specifying the function f. There are MAL equations (or, equivalently, expressions specifying the chemical potentials of species in the AL) which must be modified. Adsorption layer is not to be considered as an usual phase. There, reactants concentrations are anomalously high, distribution of ligands on the support surface is inhomogeneous, a distorsion of coordination spheres of anchored complexes are possible, etc. As a result, the grafted species are energetically inhomogeneous, compounds may build up having no analogues in solutions, the possibility of lateral interactions of fixed ligands and complexes must be taken into account. Models which bring several modifications into the MAL, have accounted for distinct AC features.

The great diversity of models complicates significantly achieving the QPCA main objective — the generalization of great data arrays concerning the composition and stability of fixed complexes — and hinders the creation of a complete molecular-statistical model of chemisorption on CCMS. In this connection, we believe that it is necessary to present the unified system of models instead of odd individual ones and to demonstrate how the parameters of different models are related to each other. Moreover, for all models, the possibility of transition from "subcomponents" Q, M_mQ_q to the true thermodynamic components is to be estimated.

The unified system for models of chemisorption on CCMS

All models are subdivided into two groups. Those taking into account explicitly the energetic inhomogeneity of the absorption layer are belonging to the first group. It is advantageous to use them when, at the interaction of M with a fixed group Q, the only fixed complex MQ is formed

$$\mathrm{M} + \mathrm{Q} = \mathrm{MQ}. \qquad (13)$$

What is considered is degree of complex MQ formation

$$\theta = [\mathrm{MQ}]/t(\mathrm{Q}) = \{t(\mathrm{M}) - [\mathrm{M}]\}/t(\mathrm{Q}), \quad (14)$$

which is proportional to the adsorption

$$\theta = g \cdot a/\{V \cdot t(\mathrm{Q})\}, \qquad (15)$$

as well as the concentration equilibrium constant

$$K = [\mathrm{MQ}]/[\mathrm{M}][\mathrm{Q}] = \theta/\{[\mathrm{M}] \cdot (1-f)\}. \quad (16)$$

Model of continuous distribution of the equilibrium constants. The energetic inhomogeneity of CCMS is meant to be a distinction between the

standard chemical potentials of fixed species having the same stoichiometric composition. In other words, in the case of the energetic inhomogeneity of complexing silica, the standard states of Q and MQ do describe not the unique values μ^0_Q and μ^0_{MQ}, but sets of values $\{\mu^0_Q\}$ and $\{\mu^0_{MQ}\}$. Since the equilibrium constant of reaction (13) is specified as follows

$$K = \exp\{-(\mu^0_{MQ} - \mu^0_M - \mu^{0)}_Q / R\,T\}, \qquad (17)$$

the equilibrium constant will be represented, too, by a set of values $\{K_i\}$. To define the energetic inhomogeneity of a CCMS, we must determine, what part of fixed groups (in relation to their total number) is characterized by a given value of the constant. In other words, one should found the distribution function of groups in the constant values, $p(K)$ (the probability density of equilibrium constants). Often, it is more convenient to use, instead of the differential distribution function $p(K)$, the integral one

$$P(K) = \int_0^K p(x)\,dx, \qquad (18)$$

Assuming the formation of unique fixed complex MQ and absence of lateral interactions, we have obtained an expression relating the experimental θ values to the sought for function $p(K)$ [21]:

$$\theta([M]) = \int_0^\infty p(K)\,Y(K,[M])\,dK, \qquad (19)$$

where

$$Y(K,[M]) = K \cdot [M]/(1 + K \cdot [M]). \qquad (20)$$

Eq.(19) is mathematically identical with the Langmuir equation for the physical adsorption on a heterogeneous surface [22,23] and with equations describing inhomogeneity of humic acid [24] and proteins [25]. The parametric identification of the model, that is the $p(K)$ calculation on the basis of an experimentally measured function θ([M]), is a difficult problem, since the solution of integral equation (19) (Fredholm 1st type) is a typical example of an ill-posed problem [27] (many possible solutions exist consistent with experimental data). By now, however, methods have been developed to evaluate, reliably enough, the energic inhomogeneity [23,28,29], therewith the integral distribution function $P(K)$ is determined more accurately than $p(K)$.

The model of continuous distribution allows to go from "subcomponents" Q to the true thermodynamic component $\{(SiO_2)_xQ_s\}$. The chemical form $\{(SiO_2)_xQ_s\}$ is an s-dentate bonding center to which, in step-by-step manner, low-molecular particles M add to create chemical form $\{(SiO_2)_xQ_3M\}$, $\{(SiO_2)_xQ_3M_2\}$, etc. The complexing process is described with an array of stability constants

$$\kappa_i = [(SiO_2)_xQ_sM_l]/\{[(SiO_2)_xQ_s] \cdot [M]^l\}, \qquad (21)$$

where bracketed symbols mean equilibrium concentrations. The titration curve of s-atomic acid or base is known to be identical to that of solution containing s monoatomic acids (or bases) in equal concentrations, if protonizations constants (K_l) of conjugated monoatomic bases and overall protonizations of s-atomic base are such that

$$\kappa_l = \sum_{\nu_j \in \Omega} K_1^{\nu_1} K_2^{\nu_2} \times \ldots \times K_l^{\nu_l} \times \ldots \times K_s^{\nu_s}, \qquad (22)$$

where the set Ω of allowable ν_j values is specified by the conditions $\nu_j \le 1$; $\nu_j \ge 0$; $\sum_{j=1}^{s} \nu_j = l$, $j = 1,2,\ldots,s$ [30,31]. If the continuous integral distribution function $P(K)$ is approximated with a s-stepped function, it means that we describe a chemisorption process as the addition of particles M to s monobasic bonding centers with different constants K_l. At great s values, the error of approximation of $P(K)$ with a stepwise function is negligible. Now, using Eq.(22), it is easy to go from K_l constants set to an array of constants κ_l, which do describe the experimental adsorption isotherm as good as K_l, but, unlike the latter, characterize properties of the Gibbs' component of a system (i.e. those of CCMS) as a whole.

The electrostatic model is used when species are charged, e.g. if Q is electrically neutral and M and MQ bear a charge. Bonding the charged particles with fixed groups is believed [1,14,32] to result in formation of a charged adsorption monolayer on the CCMS surface and of electric double layer (EDL) in the adjacent solution volume. The influence of the AL electrostatic field on the charged ions in solution is accepted to be the cause of the EDL inhomogeneity. The actual discrete distribution of charges on the surface is replaced to homogeneous continuous one. Ions in solution are considered as point charges. The change of Gibbs energy associated with the bonding of 1 mol of M to 1 mol of grafted groups Q is subdivised into two items:

$$\Delta G = -2.3\,R\,T\,lg\,K = \Delta G_{chem} + \Delta G_{el}, \qquad (23)$$

where K is the quantity being calculated according to Eq.(16), ΔG_{chem}, the contribution due to the chemical interaction:

$$\Delta G_{chem} = \mu^0_{MQ} - \mu^0_M - \mu^0_Q = -2.3\,R\,T\,lg\,K^0, \qquad (24)$$

where K^0 is the "intrinsic" equilibrium constant; ΔG_{el}, the transfer work of 1 mol of ions M from the bulk solution onto the charged surface. The bonding of each new M particle requires an ever-increasing work expenditure ΔG_{el} against electrostatic field forces. Consequently, the equilibrium constant calculated from Eq.(16) must decrease when θ raises.

To recognize the type of $K(\theta)$ relationship, i.e. to perform the structural identification of the electrostatical model, one must be able to calculate ΔG_{el}. Several EDL models and respective expressions for ΔG_{el} are discussed in literature [32-34].If EDL is considered as a flat condenser, then

$$\Delta G_{el} = 2.3\,R\,T\,b\,\theta, \qquad (25)$$

where b is positive factor depending on the EDL thickness, CCMS specific surface area, dielectric constant of the medium in EDL, and Q groups concentration. Combining Eqs.(16),(19), and (20), we obtain [35]

$$lg\,K = lg\,K^0 - b\theta = lg\,[\theta/(1-\theta) + pM, \qquad (26)$$

where $pM = -lg\,[M]$. Equation (26) specifies the function $\theta\,(pM)$ unexplicitly: at known lgK^0, b and prescribed pM, the calculation of θ is performed numerically. To determine parameters $lg\,K^0$ and b, it is necessary: 1) to calculate lgK according to Eq.(16) from measured θ and pM values; 2) to construct the plot of lgK vs. θ. If this relationship is linear, it means that it is possible to use the model. The free term gives an estimation of lgK^0, the slope, that of b parameter. The transition from parameters lgK^0 and b to constants ξ_l is evident enough: it is sufficiently to approximate discrete ξ_l values by means of the function $\kappa(\theta) = K^0 \cdot 10^{-b\theta}$ [36].

The relationship between electrostatic and continuous constants distribution models. To reveal the relationship between models, one must establish how the function $p(lgK)$ and its moments (average, dispersion, and asymmetry)

$$E = \int_{-\infty}^{+\infty} lg\,K\,p(lg\,K)\,d\,lg\,K;$$

$$D = \int_{-\infty}^{+\infty} (lg\,K - E)^2\,p(lg\,K)\,d\,lg\,K; \qquad (27)$$

$$A = \int_{-\infty}^{+\infty} (lg\,K - E)^3\,p(lg\,K)\,d\,lg\,K$$

are associated with the parameters lgK^0 and b describing the same adsorption system. It is shown [35] that

$$E = lg\,K^0 - b/2;\ D = b\,(b/12 + 0.434);\ A = 0. \qquad (28)$$

In the case if an adsorption isotherm is described by the electrostatic model with parameters lgK^0 and b, that isotherm will be described in just the same quality by the continuous constants distribution with a symmetrical distribution function $p(lgK)$, the average and dispersion being determined by Eq.(28). On the other hand, if the function $p(lgK)$ is asymmetric, then the electrostatic model corresponding to it does not exist. Therefore, the electrostatic model as described by Eq.(26) must be considered as a special case of the continuous distribution model, and only the latter is to be used to treat the experimental data. The result of calculation performed according to this model will allow to recognize if the inhomogeneity effects can be interpreted on the basis of electrostatic motions.

Models of chemical reactions, fixed and statistical polydentate centers. In those models, the adsorption layer inhomogeneity is not taken into account explicitly. The features of that layer can manifest themselves in an anomalous stoichiometry and/or stability of fixed complexes. In those models, the form of MAL traditional for solution is modified by different manners (see Table). For the statistical polydentate centers, a justification based on the statistical thermodynamics method has been given [37,38]. CCMS is considered as a two-dimensional lattice whose points are occupied by bounding centers. Lateral interactions, unhomogeneity effects, etc., are not taken into account.

The fitting parameters for those models are determined either by simplified graphical and manual calculation methods based on the use of auxiliary functions (e.g. Bjerrum, Lejden, etc.) [7—9], or by modern computational ones [7,9,20,39,40] to obtain the best possible agreement between measured and calculated adsorption values. The fundamental difference between the application of auxiliary functions to study equilibria in solutions and on CCMS surface has been pointed out first by Tertykh and Yanishpolsky [41]. The parametric identification of models is performed in several steps [20,39]. First, the discrete parameters are fixed, namely, the number of fixed species and stoichiometric indices in their formulas. For a prescribed hypothese dealing

Table. Models accounting explicitly for the variety of chemical forms in the adsorption layer

Name	Model characteristic	Reactions of the complexing silica with components M being sorbed	Expressions for stability constants	Characteristic parameters
Fixed polydentate centers (FPC) [15,16]	CCMS is an array of quasi-independent fragments containing some number (y) of grafted groups. The reaction with the number y of groups Q is considered as that with one y-dentate ligand (Q_y)	$(Q_y) + M = M\,Q_y$ $(Q_y) + 2M = M_2Q_y$ ... $(Q_y) + pM = M_pQ_y$	$\sigma_p = [M_pQ_y]/([M]^p \times [(Q_y)]$	y, σ_π
Statistical polydentate centers (SPC) [37,38]	The aggregation of some number (i) of grafted groups Q resulting in the formation of an i-dentate ligand takes place immediately in the course of the MQ_i complex formation	$Q + M = M\,Q$ $2Q = Q_2;\ Q_2 + M = M\,Q_2$ ... $iQ = Q_i;\ Q_i + M = M\,Q_i$	$\beta_i^0\,\tau_i = [MQ_i]/([M] \times [Q]^i) \times i(l_{Q)}^{i-1}$	$y = \max i$, τ_i, i.e. number of groups consisting of i ligands Q, including fixed one, capable to form the complex MQi; $(\beta_i^0\tau_i)$
Chemical reactions (CR) [17]: a) without regard for the heterogeneity; b) accounting for the heterogeneity	Do not introduce a priori any assumptions about reactions of grafted groups; the features of the system may manifest themselves as anomalous composition and/or stability of fixed complexes	$Q + M = MQ$ $iQ + pM = M_pQ_i$ $p = 1$, if Q is monodentate; $p \geq 1$, if Q is polydentate	$\beta_{ip} = [M_pQ_i]/([M]^p \times [Q]^i)$	β_{ip}

with reactions, a criterial function is minimized in respect to the stability constants of fixed complexes; such a function can have, for example, the form

$$s_0^2 = (1/(N-t)) \cdot \sum_{k=1}^{N} w_k\,\Delta_k^2, \qquad (29)$$

where N is the number of experimental points of the composition-property dependence; Δ_k, the discrepancy between the calculated and measured values of adsorption $\Delta_k = g_k^{model} - g_k^{meas}$; w_k, the statistical weight of the k-th measurement, $w_k = [\sigma_k \cdot g_k^{meas}]^{-2}$, σ_k, estimation of the relative error for g_k measurement. If errors are estimated properly, the model under testing describes adequately the experimental data at s_0^2 of order of unity [42]. If s_0^2 is too large, new complexes are introduced into the model, and the calculation is repeated. It should be noted that least squares problem (29) is of ill-posed nature: there are many sets of fitting parameters compatible with experimental data [43]. from the chemical viewpoint, it means that a specific chemisorption model can include redundant complexes with fictive stability constants and the used computational programs must contain means to eliminate the redundancy.

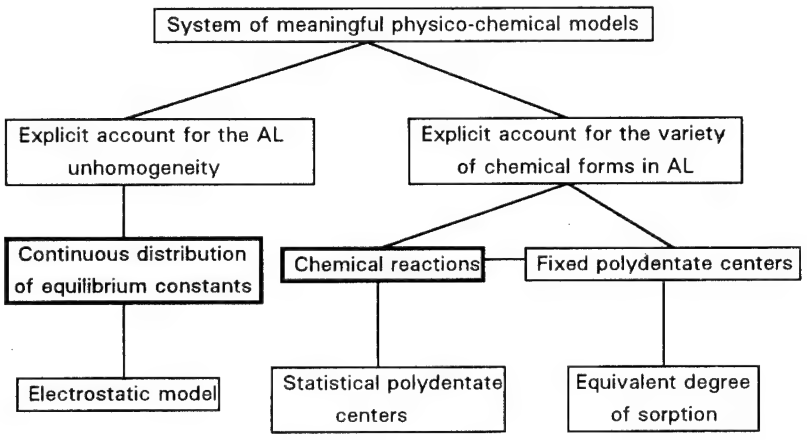

Fig.1.

It seems at first glance that models based on chemical reactions (CR), fixed polydentate centers (FPC), and statistical ones (SPC) describe isotherms of the adsorption on CCMS surface in different manners. All these models, however, are in effect several versions of the lattice model which does not include special parameters accounting for the AL inhomogeneity and lateral interaction therein. Comparising the expressions for β_{ip} (CR model) and $\beta_i^0\tau_i$ (SPC model) we can see [17] that

$$lg\ \beta_{i1}^{*} = lg\ (\beta_i^0 \cdot \tau_i) + (1-i)\ lg\ t\,(\mathbf{Q}) - lg\ i, \qquad (30)$$

$$lg\ \beta_{i1} = lg\ (\beta_i^0 \cdot \tau_i) + (1-i)\ lg\ \{t\,(\mathbf{Q} \cdot a/V\}) - lg\ i, \qquad (31)$$

where stability constants marked by asterisk are referred to the "heterogeneous" version of the CR models (i.e. when concentrations of fixed species are related to the CCMS mass). The SPC model is applicable when complexes forming on the surface are mononuclear with reference to the metal. The area of the CR model application is wider, and it can be considered as a generalization of the SPC model.

The interrelation between FPC and CR model parameters is less evident. To look for it, the common base for both models, namely, lattice model was considered. The necessary relations for several versions of models have been obtained [44]. So, for a special case when fixed complexes MQ and MQ_2 are formed having, in the context of CR model, the stability constants β_{11} and β_{21}, the following expression is valid:

$$\sigma_l = \sum_{\nu_j \in \Omega} \frac{G!}{\nu_1!\ \nu_2!\ \nu_3!}\, 2^{\nu_2}\, \beta_{11}^{\nu}\, \beta_{21}^{\nu_2}\, t\,(\mathbf{Q})^{\nu_2}, \qquad (32)$$

$$l = 1,2,\ldots,y,$$

where y is the number of grafted groups forming a single polydentate bonding center; the set Ω is determined by conditions $\nu_1 = 0$; $\nu_2 = 0$; $\nu_3 = 0$; $y = \nu_1 + 2\nu_2 + \nu_3$; $l = \nu_1 + \nu_2$; $G = \nu_1 + \nu_2 + \nu_3$. In particular, at $y = 2$, $\sigma_1 = 2\beta_{11} + 2\beta_{21} t\,(\mathbf{Q})$, $\sigma_2 = \beta_{11}^2$. If the size of a fixed polydentate center (y) coincides with the number of functional groups (s) grafted to a CCMS supermolecule, the parameters σ_l transform to κ_l, $l = 1,2,\ldots,s$. Thus, equation (32) and its analogues [44,45] allow to go from the chemical reactions model and the polydentate bonding one to the description of a CCMS as a single complexing agent. A quantity depending on experimental conditions, namely, the concentration $t(\mathbf{Q})$ is included in Eq.(32). It would seem that, by varying $t(\mathbf{Q})$, the FPC and CR models can be discriminated (it is possible to establish which of them is more realistic): for this purpose, one must vary $t(\mathbf{Q})$ and recognize, by observation, which parameter — β or σ-varies. When the homogeneous version of the CR model is used, $t(\mathbf{Q})$ can be varied by changing the a/V ratio. In the case of the heterogeneous version application, the a/V changes do not influence on $t(Q)$ value (mol/kg). Therefore, both models mentioned are equivalent, and adsorption isotherms obtained from each of them will coincide with each other.

The "equivalent sorption degree" model (ESDM) [46] is the last those under consideration. It is proposed as an alternative to the approach using the stability constants to describe

the equilibria of fixed complex compound formation. The equilibrium of reaction

$$M + (Q_y) = MQ_y, \qquad (33)$$

where Q_y is y-dentate bonding center, is supposed to be characterized, instead of the stability constant, by the equivalent sorption degree

$$a_e = [MQ_y]/t(M) = \frac{t(M) - [MQ_y]}{t(M)}, \qquad (34)$$

where total and equilibrium concentration are related to the solution volume (mol/dm^3), $t(M)$ is the known total concentration of M equal to $t(Q_y)$ concentration. The application of ESDM, according to [46], is justified when the only complex MQ_y is formed on the surface, lateral interactions between grafted species do not take place, ligands are grafted to the surface uniformly. It is obvious that the formation of the only fixed complex is described with the only parameter, be it the stability constant or a_e. At the specified $t(M)$, there is an unique correspondence between a_e and σ, thus, the ESDM is a special case of the FPC model.

The analysis performed allows to establish the unified, thermodynamically justified system of meaningful physico-chemical models for the interpretation of the QPCA results (see Figure). Names of models which are recommended for the treatment of original experimental data are given in bold frames.

References

1. Chemically Modified Silicas in Sorption, Catalysis, and Chromatography [in Russian], G.V.Lisichkin, Ed., Khimia, Moscow (1986).
2. V.A.Tertykh, L.N.Belyakova, Chemical Reactions Involving Silica Surface [in Russian], Naukova dumka, Kiev (1991).
3. G.V.Lisichkin, *Zhurn.Vses.Khim.Obshch. im.Mendeleeva,* **34**, 291 (1989).
4. V.Ya.Anosov, M.I.Ozerova, Yu.Yu.Fialkov, Principles of the Phys.-Chem.Analysis [in Russian], Nauka, Moscow (1976).
5. L.G.Sillen, A.E.Martell, Stability Constants of Metal-Ion Complexes, Chem.Soc. London. 1064p, No.17 — 754p. 1971, No.25 — 865p.
6. Critical Stability Constants, **1—5**, Plenum Press (1974-1982).
7. M.Beck, I.Nagypal, Chemistry of Complex Equilibria, Akadémiai Kiado, Budapest (1989).
8. F.J.C.Rossotti, H.Rossotti, *The Deterination of Stability Constants and Other Equilibrium Constants in Solution, McGraw-Hill Book Company, New York — Toronto — London (1961).*
9. F.R.Hartley, C.Burgess, R.M.Alcock, Solution Equilibria, Elwis Horwood, Chichester (1980).
10. A.V.Suvorov, Mathematical Methods of Chemical Thermodynamics [in Russian], Nauka, Novosibirsk (1982).
11. V.B.Aleskovski, Course of Supermolecular Compound Chemistry, [in Russian], LGU Publ., Leningrad (1990).
12. A.A.Lopatkin, Theoretical Principles of the Physical Adsorption, [in Russian], MGU Publ., Moscow (1983).
13. A.A.Lopatkin, *Zhurn.Fiz.Khim.*, **67**, 2315 (1993).
14. B.V.Zhmud', A.A.Golub, *Zhurn.Fiz.Khim.*, **67**, 734 (1993).
15. A.P.Filippov, *Teor.i eksper.khimia*, **19**, 463 (1983).
16. G.V.Kudryavtsev, *Zhurn.iz.Khim.*, **61**, 468 (1986).
17. Yu.V.Kholin, V.N.Zaitsev, N.D.Donskaya, *Zhurn.Neorg.Khim.*, **35**, 1569 (1990).
18. T.P.Lishko, L.V.Glushchenko, Yu.V.Kholin, et al. *Zhurn.Fiz.Khim.*, **65**, 2996 (1991).
19. Z.A.Saprykova, G.A.Boos, A.V.Zakharov, Physico-Chemical Methods for Investigation of Coordination Compounds in Solutions [in Russian], Kazan Univ.Publ., Kazan (1988).
20. A.A.Bugaevsky, Yu.V.Kholin, *Analyt.Chim.Acta,* **241**, 353 (1991).
21. Yu.V.Kholin, S.A.Merny, *Zhurn.Fiz.Khim.*, **67**, 2223 (1993).
22. O.M.Poltorak, Thermodynamics in Physical Chemistry [in Russian], Vysshaya Shkola, Moskow (1991).
23. A.W.Adamson. Physical Chemistry of Surface, Third edition, J.Wiley, New York, (1976).
24. B.Leuenberger, P.W.Schindler, *Anal.Chem.*, **58**, 1471 (1986).
25. F.Karush, M.Soneneberg, *J.Am.Chem.Soc.*, **71**, 1369 (1949).
26. A.M.Thakur, P.G.Munson, D.L.Hunston, D.Rodbard. *Analyt.Biochem.*, **103**, 240 (1949).
27. A.N.Tikhonov, B.Ya.Arsenin, Methods for solution of ill-posed problems) [in Russian], Nauka, Moscow (1986).
28. W.A.House, M.J.Jaycock, *J.Chem.Soc. (Faraday),* Part 1, **73**, 942 (1977).
29. J.Roles, G.W.Guiochon, *J.Phys.Chem.*, **95, 4098 (1991).**
30. H.S.Simms, *J.Am.Chem.Soc.*, **48**, 1239 (1926).
31. A.A.Bugayevsky, Study of Equations Describing Systems with Stepwise Equilibria [in Russian], Chim.Cand.Thesis, KhGU, Kharkov (1965).
32. B.V.Zhmud', A.A.Golub, *Ukr.Khim.Zhurn. (Ukr.Chem.J.),* **58**, 976 (1992).
33. M.J.Jaycock, G.D.Parfitt. Chemistry of Interfaces, Ellis Horwood, Chichester (1981).
34. Adsorption from Solution at the Solid Liquid Interface, Ed.by G.D.Parfitt and C.H.Rochester, Academic Press, London (1983).
35. Yu.V.Kholin, S.A.Merny, *Zhurn.Fiz.Khim.*, **67**, 2229 (1993).
36. V.M.Tolmachov, N.I.Gulayeva, L.A.Lomako, I.K.Ishchenko, High-Molecular Complex Compounds [in Ukrainian], KhDU, Kharkov (1991).
37. V.V.Yagov, A.A.Lopatkin, *Zhurn.Fiz.Khim.*, **62**, 2222 (1988).
38. G.V.Kudryavtsev, D.V.Miltchenko, V.V.Yagov, A.A.Lopatkin, *J.Colloid Interf.Sci.*, **140**, 114 (1990).
39. M.Meloun, J.Havel, Computation of Solution Equilibria. 1.Spectrophotometry, (1984) 184p. 2.Poten-

tiometry, (1985) 145 p. Brno: Univerzita J.E.Purkyne — prirodovedecka faculta.
40. A.M.Evseev, L.S.Nikolaeva, Mathematic Simulation of Chemical Equilibria [in Russian], MGU Publ., Moscow (1988).
41. V.A.Tertykh, V.V.Yanishpolsky, *Teor.i Eksper.Khim.*, **27**, 361 (1991).
42. J.A.F.Seber, Linear Regression Analysis, J.Wiley and Sons, New York (1977).
43. A.N.Kornilov, Unformal Mathematical Models in Chem.Thermodynamics [in Russian], Nauka, Novosibirsk (1991).
44. V.V.Skopenko, Yu.V.Kholin, V.N.Zaitsev et al. *Zhurn.Fiz.Khim.*, **67**, 727 (1993).
45. A.M.Yevseev, L.S.Nikolayeva, *Zhurn.Fiz.Khim.Phys.Chem.*, **67**, 509 (1993).
46. A.K.Trofimchuk, *Ukr.Khim.Zhurn.*, **56**, 930 (1990).

Количественный физико-химический анализ хемосорбции на комплексообразующих кремнеземах.

Ю.В.Холин

В статье рассмотрен один из наиболее распространенных методов исследования комплексообразующих химически модифицированных кремнеземов — количественный физико-химический анализ (КФХА). Проанализировано, как следует изменить методики КФХА, предложенные для исследования комплексообразования в растворах, чтобы корректно учесть особенности хемосорбции на комплексообразующих кремнеземах. Представлен обзор содержательных физико-химических моделей, используемых для интерпретации первичных данных КФХА. Рассмотрены методы структурной и параметрической идентификации моделей. Обсуждена термодинамическая обоснованность моделей, найдены связи между их параметрами. Предложена иерархическая система моделей и даны рекомендации по их использованию.

Functional Materials 2, No.1 (1995)

The silicas chemically modified with amino-di(methylene phosphonic) and ethylenediamine-di(methylene phosphonic) acids

V.N.Zaitsev, L.S.Vassilik, J.Evans* and A.Brod**

T.Shevchenko Kiev University, 64 Vladimirskaya St., 252017, Kiev Ukraine

*Southhampton University, Great Britain

**Oxford University, Great Britain

The synthesis and properties of two representatives of a new class of chemically modified silicas, containing organophosphorus complexones bonded to surface of silica are described. These are amino-di(methylene phosphonic) and ethylenediamine-N',N'-di(methylene phosphonic) acids. The new substances have been characterized by elemental analysis, FTIR and high-resolution solid-state NMR spectroscopy on ^{31}P and ^{13}C. Protolytic and complexing properties of mentioned compounds with some *s*-, *f*- and *d*-metals are investigated. The high selectivity of interaction of fixed acids with ions Ca^{2+}, La^{3+} is found out.

Описано синтез та охарактеризовано два представника нового класу хімічно модифікованих кремнеземів, що містять на поверхні фосфорорганічні комплексони: N-пропіламіно-ди(метиленфосфонову) та N-етилендіамін-N',N'-ди(метиленфосфонову) кислоти. Нові сполуки охарактеризовано даними елементного аналізу, ІК-спектрометрії з Фур'є перетворенням спектроскопії ЯМР високої роздільної здатності в твердому тілі на ядрах ^{31}P і ^{13}C. Вивчено протолітичні та комплексоутворюючі властивості вказаних сполук з рядом *s*-, *f*- і *d*-металів. Виявлено високу селективність взаємодії закріплених кислот з іонами Ca^{2+}, La^{3+}.

Inorganic materials with chemically modified surface nature (CMM) have practically excluded the organic polymers in such areas as chromatographic stationary phases [1], catalysts [2], carriers for enzymes immobilization [3], owing to their advantages over the polymeric materials. Various modifications of silica are the main and most comprehensively studied bases for the CMM creation [4]. Silica is chemically inert and does not effect substantially on the CMM properties because contains no strongly acid or basic centers, in opposed to, for example, Al_2O_3 or TiO_2 [5]. Wide varieties of organic compounds have been fixed on silicas by means of covalent immobilization, e.g. alkyl and aryl derivatives [6], alcohols and amines, heterocyclic and sulphur-containing [4] compounds.For the ion-exchange properties development, CMM have been obtained containing fragments of carboxylic and alkyl sulphonic acids [8] as well as of quarternary ammonium salts [8,9]. Yet, the methods for obtaining silicas having the organophosphoric complexing agents are not sufficiently advanced. Phosphorus-containing silicas obtained previously are hydrolytically unstable and have low coating degree of the surface by modifying agent [10]. In the same time, it can be suggested that unique properties of amino phosphonic acids [11] allow to obtain promising CMM that could have prospective properties as medium-acidity ion-exchangers having increased affinity to *s*- and *f*-metals, stationary phases for the ligand-exchange chromatography, adsorbents, etc.

The aim of the present research is to develop a procedure for obtaining a new class of chemically

modified silicas containing organophosphorus complexing groups with general formula

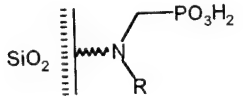

[where R=H, CH_3, $CH_2PO_3H_2$, $CH_2CH_2N(CH_2PO_3H_2)2$]
which combine the properties of ion-exchangers and chelating ligands. We also intend to describe the physico-chemical properties of two compounds from this class, namely, of amino-di(methylene phosphonic) acid (ADPA-SiO_2) and ethylenediamine-N',N'-di(methylene phosphonic) acid (EnDPA-SiO_2) covalently bonded to the silica surface via propylsilyl spacer:

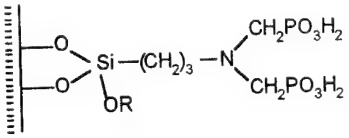

ADFK-SiO_2

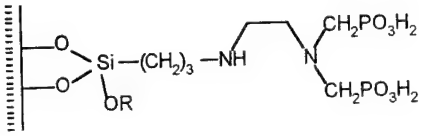

EnDFK-SiO_2

Experimental

Instruments

IR spectra were recorded on the Perkin-Elmer Fourier transform spectrophotometer, samples being prepared as thin films between KBr windows. NMR spectra on ^{31}P and ^{13}C nuclei were taken for wetted and air-dried powders in the temperature range 180-300 K on the Durham instrument (200 MHz) in the static regime as well as with "magic angle" speening and cross-polarization.The contact time was varied from 0.1 to 20 ms. The pH-metric titrations were performed on the EV-74 ionometer with the silver chloride operating electrode and glass auxiliary one (ESL 43-07 type).

Procedures

The elemental analyses (C, N, H) were performed on an elemental analysator by Dumas method. The phosphorus content was determined in London Analytical Laboratory service as well as in authors' one by following method [12]: to the certain amount of sorbent (0.1 g) placed in the volumetric flasks of 50 ml volume, 0.6 cm^3 of glacial acetic acid and 0.2 cm^3 of bromine were added. The flasks were heated on a sand bath until solution discoloration, then 5 cm^3 of 25 % H_2SO_4, 10 cm^3 of 0.25 % potassium vanadate solution and 10 cm^3 of 5 % ammonium vanadate solution were added to flask and diluted with water. The solutions were allowed to stand for 30 min to colour development. The absorption was measured at λ=430 nm, l=1 cm. The calibration plot was obtained with potassium dihydrophosphate solution. Instead of the phosphorus-containing sorbent, an amino silica was used in that case. The dependence of the solution optical density on the phosphorus concentration can be described by the straight line $y = 1.1323x+0.0519$ with the correlation coefficient r=0.998.

The immobilized groups concentration was determined by pH-potentiometric titration and additionaly from elemental analysis data. Since, at pH>8.5, SiO_2 is beginning to react appreciably with alkali, the titrations were performed in 1 N KCl solution, what diminishes the matrix dissolution rate. A sample of sorbent was placed into a glass containing 25 cm^3 of KCl solution, and 0.1 N sodium hydroxyde was added under continuous mixing.

The complexing properties of sorbents were examined potentiometrically. To this end, the sorbent (0.2 g) was placed into a glass containing 25 cm^3 of 1 N KCl solution; then, a solution of a metal salt was added in the amount required to achieve the molar ratio M(*soln.*):L(*surf.*)=1:1 and the slurry was mixed for 20-30 min. Then, under continuous mixing, the mixture was titrated with 0.1 N NaOH solution.

The non-linear least-square method [13] was used to calculate the stability constants values for the fixed complexes, by minimizing the function

$$s_0^2 = [1/(N - V)] \cdot \Sigma\, W_k \left(pH_k^b - pH_k^e\right)^2$$

where k is the No. of the experimental point; N, the number of points; V, the number of unknown constants (indices b and e meaning the value calculated using estimated constant and the experimental one, respectively); W_k, the statistical weight of k-th measurement (the estimated error ΔpH=0.1). At each iterative step, the correction lg K_n to approximate lg K_n estimations was determined using Gauss-Newton method [14,15]. The iterative process was continued until the lg K_n values were converged, and the information was

Table 1. Results of independent determination of the fixed groups concentration on various CMM

Silica	Method of determination							
	Elemental analysis							pH-potentiometry
	C		H		N		P	
	%	C_L, mmol/g	%	C_L, mmol/g	%	C_L, mmol/g	C_L, mmol/g	C_L, mmol/g
ADPA-Silochrom	1.53	0.255	0.34	0.28	0.3	0.214	0.25	0.28
EnDPA-Aerosil	4.74	0.56	0.87	0.49	1.45	0.517	0.5	0.6

obtained about their co-variation matrix, equilibrium compositions for all points, and $(pH_K)^B$ values. The algorithm is realised in the form of a computer program.

Synthesis of the chemically modified silicas

Synthesis of the silica with surface fixed amino-di(methylene phosphonic) acid was performed similarly to the procedure described in [16] according to scheme

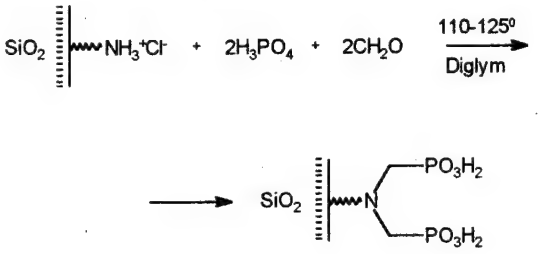

20 g of aminopropyl silochrom with $2 \cdot 10^{-4}$ mol/g (C_L) concentration of bonded aminogroups were placed into a reaction vessel with diglym and, under mechanic mixing, a hydrogen chloride flow was allowed to pass. Then, under continuous mixing and heating (110 °C), the solution of 0.98 g H_3PO_4 in diglym was added to the protonated sorbent, and, additionally, 0.51 g of ^{13}C enriched formaldehyd in diglym was added dropwise during 1 h.After cooling, the precipitate was washed with dioxan in a Soxhlet apparatus, then with water, and dried in air at 110 °C.

The synthesis of the ethylenediamine-N',N'-di(methylene phosphonic) acid bonded to the silica surface was performed similar to the above-described one; 6.3 g of protonated ethylene diamino propyl aerosil (C_L=$5 \cdot 10^{-4}$ mol/g) were used and 0.93 g of H_3PO_4, 0.34 g of CH_2O were added.

To the prompt control of the completeness of the silica modification, the presence of residual amino groups was monitored by means of ninhydrine.

Results and discussion

The fact of organophosphorus ligand immobilizing to the silica surface is confirmed by elemental analysis data, NMR and IR spectroscopy.

Table 1 shows the results of CMM elemental analysis and values of the bonded groups concentration calculated both from pH-metric titration and chemical analysis. The good agreement of the data obtained provides the evidence of the completeness of modification reactions.

Only narrow parts of IR spectra can be successfully used for silica sorbents characterization due to strong matrix effect (Fig.1). An intensive absorption of the Si—O bond stretching vibration in the 950-1200 cm^{-1} range gives no chance to observe the vibration bands ν_{as}(PO) of phosphonic groups falling in the 918-1190 cm^{-1} range. In the spectrum of ADPA-SiO_2, an intense band near to 1516 cm^{-1}, characteristic for protonated amino group, disappears; instead, other band arises in the range of 1698 cm^{-1}. For ADPA-SiO_2 vacuum-treated at 110 °C over P_2O_5, in the region of stretching vibrations, the band at 3689 cm^{-1} related to the absorption of hydroxyls contained in phosphonic groups, and other band near to 3350 cm^{-1} are observed. The broadening of this latter being indicative for the zwitter-ionic form of immobilized ligand.

NMR spectra of ADPA-SiO_2 are in general relatively insensitive to the excitation methods. Poor resolution is feature for the spectra of ^{13}C nuclei, in static and with "magic angle" speening. This fact can be explained whether by unhomogeneous micro-environment of several fixed groups, or by the absence of the grafted groups

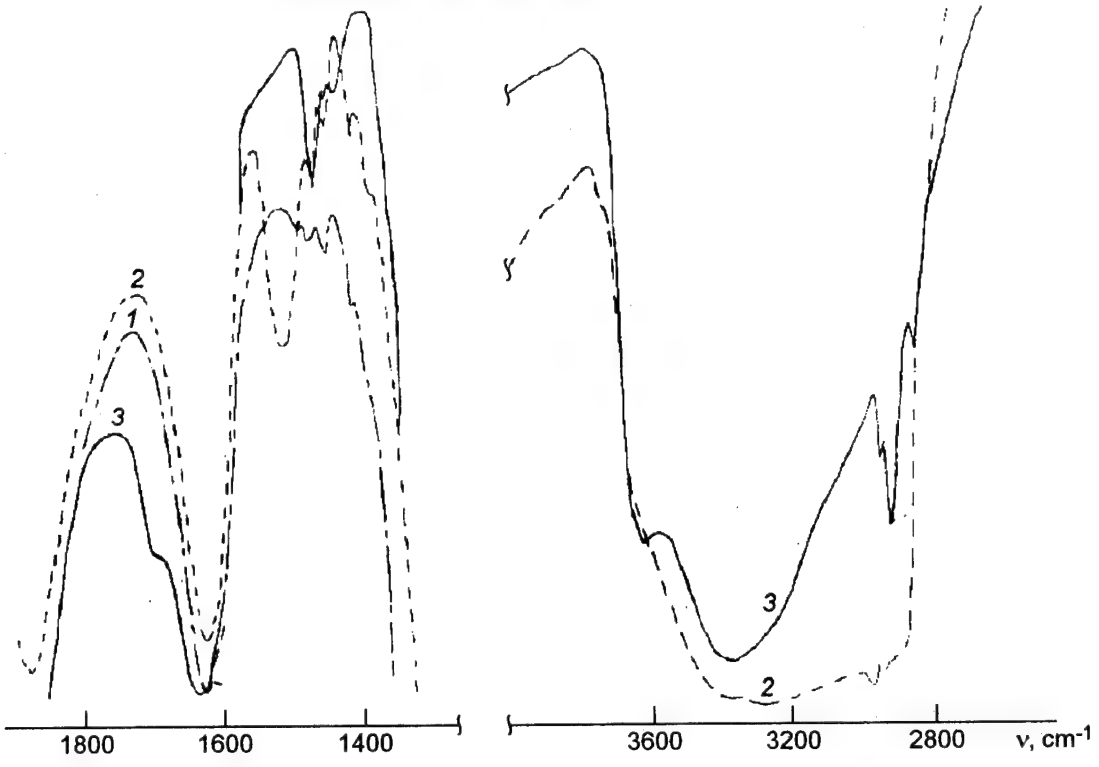

Fig.1. IR spectra of SiO_2-NH_2 (1), $SiO_2NH_3^+Cl^-$ (2), and ADPA-SiO_2 (3).

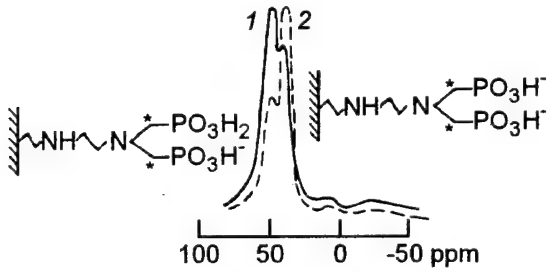

Fig.2. NMR spectra on ^{13}C nuclei of monopotassium (1) and dipotassium (2) salts of ADPA-SiO_2.

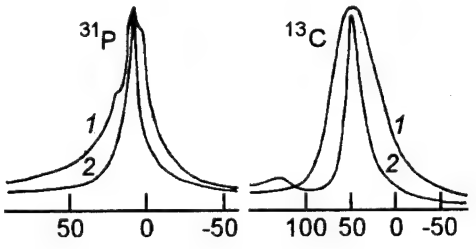

Fig.3. NMR spectra on ^{31}P (a) and ^{13}C nuclei (b) recorded at rotation at "magic angle" for air-dried samples (1) and without rotation for wetted ones (2).

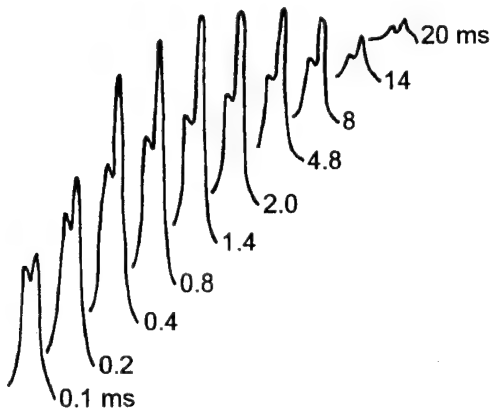

Fig.4. NMR spectra on ^{13}C for various resonance excitation times (from 0.1 to 20 ms).

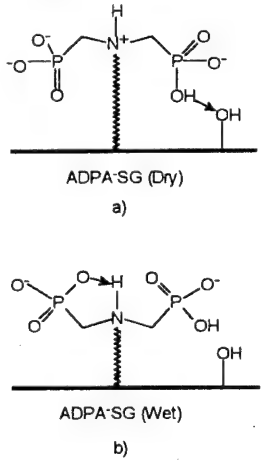

Fig.5. ADPA-SiO_2 structure as depended on the treatment conditions: air-dried (a) and wetted (b).

rotation on the SiO_2 surface. The static spectrum of ADPA-SiO_2 remained unchanged between room temperature and 180 K, indicating that the line width in the "magic angle" speening spectrum results from a range of isotropic chemical shifts, and not from bonded groups motion.

The ^{13}C spectrum has two (instead of one being expected) lines for the equivalent carbon atoms of the aminomethyl phosphonic acid methylene link, namely, at 44 and 53 ppm; the intensity ratio of these bands being changed when passing from mono-potassium salt to the di-potassium one (Fig.2). This allowed to assign the observed bands to the absorption of —$CH_2PO_3H^-$ and —$CH_2PO_3H_2$ groups, respectively.

NMR spectra on ^{31}P nuclei show also the presence of several chemical forms of the bonded amino-di(methylene phosphonic) acid. In a broad multiplet having maximum at 10 m.p., three components can be distinguished corresponding to the grafted groups having different ionization (Fig.3). To clarify the nature of this signal splitting, spectra of ^{13}C were taken for a range of contact times. It can be seen from the spectra (Fig.4) that the two peaks differ quite markedly in their behaviour, reflecting differences in their environment relative to the nearest protons. This fact confirms the assignation of 44 and 53 ppm bands to methylenic carbons of distinct branches of the amino-di(methylene phosphonic) acid; the distinctions observed effect the various chemical environments as well as various mobility features of the fragments of grafted groups (Fig.5). The splitting in NMR spectra of the bonded groups and a significant signal broadening allow make the suggestion about the strong hydrogen bonds between the grafted molecule and silica surface, what, on the one side, prevents the free rotation of grafted groups and, on the other, causes their differentiation. This conclusion is confirmed by a sharp narrowing of ^{13}C NMR signals in static spectra of bonded aminophosfonic acids for the wetted samples (Fig.3) since the hydratation of silica surface results in the breaking of intermolecular bonds and is favourable to the grafted molecules free rotation (Fig.5,b). The ^{31}P static spectra for hydrated ADPA- and EnDPA-SiO_2 was found to be very narrow, with line shapes indicating motion nearly in the fast limit at room temperature.

The analog of ligands fixed to the surface of ADPA-SiO_2 and EnDPA-SiO_2, is N-ethyl imino di(methylene phosphonic) acid which exists in the solid state in form of a zwitter-ion, and in solution in the following forms [17]:

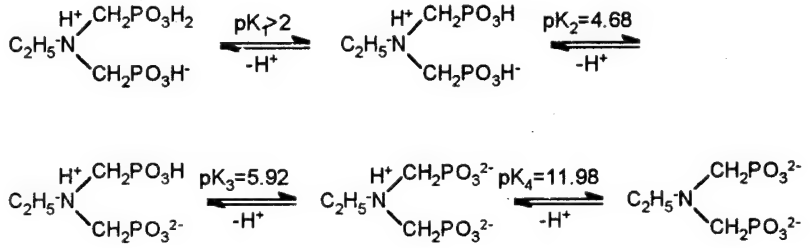

The calculation of protonization constants for the fixed ligands was performed assuming that acid-base equilibrium on the surface can be described by the same constants set. We failed to calculate pK_1 values. The second acidic dissociation constant is near to that for the homogeneous analog (4.53±0.22 for ADPA-Silochrom and 5.88±0.15 for EnDPA-Aerosil). The third stage of dissociation occurs significantly weaker for fixed ligands then for similar ligands in solution (8.39±0.2 and 8.56±0.2 for ADPA-Silochrom and EnDPA-Aerosil, respectively). The pK_H^4 value cannot be calculated, since the range of existence, for that form, falls within the basic medium where a sensible dissolution of the silica matrix is observed.

At the contact of metal salts with bulk silicas, no substantial physical adsorption of metal ions is observed (it can be at least stated with assurance that metal adsorption value is within the range of titration error [18]). Therefore, the adsorption observed at the contact of metal salts with ADPA-Silochrom and EnDPA-Aerosil must be assigned mainly to the complexes formation between the surface-fixed complexing agents and metal cations of the solution. On Fig.6 and 7, the experimental data are shown characterizing the adsorption features for some metall ions as depending on the solution acidity. It follows from the potentiometric titration curves presented on Fig.6 that ADPA-Silochrom possess a high affinity to La^{3+} and Eu^{3+} ions. Thus, at pH=4.0, the shift of the ADPA-Silochrom titration curve by 1 mol of H^+ is observed in the presence of equimolar amount of La^{3+} ions as compared to the similar curve obtained in the absence of the metal. Since free protons can arise in solution only from the reaction

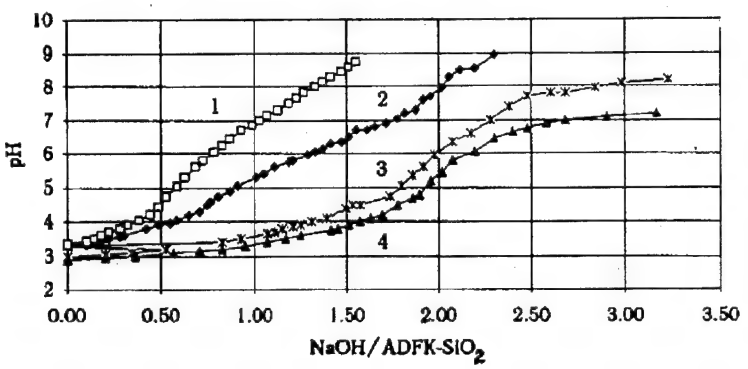

Fig.6. Potentiometric titration curves for ADPA-SiO_2 (1) and for the same in the presence of cations Sr^{2+} (2), La^{3+} (3), and Eu^{3+} (4).

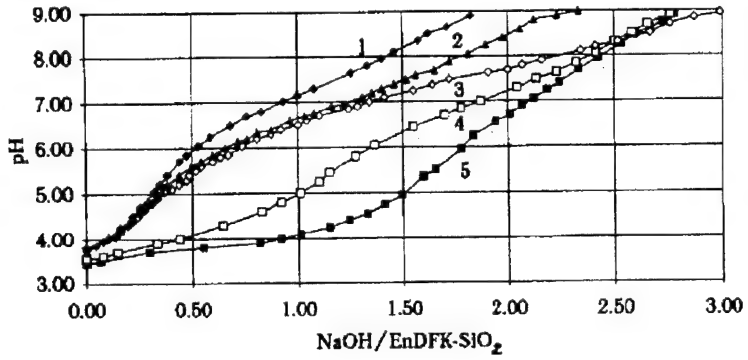

Fig.7. Potentiometric titration curves for EnDPA-SiO_2 (1) and for the same in the presence of cations Sr^{2+} (2), Ca^{2+} (3), Cu^{2+} (4), and La^{3+} (5).

Table 2. Equilibrium constants logarithms for the complexing reactions involving EnDPA-Aerosil.

Ions	lgK_2	lgK_1	lgK_3	lgK_4	S_0^2
Ca^{2+}	2.42±0.16	3.41±0.24	-8.08±0.3	-9.9±1.0	2.0
Sr^{2+}	2.47±0.21	3.38±0.23	-9.38±0.4	-	3.1
Cd^{2+}	2.71±0.17	3.72±0.9	-6.3±0.18	-8.13±0.2	0.7
Cu^{2+}	-	8.71±0.3	-4.99±0.4	-7.0±0.3	1.4
La^{3+}	-	8.68±0.21	-6.8±0.12	-9.34±0.3	1.1

Table 3. Equilibrium constants logarithms for the complexing reactions involving ADPA-Silochrom.

lgK	Metal ions							
	Ca^{2+}	Sr^{2+}	Ni^{2+}	Pb^{2+}	Cu^{2+}	La^{3+}	Dy^{3+}	Eu^{3+}
lgK_2	2.85±0.17	2.84±0.1	4.46±0.14	4.41±0.16	3.14±0.3	4.83±0.3	4.41±0.5	4.45±0.5
lgK_1	5.75±0.16	4.87±0.09	7.51±0.13	8.95±0.4	8.5±0.4	8.87±0.4	8.76±0.38	9.05±0.4
lgK_3	-8.69±0.1	-9.32±0.12	-6.62±0.05	-5.45±0.14	-5.21±0.27	-7.58±0.15	K_3 and K_4 inversion	-7.0±0.17
lgK_4	-	-	-9.42±0.14	-7.4±0.12	-8.1±0.2	-8.58±0.36	-	-7.1±0.21
S_0^2	1.3	1.0	0.3	1.2	1.8	2.0	1.3	1.25

$$H_3L^- + La^{3+} \rightarrow H_2LaL^+ + H^+$$

it may be concluded that the lanthanum and europium ions are nearly completely adsorbed on the modified silicagel surface at pH=4.0, and equimolar complexes being formed. When the medium acidity increases, titration curves remain parallel to each other, i.e. complexes of different composition do not form up to pH=8.0. The Ca^{2+} ions affinity is lower comparising to that of La^{3+}, both for ADPA-SiO_2 and EnDPA-SiO_2. That fact is indicated by a poor shift of the titration curve in the presence of Ca^{2+} in comparison with free acid titration, especially, for EnDPA-SiO_2. The last-mentioned adsorbent also shows considerable affinity to copper ions. These ions are adsorbed from solution by the EnDPA-SiO_2 at pH>5.0, where the most essential shift is observed between the titration curves recorded with and without copper ions (Fig.7).

The heterogeneous equilibrium constant were calculated assuming that the metal ions interact with fixed ligands according to scheme

$$M^{2+} + H_2L^{2-} = MH_2L \quad lgK_1$$
$$M^{2+} + H_3L^{2-} = MH_3L^+ \quad lgK_2$$
$$MH_2L = MHL^- + H^+ \quad lgK_3$$
$$MHL^- = ML^{2-} + H^+ \quad lgK_4$$

The calculated constants values are given in Tables 2 and 3. These data show that the stability of surface fixed complexes is higher then that for similar homogeneous ones. For the functionalised silicas studied, the metal complexes stability decrease through the series:

ADPA-SiO_2: Eu≈Dy≈La≈Pb>Cu>Ni>Ca>Sr

EnDPA-SiO_2: La≈Cu>Cd>Ca>Sr

As would be expected, the phosphorus-containing modified sorbents have the maximum affinity to lanthanum. The EnDPA-SiO_2 forms strong complexes with *d*-metals, too.

References

1. E.L.Styskin, L.B.Itsikson, E.V.Braude, Practical High-Performance Liquid Chromatography [in Russian], Khimia, Moscow (1986).
2. Yu.I.Ermakov, V.A.Zakharov, B.N.Kuznetsov, Fixed Complexes on Oxide Supports [in Russion], Nauka, Novosibirsk (1980).
3. Immobilized Cells and Enzymes: Practical Approach, by J.Woodward, IRL Press, Oxford, Washington DC (1985).
4. T.V.Lisichkin, T.V.Kudryavtsev, A.A.Serdan, S.M.Staroverov, Modified Silicas in Sorption, Catalysis, and Chromatography [in Russian], Khimiya, Moscow (1986).
5. I.E.Neimark, Synthetic Mineral Adsorbents and Catalyst Supports [in Russian], Naukova Dumka, Kiev (1986).
6. J.Chmielowiec, B.A.Morrow, *J.Colloid and Interface Science*, **94**, 319 (1986).
7. L.A.Belyakova, I.N.Polonskaya, V.A.Tertykh, *R.Zh.Kh.*, **24**, 9-16 (1986).
8. B.B.Wheals, *J.Chromatography*, **177**, 263 (1979).
9. G.V.Kudryavtsev, S.Z.Bernadyuk, G.V.Lisichkin, *Usp.Khimii*, **18**, 684 (1989).
10. USSR Pat. 1613129.
11. N.M.Dytlova, V.Ya.Temkina, K.I.Popov, Complexones and Metal Complexonates, Khimia, Moscow (1988).
12. L.Mazor, Organic Analysis Methods, Mir, Moscow (1986), p.556 [cited by Russian Ed.].
13. V.V.Skopenko, V.N.Zaitsev, Yu.V.Kholin, A.A.Bugayevsky, *Zhurn.Neorg.Khim.*, **32**, 1626 (1987).
14. G.Forsyte, M.Malcolm, K.Moler, Computer Methods of Mathematical Calculations, Prentice Hall, Inc. (1977).
15. A.A.Bugayevsky, Yu.V.Kholin, *Radiokhimia*, **5**, 594 (1985).
16. K.Moedridzer, R.R.Irani, *J.Org.Chem.*, **31**, 1603 (1966).
17. R.P.Carter, R.L.Carrol, R.R.Irani, *Inorg.Chem.*, **6**, 939 (1967).
18. A.K.Trofimchuk, L.V.Glushchenko, *Ukr.Khim.Zhurn.*, **43**, 991 (1978).

Кремнеземы,химически модифицированные амино-ди(метиленфосфоновой) и этилендиамин-ди(метиленфосфоновой) кислотами

В.Н.Зайцев, Л.С.Василик, Дж.Эванс, А.Брод

Описан синтези охарактеризованы два представителя нового класса химически модифицированных кремнеземов, содержащих на поверхности фосфорорганические комплексоны: N-пропиламино-ди(метиленфосфоновую) и N-этилендиамин-N',N'-ди(метиленфосфоновую) кислоты. Новые вещества охарактеризованы данными элементного анализа, ИК-спектрометрии с Фурье преобразованием и спектроскопии ЯМР высокого разрешения в твердом теле на ядрах ^{31}P и ^{13}C. Изучены протолитические и комплексообразующие свойства указанных соединений с рядом *s*-, *f*- и *d*-металлов. Обнаружена высокая селективность взаимодействия закрепленных кислот с ионами Ca^{2+}, La^{3+}.

Functional Materials 2, No.1 (1995)

Chemisorption of dithiooxamide on silica surface

I.N.Polonskaya and L.A.Belyakova

Institute of Surface Chemistry, National Academy of Sciences of Ukraine,
31 Nauki Ave., 252022 Kiev, Ukraine

Organosilica sorbent with grafted dithiooxamide groups was obtained as the result of a two-stage chemical modification of the SiO_2 surface. Mechanism of surface chemical reaction and concentration of grafted thiooxamide groups were determined by means of IR-spectroscopy and differential thermographic technique. The possibility of the synthesized organosilica application for selective extraction of cobalt, copper, silver and palladium cations from aqueous solutions was tried and found to be effective.

Внаслідок двостадійної хімічної реакції модифікування поверхні аморфного кремнезему одержано органокремнеземний сорбент з закріпленими дитіооксамідними групами. За допомогою методів ІЧ-спектроскопії та дериватографії досліджено механізм реакції і встановлено концентрації прищеплених органічних лігандів. Показана можливість застосування одержаного сорбенту для селективного вилучення кобальту, міді, срібла та паладію з розведених водних розчинів.

Dispersed silicon dioxides with nitrogen- and sulphur-containing organic ligands chemically bonded onto their surface possess a special place among the wide group of modified supported silicas due to strong complex formation properties of grafted ligands. The application areas of such organosilicas are concentration, separation, extraction and analytical determination of metal ions in different organic and inorganic solutions including very dilute ones.

In the present work, the chemisorption of dithiooxamide (reagent that forms stable chelate complexes with some transition and heavy metals in solutions) on silica was studied.

It is known [1] that dithiooxamide is able to form N,N'-dialkyl-derivatives while treated with primary amines in a solutions. So the preparation of organosilica with grafted aminopropyl groups was the first stage of chemical modification process. For this purpose, the silica surface was modified with γ-aminopropyltriethoxysilane [2]. The second stage of immobilization process consisted in treatment of the obtained aminopropylsilica with dithiooxamide in aceton solution.

Surface chemical reactions proceeding was controlled by means of IR-spectroscopy (Fig.1). In the IR-spectrum of aminopropylsilica the stretching vibration bands at 3300 cm^{-1} and 3375 cm^{-1}, and the bending vibration one at 1580 cm^{-1} of primary amines N–H bond are observed. But in the IR-spectrum of dithiooxamide treated silica these absorption bands are absent.

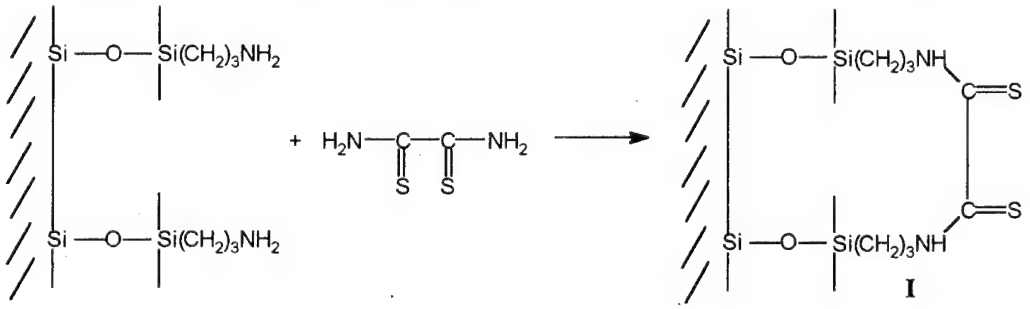

I

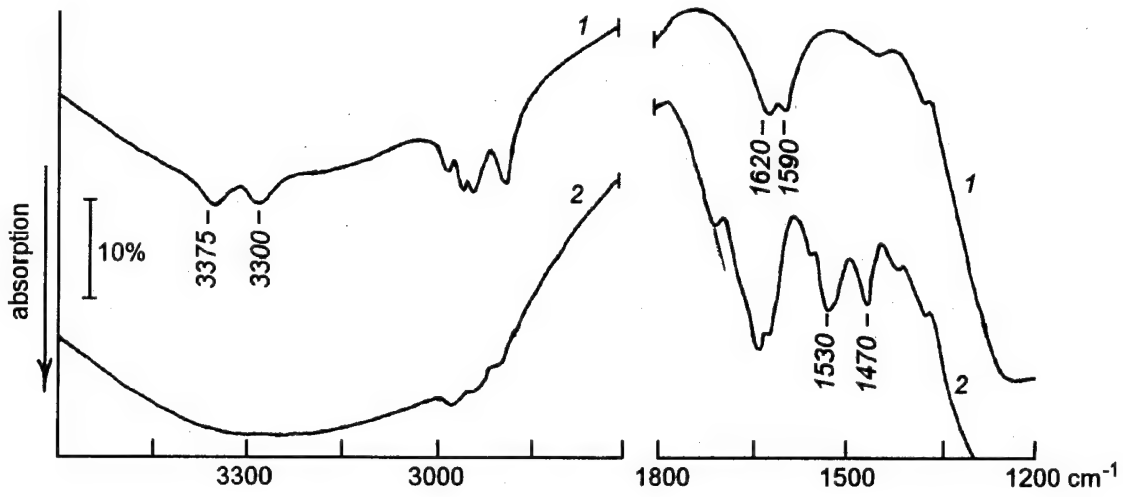

Fig.1. IR-spectrums of aminopropylsilica (1), dithiooxamide supported silica (2).

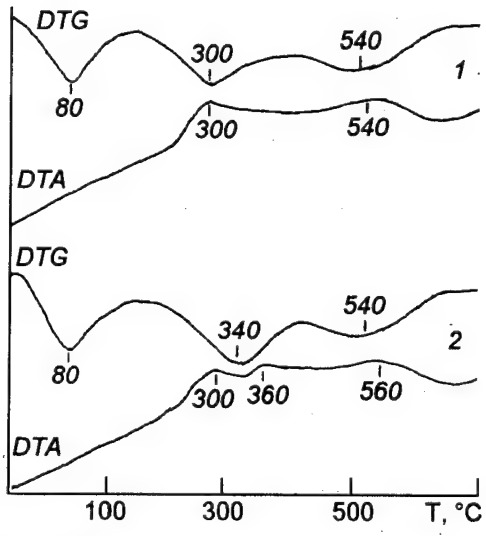

Fig.2. DTG and DTA curves of aminopropylsilica (1) and dithiooxamide supported silica (2).

At the same time, the absorption band at 1530 cm^{-1} of N–H bond of –NH–C–S group and the adsorption band of C–S bond with maximum at 1470 cm^{-1} appear in spectra of these samples [3]. These facts prove the performance of chemical immobilization of dithiooxamide on aminopropylsilica surface.

Additional evidences of immobilization are seen from data of the differential thermographic analysis (DTA) (Fig.2). The interpretation of the DTA curves are as follows: heating to 200 °C promotes desorption of physically adsorbed water molecules, then in the range from 220 to 320 °C the residual ethoxy groups decomposed, this process is followed by an exothermic effect with a maximum close to 360 °C which is related to the destruction of sulphur-containing groups. Aminopropyl groups are removed from the silica surface at temperatures above 480 °C. The concentration of grafted groups was calculated from the curves of mass loss. These results give evidence for a chemical interaction between one dithiooxamide molecule and two grafted aminopropyl groups (Table 1). So the cyclic structure is formed on the silica surface.

Table 1. Concentration of grafted organic groups

Grafted organic layer	NH_2-group aminopropylsilica (mmol/g)	Dithiooxamide-group (mmol/g)
I	0.20	0.08
	0.26	0.10
	0.46	0.24

In order to investigate sorptional ability of dithioxamide-containing organosilica, the uptake of copper, nickel, cobalt, silver, and palladium ions from aqueous solutions was studied.

The values of static sorptional capacities calculated for the case of maximum saturation are presented in Table 2 and found to be high. The affinity to metals studied is also proved to be rather high as the values of the distribution coefficients show calculated for the case of cations extraction from very dilute solutions (Table 2).

The intensive colours (Table 2) that dithiooxamide treated silica samples get just after the contact with metal salts solutions reveal that cations

Table 2. Sorptional properties of dithiooxamide treated silica

Concentration of grafted ligands (mmol/g)	Cation sorption capacities (mmol/g)				
	Co(II)	Cu(II)	Ni(II)	Ag(II)	Pd(II)
0.08	0.08	0.08	0.03	0.08	-
0.10	0.09	0.10	0.04	0.13	0.07
0.24	0.09	0.23	0.07	0.24	-
Distribution coefficients	915	1000	432	2300	1800
Colour of metal-saturated sorbent	dark-green	green	red	orang.	red

extraction from the solutions is due to the metal complex formation with grafted ligands. This is confirmed by the IR-spectral investigation of metal saturated dithiooxamide-containing organosilica (Fig.3). For example, the absorption band related to the vibration of the C=S bond with maximum at 1470 cm^{-1} is not observed in the IR-spectrum of Co^{2+}-containing sample at all. In the IR-spectr of samples saturated with copper, silver, and palladium ions, the intensivity of this band is much less than in the IR-spectrum of initial dithiooxamide containing silica. The observed splitting of the band in IR-spectra of metal-containing samples related to the bending vibration of N–H bond in –NH–C–S group with maximum at 1530 cm^{-1} on two bands in the range of 1510—1550 cm^{-1} is caused both by metal interaction with nitrogen atom and by increase of C–N bond multiplicity [3]. This fact proves the interaction between metal cations and the bonded groups.

Conclusion

A rather simple and effective method has been created for preparation of chemically stable organosilica sorbents with high concentration of grafted dithiooxamide ligands. The comparison of IR-spectroscopy data and the results of the DTA analysis of organosilicas made it possible to determine the concentration of grafted functional groups and the structure of surface organic layer. The high level of sorption capacities and observed

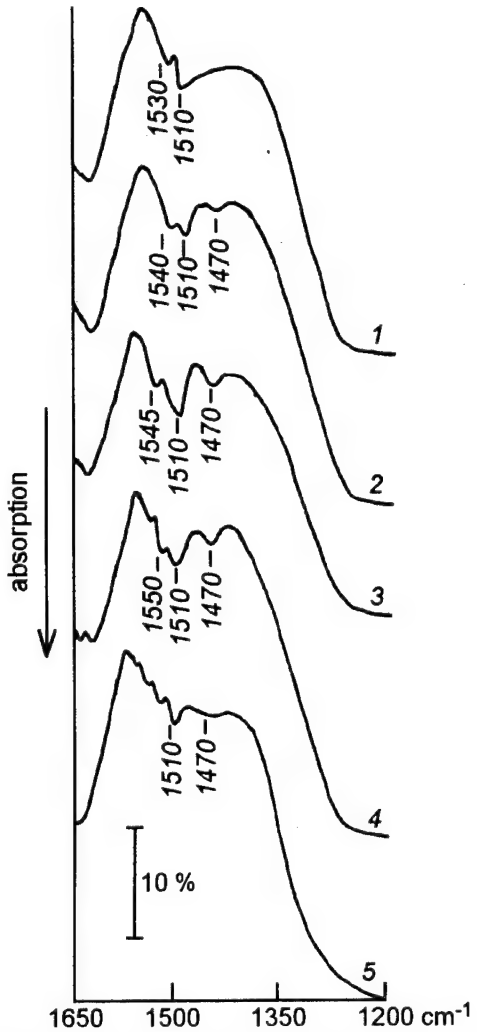

Fig.3. IR-spectrums of dithiooxamide treated silica saturated with Co^{2+} (1), Cu^{2+} (2), Ni^{2+} (3), Ag^{2+} (4), Pd^{2+} (5).

differences in distribution coefficients of metal cations indicate the prospectivity of dithiooxamide-containing silica sorbent utilization for metal cations extraction, separation and analytical determination.

References

1. I.O.Sozerland, in: Comprehensive Organic Chemistry [in Russian], Khimia, Moscow (1983) vol.5.
2. V.A.Tertykh, L.A.Belyakova, Chemical reactions with silica surface participation [in Russian], Naukova Dumka, Kiev (1991).
3. L.J.Bellami, The Infrared Spectra of Complex Molecules, Methuem & Co. Ltd., London (1957).

Хемосорбция дитиооксамида на поверхности кремнезема

И.Н.Полонская, Л.А.Белякова

В результате двухстадийной реакции химического модифицирования поверхности аморфного кремнезема получен органокремнеземный сорбент с привитыми дитиооксамидными группами. С помощью методов ИК-спектроскопии и дериватографии исследован механизм реакции и определены концентрации привитых органических лигандов. Показана возможность применения полученного сорбента для селективного извлечения кобальта, меди, серебра и палладия из разбавленных водных растворов.

Functional Materials **2**, No.1 (1995)

Thermodynamic and kinetic study on protolytic and complex formation reactions at the surface of porous matrices

B.V.Zhmud, A.B.Pecheniy* and A.A.Golub*

Institute for Physical Chemistry, Friedrich Schiller University,
Lessingstraße 10, D-07743 Jena, Germany

*T. Shevchenko Kiev University, 60 Vladimirskay St., 252017 Kiev, Ukraine

Basing on the formal thermodynamics, we have derived a generalized law of mass action which can be applied to describe protolytic and ionic reactions at the surface of rigid matrices in contact with electrolytes solutions. Using this law, we have made an attempt at theoretical reanalyzing and systematizing of influence of various factors, such as porous structure, fractality, and mechanism of surface charge formation, on the protolytic properties of porous silica gels modified with organic ligands. In the framework of a semi-infinite diffusion model, we have investigated the kinetics of chemisorption of hydrochloric acid and a number of sulpho-substituted phthalocyanine complexes of cobalt (II) onto such silica gels.

З використанням апарату формальної термодинаміки виведено узагальнений закон діючих мас, котрий може бути використаний для опису протолітичних та іонних реакцій на поверхні твердих матриць в контакті з розчинами електролітів. На основі цього закону зроблено спробу теоретичного переосмислення та систематизації впливу різноманітних факторів, таких як пориста структура, фрактальність та механізм формування поверхневого заряду, на протолітичні властивості пористих силікагелей, модифікованих органічними лігандами. В рамках моделі напівнескінченної дифузії досліджено кінетику хемосрбції соляної кислоти та ряду сульфозаміщених фталоціанінових комплексів Co(II) на цих матрицях.

Introduction

Protolytic and complex formation reactions when proceeding at the surface of rigid matrices, reveal some new features as compared to the same reactions in solutions, among which we should mention (i) the simultaneous formation of many sorts of interfacial compounds, (ii) the dependence of the stability of these compounds on the degree of reaction completeness, as well as on the topology of the supporting surface, and (iii) the excess free electrostatic energy as a result of the electrostatic interactions. All these factors can be accounted for in the framework of a generalized equilibrium constant concept. In this communication, we have restricted ourselves to application of this concept to the protolytic equilibria involving ligands immobilized at the silica gel surface. However, most of the results obtained here remains valid in a more general case of complex formation reactions.

Thermodynamic study

The main thermodynamic relation

As far as modified silica gels are usually considered as rigid matrices, we will think of chemical equilibria involving their surface as equilibria between a two-dimensional surface phase - as it was understood by van der Waals (jr.) and Bakker [1] - and a bulk solution phase. Then, the equilibria must obey the following generalized law of mass action [2]:

$$K_j^{ef} = \prod_i x_i^{\nu_{ij}} = K_j^0 \exp[-(kT)^{-1} \sum_i \nu_{ij} (\partial\gamma/\partial\{i\}] \qquad (1)$$

where x_i is the mole fraction , $\{i\}$ the superfacial concentration of the i-th component involved in

the j-th reaction with the stoichiometric coefficient ν_{ij}; K_j^0 is the intrinsic equilibrium constant of that reaction, whereas K_j^{ef} is usually termed as its apparent or effective equilibrium constant; and γ is the surface tension. We can point out a lot of factors which contribute to γ, yet there is little doubt that, for sorbents in contact with electrolytic solutions, the main contribution to γ is made by electrostatic interactions. Therefore, we can assume that $\gamma \cong F_e$, the latter being the electrostatic contribution to the surface tension.

Calculation of F_e

Let us consider a porous sorbent in contact with an electrolytic solution. As usually, it is suggested that pores are infinitely long and of cylindrical symmetry. Introduce the dimensionless potential, $u = e\psi/kT$, and radius $\rho = \chi r$, $0 \le r \le R$, χ being inverse Debye's length and R the radius of pores. The free electrostatic energy per unit surface area of such a cylindrical pore can be expressed through the potential by means of Derjaguin's formula [3]

$$F_e(\sigma_\lambda) = \frac{\chi\varepsilon_0\varepsilon(kT)^2}{2\pi\lambda e^2}\int_{\rho=0}^{\rho=\lambda}\left[u^2(\sigma_\lambda,\rho) + (u')^2(\sigma_\lambda,\rho)\right]\rho d\rho$$

$$u(\sigma_\lambda,\rho) = \alpha_\lambda I_0(\rho);\ \alpha_\lambda = \frac{e\sigma_\lambda}{kT\varepsilon_0\varepsilon\chi I_1(\lambda)};\ (u' = d/d\rho) \qquad (2)$$

where the upper limit of integration is $\lambda = \chi R$, σ_λ is the charge density at the pore surface, ε is the dielectric constant of the solution, ε_0 is the permittivity of vacuum, e is the proton charge, and $I_n (n = 0;1)$ are Bessel's functions. Integration yields

$$F_0(\sigma_\lambda) = \frac{\sigma_\lambda I_0(\lambda)}{2\varepsilon_0\varepsilon\chi I_1(\lambda)} = \frac{kT\sigma_\lambda u(\sigma_\lambda)}{2e} \qquad (3)$$

Let $\Lambda(\lambda)$ be the pore size distribution for the sorbent in question, and let us choose it to meet the conditions

$$\Lambda(0) = \Lambda(\infty) = 0 \quad \text{and}$$

$$\int_0^\infty \Lambda(\lambda)d\lambda = \chi^3 V_{tot} \qquad (4)$$

where V_{tot} is the total volume of all pores per unit mass of the sorbent. Consequently, $\Lambda(\lambda)/\lambda$ is the corresponding distribution of the surface area, herewith

$$\int_0^\infty \Lambda(\lambda)d\lambda = \chi^2 S_{sp}/2 \qquad (5)$$

S_{sp} being the specific surface area. The combination as follows:

$$F_e(\sigma_\lambda)\,\Lambda(\lambda)/\lambda \qquad (6)$$

will, therefore, represent the distribution of the free electrostatic energy over the sorbent surface.

The mechanism of charge formation

The above thoughts would be of little interest if the surface charge density were assumed to be a constant independent of the pores size [2,4]. Yet this is not the case. The surface charge is known to take rise from equilibrium processes of adsorption of ions and dissociation of surface ionizable groups [5]. In that case, in particular when there is no specific adsorption, it is called forth by protolytic reactions [6], such as

$$\mathrm{AH} \overset{K_1^{ef}}{\leftrightarrows} \mathrm{A^-} + \mathrm{H^+}$$

$$\mathrm{B} + \mathrm{H^+} \overset{K_2^{ef}}{\leftrightarrows} \mathrm{BH^+} \qquad (7)$$

where AH is some acidic group and B is some basic group, herewith being possible that B = AH and then $\mathrm{BH^+} = \mathrm{AH_2^+}$. Thus,

$$\sigma_\lambda = eN_a\left(\{\mathrm{BH^+}\}_\lambda - \{\mathrm{A^-}\}_\lambda\right) = eN_A\sum_i z_i\{i\}_\lambda \qquad (8)$$

where ez_i is the charge of the i-th species, and N_A is Avogadro's number. By subsequent substitution of Eq.(8) into Eq.(3), and what results, into Eq.(1), we come to a well-known form of the law of mass action [2,7,8],

$$K_j^{ef}(\sigma_\lambda) = \prod_i x_i^{\nu_{ij}} = K_j^0 \exp[-\sum_i \nu_{ij} z_i u(\sigma_\lambda)] \qquad (9)$$

From Eq.(14), one can draw the conslusion that the equilibrium state of a given ionic process proceeding at the surface of pores of different radius is characterized by different local equilibrium constants. Experimentally, we can only determine the average of the local constants over the sorbent surface [2],

$$<\ln K_j^{ef}(\sigma_\lambda)> =$$

$$= 2\left(\chi^2 S_{sp}\right)^{-1}\int_0^\infty \lambda^{-1}\Lambda(\lambda)\ln K_j^{ef}(\sigma_\lambda)d\lambda \qquad (10)$$

Suppose now that total surface concentrations of acidic and basic groups amount correspondingly to C_A^{tot} and C_B^{tot}, not depending on the pores size and not changing in the course of reactions. Then the concentrations of the charged species, $\mathrm{A^-}$ and $\mathrm{BH^+}$, are

$$\left\{A^-\right\}_\lambda = \frac{ab(\sigma_\lambda)K_1^0 C_A^{tot}}{\left[H^+\right] + ab(\sigma_\lambda)K_1^0}$$

$$\left\{BH^+\right\}_\lambda = \frac{K_2^0\left[H^+\right]C_B^{tot}}{ab(\sigma_\lambda) + K_2^0\left[H^+\right]} \qquad (11)$$

$a \approx 55.56$ mol·l^{-1} and $b(\sigma_\lambda) = \exp u(\sigma_\lambda)$

Substitution of Eq.(11) into Eq.(8) yields a transcendental equation, whose solution makes it possible to see that σ_λ does really depend on λ. In particular, we come to the conclusion that $\sigma_\lambda \sim \lambda$ as $\lambda \to 0$, and therefore

$$\lim_{\lambda\to 0}\left\{A^-\right\}_\lambda = \lim_{\lambda\to 0}\left\{BH^+\right\}_\lambda = \left\{A^-\right\}_{pzc} = \left\{BH^+\right\}_{pzc} \qquad (12)$$

so that the equilibrium concentrations of charged species become independent of the real pH and approximate to each other as if pH were going to the pH_{pzc}. Yet, this situation is quite different from that in the *pzc*, for the potential $u(\sigma\lambda)$ takes now on a finite value, $u_{\lambda\to 0} \neq 0$, which thereto appears to be independent of λ, whereas at pH_{pzc}

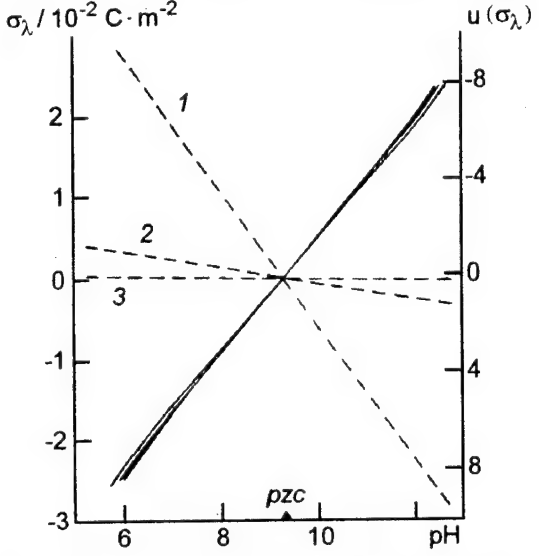

Fig.1. Surface chaarge density, σ_λ (broken lines), and surface potential, $u(\sigma_\lambda)$ (solid lines), versus *pH* for a hypothetical uni-pore-sized sorbent with $R = 50$ Å in contact with an electrolytic solution whose ionic strength equals (1) 10^{-2}, (2) 10^{-3}, and (3) 10^{-4} mol·dm^{-3}, respectively. A tenfold decrease in the ionic strength in the sequence (1) → (2) → (3) entails an 8.3-times' decrease in σ_λ, whereas $u(\sigma_\lambda)$ remains almost unchanged and increases only by 1.6 and 0.2%, respectively. In the calculations, we have used $K_1^0 = 3\cdot10^{-12}$; $K_2^0 = 4\cdot10^{10}$ [20]; and $C_A^{tot} = C_B^{tot} = 5\cdot10^{-6}$ mol·m^{-2}.

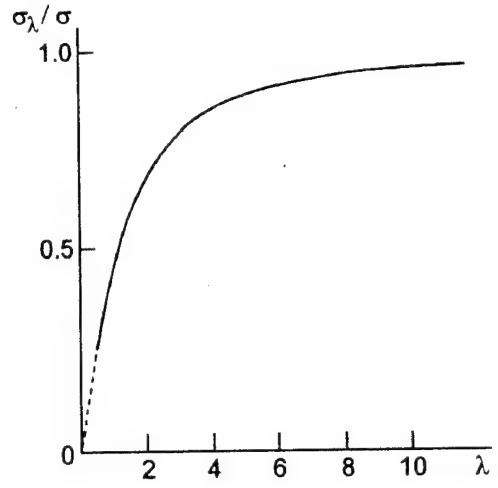

Fig.2. The distribution of σ_λ over λ (σ) has been determined in Eq.(26)).

this potential is equal to zero. It can be proven that when $\lambda \to 0$, the surface of porous sorbents tends to be of equal potential rather than of equal charge density. The influence of porosity becomes appreciable as soon as λ reaches unity and rises dramatically as λ becomes lower and lower. In Fig.1 and 2, we have pictured some results of our calculations for a hypothetical sorbent whose pores are all of the same size. These results help to realize how real and how pronounced the discussed effects are.

The conclusion that σ_λ falls down together with λ is of importance for studies of protolytic processes at the surface of the so-called fractal sorbents, some of which can be imagined as an infinite set of self-similar cylinders with a power-law-like pore-size distribution [9],

$$\Lambda(\lambda) \approx \lambda^{2-D}, \quad 2<D<3 \qquad (13)$$

The mean electrostatic contribution to the surface tension of such sorbents becomes negligible as $\lambda \to 0$:

$$< F_e(\sigma_\lambda) > = \frac{\int_0 F_e(\sigma_\lambda)\Lambda(\lambda)d\lambda/\lambda}{\int_0 \Lambda(\lambda)d\lambda/\lambda} \approx \lambda^{D-2} \to 0 \qquad (14)$$

Nevertheless, the average of the local equilibrium constants does not come to the corresponding intrinsic constant but takes on the value

$$< \ln K_j^{ef}(\sigma_\lambda) > = \ln K_j^0(\sigma_\lambda) - \sum_i \nu_{ij} z_i u_{\lambda\to 0} \qquad (15)$$

It should also be pointed out that, for fractal sorbents, the mean surface charge density, degree of protonation, degree of dissociation, etc., are all

equal to zero independent of pH. So, the chemistry of protolytic and ionic reactions at the surface of fractal sorbents would be of little interest if there were no mechanism for compensation of the surface charge arising from adsorption of ions or dissociation of surface ionizable groups. And it is association with counterions that provides such a mechanism.

Ion association

Consider, in addition to reactions (11), two other association reactions,

$$A^- + Me^+ \overset{K_3^{ef}}{\leftrightarrows} AMe$$

$$BH^+ + X^- \overset{K_4^{ef}}{\leftrightarrows} BHX \qquad (16)$$

where Me^+ is a cation, and X^-, an anion, of the background univalent electrolyte. Reasoning in the same manner as has led us to Eq.(11), we find that

$$\{AMe\}_{\lambda\to 0} = C_A^{tot} \text{ and } \{BHX\}_{\lambda\to 0} = 0 \text{ as } [H^+] \to 0,$$

and (17)

$$\{AMe\}_{\lambda\to 0} = 0 \text{ and } \{BHX\}_{\lambda\to 0} = C_B^{tot} \text{ as } [H^+] \to \infty$$

herewith $\{A^-\}_{\lambda\to 0} = \{BH^+\}_{\lambda\to 0}$ in both cases. Thus, the association with counterions makes possible, at least in principle, the quantitative participance of surface groups in protolytic transformations.

The influence of space dispersion of the dielectric constant

It is known that the dielectric constant of a solution in the neighbourhood of a surface is different from that of the bulk solution [10,11]. A change in the dielectric constant results inevitably results - according to the Born equation [12] - in a change of the dissociation ability of ionizable groups. It seems to be of concern to analyze how does this effect on the protolytic properties of porous sorbents.

The simplest and commonly applied way to take into account the space dispersion of the dielectric constant is to introduce into consideration a dense part of the electric double layer. That is, we are to put forward

$$\varepsilon(\rho) = \begin{cases} \varepsilon_1, & 0 < \rho < \lambda - \eta \\ \varepsilon_2, & \lambda - \eta < \rho < \lambda \end{cases} \quad (\varepsilon_1 > \varepsilon_2, \rho > \eta) \qquad (18)$$

where ε_1 and ε_2 are the dielectric constants of the bulk solution and of the dense part, respectively, and η is the thickness of the dense part. Herewith, we assume that the area $\lambda - \eta < \rho < \lambda$ is free of charges and that there is no specific adsorption on the interface $\rho = \lambda - \eta$. A solution the Debye-Hueckel equation for such a task [4,13] can be represented as

$$u(\lambda) = \frac{e\lambda\sigma_\lambda}{kT\varepsilon_0\chi}\left[\frac{I_0(\lambda-\eta)}{(\lambda-\eta)\varepsilon_1 I_1(\lambda-\eta)} - \frac{1}{\varepsilon_2}\ln\left(1-\frac{\eta}{\lambda}\right)\right] \qquad (19)$$

Now, the same situation as expressed in Eq.(12) occurs when $\lambda \to \eta$, yet the surface charge density falls down steeper, as $\sigma_\lambda \sim (\lambda - \eta)^{-2}$.

Another kind of dielectric constant dispersion takes rise from electrostatic saturation effect [11,14-16]. It is described by the Booth-Kirkwood formula [14],

$$\varepsilon(\rho) = \varepsilon_1[1 - \theta(\text{grad } u)^2](\rho) \qquad (20)$$

where $\theta = q(\chi kT/e)^2$, q being a parameter of the order magnitude 10^{-17} m^2V^{-2}, and u is the dispersion-disturbed potential. The Debye-Hueckel equation for u, in the case of cylindrical symmetry, takes on the form

$$\frac{1}{\rho}\frac{d}{d\rho}\left[\rho\frac{d}{d\rho}\left[1 - \theta\left(\frac{du}{d\rho}\right)^2\right]\right] = u \qquad (21)$$

Because of the smallness of θ, we can look for a solution to Eq.(21) in the following approximate form

$$u(\rho) = u_0(\rho) + \theta u_1(\rho) \qquad (22)$$

where $u_o(\rho)$ is the undisturbed solution given in Eq.(2), and $u_1(\rho)$ is a correcting function given by the power series

$$u_1(\rho) = \sum_{n=0}^{n=\infty} a_n \rho^{2n} \qquad (23)$$

$$a_n = b_n\left[a_0 + \sum_{k=0}^{k=n-1} b_k^{-1}\Phi_k\right];\ b_n = \left(2^n n!\right)^{-2}$$

$$\Phi_n = 4\sum_{k=0}^{k=n}\frac{3(n-k)+2}{n-k+1} b_{n-k} \times \sum_{m=0}^{m=k} m(k-m+1) b_m b_{k-m+1}$$

The free coefficient, a_o, as found from the electroneutrality condition:

$$\chi\lambda\sigma_\lambda - 2en_0\int_0^\lambda \rho u(\rho)d\rho = 0 \qquad (24)$$

where n_0 is the density of background (1-1)-electrolyte ions, is

$$-a_0(\lambda) = \frac{\sum_{n=0}^{n=\infty}(2n+2)^{-1}b_n\lambda^{2n+2}\sum_{k=0}^{k=n-1}b_k^{-1}\Phi_k}{\sum_{n=0}^{n=\infty}(2n+2)^{-1}b_n\lambda^{2n+2}} \qquad (25)$$

As $\lambda \to 0$, we get the asymptotical formulas,

$$-a(\lambda) \approx \frac{1}{6}\left(\frac{\lambda}{2}\right)^4 + 0\left(\lambda^6\right) \qquad (26)$$

$$\alpha_\lambda^{-3}u_1(\lambda) \approx a_0(\lambda)\left[1 + \left(\frac{\lambda}{2}\right)^2 + \frac{1}{4}\left(\frac{\lambda}{2}\right)^4\right] +$$

$$+ \frac{1}{2lef}\left(\frac{\lambda}{2}right\right)^4 + 0\left(\lambda^6\right)$$

which allow to see that when $\lambda \to 0$, the influence of the dielectric constant dispersion brought about by the saturation effect gets vanishing.

To investigate another limiting case as $\lambda \to \infty$, it is convenient to introduce preliminary a new variable, $\rho^* = \lambda - \rho$, that is the distance from the cylinder surface to a given point within the cylinder cavity, whereas ρ has been the distance to the same point from the cylinder axis. Then the correcting function, $u_1(\rho^*)$, meeting the condition (24) is

$$u_1\left(\rho^*\right) = \lim_{\lambda\to\infty}\alpha_\lambda^3 I_1^3(\lambda)\left[1/8\exp\left(-3\rho^*\right) - \right.$$

$$\left. - 1/24\exp\left(-\rho^*\right)\right] \qquad (27)$$

And in this case, the dispersion of the dielectric constant will decrease the dissociation ability of ionizable groups at the surface, affecting their dissociation constants in accordance with Born's equation [8,11,12]:

$$K_{dis}(\varepsilon) = K_{dis}\left(\varepsilon_1\right)\exp\left[\omega\left(\varepsilon_1^{-1} - \varepsilon^{-1}\right)\right]$$

$$\approx K_{dis}\left(\varepsilon_1\right)\exp\left[-\frac{\theta\omega e^2\sigma^2}{\left(kT^3{}_0\chi\right)^2\varepsilon_1^3}\right] \qquad (28)$$

where $\sigma = \lim_{\lambda\to\infty}\sigma_\lambda$, and $\omega \cong 2\cdot10^2$ if dissociation yields two unicharged ions.

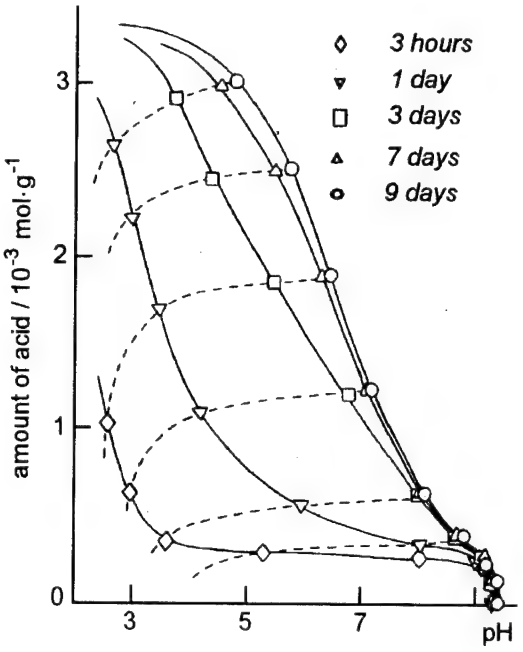

Fig.3. Changing of the titration curve in the time course: in the case considered, the equilibration time is over a week.

Kinetic study

Application of the semi-infinite diffusion model

Many reactions, which are very fast in solution, get considerably slowed down when proceeding at surface. A reason for this is quite evident: the rate-determining of surface reactions is more often than not the stage of diffusion one [17,18]. Consequently, it can take a long time for a surface equilibrium to be established. As an indicative example, we have pictured in Fig.3 how the titration curve for a porous amino-containing matrix was changing in the course of time until it took its final equilibrium form.

To examine the diffusion effects like that mentioned, let us consider a long tube filled up with a sorbent and connected with a bowl filled up with a solution containing some adsorbate. Our task is to study the time dependence of the adsorbate concentration in the solution. If the length of the tube is much larger than the dimensions of the bowl and the starting concentration of the adsorbate is low enough, the drift of adsorbate within the sorbent phase at the beginning of the diffusion process can be described using the semi-infinite diffusion model [18]. In its framework, the time dependence of the adsorbate concentration in the overlying solution is expressed as follows:

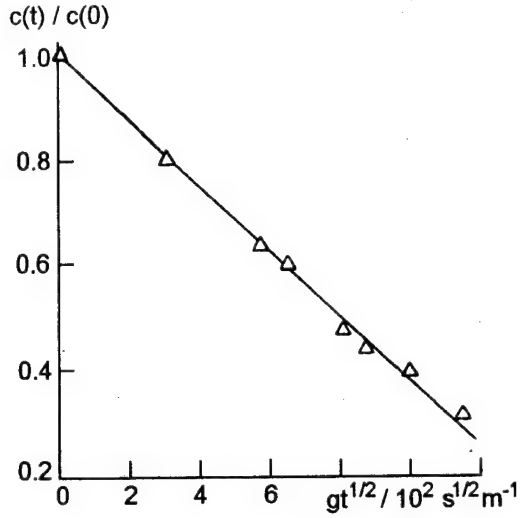

Fig.4. Determination of the diffusion coefficient by using Eq.(28): the experimental points (Δ) are approximated by a straight line with $g = 1.96\ m^{-1}$; $p = 0.5$; $\Gamma = 10^{7.6}$ and $D = 1.5 \cdot 10^{-13}\ m^2 \cdot s^{-1}$ [20].

$$c(t) = \frac{2c(0)}{\pi^{1/2}} \exp[\pi\beta^2 t] \int_{\beta(\pi t)^{1/2}}^{\infty} \exp(-\tau^2) d\tau;$$

$$\beta = g\left(\frac{p(1+\Gamma)D}{\pi}\right)^{1/2} \qquad (29)$$

where $c(0)$ is the starting concentration of the adsorbate, $c(t)$ is its concentration at the time t, p is the porosity coefficient, Γ is the Henry coefficient, D is the diffusion coefficient, and g is the geometrical factor, $g = S_{cr}/V_{sol}$, S_{cr} being the tube cross-section area, and V_{sol} the solution volume. As $t \to 0$, Eq.(27) can be brought to the form

$$c(t)/c(0) \approx 1 - 2\beta t^{1/2} + 0(\pi\beta^2 t) \qquad (30)$$

The latter equation was used to study the adsorbtion kinetics of hydrochlorid acid and a number of Co(II) phthalocyanine complexes onto a series of porous organopolysiloxane sorbents having recently been described elsewhere [19]. The corresponding $c(t)/c(0)$ vs $gt^{1/2}$ lines are represented in Fig.4 and 5.

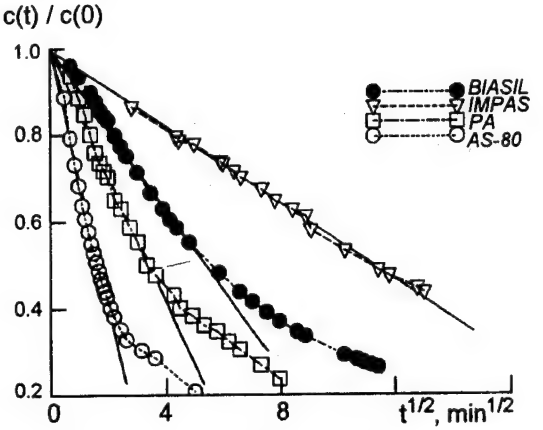

Fig.5. The sorption kinetics of cobalt(II) tetrasulphophthalocyanine onto organo-grafted silica gels bearing benzimidazole (BIASIL), imidazole (IMPAS), and aminopropyl (PAS and AS-80) [19] groups. In the indicated sequence, the diffusion coefficient calculated according to Eq.(28) proved to be equal to 10^{-12}, $3 \cdot 10^{-14}$, $2\ 10^{-14}$ and $3 \cdot 10^{-13}\ m^2 \cdot s^{-1}$; the Henry coefficients were put to be equal to 10^5, 10^6 and $10^{7.6}$, respectively.

Acknowledgements

Hospitality of the staff of the Institute for Physical Chemistry and financial support provided by Daimler-Benz Foundation were invaluable for one of us.

References

1. E.A.Guggenheim, Thermodynamics, North-Holland Publ. Co., Amsterdam, (1957), p.46.
2. B.V.Zhmud, A.A.Golub, *Zh.Fiz.Khim.*, **67**, 734 (1993).
3. B.V.Derjaguin, Theory of the Stability of Colloids and Thin Films [in Russian], chap.7, Nauka, Moscow (1986).
4. T.L.Hill, *Arch.Biochem.Biophys.*, **57**, 229 (1955).
5. B.V.Derjaguin, N.V.Churaev, V.M.Muller, Surface Forces, Consultants Bureau, New York, Chap.1 and 6. (1987).
6. J.Lyklema, *J.Colloid Interface Sci.*, **99**, 109 (1984).
7. W.Pauli, E.Valko, Electrochemie der Kolloide, Springer, Wien, (1929).
8. B.V.Zhmud, A.A.Golub, *J.Colloid Interface Sci.*, **167** (1994) (in print).
9. A.B.Neymark, *Zh.Fiz.Khim.*, **64**, 2593 (1990).
10. J.Bockris, M.Devanathan, K.Muller, in Proc.R.Soc. (London), **274**, 55 (1963).
11. Y.Gur, I.Ravina, A.J.Babchin, *J.Colloid Interface Sci.*, **64**, 326 (1978).
12. M.Born, *Z.Physik*, **1**, 45 (1920).
13. G.P.Dube, *Indian J.Phys.*, **17**, 189 (1943).
14. F.Booth, *J.Chem.Phys.*, **19**, 391 (1951).
15. J.Frahm, S.Dickman, *J.Colloid Interface Sci.*, **70**, 440 (1979).
16. H.Hurwitz, A.Sanfeld, A.Steinchen, in: Fundamental Aspects of Modern Theoretical Electrochemistry, Proc. 14th Conference of the International Committee of Electrochemical Thermodynamics and Kinetics [in Russian], Ed. by A.N.Frumkin, Mir, Moscow, (1965), p.141.
17. F.Helfferich, Ionenaustauscher, Verlag Chemie, Weinheim, (1959).
18. B.V.Zhmud, A.B.Pecheniy, V.A.Kalibabchuk, *Ukr. Khim. Zh.*, **60**, (1994) (in print).
19. B.V.Zhmud, A.B.Pecheniy, *J.Colloid Interface Sci.*, (submitted).
20. G.V.Kudrayavtsev, G.V.Lisichkin, *Zh.Fiz.Khim.*, **51**, 1352 (1981).

Термодинамическое и кинетическое исследование реакций протолиза и комплексообразования на поверхности пористых матриц

Б.В.Жмудь, А.Б.Печеный, А.А.Голуб

С использованием аппарата формальной термодинамики выведен обобщенный закон действия масс, который может быть использован для описания протолитических и ионных реакций на поверхности жестких матриц в контакте с растворами электролитов, На основе этого закона сделана попытка теоретического переосмысления и систематизации влияния различных факторов — пористой структуры, фрактальности и механизма формирования поверхностного заряда — на протолитические свойства пористых силикагелей, модифицированных органическими лигандами. В рамках модели полубесконечной диффузии исследована кинетика хемосорбции соляной кислоты и ряда сульфозамещенных фталоцианиновых комплексов Co(II) на этих матрицах.

Functional Materials 2, No.1 (1995)

Catalytic hydrosilylation reactions involving modified silica surfaces

O.V.Simurov, L.A.Belyakova and V.A.Tertykh

Institute for Surface Chemistry, National Academy of Sciences of Ukraine,
31 Nauki Ave., 252022 Kiev, Ukraine

The systematic investigation of transformations silica surface taking place at ≡Si—H groups of different nature and olefins contacts as well as at ≡Si—CH=CH$_2$ groups and hydrosilane contacts is first carried out. The principal possibility of proceeding of the hydrosilylation reaction on silica surface is shown and the optimal condition are found. The reaction mechanism and physico-chemical properties of obtained organosilicas are investigated.

Нами вперше було проведено систематичне вивчення хімічних перетворень на поверхні кремнезему при контакті ≡Si—H (різної природи) та олефінів, а також ≡Si—CH=CH$_2$ груп гідридсилану. Показано принципову можливсть проведення реакції гідросилілювання на поверхні кремнезему, знайдено оптимальні умови. Досліджено механізм реакції. Вивчено фізико-хімічні властивості одержаних органокремнеземів.

It is known that a wide variety of objectives can be achieved using chemically modified silicas (CMS). Such silicas are widely used, e.g., as high-specific adsorbents, selective catalysts, active fillers for polymers, effective thickeners of dispersive media, etc. [1]. Yet, the wider CMS are used, the more critical becomes the problem of their hydrolytical and chemical stability which should assure the long-term and repeated use of modified matrices without loss of their properties. At the same time, for various reasons, the known methods of chemical treatment of silicas do not always consistent with the requirement mentioned. Therefore, the development of new methods for silicas modification with the aim to form, on their surfaces, thermally and hydrolytically stable coatings remains to be of great importance. In this connection, the hydrosilylation reaction has drawn our attention. The idea of the using of this reaction to obtain CMS has its own history. This can be traced from the first suggestions and realization attempts [2-4] to serious theoretical works [5].

As a whole, the following situation is set up at present:

a) the hydrosilylation reaction with the participation of homogeneous reagents is well studied and widely used to obtain various organo silicon compounds [6,7];

b) the introduction of hetegeneous catalysts has allowed to obtain some experience of the process performing on the phase interface [7];

c) there is a sufficient amount of information concerning the synthesis and properties of silicas containing the surface-fixed ≡Si—H and ≡Si—CH=CH$_2$ groups [1,8].

Thus, as a whole, it seems to be logically enough that we set ourselves the following tasks:

1) to study comprehensively the chemical transformations on the silica surface at the contact of ≡Si—H groups (being of various origins) with olefins, as well as of grafted ≡Si—CH=CH$_2$ groups with silicon hydrides;

2) to investigate the course and mechanism of these reactions;

3) to study the physico-chemical properties of the modified silicas obtained by these reactions.

As is known, one of most widely used techniques for obtaining of silicohydride groups on a silica surface is the treatment of the substrate

with the respective silane. We have used the methyldichlorosilane:

$$\equiv Si—OH + CH_3SiCl_2H \rightarrow$$
$$\equiv Si—O—Si(CH_3)(Cl)H + HCl$$

In the IR spectrum of such silica hydride, the absorption band 3750 cm^{-1}, corresponding to the stretching vibration of ≡Si—OH groups, does not observed; instead, the band 2204 cm^{-1} ν(Si—H) appears as well as those corresponding to $\nu_{as,s}$(C—H) (2984 and 2931 cm^{-1}) and to δ(C—H) of methyl groups (1400 $^{-1}$).

The silica hydride so obtained was brought into contact with olefins under progressively changed reaction conditions. The investigations performed have shown that the reaction of ≡Si—O—Si—H groups fixed on the silica surface with the simple terminal olefins does not proceed effectively neither in gas nor liquid phase in the absence of catalyst and at moderate temperatures. The use of Speier catalyst (0.1 N of the chloroplatinic acid in the *iso*-propyl alcohol) allows almost quantitative reaction to be performed. In the IR spectra, this fact manifests itself as follows: the intensity of the Si—H bonds absorption band diminishes (more then by 90 per cent); that of the methyl groups ν(C—H) increases; the 2880 cm^{-1} band of methylene links ν(C—H) appears. The increase of the surface concentration of C—H bonds makes itself evident also as the absorption in the 1500-1300 cm^{-1} range which corresponds to the bending vibrations of the methyl and methylene groups (Fig.1, curve 3). The band corresponding to the stretching vibrations of C—H bonds contained in the CH_2=CH— groups (3090 cm^{-1}), which is present in the spectrum of initial octene (Fig.1, curve 2), is vanished in that of modified silica. These results establish that, on the silica hydride surface, the hydrosilylation reaction occurs:

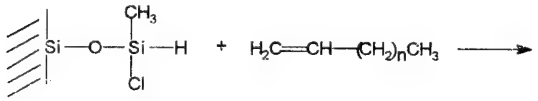

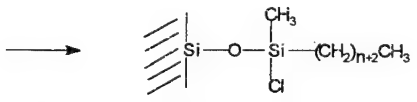

The hydrolytic stability of the organosilicas obtained by hydrosilylation reaction serves as an additional verification of the Si—C bonds formation on the silica surface. The treatment of the specimens synthesized by the water vapour in the pyridine presence does not result in any significant change of the IR spectrum (Fig.1, curve 4). The appearance of the 3750 cm^{-1} band corresponding to silanol groups can be explained easily by the hydrolysis of ≡Si—Cl groups presented in surface compounds of ≡Si—O—Si(C_nH_{2n+1})(CH_3)Cl type.

Besides, it is established that following reactions may take place in parallel with the solid-phase hydrosilylation process:

1) the hydrolysis of ≡Si—H group in surface compounds similar to ≡Si—O—Si(Cl)(CH_3)H;

2) the *iso*-propanol addition to the surface of initial silica as well as to that of of silica hydride;

3) the chemisorption of 1-olefins on the initial silica surface.

However, the side reactions can be kept to a minimum by using the proposed optimum reaction conditions (1 to 1.5 h at 100 °C in the presence of the Speier catalyst) as well as by the pre-drying of reactants and ensuring the maximum conversion of ≡Si—OH to ≡Si—O—Si—H groups [9].

To reveal the potential possibilities of the solid-phase catalytic hydrosilylation as applied to polyfunctional unsaturated compounds, the silica with fixed ≡Si—O—Si—H groups was treated by trimethylvinylsilane or by trichlorovinylsilane for 1 h at the boiling temperature in the presence of the Speier catalyst. It is found [10] that, after the contact with vinylsilanes mentioned, a significant intensity drop (by 80-85 %) of absorption band of the Si—H bond stretching vibrations (2204 cm^{-1}) is observed in the IR spectra of modified silicas (see Fig.2), as well as the appearance of the absorption bands corresponding to the asymmetrical (2926 cm^{-1}) and symmetrical (2853 cm^{-1}) stretching vibrations of the methylene C—H bonds (Fig.2, curves 2,4). In the case of the silica hydride-trimethylvinylsilane interaction, the intensity of absorption bands corresponding to of methyl C—H bonds, also increases (Fig.2, curve 4). Besides, in the IR spectra of the silicas modified by vinylsilanes, the following absorption bands are absent: one of ν(C—H) attaching to carbon-carbon double bond (3080 to 3000 cm^{-1} range) and one corresponding to the C—C stretching vibrations (near to 1600 cm^{-1}) (Fig.2, curves 2,4), while these bands are easy to observe in the spectra of individual vinylsilanes, namely, 3082; 3032; 3004, and 1602 cm^{-1} for the vinyltrichlorosilane (Fig.2, curve 3) and 3052; 3010, and 1596 cm^{-1} for the vinyltrimethylsilane (Fig.2, curve 5). The described changes in IR spectra indicated that, already in the conditions mild enough, Si—H bonds transform in Si—C ones as

a result of the hydrosilylation reaction in the surface layer of the silica hydride:

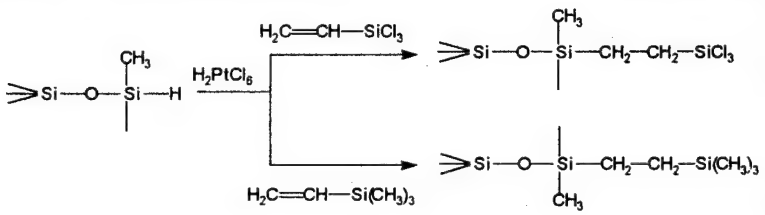

Thus, the reaction proposed can be used for the synthesis of the functional organosilicas.

It is known that the proposed method in the silica hydride synthesis is not the only possible. We believe that the method based on the methoxy silica thermal destruction can be a promising one:

$$\equiv Si—OCH_3 \rightarrow \equiv Si—H + H_2CO$$

Therewith, in the IR spectrum, a sharp intensity drop was observed for the adsorption bands of the methoxy groups, the appearance of a rather intensive 2280 cm^{-1} band (ν(Si—H)) as well as of a moderately intensive

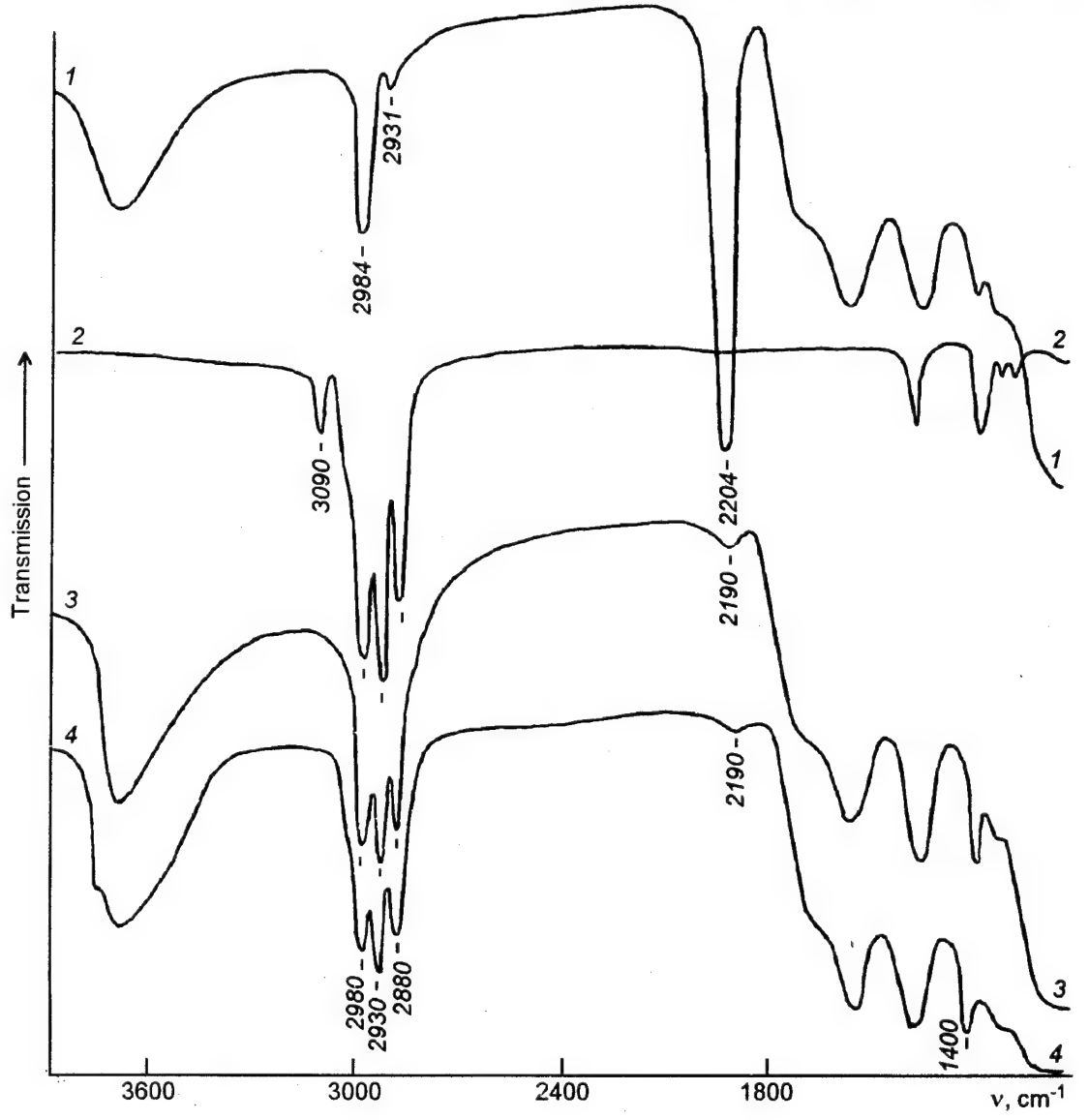

Fig.1. IR absorption spectra of the silica hydride with the fixed ≡Si-O-Si-H groups (1); after interaction with 1-octene at 100 °C in the presence of the Speier catalyst (3); after the water vapour treatment in the presence of pyridine at 25 °C for 1 h and subsequent vacuum exposure at 300 °C for 1 (4); the IR spectrum of the 1-octene (2).

one of silanol groups (3750 cm^{-1}). To eliminate the possible side effects associated with the arising of silanol groups, the surface was additionaly treated by the hexamethyldisilazane vapour at 100 °C.

Under the interaction of surface ≡Si—H groups of the silica hydride obtained with 1-octene in the presence of Speier catalyst (100 °C, 1 h), in the IR spectrum (Fig.3, curve 2),

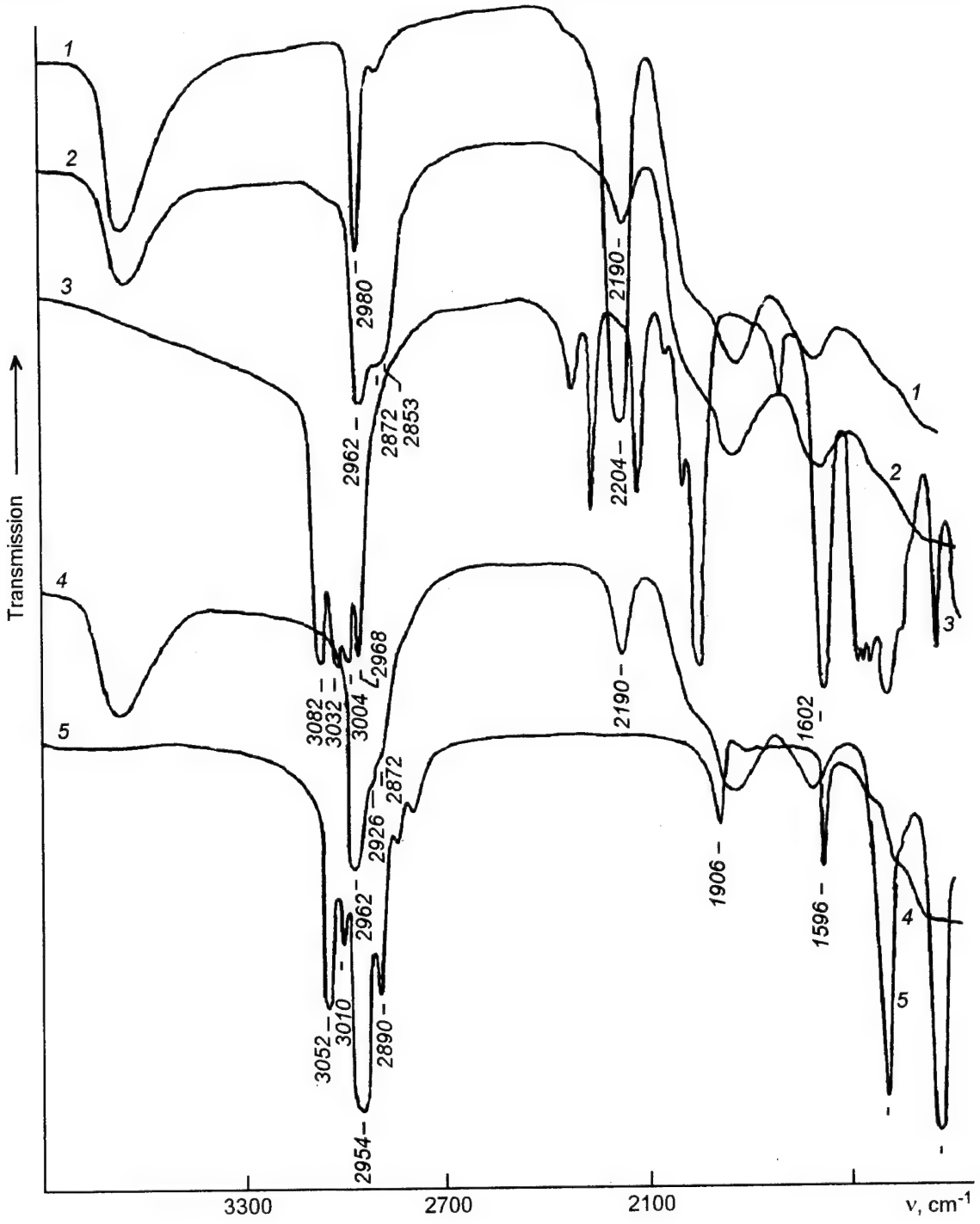

Fig.2. IR absorption spectra of the silica hydride (1); of that treated by the vinyltrichlorosilane (2) or vinyltrimethylsilane (4) in the presence of the Speier catalyst and exposed to vacuum at 300 °C for 1 ; the IR spectra of the vinyltrichlorosilane (3) and the vinyltrimethylsilane (5).

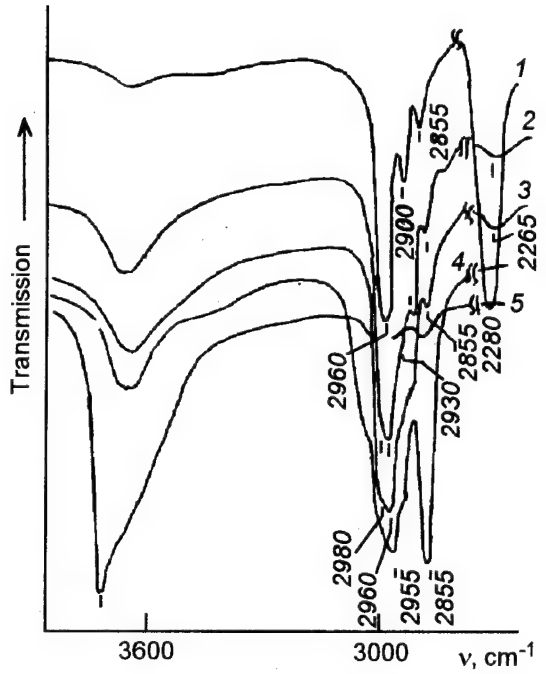

Fig.3. IR absorption spectra of the silica hydride with surface-fixed ≡Si-H groups (obtained by the methoxy-silica thermal destruction and post-treated by the hexamethyldilazane) (1); after the interaction with 1-octene (100 °C, 1 h) and subsequent vacuum exposure (300 °C, 1) (3); IR spectrum of methoxy silica before (4) and after hydrolysis in the pyridine presence (25 °C, 1 h) and subsequent vacuum treatment (300 °C, 1 h) (5).

a significant (more than by 90 per cent) weakening of the absorption band belonging to ≡Si—H groups. Simultaneously, the bands corresponding to the stretching vibrations of C—H bonds in methylene (2930; 2855 cm^{-1}) and methyl (2980; 2900 cm^{-1}) groups become more intensive. This evidences the transformation of the ≡Si—H groups into the chemically bonded hydrocarbon radicals:

$$\equiv Si{-}H + CH_2{=}CH{-}(CH_2)_5{-}CH_3 \xrightarrow{H_2PtCl_6} \equiv Si{-}(CH_2)_7CH_3$$

The data concerning the hydrolytic stability of the organosilicas obtained by solid-phase hydrosilylation form the additional prove for the surface -Si—C bonds formation. In the same time, for the methoxy silica, the Si—O—C bond destruction and the silanol groups formation is observed, what is indicated by the weakening of the bands intensity in the 3000-2800 cm^{-1} range, corresponding to the ether groups, and the appearance of the 3750 cm^{-1} band (Fig.3, curves 4,5; see [11,12]).

Thus, it is established that the sythesized ≡Si—H groups on the silica surface possess a high reactivity toward 1-olefins. The method proposed can be used to synthesize the organosilicas having thermally and hydrolytically stable Si—C bonds between the silica support and organic functional groups, without use of organo silicon reactants. This results in a substantial extending of the experimental possibilities at the obtaining of dispersed silicas with chemically modified surfaces.

To elucidate the influence of the phase state of the compounds containing CH_2=CH— groups on the hydrosilylation reaction, the interaction between the silica having fixed ≡Si—O—Si—CH=CH_2 groups and the methyldichlorosilane in the presence of the Speier catalyst was studied.

The vinyl silica was obtained by the silica treatment with the vinyldichlorosilane vapour at 300 °C for 2 h:

$$\equiv Si{-}OH + Cl_3SiCH{=}CH_2 \rightarrow$$
$$\rightarrow \equiv Si{-}O{-}Si(Cl_2)CH{=}CH_2 + HCl$$

Therewith, in the IR spectrum the absorptions bands appear of ν(C—H) attached to C=C (3082; 3032, and 3004 cm^{-1}), as well as ν(C=C) band at 1602 cm^{-1}; while absorption band of the stretching vibrations of the isolated silanol groups nearly vanishes. To elemenate the residual ≡Si—OH groups the vinyl silica was end-capped by the hexamethyldisilazane. Therewith, the absorption bands of ν(C—H) in the trimethylsilyl groups (2970 and 2910 cm^{-1}) were observed in the IR spectrum.

After the interaction of the vinyl silica with the methyldichlorosilane, the absorption bands characteristic for the CH_2=CH- groups (3082; 3032; 3004, and 1602 cm^{-1}) are vanished in IR spectra. The band belonging to ≡Si—H groups is not observed after the vinyl silica treatment by the methyldichlorosilane. In the IR spectrum of the product obtained, only the stretching vibrations bands of the C—H bonds belonging to methyl and methylene groups are presented. Consequently, the following transformations of the modifying groups occur on the silica surface:

$$\equiv Si{-}O{-}\underset{|}{Si}{-}CH{=}CH_2 + H{-}\underset{|}{Si}{-}CH_3 \xrightarrow{H_2PtCl_6}$$
$$\rightarrow \equiv Si{-}O{-}\underset{|}{Si}{-}CH_2{-}CH_2{-}\underset{|}{Si}{-}CH_3$$

Table 1. Structural and sorption characteristics of the C_nH_{2n+1}-silicas obtained by the solid-phase hydrosilylation in the presence of the Speier catalyst

Silica	Solid-phase hydrosilylation with the Speier catalyst					After trimethyliodosilane end-capping			
	C		S_p, m^2/g	V_p, cm^2/g	d_c, Angstroms	C, mg/g	S_p, m^2/g	V_p, cm^2/g	Θ, degrees
	mg/g	μmol/m^2							
Silochrom 120	24.0*	3.78	140	1.16	330	24.0	141	1.16	90
Silica hydride	13.6	2.94	132	1.12	340	-	132	1.12	105
|-C_6H_{13}	57.2	3.47	132	1.08	323	72.4	116	0.99	-
|-C_8H_{17}	61.6	3.01	131	1.06	323	-	113	0.98	96
|-$C_{10}H_{21}$	50.1	2.05	128	1.05	330	63.9	112	0.96	-
|-$C_{14}H_{29}$	32.0	0.99	127	1.05	330	47.6	111	0.94	-
|-$C_{16}H_{33}$	31.9	0.88	125	1.04	335	45.3	101	0.92	-
|-$C_{18}H_{37}$	28.5	0.71	125	1.04	335	39.8	101	0.92	106

* determined by the trimethyliodosilane chemisorption.

No difference is found to exist in the reactivities of the modified silicas containing vinyl or ≡Si—H groups: the hydrosilylation reaction of the fixed groups resulting in the surface compounds containing Si—C bonds occurs substantially to completion.

Among the main problems occuring during the study of any synthesis process is the reaction mechanism investigation.

Using the IR spectroscopy we have recognized that the contact of the Speier catalyst with the silica hydride as well as with the vinyl silica results in the activation of the Si—H bonds as well as of C=C ones. In the silica hydride spectrum, this phenomenon manifests itself as the intensity lowering (or the complete vanishing) of the 2204 cm^{-1} band belonging to the ≡Si—H groups adsorption; while, in the vinyl silica spectrum, the —$CH=CH_2$ group bands at 3070 and 1650 cm^{-1} became not observable.

The electron spectra of the system consisting of the Speier catalyst, silica hydride, and 1-decene, have shown that, regardless of the reactants and catalyst introduction sequence, the solid-phase catalytic hydrosilylation reaction is preceded by the formation of the catalytically active intermediate including both reactants and the catalyst.

The consideration of the structure of these intermediate complexes permits the conclusion that the intracomplex transformations which result in the formation of the hydrosilylation products can be related to the nucleophilic addition processes at the silicon atom. Generally, the increase of the silicon atom electrophilness in the silica hydride (or in the hydrosilane) and enhancement of the complexing ability of the olefine (or olefine-silica) should be lead to the yield increase of the solid-phase hydrosilylation product. The role of the modified silica surface in the simultaneous activation both of Si—H and C=C bonds by the Speier catalyst should be noted as well as the increasing importance of the steric factors and adsorption interactions in the course of the formation of the intermediate surface complexes which result in the solid-phase hydrosilylation products.

The investigation of the structure and adsorption-structural characteristics of the porous silicas with the long-chain alkyl groups fixed on the surface by the solid-phase hydrosilylation have shown that the proposed method allows to obtain the effective and stable modifying coatings. Moreover, it is found that, with increasing length of the fixed hydrocarbon radical, the water adsorption diminishes, and such a relationship is observed on the backgroud of the diminishing grafted organic groups concentration (see Table 1). This apparent inconsistency can be explained as follows. In Table 2, the data about the thickness of the organic layer for the C_nH_{2n+1}-silicas are presented which are obtained experimentally (as the difference between the pore radii before and after the modification) and by calculation. The organic layer thickness obtained from experimental data is obviously significantly less then the calculated length of the corresponding organic radical, except for the value for n=6. Thus, the C_nH_{2n+1} groups fixed on the silica surface do not a brush-like structure; on the contrary, the hydrocarbon chains are placed

Table 2. The length of C_nH_{2n+1} radicals fixed on the silica surface by the solid-phase hydrosilylation

Radical –Si–O–Si– C_nH_{2n+1}		n				
		6	10	14	16	18
Length*, Angstroms	Calculated value	11	16	22	24	26
	Experimental data	7	5	5	10	15

* rounded to the nearest integer.

obliquely to the silica surface. This explains the enhancement of the hydrophobic properties of the C_nH_{2n+1}-silica surface as well as of the angle of contact at the wetting with the increase of *n*, in spite of the substantial lowering of the grafted alkyl group content (Table 1).

References

1. Modified Silicas in Sorption, Catalysis and Chromatography [in Russian], Ed. by G.V.Lisichkin Ed., Khimiya, Moscow (1986).
2. A.A.Chuyko, V.A.Tertykh, V.A.Khranovsky, et al., *Teoreticheskaya i eksperimental'naya khimiya*, **2**, 247 (1966).
3. G.E.Pavlik, Cand. Thesis Autoref., Kiev (1968).
4. G.H.Wagner, A.N.Pines, *Ind.Eng.Chem.*, **44**, 321 (1952).
5. J.E.Sandoval, J.J.Pesek, *Anal.Chem.*, **61**, 2067 (1989).
6. E.Ya.Lukewitz, M.G.Voronkov, Hydrosilylation, Dihydrogermylation, Dihydrostannylation [in Russian], AN Latv. SSR Ed., Riga (1964).
7. V.P.Yur'ev, I.M.Salimgareeva, Olefines Dihydrosilylation Reaction [in Russian], Nauka, Moscow (1982).
8. V.A.Tertykh, L.A.Belyakova, Chemical Reactions Involving Silica Surface [in Russian], Naukova dumka, Kiev (1991).
9. V.A.Tertykh, L.A.Belyakova, A.V.Simurov, *Zhurn. Fiz. Khim.*, **64**, 1410 (1990).
10. L.A.Belyakova, A.V.Simurov, D.Yu.Lyashenko, V.A.Tertykh, *Ukr.Khim.Zhurn.*, **58**, 630 (1992).
11. V.A.Tertykh, L.A.Belyakova, A.V.Simurov, *Mendeleev Commun.*, No.2, 46 (1992).
12. V.A.Tertykh, L.A.Belyakova, A.V.Simurov, *Dokl. AN SSSR*, **318**, 647 (1991).

Реакции каталитического гидросилилирования с участием поверхности модифицированного кремнезема

А.В.Симуров, Л.А.Белякова, В.А.Тертых

Нами впервые было проведено систематическое изучение химических превращений на поверхности кремнезема при контакте ≡Si—H (различной природы) и олефинов, а также ≡Si—CH=CH_2 групп и гидридсилана. Показана принципиальная возможность проведения реакции гидросилилирования на поверхности кремнезема, найдены оптимальные условия. Исследован механизм реакции. Изучены физико-химические свойства полученных органокремнеземов.

Functional Materials **2**, No.1 (1995)

Chemisorption of styrene on the silica hydride surface

V.A.Tertykh and S.N.Tomachinsky

Institute for Surface Chemistry, National Academy of Sciences of Ukraine,
31 Nauki Ave., 252650 Kiev, Ukraine

The reaction of solid-phase hydrosilylation between styrene and silica hydride in the presense of Speier catalyst was carried out. Analysis of IR spectra shows that the degree of transformation of bonded Si—H groups in various experiments was amounted to 82-88 %. This value did not depend from presence of 1 % hydroquinone in reaction mixture. The optimal reaction conditions were found preventing side reactions and polymerization of styrene.

Здійснено реакцію твердофазного гідросилілювання між стиролом і гідридкремнеземом у присутності каталізатора Спейера. Аналіз ІЧ-спектрів показав, що ступінь перетворення поверхневих Si—H груп у різних дослідах становив 82-88 %. Ця величина не залежить від присутності 1 % гідрохінону у реакційній суміші. Було знайдено оптимальні умови проведення реакції, що запобігають перебігу побічних реакцій та полімеризації стиролу.

Recently, the realization possibility of solid-phase hydrosilylation reaction was shown [1-5] involving the Si—H groups linked to the silica and a series of various structure olefins, such reactions result in the forming of surface chemical compounds containing Si—C bond. The fixation of styrene on the silica hydride surface is no doubt of interest in terms of the functional matrices obtaining by such a method. The mentioned reaction in the silica surface layers is yet not investigated. It is known, however, that, in the liquid phase silylation reactions, styrene is almost twice less active as compared to the terminal olefins [6]. The purpose of this work is to study the realisation possibilities and performing conditions for the styrene hydrosilylation resulting in the obtaining of silica modified by phenyl ethyl groups. As in the case of styrene — divinyl benzene copolymers, such matrices are of interest for the incorporation of required functional groups in the course of the chloromethylation, nitration, and azo combination [7].

The IR spectra of the styrene as well as of initial silica (aerosil, the specific surface 300 m^2/g, measured using methanol) and modified ones, were recorded by means of IKS-29 spectrophotometer in the frequency range from 4000 to 1200 cm^{-1}; the thickness of pressed plates corresponded to 10-15 mg/cm^2; the tabletting pressure was $1.72 \cdot 10^8$ Pa. To obtain the silica containing Si—H surface groups, the initial silica, according to the method described in [5], was vacuum treated at 400 °C for 2 h in a quartz cell with CaF_2 windows and then brought into contact with methyldichlorosilane vapour for 2 h at 300 °C. The silane excess and gaseous reaction products were removed by vacuum treatment for 2 h at 300 °C. Therewith, in the IR spectrum of silica hydride obtained (see Fig.1, curve 3), the 3750 cm^{-1} absorption band of the initial silica (Fig.1, curve 2) vanishes, while that of Si—H bond valence vibrations (2204 cm^{-1}) arises as well as bands at 2984 and 2931 cm^{-1} corresponding to the valence vibrations and at 1400 cm^{-1} — to the deformational one of methyl C—H bonds [10-12]. The «chemically pure» styrene stabilized by 1 per cent of hydroquinone was used. The polymerization stabilizer was removed by multiple washing with 10 per cent KOH solution. Next, the styrene was washed with distilled water up to neutral reaction, and dried over 4 Å molecular sieves at 0 °C for a day [8]. IR spectrum of the styrene

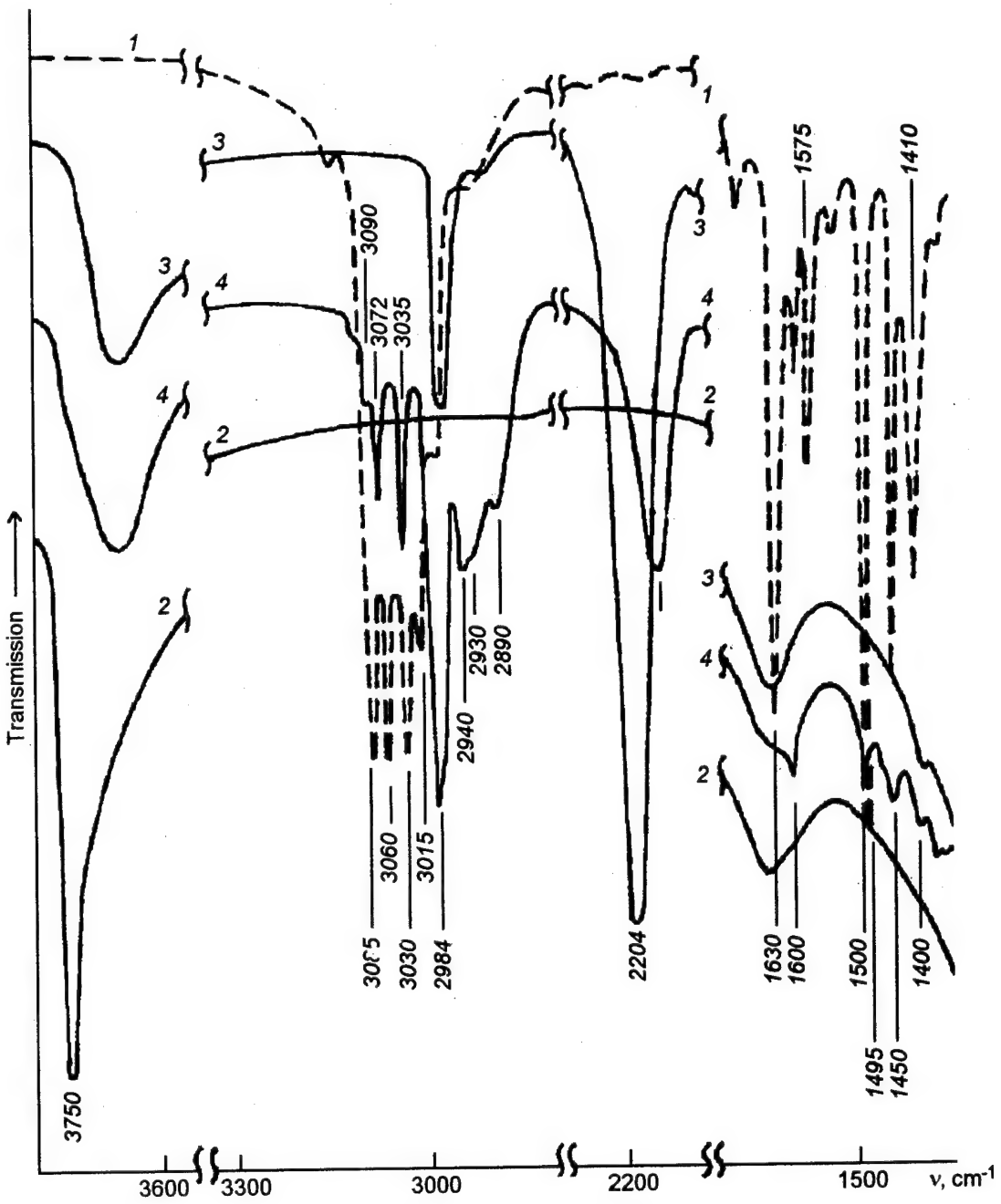

Fig.1. IR spectra: styrene, *l*=0.011 mm (1); silica vacuum-dried at 400 °C for 2 h (2); after methyldichlorosilane treatment at 300 °C for 2 h and vacuum treatment at 300 °C for 2 h (3); after subsequent modification by styrene, washing by boiling CCl_4 for 1 h and vacuum drying at 300 °C for 2 h (4).

(Fig.1, curve 1) was identical to that given in the literature [9].

The hydrosilylation reaction was performed in the liquid phase without solvent use, in a shaded reactor, at 100 °C for 3 h, in the presence of 0.1 N platinumhydrochloric acid in *iso*-propyl alcohol (Speier catalyst). Next, the modified silica was washed by carbon tetrachloride in the Soxhlet apparatus for 1 h and vacuum treated at 300 °C during 2 h.The reaction results in a significant diminishing of the intensity of Si—H bond absorption band in the IR spectrum of modified

silica. The maximum of this band was shifted to 2190 cm^{-1} due to partial hydrolysis of Si—Cl bonds [10,11] taking place at the contact of modified silica with atmospheric moisture during transfer from one vessel to another. The silanol groups formation is accompanied by the appearance of an absorption band near to 3859 cm^{-1}. Besides, the absorption bands at 3090; 3072, and 3035 cm^{-1} are observed corresponding to the valence vibrations of C—H bonds in the benzene ring. The intensities ratio of these bands differs from that in the styrene spectrum and is characteristic for benzene derivatives having no double bond in side chain. Moreover, in the spectrum of the modified silica, the characteristic bands of the styrene are absent, namely, 1630 cm^{-1} (valence vibrations of vinyl C=C group) and 1575 cm^{-1} (benzene ring plane vibrations), the latter appearing when the conjugation of benzene π electron cloud with π electrons of a double bond or with the lone pair of the substituent takes place [13]. It follows herefrom that styrene is entered into hydrosilylation reaction with the Si—H groups of the surface. The absorption bands in 1600 and 1500 cm^{-1} ranges correspond to the plane vibration of the benzene rings; the 1450 cm^{-1} band, to the same vibrations of the aliphatic bridge C—H bonds. A significant intensity increase of 2984 and 2930 cm^{-1} absorption bands (methyl groups) as well as appearance of 2940 cm^{-1} (methylene groups) and 2890 cm^{-1} (the combined methylene and methine groups absorption) bands [10-12] point to the fact that styrene adds to the silicium atoms of surface Si—H groups in form of 1-phenylethyl radicals (I) as well as in form of 2-phenylethyl ones (II):

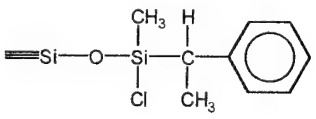

I

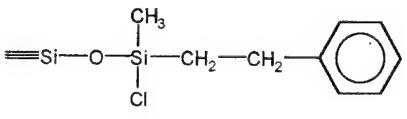

II

This conclusion is supported by the fact that, if the reaction is performed in the homogene medium at 100 °C in the presence of Speier catalyst and at styrene to methyldichlorosilane ratio 1.8:1 during 16 h, a mixture of products is formed having structures similar to (I) and (II) in the ratio 39 to 61 per cent, respectively [14]. The conversion degree (η) of the surface Si—H groups was calculated by the formula [15,16]

$$\eta = (d_0 - d)/d_0$$

where d_0 and d are optical densities of Si—H groups absorption band before and after the reaction, respectively. The calculated degree of reaction completeness amounted to 82-88 per cent in various experiments. The surface concentration of phenyl ethyl group in the modified silica obtained was 0.46 mmol/g, as follows from thermogravimetric analysis. At the repeated treatment of a silica specimen having the Si—H group conversion degree 87 % in the identical conditions during 3 h, the additional 3 % of Si—H groups were converted. Yet, a reference specimen of the initial silica hydride placed in the same reactor showed the conversion degree 88 %. Such a slowing of the Si—H groups reaction at high conversion degrees appears to be due to steric hindrances formed by phenyl ethyl radicals attached to the surface.

A specific feature of styrene-silica hydride interaction should be pointed out. If the Speier catalyst is added to a styrene- silica hydride mixture at ambient temperature, on light, the resulting mixture is progressively heated to 100 °C and exposed for 3 h in these conditions, then, in IR spectra of specimens obtained, a poor reproducibility of intensities is observed for absorbtion bands in the range 3000-2850 cm^{-1}, as compared with those of 3150-3000 cm^{-1} range and 1500 cm^{-1} band. This effect is to be assigned to side reactions. Thus, *iso*-propanol containing in the Speier catalyst may react with Si—Cl bonds even at ambient temperature [17,18]. Besides, acetone which is formed in the Speier catalyst [19,20] reacts on light quantitatively with Si—H groups [21]. The both reactions result in the formation of $SiOCH(CH_3)_2$ groups on the silica surface. The IR spectra of the oxy-*iso*-propyl groups are very similar to these of aliphatic part of 1-phenylethyl group in 3000-2850 cm^{-1} range, and that fact complicates the interpretation of spectra. However, if we add the Speier catalyst to the styrene-silica hydride system heated to 100 °C in the shaded reactor, then, because of the small catalyst quantity (0.04-0.06 cm^3), the dominant part of *iso*-propanol (Bp. 82.4 °C) and acetone (Bp. 56.2 °C) evaporates rapidly. Therefore, a good reproducibility of the intensities ratio in IR spectra is observed for specimens obtained in these conditions. The same result is achieved when we add to the styrene heated to 100 °C, first, the Speier catalyst, and then, after 1 to 2 min, silica hydride.

It is known that the bond in alkoxy groups on the surface is unstable and breaks easily under the action of water in presence of organic bases, such as pyridine or aniline [22]. After the boiling water

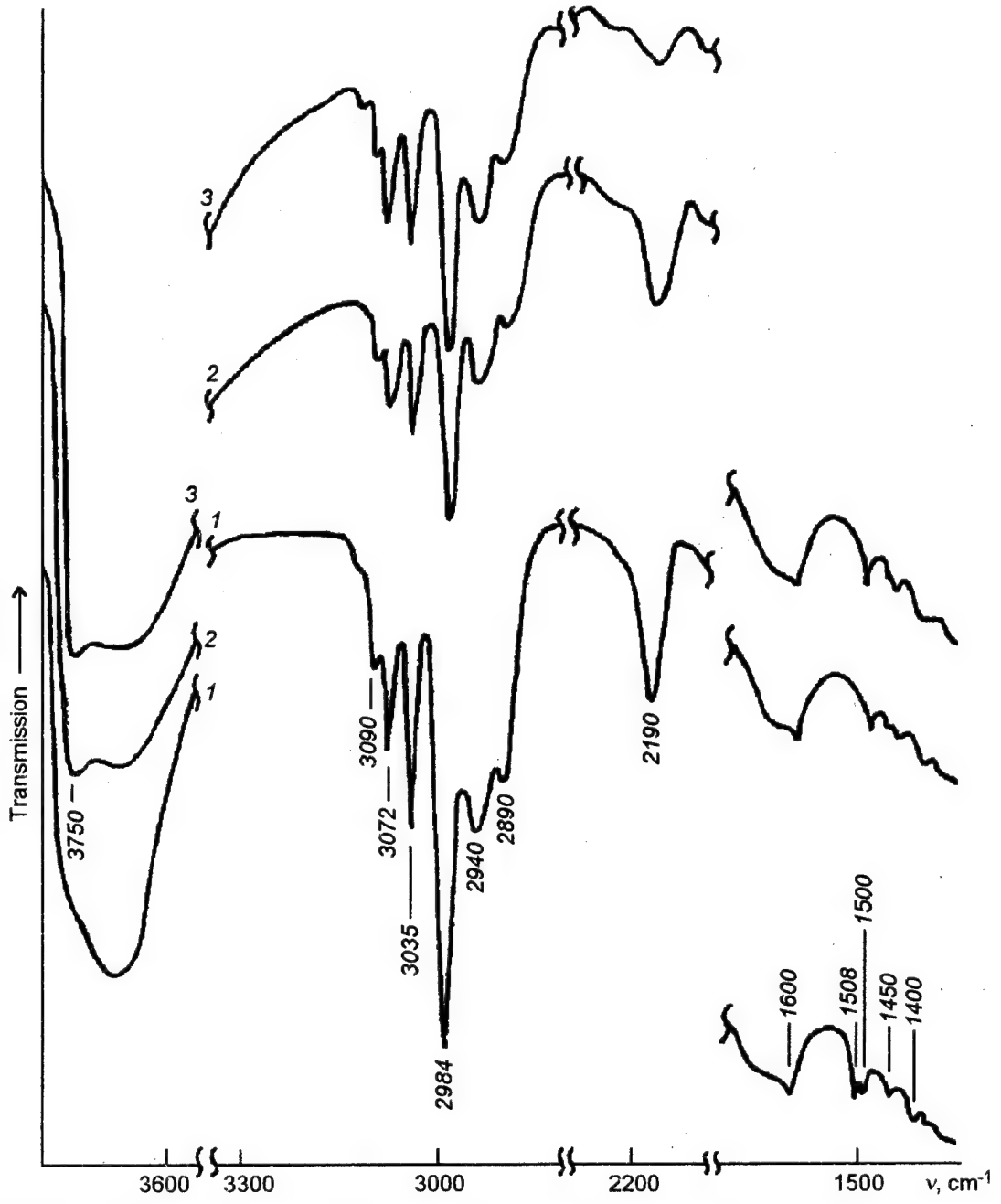

Fig.2. IR spectra: silica after modification by styrene in the presence of hydroquinone, washing by boiling acetone for 2 h (1); after washing by boiling water for 1 h and 2 h with subsequent drying in vacuum at 300 °C for 2 h (2,3).

action on the modified silica for 2 h and subsequent vacuum treatment, the IR spectrum of the material in the range 3000-2850 cm^{-1} remained substantially unchanged. This fact indicates that the formation of oxy-*iso*-propyl groups on the silica surface as a result of side reactions can be substantially ruled out by the appropriate control of the reactants addition sequence and reaction conditions.

By analogy with the homogeneous reaction [23], the interaction of the silica hydride with styrene was studied in the presence of a polymerization inhibitor (as the inhibitor, the benzoquinone was served which forms due to hydroquinone oxydation by air oxygen during the storage and in

the course of the reaction [8]). In this case, the styrene grafting to the silica surface was also observed. It was shown, by separate experiments, that the boiling of the silica hydride in the 30 % *iso*-propanolic hydroquinone solution does not result in any intensity changes of the Si—H bonds absorption band. Thus, the intensity loss of the Si—H groups band in the course of the modification is to be assigned to the interaction with styrene. This permits to calculate the fraction of Si—H groups reacted with styrene. The conversion degree value with and without presence of hydroquinone appeared to be substantially the same.

The absorption band 1508 cm^{-1} in the IR spectrum of modified silica (Fig.2, curve 1) indicates the presence of hydroquinone on its surface (the other hydroquinone adsorption bands are hided by the phenylethyl fragments absorption). The intensity of that band does not changed when IR spectra are recorded after the specimen washing by the boiling acetone or *iso*-propanol for 2 h, the solvent being changed three times. Yet, the 1508 cm^{-1} band is substantially vanished after the washing of the specimen by distilled water in the Soxhlet apparatus for 1 h (Fig.2, curve 2). Simultaneously, the hydrolysis of Si—Cl and Si—H groups occurs, what is seen from intensity decrease of the 2190 cm^{-1} absorption band near 3750 cm^{-1}. Without a catalyst, the Si—H bonds hydrolysis does not take place. The anomalously high hydrolysis rate of Si—H bonds is due perhaps to the catalytic effect of acids [24], in this case, of hydrochloric one, formed as result of bonds hydrolysis, and of platinum hydrochloric one, which was adsorbed, in the trace amounts, on the silica surface. After the repeated specimen washing by water in the Soxhlet apparatus for 2 h, the further intensity increase of the Si—OH group band (at 3750 cm^{-1}) and decrease of the intensity of Si—H absorption band occur. Other parts of spectrum remained unchanged. This indicates that hydroquinone was fully removed from the silica surface during the first water washing (for 1 h). The fraction of remaining groups amounts 3.8-4.0 % from the initial one.

The possibility of the polystyrene formation grafted to the silica surface [25,26], as a result of a side reaction, in the course of solid-phase styrene hydrosilylation, requires to be discussed separately. In the IR spectra of modified silicas, the absorption bands 2856 and 2924 cm^{-1} do not observed, in contrast to the high intensity of these bands in polystyrene spectrum. Both these bands are very characteristic for the polystyrene [9,13]. Moreover, the intensities ratio of absorption bands in the 3000-2850 cm^{-1} range is substantially identical for the IR spectra of specimens modified with (Fig.2, curve 1) and without (Fig.2, curve 4) the presence of a polymerization inhibitor. This indicates that, in both cases, there is no significant polymer amount on the silica surface. This can be assigned to the inhibiting effect of the colloidal platinum forming in the Speier catalyst [19,20] upon styrene polymerization [27].

If silica is vacuum treated at 400 °C for 3 h, then exposed, in the presence of Speier catalyst, with styrene at 100 °C for 3 h, next washed by CCl_4 in a Soxhlet apparatus for 1 h and vacuum dried at 300 °C for 2 h, then, in its IR spectrum, wery weak bands in the 3150-3000 cm^{-1} range are observed. These bands should be assigned likely to the polystyrene located on the silica surface. The polystyrene amount calculated from the optical density of the 3035 cm^{-1} band, is 1.5 to 2 per cent of the phenylethyl radicals content in the modified silica. Thermogravimetric analysis gives a value of 3.4 %. The scatter of values is due, to obviously, to the error of optical density measuring for very low-intensity bands. These results point out that, in the process of solid-phase styrene hydrosilylation, polystyrene grafted to the silica surface do not form in substantial amounts.

References

1. A.V.Simurov, L.A.Belyakova, Abstracts of Reports of 2nd School-Seminar on the Surface Chemistry of Dispersed Solids [in Russian], Slavsko (1989).
2. V.A.Tertykh, L.A.Belyakova, A.V.Simurov, *Zhurn.Fiz.Khim.*, **64**, 1410 (1990).
3. V.A.Tertykh, L.A.Belyakova, A.V.Simurov, *Dokl. AN SSSR*, **318**, 647 (1991).
4. V.A.Tertykh, L.A.Belyakova, A.V.Simurov, *Mendeleev Commun.*, No.2, 46 (1992).
5. L.A.Belyakova, A.V.Simurov, D.Yu.Lyashenko, V.A.Tertykh, *Ukr.Khim.Zhurn.*, **58**, 630 (1992).
6. E.Ya.Lukewits, *Usp.Khimii*, **46**, 507 (1977).
7. G.V.Myasoedova, S.B.Savvin, Chelate-Forming Sorbents [in Russian], Nauka, Moscow (1984).
8. V.V.Korshak, High-Molecular Organic Chemistry Methods [in Russian], AN SSSR Edition, Moscow (1953), vol.1.
9. C.J.Pouchert, The Aldrich Library of FT-IR Spectra, Aldrich Chem, Milwaukee, WI (1985), p.p.4800.
10. A.A.Chuyko, V.A.Tertykh, V.A.Khranovsky et al., *Teoreticheskaya i eksperimental'naya khimiya*, **66**, 247 (1966).
11. P.M.Wainstein, S.I.Kol'tsov, Yu.K.Ezhovsky et al., *Zhurn.Fiz.Khim.*, **57**, 1728 (1983).
12. N.A.Chumayevsky, Vibrational Spectra of the Elemento-Organic Compounds of IVB and VB Group Elements [in Russian], Nauka, Moscow (1971).
13. K.Nakanishi, Infrared Absorbtion Spectroscopy, Practical Holding-Day, San Francisco and Nankodo Company Ltd., Tokyo (1962).

determined by elemental analysis and potentiometric titration [8,9].

The standard beryllium sulphate solution with the concentration C_{Be}=1 mg/cm^3 was prepared according to [10]. The working solutions of minor concentrations were prepared immediately before use by the dilution of the initial one. The copper, cobalt, nickel, iron, aluminium, calcium, magnesium, lead, manganese and cadmium nitrates were prepared by dissolution of corresponding weighted amounts of metal salts ("pure for analysis" grade) in distilled water [10]. The required pH values of solutions were established by the introducing of 0.1 M hydrochloric acid or 0.1 M sodium hydroxide. The pH values were measured by means of EV-74 ionometer.

The recovery of berylium ions was performed in the dynamic condition. In this case, the solution under study was passed through a column filled with sorbent by means of a peristaltic pump (the sorbent mass was 0.3 g, layer height 10 mm, column diameter 5 mm, the rate of passage 7 to 10 cm^3/min).

The dependence of beryllium desorption from the sorbent phase on the medium acidity was studied in the dynamic regime, too, by passing the hydrochloric acid solution with concenrations of $1\cdot10^{-4}$ to $1\cdot10^{-2}$ mol/dm^3 through the column. For the analysis, the eluate portions of 1 cm^3 volume each were sampled.

The beryllium content in the column eluate was determined with two independent methods: atomic absorption, on the CPQ-800 of Pye-Unicam (N_2O-acetylene flame, the radiation source being the hollow-catode lamp with beryllium) and photometry (after the reaction with the Chromazurol S, CAZ, in presence of a non-ionic surface-active agent, SAA) on the Specol-11 spectrophotometer.

As stated previously [8,9], the beryllium ions are sorbed quantitatively on APA-SiO_2 at pH $\geq$ 4.3. Therewith, if the sorbent capacity exceeds the total beryllium amount in solution, the sorption process obeys to Henry law. Distribution coefficients are constant throughout this area and achieve to values of 10^5 cm^3/g. Therefore, the beryllium ions concentration in the dynamic regime was performed at pH 4.5. The results of the study of the berillium concentration on the APA-SiO_2 in the Henry range are presented in Table 1. They show that, in the experiment conditions, the quantitative extraction of the element from the solution is achieved regardless of its volume. The difference between the initial beryllium content in solution and that found

Table 1. Results of beryllium concentration on the silica gel with grafted aminophosphonic acid groups from different volumes of solution to be analysed (m=0.3 g, pH=4.5, n=3, eluent 0.01 M HCl, V_{el}=5 cm^3)

Volume of solution under analysis, dm^3	Method of Be determination in eluate	Introduced Be, μg	Found Be, μg	S_r	Desorption degree, %	Concentration coefficient
0.2	Photometric	1.0	1.00	0.01	100	40
0.5	Photometric	1.0	0.99	0.02	99	99
1.0	Photometric	1.0	0.97	0.02	97	194
1.0	Photometric	0.5	0.48	0.03	96	192
1.0	Photometric	0.2	0.18	0.05	90	180
2.0	Photometric	0.5	0.47	0.06	94	376
2.0	Photometric	0.3	0.28	0.09	93	372
0.5	Atomic absorption spectroscopy	0.2	0.20	0.01	100	100
1.0	Atomic absorption spectroscopy	0.2	0.20	0.02	100	200
1.0	Atomic absorption spectroscopy	0.1	0.09	0.05	90	180
2.0	Atomic absorption spectroscopy	0.4	0.39	0.04	98	390
2.0	Atomic absorption spectroscopy	0.2	0.17	0.07	85	340

in column eluate indicates that, after the sorbent contact with the solution under investigation, the beryllium content drops to the values less of the MPC at least by an order of magnitude. This fact is the evidence of the sorbent high effectivity in the concentration as well as in water purifying for the removal of that high-toxic element.

As is seen from Table 1, the sorption-desorption cycle does not cause the sorbent efficiency lowering and indicates to the reversibility of the absorption process.

For the quantitative desorption of ≤2 μg of beryllium, 3 cm^3 of 0.01 H HCl solution are found to be sufficient. The concentration coefficients, in these conditions, have values of $(1...3)\times10^2$ (see Table 1).

The alkali metals cations and chloride, sulphate, nitrate and acetate ions when present in the solution in concentrations not exceeding 1 mol/dm^3, are established to do not influence the degree of beryllium extraction on APA-SiO_2.

The presence of complexing agents such as EDTA, oxalic acid, and ascorbic acid ($C \le 0.05$ mol/dm^3) does not hinder the quantitative beryllium recovery by means of APA-SiO_2. The aforesaid makes the evidence of the formation of a strong complex of beryllium with aminophosphonic acid groups bonded to the carrier surface, the stability of this complex exceeds that of the beryllium complexes with the complexing agents mentioned in solution.

The specifity of the grafted aminophosphonic groups reaction with beryllium ions allows for the selective concentration of that high-toxic element in the presence of great excesses (up to 10^4 times) such *s*-, *p*-, and *d*-metals as calcium, magnium, strontium, zink, cadmium, lead, copper, nickel, manganese, and tin.

In conditions optimal to concentrate beryllium on APA-SiO_2, the sorbent is found to remove from solution aluminium and iron (III) ions as well. It was established, however, that the masking of these elements with the EDTA solution (0.02 mol/dm^3) allows for the selective beryllium concentration in the presence of great excess (to 10^4 times) of metals mentioned.

On the basis of the research results, the procedure involving beryllium ions preconcentration and subsequent atomic absorption or photometric determination has been proposed. This procedure has been worked out on the model solutions containing aluminium, iron, nickel, alkali and alkali-earth metals; method was tested also in the analysis of waste waters. The results obtained are presented in Tables 2 and 3. To estimate the validity of the method proposed, the beryllium content in the samples was determined in parallel by the methodof additions. The data shown in the tables bear out the sufficient accuracy and reproducibility of the proposed procedure which allows to perform the determination of beryllium ions at concentrations on the level of MPC and lower.

Table 2. Results of beryllium determination in a model solution containing (mg/dm^3): Fe 2.0; Al 0.5; Cu 1.0; Ni 1.0; Sn 1.0; Mn 1.0; alkaly-earth metals 2.0 (V=1 dm^3, n=3,P=0.95)

Method of beryllium determination in eluate	Introduced Be, μg	Found Be, μg/dm^3	S_r
Photometric	2.00	2.00±0.02	<0.01
Photometric	1.00	0.99±0.02	0.01
Photometric	0.50	0.48±0.03	0.03
Photometric	0.20	0.17±0.05	0.12
Atomic absorption spectroscopy	1.00	1.00±0.01	<0.01
Atomic absorption spectroscopy	0.50	0.48±0.01	0.01
Atomic absorption spectroscopy	0.20	0.18±0.02	0.04

Thus, APA-SiO_2 sorbent can be used to concentrate the trace amounts of beryllium from solutions having complex composition. The preconcentration of beryllium with APA-SiO_2 allows to reduce the detection limits (DL) for this element at its determination in the concentrate by atomic absorption (DL=$8\cdot10^{-5}$ μg/cm^3) or by photometry (DL=$5\cdot10^{-5}$ μg/cm^3 after reaction with Chromazurol S in the presence of OP-7) by two decimal orders.

Analytical procedure

To 1 dm^3 of wastewater add 20 cm^3 of sulphuric acid (1:1) and boil for 10 min. After cooling filtrate the solution, add 20 cm^3 1 M EDTA, then 0.1 M sodium hydroxide to pH 4.5 and pass through the column filled by APA-SiO_2 (prewashed with 0.02 M EDTA and HCl solution with pH 4.5) by means of a peristaltic pump with a rate of 7 to 10 cm^3/min. Then, wash the column with 10 cm^3 of 0.02 M EDTA solution and 5 cm^3 of 0.01 M hydrochloric acid solution. Determine the beryllium content in the aluate using atomic absorption or photometric method.

Table 3. Results of beryllium determination in industrial wastewaters

Sample	Method of beryllium determination in eluate	Introduced Be, μg	Founded Be, μg/dm^3	Be content in wastewater, μg/dm^3
1	Atomic absorption spectroscopy	-	0.48±0.03	0.48±0.03 (S_r=0.03)
		1.00 0.50	1.51±0.03 1.00±0.02	0.51±0.01 (S_r=0.03)
	Photometric	-	0.49±0.03	0.49±0.03 (S_r=0.04)
		1.00 2.00	1.51±0.03 2.53±0.05	0.52X0.01 (S_r=0.03)
2	Atomic absorption spectroscopy	-	0.21±0.06	0.21±0.06 (S_r=0.11)
		1.00 0.50	1.24±0.02 0.73±0.02	0.24±0.01 (S_r=0.04)
3	Atomic absorption spectroscopy	-	0.37±0.04	0.37±0.04 (S_r=0.04)
		1.00 0.50	1.38±0.02 0.87±0.02	0.38±0.01 (S_r=0.02)
4	Atomic absorption spectroscopy	-	0.10±0.05	0.10±0.05 (S_r=0.18)
		1.00 0.50	1.14±0.02 0.61±0.02	0.12±0.02 (S_r=0.12)

Atomic absorption is to be measured at λ=234.9 nm, slot spectral width 0.2 mm, the lamp operating current 12 mA.

To determine beryllium by the photometric method, neutralize the eluate at continuous mixing with 5 to 10 per cent ammonia solution to pH 4-5, add to the mixture 1 ml of $1\cdot10^{-3}$ M CAZ solution, 1 ml of $1\cdot10^{-3}$M OP-7 solution, 0.5 ml of $5\cdot10^{-2}$ M EDTA solution and bring the volume to 10 ml with acetate buffer solution having pH 6.0. After 15 min, perform the photometric measurements at λ=630 nm, l=10 mm.

In parallel, perform the blank experiment using all the reagents and sorbent.

References

1. V.Yu.Novikov, K.O.Lastochkina, Z.N.Boldina, Method for Determination of Harmful Substances in Water Bodies [in Russian], Medizina, Moscow (1981).
2. A.V.Novoselova, L.R.Batsanova, Analytical Chemistry of Beryllium [in Russian], Nauka, Moscow (1966).
3. A.Mizuike, Enrichment Techniques for Inorganic Trace Analysis, Springer Verlag (1983).
4. N.M.Kuz'min, Yu.A.Zolotov, Trace Elements Concentration [in Russian], Nauka, Moscow (1988).
5. M.Marhol, Ion Exchangers in Analytical Chemistry, Their Properties and Use in Inorganic Chemistry, Academia, Prague (1982).
6. I.A.Tarkovskaya, Oxidized Coal [in Russian], Naukova dumka, Kiev (1981).
7. Modified Silicas in Sorption, Catalysis and Chromatography [in Russian], Ed. by G.V.Lisichkin, Khimia, Moscow (1986).
8. USSR Pat. 1773475, Cl. B01D15/08.
9. G.N.Zaitseva, O.P.Ryabushko, *Ukr.Khim.Zhurn.*, **58**, 965 (1992).
10. P.P.Korostylev, Preparation of Solutions for Chemical Analysis [in Russian], Nauka, Moscow (1974).
11. S.B.Savvin, R.K.Chernova, L.N.Kudryavtseva, *Zhurn.Anal.Khim.*, **34**, 66 (1979).

Кремнезем с ковалентно закрепленными группами аминофосфоновой кислоты для концентрирования ионов бериллия

Г.Н.Зайцева, О.П.Рябушко , О.Н.Желиба , В.В.Стрелко, С.А.Хайнаков

Предложен метод сорбционного концентрирования бериллия, основанный на извлечении элемента из водных растворов с помощью аминофосфоновой кислоты, ковалентно закрепленной на поверхности силикагеля, с последующим определением бериллия в элюате атомно-адсорбционным либо фотометрическим (по реакции с хромазуролом S в присутствии ОП-10) методом. Метод дает возможность снизить пределы обнаружения бериллия на два порядка. Специфичность реакции закрепленных групп аминофосфоновой кислоты с ионами бериллия позволяет проводить селективное концентрирование этого элемента в присутствии 10^4 кратных избытков многих *s*-, *p*- и *d*-металлов. Метод тестирован при анализе сточных вод.

Functional Materials 2, No.1 (1995)

Copper (II) complexes on silica surfaces with covalently bonded methylamino and ethylenediamino silanes

V.N.Zaitsev, V.D.Oleynyk, V.V.Skopenko and V.V.Antoschuk

T.Shevchenko Kiev University, 64 Vladimirskaya St., 252017 Kiev, Ukraine

By chemical modifying of fumed silica surface the materials with covalently bonded (N-methylamino)propyl and (N-aminoethyl)-aminopropyl (En-AS) silanes have been prepared. Interaction of bonded ligands with CH_3CN solution of $Cu(BF_4)_2$ has been studied. By physico-chemical analysis, ESR, FTIR and UV-VIS spectra, formation of complexes such as CuL_2 (where L is bonded ligands) with axial-elongated (for En-AS) stereochemistry and $g_\perp$=2.01, $g_\parallel$=2.21 has been proved. It was found that thermal tratment increase tetrahedral distorsion of coordination polyhedral.

Шляхом хімічного модифікування поверхні непористого аморфного диоксиду кремнію отримано матеріали з ковалентно закріпленими групами N-метиламінопропіл і N-(аміноетил)-амінопропіл (En-AS) силанами. Вивчено взамодію закріплених лігандів з ацетонітрильним розчином $Cu(BF_4)_2$. За даними фізико-хімічного аналізу, спектроскопії ЕПР, ІЧ з Фур'є-перетворенням та електронної спектроскопії дифузійного відбиття встановлено утворення комплексів складу CuL_2 (де L — прищеплений ліганд), що мають у випадку En-AS аксіально-витягнутий координаційний поліедр з $g_\perp$=2.01 та $g_\parallel$=2.21. Термічна обробка приводить до підсилення тетраедричного викривлення координаційного вузла.

Silicas chemically modified with covalently bonded organic ligands are used in the modern biotechnology and pharmaceutics, as stationary phases for the ligand-exchange chromatography, for the separation of optical isomers [1,2], bio-active substances [3], etc. Their use is based on the ability of fixed ligands to form a mixed-ligand complex compounds according to scheme

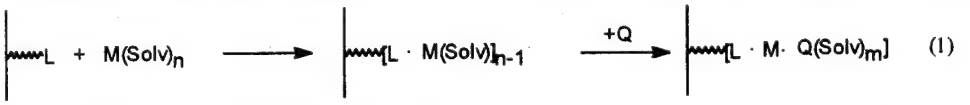

(1)

where M is a metal ion, usually Cu^{2+}; Q, an analyte to be separated. Scheme (1) is simplified since metal ions and grafted ligands are assumed to form a complex with 1:1 composition. In fact, the surface complexes can contain up to 3 fixed ligands [4]. It is easy to see that this fact affects significantly the ligand-exchange ability of the material. The stationary phases containing bidentate grafted ligands are usually unsuitable for the ligand-exchange chromatography, if a complex of M:L=1:2 composition is formed on the surface. In this case, the metal coordination sphere is saturated (the coordination number for copper is 4), and the substance to be separated does not interact chemically with the surface to give the mixed ligand complex according to scheme (1). And conversely, the fixed complex with equimolar composition is the best suited one for chromatographic purposes. Hence, the effective use of silicas with chemically modified surface in the ligand-exchange chromatography is only possible under the condition that composition, stability, and structure of the surface complexes are comprehensively studied.

Ligands fixed on the amino propyl silica surface are known to form copper complexes mainly of ML_2 composition. Moreover, that composition does not change if the concentration of the grafted groups is varied [5]. This fact, in particular has allowed, to suggest the cluster-like distribution of amino groups bonded to a silica surface [6].

In this work, an attempt is made to trace the influence of hydrophilic and hydrophobic substituents on the composition and structure of complexes formed on the amino silicas surfaces in the course of interaction with acetonitrile solution of copper (II) tetrafluorborate and, by this means, to clarify the influence of such substituents on the character of groups distribution over the support surface. Two substances related to amino silicas were studied with general formula

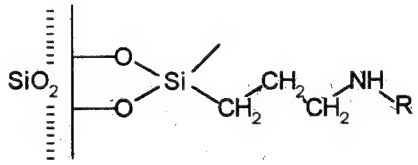

where R=CH_3 and $CH_2CH_2NH_2$.

The methyl group at the nitrogen atom causes the increase of its basicity but reduce the hydrophility. The aminoethyl group rises both the basicity and the hydrophility.

The composition and structure of complexes were studied by means of the chemical equilibrium data, as well as by electron diffuse reflection, IR and ESR spectroscopies of fixed complexes.

Experimental

The water-free acetonitrile was obtained with the distillation of "pure" grade solvent over P_2O_5 and CaH_2. Toluene was distilled over Na. (N-methylamino)propyl triethoxy silane obtained from ***Merck*** and (N-ethylamino)aminopropyl triethoxy silane from ***Fluka*** were purified by the vacuum distillation before use.

IR spectra of compounds were recorded in the 1200-4000 cm^{-1} range on the UR 10 spectrometer. IR spectra with Fourier transformation in the 400-4000 cm^{-1} range at 0-2 smoothing cycles were taken on the FTIR 171 ***Perkin-Elmer***. spectrometer. The specimens were prepared as thin pressed tablets. Silica gels and silochroms were grinded in an agate mortar before pressing.

Elemental analyses (H, C, N) were made by the service group of London University. The bonded groups concentration was calculated from the analytical data according to formula

$$C_L^{(mmol/g)} = \frac{\% \cdot 10^3}{100 \cdot n \cdot M}$$

where % is the per cent content of the element determinated; n is the element atoms number in the immobilized molecule; M is the element molar mass.

The copper (II) tetrafluorborate was prepared from the basic copper carbonate by action with 70 per cent HBF_4. The acetonitrile solvate $Cu(BF_4)_2$ was recovered from hexahydrate by dissolution of 5 g of crude salt in 50 cm^3 of acetonitrile. Then, benzene was added to the solution (20 cm^3 to 50 cm^3 of soln.) and the triple azeotrope acetonitrile-benzene-water was distilled out (Bp. 66 °C). The residue was cooled and the $Cu(BF_4)_2(CH_3CN)_4(H_2O)_2$ crystals were separated by filtration. The product was recrystallized from acetonitrile : ethylacetate (1:4) mixture and dried in vacuum. The chemical composition was checked by means of copper analysis.

The equilibrium studies and the synthesis of mixed complexes were performed by bringing the $Cu(BF_4)_2$ acetonitrile solution into contact with chemically modified silica (CMS). Therewith, the metal concentration in the solution was varied from 1 to 20 mmol/dm^3 while the CMS weight was kept constant (0.25 g and 0.2 g for $NHCH_3$-AS and En-AS, respectively). After mixing in sealed vessels for 1 h, the solid phase was separated by centrifugation, the solution being checked for the metal presence by trilonometric titration. Before study the structure and composition of fixed complexes, the products were dried in air at 50 °C and in vacuum at 110 °C over P_2O_5 for 24 h.

Synthesis of chemically modified silicas

To obtain silicas with chemically modified nature of surface and monolayer of covalently bonded groups, the modification was performed in the water-free toluene. To this purpose, fumed silica-aerosil A-200 (Degussa, Germany) was used after activation at 550 °C for 8 hours. The (N-methylamino)propyl triethoxy silane was immobilized on the aerosil surface according to following scheme (2):

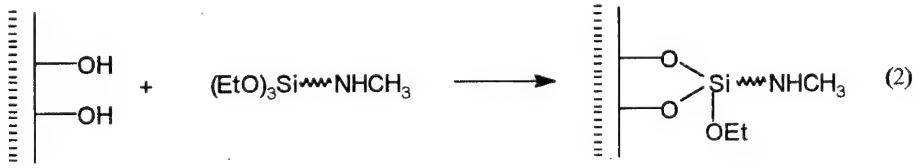

(2)

To this end, to 17 g of aerosil ($1.7 \cdot 10^{-3}$ mol SiOH groups) in 200 cm^3 of toluene, the solution containing 3.28 g ($1.6 \cdot 10^{-3}$ mol) of ethylamino propyl triethoxy silane in toluene was added. The reaction mixture was heated at 100 °C under mixing for 10 h. Then, the solid phase was separated by filtration and washed with toluene in a Soxhlet apparatus to remove the excess of modifying agent. The washing completeness was checked by the reaction of the washing solution with bindone [7]. The chemically modified silica was dried in vacuum (10^{-2} Torr) for 3 h at room temperature and 7 h at 110 °C.

IR spectroscopy and chemical analysis data were used to control the chemical modification of the silica surface. According to the elemental analysis results, the concentration of anchored methylamino groups is $5.3 \cdot 10^{-4}$ mol/g.

The synthesis of ethylenediamino aerosil (En-AS) was performed similarly to that of CH_3NH-AS according to scheme (3):

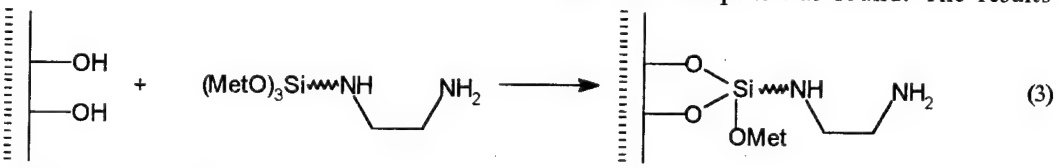

(3)

Silane (1 g, $2.5 \cdot 10^{-4}$ mol) was used to modify 16 g ($1.6 \cdot 10^{-3}$ mol of SiOH groups) of the aerosil. The bonded groups concentration as determined from the elemental analysis data was 0.26 mmol/g. The potentiometric pH titration gave 0.29 mmol/g.

Results and discussion

After silanes immobilisation, in the IR spectra of silicas, the absorption band at 3750 cm^{-1}, related to stretching vibrations of isolated OH groups on the SiO_2 surface, disappears; the bands arise indicating the presence of alkyl and amino groups (Table 1).

The character of the IR spectrum changes bears out that the covalent immobilisation of aminosilanes on the silica surface occurs, according to schemes (2) and (3).

The reaction of $Cu(BF_4)_2$ with ligands attached to aerosil surface can be described by the equation

$$SiO_2 \sim NHR + Cu^{2+} \rightleftharpoons [SiO_2 \sim NHR]_n Cu^{2+},\ n=1\text{-}3$$

where R=CH_3 for CH_3NH-AS, or $CH_2CH_2NH_2$ for En-AS.

Table 1. The main characteristic frequencies in the IR spectra of fixed complexes and ligands

The compound fixed	νNH, cm^{-1}	νCH_2, cm^{-1}	σNH_2, cm^{-1}	σCH_3, cm^{-1}
CH_3NH-Ac	3317	2946, 2880, 2850, 2808	-	1473
CH_3NH-Ac-Cu	3220	2946, 2880, 2850, 2808	1620	1470
En-Ac	3378, 3309	2946, 2880	1650	-
En-Ac-Cu	3340, 3280	2946, 2880	1650	-

The complex formation causes the copper ions chemisorption from the solution. From the value of difference between the introduced metal amount and that determined in the solution after adsorption, the average metal-to-ligand ratio in the fixed complex was found. The results obtained are given in Tables 2 and 3.

Consideration of sorption isotherms plotted using the data of Tables 2 and 3 shows that the complex of M:L=1:2 composition is formed on the surface of CH_3NH-AS and En-AS. In the case of En-AS with grafted bidentate ligand (ethylenediamine) fixed on its surface, such a ratio leads to the conclusion that a complex is formed with the CuN_4 chromophore, while for CH_3NH-AS, with CuN_2 one.

It is established from IR spectra of complexes recovered at 50 °C that the solvent is not included into the inner coordination sphere, nor is it adsorbed on the silica (the stretching vibration band of CN group is absent). Therefore, to adjust the co-ordination sphere composition for the complexes recovered as well as their structure, the EDR and ESR spectra were considerated.

Fig.1 shows that the ESR spectra of En-AS complexes with $Cu(BF_4)_2$ are characterized by the unusually high resolution for fixed complexes; this allowed to determine the spin-hamiltonian characteristics ($g_\perp$ and $g_\parallel$).

It is found that the ESR spectrum is of axial type, and the $g_\parallel$ value indicates that the octahedric structure of the complex is deformed (see Table 4). Of importance is the fact that the g-factors value do not

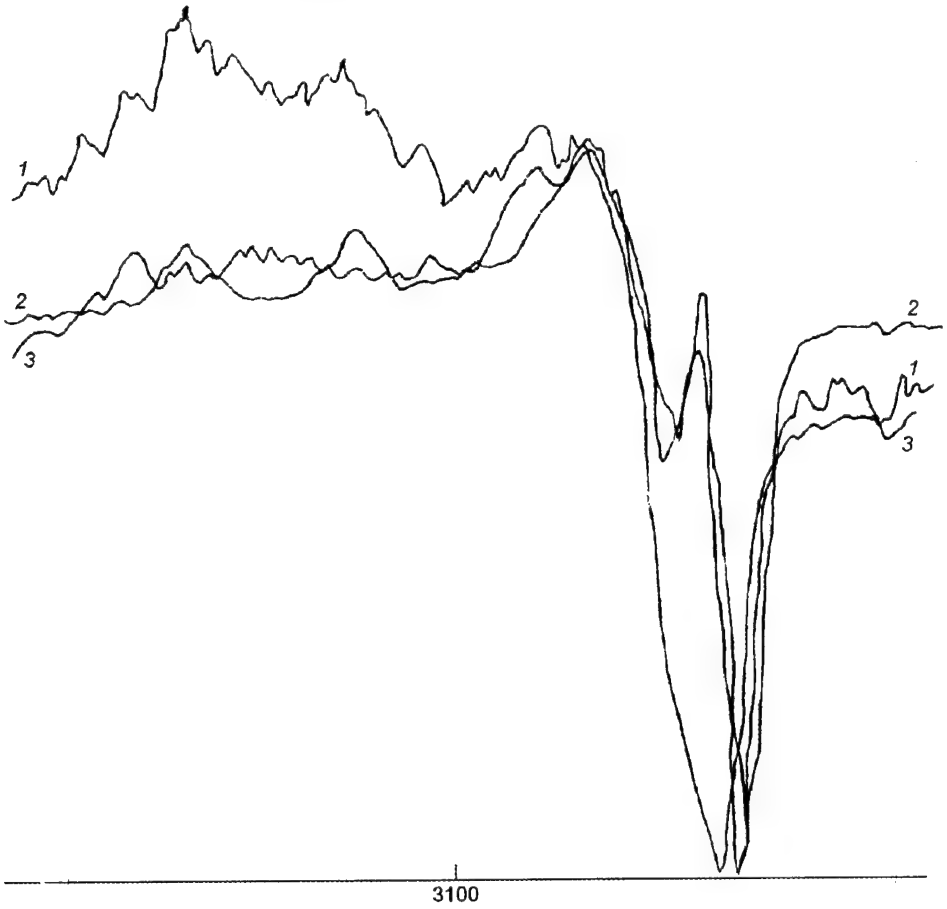

Fig.1. ESR spectra of $Cu(BF_4)_2$ complexes with En-AS (1,2) and CH_3NH-AS (3) recovered from CH_3CN at L:M ratio: 1) 41.6; 2) 20.8; 3) 8.5.

Table 2. The adsorption isotherm of $Cu(BF_4)_2$ on CH_3NH-AS (C_L = 530 μmol/g). V = 25 cm^3, m = 0.25 g, C_{Cu} = 12.5 mmol/dm^3.

Cu added		Cu concentration in solution after adsorption, mmol/dm^3	molar ratio M:L on the silica surface
N, mmol/dm^3	molar ratio $[M]_{sol}$:L		
0.52	0.049	0.4	0.011
1.04	0.098	0.6	0.041
1.76	0.166	1.1	0.062
2.11	0.199	1.2	0.085
2.64	0.249	1.4	0.117
5.28	0.498	2.5	0.262
5	0.471	2.4	0.245
7.5	0.707	3.9	0.339
10	0.943	5.8	0.396

Table 3. The adsorption isotherm of $Cu(BF_4)_2$ on EP-AS (C_L = 260 μmol/g). V = 25 cm^3, m = 0.2 g, C_{Cu} = 12.5 mmol/dm^3.

Cu added		Cu concentration in solution after adsorption, mmol/dm^3	molar ratio M:L on the silica surface
N, mmol/dm^3	molar ratio $[M]_{sol}$:L		
0.1	0.024	0	0.024
0.7	0.168	0.5	0.048
1	0.240	0.8	0.048
2	0.480	1.2	0.192
5	1.201	3.5	0.380
7.5	1.802	5.8	0.440
10	2.403	8.3	0.434

change when the average M:L ratio increases. This fact gives the evidence that, in the experimental conditions, the complex of only one composition is formed. The comparison of results obtained from the sorption isotherms and calculations of *g*-factors shows that this complex is just the compound $Cu(En\text{-}AS)_2(BF_4)_2$. It can be supposed that $(BF_4)^-$ anion is not included in the inner coordination sphere, and a markedly stretched octaheder arises on the En-AS surface. This supposition is confirmed by the EDR spectra of complexes with the grafted ethylenediamine (Fig.2). The position of the *d-d* transition band in the electron spectrum of the ethylenediamine complex does not change when the M:L ratio is varied; only the band intensity increases. The absorption band of the fixed ethylenediamine complexes is positioned lower (17500 cm^{-1}) than that of similar individual ones (19000 cm^{-1} for $CuEn_2(BF_4)_2$). In our opinion, that indicates to an insignificant tetrahedric deformation of the foxed ligand as compared to their homogeneous analogs.

To consider the possibility of including surface silanol groups into the inner coordination sphere composition, we have studied the fixed complexes behaviour at heating to 110 °C. The results of *g*-factors measuring show that such conditions do not cause any essential changes of the co-ordination node. Only some increase of the tetrahonal distorsion is possible. Such changes can be due to strengthening of hydrogen bonds between the grafted ligands and silica and to lowering their mobility on the surface after physically adsorbed water is removed. The ESR spectra of the silica modified by methyl amino groups differ markedly from those of ethylenediamino silicas. The poor spectral resolution is observed regardless of the copper concentration on the surface (see Fig.1). The spin hamiltonian is found to have the axial character, the $g_\perp$ value (Table 4) indicates to a deformed octahedric structure, the deformation being substantially higher then in the case of En-AS. The poor spectrum quality can be the evidence of the mixture formation of co-ordi-

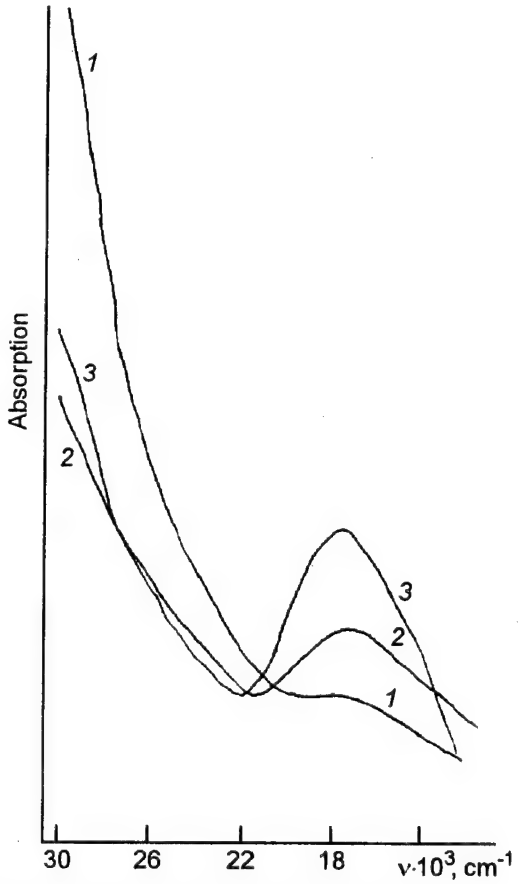

Fig.2. EDR spectra of $Cu(BF_4)_2$ complexes with En-AS at the average L:M ratio: 1) 41.6; 2) 20.8; 3) 5:2.

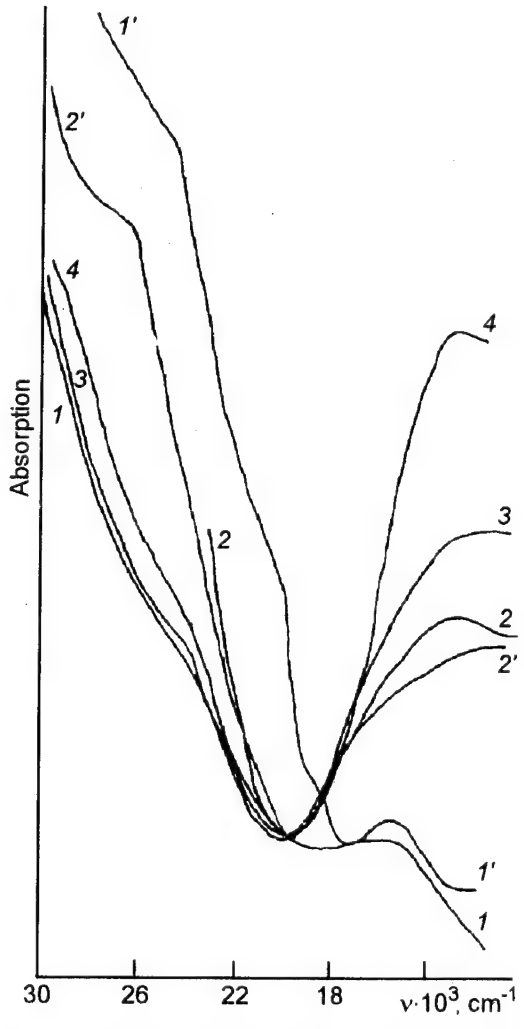

Fig.3. EDR spectra of $Cu(BF_4)_2$ complexes with CH_3NH-AS (3) recovered from CH_3CN without heating (1,2,3) and after the heat treatment (1',2') at L:M ratio: 1) 24.1; 2) 16.0; 3) 2.5.

Table 4. Spin-Hamiltonian parameters for the copper complexes with fixed ligands.

Treatment conditions	En-AS		CH_3NH-AS
	$g_\perp$	$g_\parallel$	$g_\perp$
50 °C	2.01	2.21	2.06
110 °C, vacuum	2.05	2.21	2.07

nation polyhedra on the surface even at 40-fold ligand excess. Therewith, the copper concentration increase causes only the smoothing of the spectrum in the $g_\parallel$ range but does not change the $g_\perp$ position ($g_\perp$=2.05).

In the EDR spectra of $Cu(BF_4)_2$ complexes with methylamino ligands fixed on the aerosil surface, one absorption band having the maximum in the range of 13800 cm^{-1} is observed; this band is common for the octahedric complex (Fig.3). The heating of samples to 110 °C to remove the solvent and water molecules from the coordination sphere results in significant spectral changes. The *d-d* transition band of the complex shifts toward long-wave region, and additional bands appear in the 20000 and 25000 cm^{-1} ranges. These facts can indicate to a partial formation of complexes having low coordination number (<4) on the CH_3NH-AS. The comparison of results of the copper ions sorption study, EDR and ESR spectra allows to suppose that, on the CH_3NH-AS surface, the complexes of $Cu(CH_3NH\text{-}AS)_2(BF_4)_2$ are prevailing, the inner coordination sphere of such complexes may be completed by the coordination of surface silanol groups or water molecules.

The fixed groups concentration on the En-AS is approximately half of that on the CH_3NH-AS, the former, however, is twice as dentate as the latter. Threfore, the donor nitrogen atoms density on the surface must be approximately the same for both silicas, if the fixed ligands are distributed uniformly. In spite of this fact, the substantial differences in the structure and composition of fixed complexes have been revealed. This points to the "isle-like" distribution of fixed groups on the silica surface.

References

1. V.A.Davankov, Ligand-Exchange Chromatography [in Russian], Mir, Moscow (1989).
2. Proc. of the 5-th International Symposium on Chiral Discrimination, September 25-28, 1994, Stockholm, Sweden.
3. Proc. of the 5-th International Symposium on Pharmaceutical and Biomedical Analysis, September 21-24, 1994, Stockholm, Sweden.
4. V.N.Zaitsev, Yu.V.Kholin, D.S.Konyaev, *Zhurn.Neorg.Khim.*, **38**, 1023 (1993).
5. N.D.Donskaya, V.N.Zaitsev, *Ukr.Khim.Zhurn.*, **58**, 972 (1992).
6. Yu.V.Kholin, V.N.Zaitsev, S.A.Mernyi, et al., *Ukr.Khim.Zhurn.*, **59** 910 (1993).
7. F.E.Critchfield, Organic Functional Group Analysis, Perfamon Press, Oxford-London-New York-Paris (1963).

Комплексы меди (II) на поверхности кремнеземов с ковалентно-закрепленными метиламино- и этилендиамино-силанами

В.М.Зайцев, В.Д.Олейник, В.В.Скопенко, В.В.Антощук

Путем химического модифицирования поверхности непористого аморфного диоксида кремния получены материалы с ковалентно закрепленными группами N-метиламинопропил и N-(аминоэтил)аминопропил (En-AS) силанами. Изучено взаимодействие закрепленных лигандов с ацетонитрильным раствором $Cu(BF_4)_2$. По данным физико-химического анализа, спектроскопии ЭПР, ИК с Фурье-преобразованием и электронной спектроскопии диффузного отражения установлено образование комплексов состава CuL_2 (где L - привитый лиганд), имеющий в случае En-AS аксиально-вытянутый координационный полиэдр с $g_\perp$=2.01 и $g_\parallel$=2.21. Термическая обработка приводит к усилению тетраэдрического искажения координационного узла.

Functional Materials **2**, No.1 (1995)

Two algorithms for estimating the energetic inhomogeneity of chemically modified silicas

Yu.V.Kholin and S.A.Merny

Kharkov State University, 4 Svobody Sq., 310077 Kharkov, Ukraine

Estimating of the energetic inhomogeneity of chemically modified silicas is based on solving a Fredholm integral equation of the first kind. The mathematical incorrectness of this problem, features of known methods for its solving is discussed and describe robust algorithms DAC1 and DAC2 are described. Constructing the algorithms, we have completely utilized the quantitative a priori information concerning the solution to be sought. The usefulness of the algorithms has been checked by their application to simulated and real data.

Оцінювання енергетичної неоднорідності хімічно модифікованих кремнеземів грунтується на розв'язанні інтегрального рівняння Фредгольма першого роду. В статті обговорюється математична некоректність вказаної задачі, особливості відомих методів її розв'язання і описуються чисельно стійкі алгоритми DAC1 і DAC2. Будуючи алгоритм, автор повністю використав кількісну апріорну інформацію про рішення, що його шукають. Працездатність алгоритмів перевірено при їх використанні для обробки модельних та реальних даних.

Introduction

Silicas with functional groups covalently bound to the adsorbent surface are known as chemically modified silicas. These materials are used as sorbents for separating metal ions and as supports for heterogeneous metal complex catalysts. To describe the ion sorption on modified silicas it is necessary to take into consideration specific features of grafted species compared to analogs in solutions [1—3]. In particular, the approaches which describe an energetic inhomogeneity of chemically modified silicas are needed.

The energetic inhomogeneity results from differences in topology and solvatation degree of grafted species, inhomogeneity of grafting, spread in pore sizes, etc. [4]. The phenomenon of energetic inhomogeneity manifests itself as variation of standard chemical potentials of grafted species having the same stoichiometric composition. The sorbent energetic inhomogeneity affects the character of ion adsorption isotherms on modified silicas. Hence, to investigate the energetic inhomogeneity one has to analyze the experimental adsorption isotherms.

Adsorption is the «integrated» quantity which describes the system from a macroscopic point of view. On the other hand, the energetic inhomogeneity is a microscopic concept. To connect the macroscopic adsorption and the microscopic energetic inhomogeneity one must apply models concerning the interactions on the adsorbent surface. In particular, it is necessary to know stoichiometric compositions of grafted species and to specify which chemical reactions on the surface take place.

In spite of the long history, the problem of estimating of the energetic inhomogeneity remains to be actual to the present day. This situation is caused by difficulties in a numerical calculation of inhomogeneity characteristics. The computational difficulties stem from the incorrect nature of the problem. The purpose of this paper is to investigate this problem as the mathematically incorrect one and on the basis of this analysis to propose fast and numerically stable algorithms for its solution.

Background

In this section, we deduce the equation which allows to study the energetic inhomogeneity of chemically modified silicas. We use a simple model of chemical interactions. The ion sorption is assumed to be caused by the only chemical reaction: M, the component of solution is fixed by the grafted group $\overline{Q}$ and forms the complex compound $\overline{MQ}$ grafted on the silica surface:

$$M + \overline{Q} = \overline{MQ}, \qquad (1)$$

for simplicity, the species charges in chemical formulae are omitted. Other reactions (including the side interactions) are neglected. In the case of an energetically homogeneous system, the equilibrium of reaction (1) is specified by the equilibrium constant, K:

$$[MQ] = K\,[M]\,[Q], \qquad (2)$$

from here on, the square brackets denote equilibrium concentrations. In the case of energetically inhomogeneous modified silicas, the standard chemical potentials of the grafted species $\overline{Q}$ or $\overline{MQ}$ can not be represented unambiguously. The standard chemical potentials are characterized by the sets of values $\{\mu^0_{\overline{Q}}\}$ and $\{\mu^0_{\overline{MQ}}\}$. Thus, unlike an energetically homogeneous system, the equilibrium of reaction (1) is described by a set of values $\{K_i\}$ rather then one of them. Let us denote the grafted groups with the constant K_i as $\overline{Q}_i$. Introduce the fraction of groups $\overline{Q}_i$

$$p(K_i) = t_{\overline{Q}_i}/t_{\overline{Q}}, \qquad (3)$$

were

$$t_{\overline{Q}_i} = [\overline{Q}_i] + [\overline{MQ}_i] = [\overline{Q}_i] + K_i[M][\overline{Q}_i] =$$

$$+ [\overline{Q}_i]\,(1 + K_i[M]), \qquad (4)$$

$t_{\overline{Q}_i}$ is the total (analytical) concentration of species $\overline{Q}_i$. Connect the fraction $p(K_i)$ with the adsorption isotherm parameters. For this purpose, consider the complex compound $\overline{MQ}$ formation degree:

$$f = \frac{[\overline{MQ}]}{[\overline{Q}] + [\overline{MQ}]} = \frac{[\overline{MQ}]}{t_{\overline{Q}_i}}$$

$$0 \le f \le 1. \qquad (5)$$

The f values are easy to calculate from the original experimental data:

$$f([M]) = \frac{t_M - [M]}{t_{\overline{Q}_i}} \qquad (6)$$

where t_M is the total (analytical) concentration of species M. Expression (6) gives f as the function of the measured equilibrium concentrations $[M]$. Note, that the f values are not exact because the original data (t_M, $t_{\overline{Q}_i}$ and $[M]$) are subject to experimental errors. Furthermore,the t_M, $t_{\overline{Q}_i}$ and $[M]$ values are measured only in some experimental points and, hence, the function f is specified by a table of values on the finite set of experimental points.

The equilibrium concentration $[\overline{MQ}]$ of grafted species $\overline{MQ}$ is the sum of concentrations of all species $\overline{MQ}_i$. Taking into account equation (4), one easily obtains:

$$[\overline{MQ}] = \sum_i K_i\,[M]\,\frac{t_{\overline{Q}_i}}{1 + K_i\,[M]}. \qquad (7)$$

After substitution of equation (7) for $[\overline{MQ}]$ into equation (5), the result is cast in the form:

$$f([M]) = \sum_i (t_{\overline{Q}_i}/t_{\overline{Q}}) \cdot \frac{K_i\,[M]}{1 + K_i\,[M]} =$$

$$= \sum_i p(K_i) \cdot \frac{K_i\,[M]}{1 + K_i\,[M]}. \qquad (8)$$

For practical applications, it is convenient to pass from a discrete function $p(K)$ to a continuous counterpart. Then

$$f([M]) = \int_0^\infty p(K) \cdot \frac{K\,[M]}{1 + K\,[M]}\,dK. \qquad (9)$$

The $p(K)$ is obviously a distribution function of grafted groups in equilibrium constants. It may be interpreted as a density of the probability distribution of equilibrium constants, with evident properties:

$$p(K) \ge 0; \quad \int_0^\infty p(K)\,dK = 1. \qquad (10)$$

Thus, integral equation (9) connects $p(K)$ and $f([M])$. It is a Fredholm integral equation of the first kind. Now it is necessary to find a way for solving it. This equation is mathematically identical to the Langmuir equation for gas adsorption on heterogeneous surfaces [4—7] and to equations describing the inhomogeneity of humic acids and protein substances [8—11].

Known methods for solving equation (9)

In this section we consider briefly discuss features of known methods and discuss why their application is undesirable in our problem.

It is possible to examine two ways for solving equation (9). The precise methods are based on integral transformations (such as Fourier, Laplace, Stieltjes and other ones [12]).This technique is applicable if the analytical expression for $f([M])$ is known. Unfortunately, the integral transformations are useful only for simulations. The unsuitability of these methods is due to the fact that an experimental function $f([M])$ is specified by a table of values rather than by an analytical expression.

The approximate methods are divided into two groups. The methods in which the exact expression $K[M]/(1+K[M])$ is replaced by approximate ones constitute the first group. Zeldowitch [13] and Roginskii [5] were the first to present this approach. Executing the replacement, the description of local isotherm by the Langmuir equation transforms into its description by other expressions. It is permissible in case of the physical adsorption because in the physical adsorption theory different isotherm equations (Langmuir, Freundlich, Ivanovic, Fouler—Guggenheim, etc. [4,6]) have the same physical sense and are almost interchangeable. If the chemical sorption without side interactions takes place (in particular, if hydrogen or metal ions are bound with groups grafted on the silica surface), there is only one suitable equation. It is the Langmuir isotherm equation which is in agreement with the mass action law. Hence, the replacement of the Langmuir isotherm equation by the others is undesirable from a physical point of view. And yet, methods of the first group do not provide obtaining precise solutions for $p(K)$ [4,14].

The approximate methods belonging to the second group are based on the square-law functional minimization:

$$U=\sum_j\left(f_j^{meas}-\int_0^\infty p(K)\frac{K[M]_j}{1+K[M]_j}dK\right)^2 \qquad (11)$$

where j is number of adsorption isotherm points.

Equation (9), a Fredholm integral equation of the first kind, is the typical example of the ill-posed problem. Its ill-posed nature leads to the existence of many different possible solutions for $p(K)$ which approximate the measured f values within the limits of experimental errors. That is why the classic numerical methods of optimization, which ignore this characteristic property of the problem, are numerically unstable.

To solve the problem and obtain the numerically stable algorithm, an additional a priori information about the searched function is needed.

The famous Russian mathematician Tikhonov was the first who proposed the methods for solving ill-posed (mathematically incorrect) problems. He introduced a concept of conveniently correct problems [15]. To reduce an incorrect problem to a conveniently correct one it is necessary to obtain a quantitative information that allows to choose one solution among many possible. For instance, the problem is conveniently correct if the information that narrows a set of possible solutions to a compact is accessible. The example of the compact is a set of non-decreasing functions bounded above and below. The solution of a conveniently correct problem is numerically stable on the compact.

If the desired quantitative information is not accessible, the problem falls into essentially incorrect problems [15]. To find its solution it is necessary to invoke a qualitative information about features of the searched function. Then, instead of functional (11), one should to minimize, in $p(K)$, the new criterion

$$U_\alpha = U+\alpha\cdot\Omega(p). \qquad (12)$$

where $\Omega(p)$ is a non-negative dampening function of $p(K)$, α is a positive parameter of regularization. The α-regularization method has been recently used to study the energetic inhomogeneity of sorbents [4,16]. To calculate $p(K)$, systems of linear algebraic equations were constructed and different versions of the regularized least square method accounting constraints (10) were used. But the reliable justification of the routine mathematical technique of α-regularization requires the comprehensive information on the character of the searched function (e.g., on the smoothness of $p(K)$) and on the errors of primary experimental data [15]. As it is usually absent, the α-regularization is believed to be the heuristic procedure. If the information, which allows to solve the problem as conveniently correct, is available, than the use of α-regularization is not a good practice.

The information on conditions (10) is not sufficient to narrow a set of possible solutions $p(K)$ to a compact. And yet, the integral distribution function $P(K)$, given by the expression

$$P(K)=\int_0^K p(x)\,dx, \qquad (13)$$

belongs to the compact set of restricted ($0\le P(K)\le 1$) and non-decreasing functions. Hence, a search for $p(K)$ is the essentially incorrect problem and a search for $P(K)$ is the conveniently correct one. The especially perfect algorithms for estimating an energetic inhomo-

geneity HILDA [17,18] and QA [14] are based on the Adamson and Ling method [6] and calculate the function $P(K)$ through its discretization on the compact. On the first step of those algorithms, the measured values of $f([M])$ are fitted by a function. Next, the function $P(K)$ is represented by the monotonically non-decreasing sequence of values $P(Ki)$, where K_i are equidistantly spaced arguments. The iterative improvement is accomplished to calculate $P(Ki)$ values which are in accordance with the fitted values of $f([M])$. Finally, the function $P(K)$ is numerically differentiated in respect to K to find $p(K)$. The algorithms HILDA and QA guarantee a numerical stability of computation of $P(Ki)$. And yet, there are two disadvantages of this class of algorithms. The first demerit is the iterative nature of calculating the $P(K_i)$ values. The second disadvantage is believed the evaluation of differential distribution functions $p(K)$ to be the particular step of the algorithms. As the smoothness of function $P(K)$ is not ensured by the algorithms under consideration, functions $p(K)$ may have discontinuities or spurious $p(K)$ peaks may easily arise.

In our mind, methods based on the $P(K)$ discretization on the compact can be improved.

Simplification of the discretization method — the algorithm DAC1

In this section we present the non-iterative algorithm DAC1 (Distribution of Affinity Constants-1) which calculates $P(K)$ on the compact.

We have to obtain, instead of equation (9), the appropriate equation in respect to $P(K)$. It may be received via integrating equation (9) by parts [18]:

$$\tau([M]) = 1 - f([M]) = \int_0^\infty P(K) \frac{[M]}{(1 + K[M])^2}\, dK. \quad (14)$$

It is convenient to change the variables in (14) and to pass from K and $[M]$ to their logarithms $\log_{10}K$ and $\log_{10}[M]$:

$$\tau(pM) = \int_{-\infty}^{\infty} Z(pM, \log_{10} K)\, d\log_{10} K, \quad (15)$$

where $pM = -\log_{10}[M]$,

$$Z(pM, \log_{10} K) = P\left(\log_{10} K\right) \times \frac{\log_e 10 \cdot \exp\left(\log_e 10 \cdot (\rho M - \log_{10} K)\right)}{\left(1 + \exp(\log_e 10 \cdot (\rho M - \log_{10} K))\right)^2}$$

Let us represent equation (15) in the discrete form using quadratures. For this porpose we have used the Simpson version of the Newton-Cotes quadrature formulae [19]. In the Simpson method the function Z under the integral sign is represented by the set of R polynomials of the second degree. The interval of the variation of $\log_{10}K$ is divided up into R equal subintervals and, for all those, the function Z under the integral sign is approximated by the expressions

$$\int_{[\log_{10} K_0^r]}^{[log_{10} K_0^r + 3\Delta \log_{10} K]} Z\left(pM_j, \log_{10} K\right) d\log 10\, K = S_j^r, \quad (16)$$

where index r marks the quantities characterizing the r-th subinterval, $1 \le r \le R$, $\log_{10}K_0^r$ is the left bound of the r-th subinterval, $\Delta\log_{10}K$ is the step of discretization, pM_j are the measured values of pM,

$$S_j^r = \frac{\Delta \log_{10} K}{3}\left(Z_{0j}^r + 4Z_{1j}^r + Z_{0j}^r\right),$$

$$Z_{ij}^r = P\left(\log_{10} K_i^r\right) \cdot Q_{ij}^r, \; i = 0,1,2;$$

$\log_{10}K_i^r$ are the equidistant arguments,

$$\log_{10} K_i^r = \log_{10} K_0^r + i \cdot \Delta \log_{10} K, \; i = 0,1,2;$$

$$Q_{ij}^r = \frac{\log_e 10 \cdot \exp\left(\log_e 10 \cdot \left(pM_j - \log_{10} K_i^r\right)\right)}{\left(1 + \exp\left(\log_e 10 \cdot \left(pM_j - \log_{10} K_i^r\right)\right)\right)^2},$$

Then the set of the linear equations is constructed:

$$\sum_r^R S_j^r = \tau\left(pM_j\right), \; j = 1,2,\ldots,m \quad (17)$$

where m is the number of experimental points which are used to solve the least squares problem. The unknown coefficients $P(\log_{10} K_i^r)$, $i = 0,1,2$, $r = 1,2,\ldots,R$, are calculated by the least squares method through solving least squares problem (17). To compute $P(\log_{10} K_i^r)$ on the compact the boundary constraints

$$P\left(\log_{10} K_0^1\right) \ge 0, \; P\left(\log_{10} K_2^R\right) \le 1,$$
$$P\left(\log_{10} K_0^{r+1}\right) \ge P\left(\log_{10} K_2^r\right),$$
$$P\left(\log_{10} K_i^r\right) \ge P\left(\log_{10} K_{i-1}^r\right) \quad (18)$$

are imposed on the searched values of $P(\log_{10}K_i^r)$. As result, the function $P(\log_{10} K)$ is represented by the non-decreasing sequence of numbers $P(\log_{10}K_i^r)$. The right parts of equations (17) $\tau(pM_j)$ are the

measured values. Any procedure to replace $\tau(pM_j)$ by a smooth function is not employed.

We tested the algorithm DAC1 and found that, similarly to the algorithms HILDA and QA, it produces numerically stable solutions, $P(\log_{10}K)$, but the quality of approximation of measured $\tau(pM_j)$ values and accuracy of $P(\log_{10}K)$ are not satisfactory in some cases. This fact is easy to explain. For the accurate approximation of the integral in equation (15) by the sums in equations (16), the step of discretization $\Delta \log_{10} K$ must be sufficiently small. The division of the discretization step causes the increase of the number of $P(\log_{10}K_i')$ values to be computed. But there exists a limit of this increase. The division of the discretization step gives rise to increasing the condition number of the matrix formed by the coefficients of equations set (17). These coefficients become highly correlated (nearly linearly dependent). The orthogonal decomposition methods [20], which are widely used in a modern regression analysis, detect and reject the «surplus» coefficients. For this reason, not all $P(\log_{10}K_i')$, which are necessary for a good approximation of the integral by the sums, may be determined. As a result, the error of approximation of the measured $\tau(pM_j)$ values exceeds the experimental error and the searched function $P(\log_{10}K)$ is represented only by several $P(\log_{10}K_i')$ values.

Instead of deleting the discretization step $\Delta \log_{10} K$, another way exists to increase the accuracy of calculating $P(\log_{10}K)$ and approximating $\tau(pM_j)$. It is possible to increase the degree of polynomials which are used to approximate the function Z under the integral sign in equation (15). But, as in the algorithms DACI, HILDA, QA, estimating the differential distribution functions $p(\log_{10}K)$ is not connected with calculating $P(\log_{10}K)$ and remains to be the particular step of the algorithm. For the reason, we do not adopt this modification of the algorithm and propose the algorithm DAC2.

The algorithm DAC2

Constructing the algorithm, we want 1) to calculate $P(\log_{10}K)$ on the compact; 2) to evaluate the function $p(\log_{10}K)$ simultaneously with calculating $P(\log_{10}K)$; 3) to describe $P(\log_{10}K)$ more accurately than in the algorithm DAC1 by using a high-order polynomial for approximating $P(\log_{10}K)$ instead of using the second degree polynomials for representing the function Z in the algorithm DAC1. Approximating $P(\log_{10}K)$ by a single polynomial on the whole domain of variation of $\log_{10}K$, we presume $P(\log_{10}K)$ to belong to analytical function. There exists one disadvantage of the presumption discussed. If the true integral distribution function $P(\log_{10}K)$ is of a stepwise character, the description of vicinities of points where the function has discontinuities will be rough.

Assuming that, similarly to $P(\log_{10}K)$, the function $t(pM)$ belongs to analytical functions, it is possible, instead of integral equation (15), to obtain the differential one with the some solution [21-23]:

$$P(x) = \tau(x) - \frac{pu^2}{(\log_e 10)^2 3!}\frac{\partial^2\tau(x)}{\partial x^2} + \frac{\pi^4}{(\log_e 10)^4 5!}\frac{\partial^4\tau(x)}{\partial x^4} \pm \ldots \Big|_{x=\log_{10}K=pM} \quad (19)$$

where x is $\log_{10}K$ in case of $P(x)$ and x is pM in case of $\tau(x)$. Obtaining this equation allows to avoid the iterative procedure for calculating $P(x)$. Now it is necessary to calculate the derivatives of $\tau(x)$. It is a mathematically incorrect problem [15]. To solve it we have to choose an expression for the approximation of measured $\tau(x)$ values. The simplest decision is to expand $\tau(x)$ in a power-series about the point ξ belonging to the x variation interval, remain N first terms of the expansion and drop all the rest high-order terms:

$$\tau(x) = \sum_{i=0}^{N-1} g_i(\xi)\frac{(x-\xi)^i}{i!}, \quad (20)$$

where the coefficients $g_i(\xi)$ are the i-th derivatives of $\tau(x)$ in respect to x in the point $x=\xi$. After substituting equation (20) into equation (19) we get expression to calculate $P(x)$:

$$P(x) = \sum_{i=0}^{N-1} g_i(\xi)\, D_i(x), \quad (21)$$

where $D_i(x)$ are the known functions of x:

$$D_i(x) = \begin{cases} \sum_{l=0}^{i/2} \frac{(-1)^l\ (\pi/\log_e 10)^{(i-2l)}}{(i-2l+1)!}\cdot\frac{(x-\xi)^{2l}}{(2l)!}, \\ \text{if } i \text{ is an even number,} \\ \sum_{l=0}^{(i-1)/2} \frac{(-1)^{(l+1)}\ (\pi/\log_e 10)^{(i-2l-1)}}{(i-2l)!}\cdot\frac{(x-\xi)^{(2l+1)}}{(2l+1)!} \\ \text{if } i \text{ is an odd number,} \\ 1, \text{ if } i=0. \end{cases}$$

Hence, to calculate $P(x)$ only the numerical values of coefficients $g_i(\xi)$ are needed.

For finding the coefficients $g_i(\xi)$, the system of linear algebraic equations is constructed:

$$\tau(pM_j) = \sum_{i=0}^{N-1} g_i(\xi) \frac{(pM_j - \xi)^i}{i!},$$

$$j = 1, 2, ..., m;\ m > N, \qquad (22)$$

where m is the number of the measured $\tau(pM_j)$ values. The numerical values of $g_i(\xi)$ are found by solving least squares problem (22). To solve the problem of estimating $P(x)$ as the conveniently correct one we should use the quantitative information about the features of this function on the stage when the coefficients $g_i(\xi)$ are computed. For this purpose, we have to take into account (1) that $P(x)$ is the function bounded above and below ($0 \le P(x) \le 1$) and (2) that $P(x)$ is a non-decreasing function (i.e. a differential distribution function $p(x)$ is nonnegative). It is easily to write expression for $p(x)$:

$$p(x) = \sum_{i=0}^{N-1} g_i(\xi)\, G_i(x), \qquad (23)$$

where $G_i(x) = dD_i(x)/dx$,

Imposing the restrictions on the $P(\log_{10} K)$

$$G_i(x) = \begin{cases} \sum_{l=0}^{i/2} \dfrac{(-1)^l\ (\pi/\log_e 10)^{(i-2l)}}{(i-2l+1)!} \cdot c, \\ \text{if } i \text{ is an even number,} \\ \sum_{l=0}^{(i-1)/2} \dfrac{(-1)^{(l+1)}\ (\pi/\log_e 10)^{(i-2l-1)}}{(i-2l)!} \cdot \dfrac{(2l+1)(x-\xi)^{2l}}{(2l+1)!}, \\ \text{if } i \text{ is an odd number,} \end{cases}$$

$$c = \begin{cases} 0, & \text{if } l = 0; \\ \dfrac{2l(x-\xi)^{2l}}{(2l)!}, & \text{if } l > 1. \end{cases}$$

and $p(\log_{10} K)$ values

$$0 \le P_j(\log_{10} K) = \sum_{i=0}^{N-1} g_i(\xi) \cdot D_i(pM_j) \le 1,$$

$$j = 1,2,...,m, \qquad (24)$$

$$0 \le p_j(\log_{10} K) = \sum_{i=0}^{N-1} g_i(\xi) \cdot G_i(pM_j),,$$

$$j = 1,2,...,m, \qquad (25)$$

we apply the usual technique [20] to solve the linear squares problem (22) subject to linear inequality constraints (24),(25). Thus, the function $P(\log_{10} K)$ is calculated on the compact without using an iterative procedure. Supplementarily, the function $p(\log_{10} K)$ is estimated without additional computations.

To approximate the measured $\tau(pM_j)$ values, within the limits of experimental errors, the value of N (the number of coefficients $g_i(\xi)$ to be determined) must be sufficiently large. In the algorithm DAC2 the upper threshold of N is determined by the expression

$$N = \begin{cases} m-1, & \text{if } m \le 12, \\ 12, & \text{if } m > 12. \end{cases} \qquad (26)$$

If N is too large this is an attempt to describe not only the function $\tau(pM)$ but also the experimental noise. If this situation takes place and restrictions (24) and (25) are omitted, the problem of an approximation of $\tau(pM)$ is essentially incorrect and obtaining the decreasing function $P(\log_{10} K)$ is probable. But due to constraints (24) and (25), unacceptable solutions $P(\log_{10} K)$ are rejected. Hence, discrepancies between measured and fitted $\tau(pM)$ values do not decrease without bound when the value of N is increased. Thus, the computation of $P(\log_{10} K)$ on the compact is the first reason for which the much too large values of N do not involve a numerical instability of calculations.

The second reason is connected with using the singular-value decomposition (SVD) method, which appears in the least squares algorithm [20]. Employing the SVD method we calculate the singular numbers σ_q of the matrix composed by the coefficients of equations set (22) $(pM_j - \xi)^j / i!$, set zero σ_q which are less than $\sigma_{max} \cdot \varepsilon$, where σ_{max} is the largest singular number, ε is a small number, and do not compute the linear combinations of $g_i(\xi)$ corresponding to small σ_q. The choice of ε determines the number of parameters, which are computed from the primary experimental data. It is difficult to choose unambiguously the value of ε which is suitable for handling the real chemisorption isotherms. But it is clearly that the increase of experimental errors has to give rise to increasing the appropriate values of ε. Usually, the experimental values of $\tau(pM_j)$ are exposed to

errors ranging between 10^{-2} and 10^{-1}. By a numerical simulation we have found that the values, which are suitable for processing the real chemisorption isotherms, belong to the interval $10^{-8} < \varepsilon < 10^{-4}$. The variation of ε inside this interval does not practically affect the character of calculated function $P(\log_{10} K)$ and a quality of $\tau(pM_j)$ approximation. But the choice of ε plays an important role in solving the essentially incorrect problem of calculating $p(\log_{10} K)$. A variation of ε has the same sense as a variation of the regularization parameter α in equation (12). If the primary experimental data are inaccurate (the error or $\tau(pM_j)$ exceeds $5 \cdot 10^{-2}$) using the values of ε, which are lesser that 10^{-6}, may cause an appearance of spurious maxima of $p(\log_{10} K)$. These maxima characterize not the energetic inhomogeneity but the experimental noise. It suffices to increase ε by 10—100 times and repeat calculations to detect spurious $p(\log_{10} K)$ peaks. In the algorithm DAC2, we have used the value of $\varepsilon = 10^{-6}$.

Simulation

The aim of this section is to display a numerical stability and an accuracy of the algorithm DAC2. For this aim we have used a simulation. A known (model) function $P(\log_{10} K)$ was specified. For the set of values pM integral (15) was numerically calculated and formation degrees $f(pM)$ were obtained. Then uniformly distributed random errors were inserted into $f(pM)$ and $P(\log_{10} K)$ was calculated again.

A model function has to exhibit properties of complicated distributions. It is necessary to take into consideration that $P(\log_{10} K)$ may be a superposition of some distribution functions or possess discontinuities. In our opinion, the function $P(\log_{10} K)$ satisfies these requirements if it is specified by expression

$$P(\log_{10}K) = (P_1(\log_{10}K) + P_2(\log_{10}K))/2 \quad (27)$$

where $P_1(\log_{10} K)$ is the exponential probability distribution function,

$$P_1(\log_{10}K) = \begin{cases} 0, & \log_{10}K < C, \\ 1 - \exp(-(\log_{10}K - C)/d), & \log_{10}K > C, \end{cases} \quad (28)$$

$P_2(\log_{10}K)$ is the normal (Gaussian) probability distribution function,

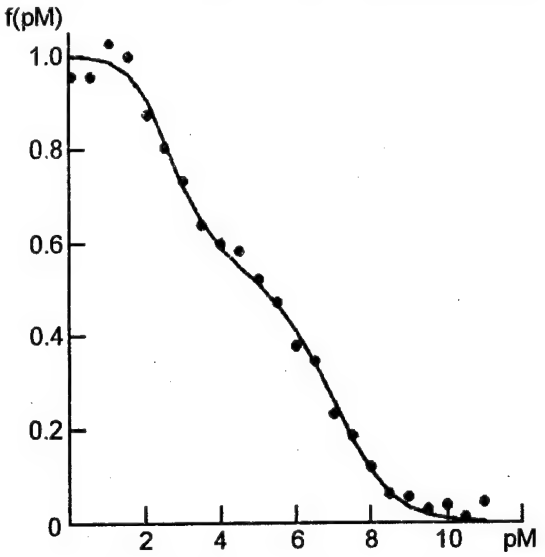

Fig.1. Complex formation degree $f(pM)$ simulated from the model distribution law. Exact values are showed by solid line, values after introducing random errors are shown by circles.

$$P_2(\log_{10}K) = \frac{1}{\sigma\sqrt{2\pi}} \int_{-\infty}^{\log_{10}K} \exp\left\{-\frac{(x-\mu)^2}{2\sigma^2}\right\} dx \quad (29)$$

where C, d, μ and σ are the parameters of the distribution laws. An example of the simulated function $f(pM)$ is presented in Fig.1. The values C=2, d=1, μ=7, σ=1 were used and the errors introduced into $f(pM)$ were uniformly distributed in the interval (–0.05; +0.05).

The obtained $f(pM)$ values were the basis for reconstructing the distribution function $P(\log_{10} K)$ by the algorithm DAC2. The results of calculations are shown in Fig.2. Note that, if $f(pM)$ values were not undergone errors or errors were belonged to interval (–0.025; +0.025), the differences between exact $P(\log_{10} K)$ values and reconstructed ones were undistincted in the scale of the picture.

For a comparison, we present results obtained by the algorithm DAC1. As illustrated in Fig.3, the algorithm DAC1 reconstructs $P(\log_{10} K)$ from exact $f(pM)$ values successfully, though the deviation of the calculated values from the model ones reaches in some points 0.1. But in case of $f(pM)$ values exposed to random errors, the reconstructed solution $P(\log_{10} K)$ is not authentic.

As mentioned above, the algorithm DAC2 allows to reconstruct thedensity distribution functions $p(\log_{10} K)$. Results of $p(\log_{10} K)$ computation from $f(pM)$, exposed to the errors in interval (–0.05; +0.05), are presented in Fig.4.

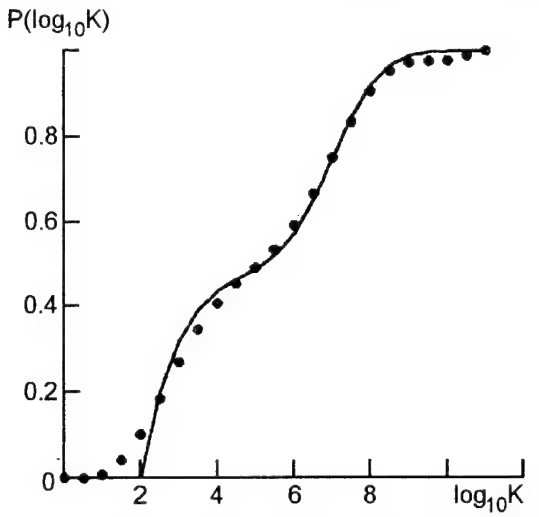

Fig.2. Plots of function $P(\log_{10} K)$. The precise (model) function is presented by solid line, the function reconstructed by the algorithm DAC2 from $f(pM)$ values in presence of errors belonging to the interval (–0.05; +0.05) is shown by circles.

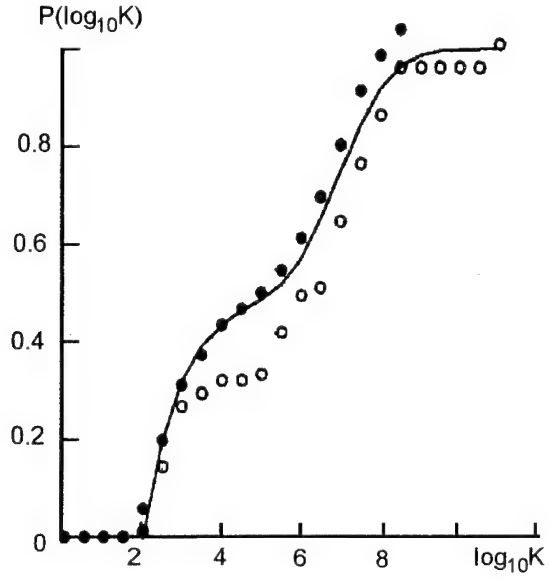

Fig.3. Plots of function $P(\log_{10} K)$. The precise (model) function is presented by solid line. The function $P(\log_{10} K)$, reconstructed from exact $f(pM)$ values by the algorithm DAC1, is presented by dark circles. The function $P(\log_{10} K)$, reconstructed by the algorithm DAC1 from the $f(pM)$ values in presence of errors belonging to the interval (–0.05; +0.05) is shown by light circles.

The reconstructed function $p(\log_{10} K)$ is close to the model one. Only in a vicinity of the point $\log_{10} K = 2$, where the function $P(\log_{10} K)$ has a discontinuity, the approximation of the model

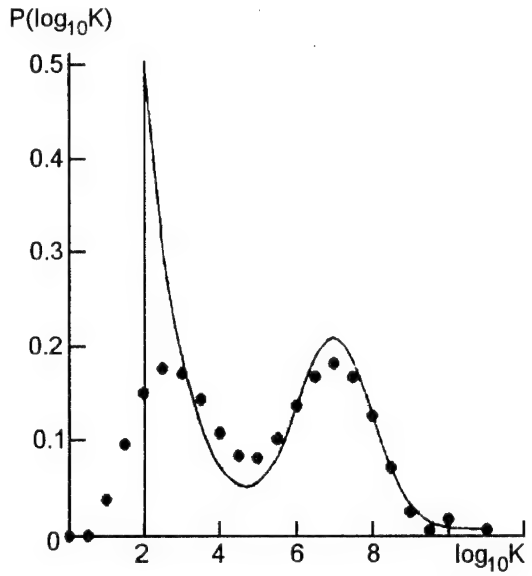

Fig.4. Plots of density distribution function $p(\log_{10} K)$. The precise (model) function is presented by solid line, the function, reconstructed by the algorithm DAC2 from $f(pM)$ values in presence of random errors belonging to the interval (–0.05;+0.05) is shown by circles.

function $p(\log_{10} K)$ by the calculated one is rough. It is due to the the supposition about the smoothness of the function $P(\log_{10} K)$.

Thus, a simulation has shown a high reliability and accuracy of the algorithm DAC2. The algorithm DAC1 based on the representation of $P(\log_{10} K)$ by a non-decreasing sequence of numbers $P(\log_{10} K_i^r)$ is not competitive.

Example

The algorithm DAC2 has been applied to describe the sorption of hydrogen ions by chemically modified silica samples with grafted *n*-propylamine and ethylenediamine (En).

A non-porous aerosil A-175 with specific surface area 175 $m^2 \cdot g^{-1}$ for grafting *n*-propylamine and A-200 with specific surface area 200 $m^2 \cdot g^{-1}$ for grafting En were used. To prepare sorbents with a «brush» structure of grafted layers, the known procedure [24] has been applied. The concentrations of groups grafted on the silica surface were determined by potentiometric titration with a strong acid and by elemental analysis, and were found to be 0.43 $mmol \cdot g^{-1}$ in case of *n*-propylamine and 0.57 $mmol \cdot g^{-1}$ in case of En. The synthesis has been performed by Dr.V.N.Zaitsev (Kiev University, Ukraine).

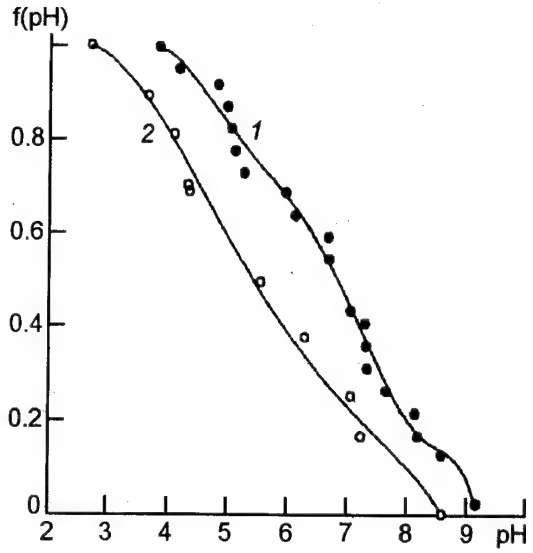

Fig.5. Plots of function $f(pM)$ for samples with grafted En and *n*-propylamine. The measured values are shown by circles (• – En, ° – *n*-propylamine), the fitted curves shown by solid lines (1 - En, 2 - *n*-propylamine).

The hydrogen ion absorption isotherms were measured by potentiometric titration of sorbent samples at 20 °C and ionic strengths of solutions 0.1 mol·l^{-1} (KNO_3). The obtained dependencies f(pH) (see Fig.5) were analyzed by the algorithm DAC2 with the purpose to estimate the energetic inhomogeneity of sorbents.

As shown in Fig.5, the measured $f(pM)$ values are precisely fitted by the computed ones: discrepancies between measured and computed $f(pM)$ values do not exceed 0.03.

The results of calculating grafted groups' distribution in logarithms of protonization constant $p(\log_{10} K)$ are shown in Fig.6. The studied sorbents are energetically inhomogeneous. For silica with grafted En, the calculated function $p(\log_{10} K)$ has three maxima. The third peak at $\log_{10}K \approx 9$ is believed to be spurious because increasing the value of ε from 10^{-6} to 10^{-5} causes its disappearance without the loss of accuracy of $f(pM)$ approximation. Hence, as one would expect, there are two types of aminogroups with the different basicities in the sample with grafted En. This fact is determined by the stepwise nature of hydrogen ions addition to the grafted En. The logarithms of aminogroup protonization constants in the sample with grafted En are about 7 and 5. At the same time, the logarithms of stepwise protonization constants of En in water solutions are equal to 10.04 and 7.22 [25]. Hence, the

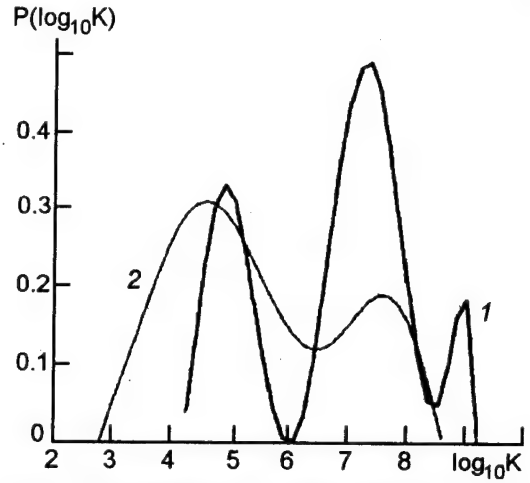

Fig.6. The distribution of grafted reagents in logarithms of protonization constants (1 - En, 2 - *n*-propylamine).

basicity of En grafted on silica surface decreases compared with that of En in solutions.The decrease of En basicity is attributed to the formation of hydrogen bounds between En and weakly acid silanol groups remaining on the sorbent surface [26]. As is seen (Fig.6), the function $p(\log_{10} K)$, which characterizes the energetic inhomogeneity of silica with grafted *n*-propylamine, has two maxima at $\log_{10}K \approx 4.5$ and $\log_{10}K \approx 7.5$. Since the protonization constant of *n*-propylamine in water solutions is equal to 10.56 [25], we can conclude that, similarly to En, the basicity of grafted *n*-propylamine decreases compared to that of analogs in solutions. The decrease of basicity is caused by the formation of hydrogen bonds between *n*-propylamine and surface silanol groups. But the existence of two classes of groups with different basicities is rather unexpected. It is impossible to explain this result by the stepwise nature of the hydrogen ions addition to the grafted *n*-propylamine. It is likely that the fixed amino-groups are grafted highly heterogeneously and form clusters (islands) on the surface [26]. In the clusters, the basicity of aminogroups is greater than in the regions with the small surface concentration of the grafted groups. In such regions, there are many hydrogen bonds of aminogroups with acid silanol hydroxyls and the basicity of *n*-propylamine decreases.

Acknowledgments

We are appreciate Ukranian Foundation of Fundamental Researches for financial support.

References

1. A.P.Filippov, *Teor.Eksp.Khim.*, **19**, 463, (1983).
2. Yu.V.Kholin, V.N.Zaitsev and N.D.Donskaja, *J.Inorg.Chem.*,**35**, 1569, (1949).
3. G.V.Kudryavtsev, D.V.Miltchencko, V.V.Yagov, A.A.Lopatkin, *J.Colloid and Interf.Sci.*, **140**, 114, (1990).
4. V.Sh.Mamleev, P.P.Zolotarev, P.P.Gldischev, Heterogeneity of Sorbents [in Russian], Nauka, Alma-Ata (1989).
5. S.Z.Roginskii,Adsorption and Catalysis on Heterogeneous Surfaces [in Russian], Nauka, Moscow—Leningrad.
6. A.W.Adamson, Physical Chemistry of Surfaces, Third edition, J.Wiley, New York, (1976).
7. O.M.Poltorak, Thermodynamics in Physical Chemistry [in Russian], Vichaya Shkola, Moskow, (1991).
8. F.Karush, M.Sonenberg, *J.Am.Chem.Soc.*, **71**, 1369 (1949).
9. A.M.Thakur, P.G.Munson, D.L.Hunston, D.Rodbard, *Analyt.Biochem*, **103**, 240 (1980).
10. B.Leunberger, P.W.Schindler, *Anal.Chem.*, **58**, 1471 (1986).
11. D.R.Turner, M.S.Varney,M.Whitfield et al., *Geochim.Cosmochim.Acta*, **50**, 289 (1986).
12. G.A.Korn, T.M.Korn, Mathematical Handbook, McGraw-Hill, New York, (1968).
13. J.B.Zeldowitch, *Acta Physicochimica URSS*, **1**, 961, (1935).
14. J.Roles,G.Guiochon, *J.Phys.Chem.*, **95**, 4098 (1991).
15. A.N.Tikhonov, B.Ya.Arsenin, Methods for Solution off Ill-posed Problems [in Russian], 3-rd Edition, Nauka, Moscow, (1986).
16. W.A.House, *J.Colloid Interface Sci.*, **67**, 166 (1978).
17. W.A.House, M.J.Jaycock, *J.Chem.Soc.Faraday Trans.* Part 1, **73**, 942 (1977).
18. M.J.Jaycock, J.D.Parfitt, Chemistry of Interfaces, Ellis Horwood, Chichester (1981).
19. N.S.Bakhvalov, N.P.Zhidkov, G.M.Kobel'kov, Numerical Methods [in Russian], Nauka, Moscow (1987).
20. C.L.Lawson, R.J.Hanson, Solving Least Squares Problems, Prentice-Hall, New Tersey (1974).
21. M.I.Temkin, V.Levitch, *Zhurnal Fizicheskoi Khimii*, **20**, 1441 (1946).
22. R.Sips, *J.Chem.Phys*, **16**, 490 (1948).
23. C.C.Hsu, B.W.Wojciechowski, W.Rudzinski, J.Narkiewicz, *J.Colloid Interface Sci.*, **67**, 292 (1978).
24. N.D.Donskaja, V.N.Zaitsev, *Ukrainskii Khimicheskii Zhurnal*, **58**, 972 (1992).
25. A.E.Martell, R.M.Smith, Critical Stability Constants, **2**, Amines, New York, London: Plenum (1975).
26. G.V.Lisitchkin, *Zhurnal Vsesojuznogo Khimicheskogo Obschestva im.D.I.Mendeleeva*, **34**, 291 (1989).

Два алгоритма оценки энергетической неоднородности химически модифицированных кремнеземов

Ю.А.Холин, С.А.Мирный

Оценивание энергетической неоднородности химически модифицированных кремнеземов основано на решении интегрального уравнения Фредгольма первого рода. В статье обсуждается математическая некорректность указанной задачи, особенности известных методов ее решения и описываются численно устойчивые алгоритмы DAC1 и DAC2. Строя алгоритмы, авторы полностью использовали количественную априорную информацию об этом искомом решении. Пригодность алгоритмов проверена при их использовании для обработки модельных и реальных данных.

Functional Materials **2**, No.1 (1995)

On semiempirical calculations of the Van der Waals interaction between a complex molecule and a surface within many-electron approach

A.V.Luzanov and V.V.Ivanov

Kharkov State University, 4 Svobody Sq., 310077 Kharkov, Ukraine

Van der Waals constants C_3^{A-S} describing the dispersion interaction of a conjugated molecule A with a surface (S) of metals and semiconductors are calculated using a phenomenological dielectric function for the material under study and treating the corresponding π-shell within full-CI approach. The method proposed requires once (for each surface) solving a PT-like equation for the correction to the unperturbated full-CI state. σ-shell contributions to C_3^{A-S} are estimated via the additive approximation to the respective frequency dependent σ - polarizabilities. The results for small polyenes, cumulenes, benzene and naphthalene are presented and some excited-state C_3^{A-S} calculations are also given.

Розраховано ван-дер-ваальсові константи C_3^{A-S}, що описують дисперсійну взаємодію супряженої молекули A з поверхнею (S) металів або напівпровідників. Для розрахунків використано феноменологічну діелектричну функцію відповідного матеріалу, а вивчення π-оболонок базувалось на методі повної конфігураційної взаємодії. Запропонований підхід потребує одноразового розв'язання рівняння за таким типом, що з'являється у теорії збурень. Внесок σ-оболонки оцінено адитивно через відповідну динамічну поляризовність. Подано результати розрахунків для нижчих поліенів, кумуленів, бензолу і нафталіну, а також C_3^{A-S} для деяких збуджених станів цих молекул.

1. Introduction

The estimations of interaction energies, E_{Int}, in case of the «molecule+surface» system, are quite a complicated problem. However, at the large distances, as the exchange repulsion is negligible, a nonpolar molecule interacts with metal surface via the dispersion forces, and no others. The latter may be presented in terms of a power series which, for the problem under consideration, is of the form [1]

$$E_{Int} = -\frac{C_3^{A-S}}{l^3} - \frac{C_4^{A-S}}{l^4} - \frac{C_5^{A-S}}{l^5} - \dots \qquad (1)$$

where l is the distance between a given molecule A and the surface, C_n^{A-S} being the Van der Waals constants of the appropriated order (see also the text-book [2], chapter 8).

The first term of Eq. (1) gives the major contribution to E_{Int}, and the corresponding Van der Waals constant for the metal surface can be expressed through the imaginary frequency dependent polarizability $\alpha^A(i\omega)$, namely [3]

$$C_3^{A-S} = \frac{\omega_s^2}{4\pi}\int_0^\infty \frac{\alpha^A(i\omega)\, d\omega}{\omega^2 + \omega_s^2} \qquad (2)$$

ω_s standing for a surface plasmon frequency, all values here in atomic units. The analogous expressions hold for the semiconductor surface.

In practice, the direct calculations of Eq. (2) by numerical integration necessitates a large number of the $\alpha(i\omega)$ values. Moreover, finding the dynamic polarizabilities is a special problem of molecular quantum mechanics, which can be handled with recourse to the approximated models such as Hartree-Fock method, multiconfigurational approaches, etc. These calculations,

however, are also laborious, so in a number of papers such as [4-6] a simple one-term dispersion formula is actually used when assuming the only characteristic frequency, ω_0, be important.

Nevertheless, the use of the current quantum-chemical approaches allows much room for treating correctly the polarizability problem [7-11]. The purpose of this paper is to give the results of our appropriate study placing it upon the least subjective formulation through the exploration of the formally exact many-electron approach allowing for electron correlation, namely the full configuration interaction method (full-CI). Some semiempirical illustrations of the technique proposed are concerned the most mobile π-electron shells of the conjugated organic molecules treated on the basis of the standard PPP π-electron scheme.

2. C_3^{A-S} calculations with PT-like approach

Consider first a more general expression for Van der Waals constant C_n^{A-S}, introducing the phenomenological dielectric function

$$g(i\omega) = g_0\omega_s^2\left(\omega^2+\omega_s^2\right)^{-1} \tag{3}$$

used in [4]; here, g_0 and ω_s are certain fitting parameters describing the material under question such as a metal or a semiconductor. Then, the use of the ensuing representation

$$C_3^{A-S} = \frac{1}{4\pi}\int_0^\infty \alpha(i\omega)g(i\omega)\,d\omega \tag{4}$$

makes it possible to estimate dispersion interaction for semiconductors as well as for metals, for the latter $g_0 = 1$ is usually taken.

It is a simple matter to perform elementary integration in (4) with reference to the common sum-over-state for the dynamic polarizability

$$\alpha(\omega) = \sum_{k=1}^{M}\frac{f_{o\to k}}{\omega^2-\omega_k^2} \tag{5}$$

ω_k being the excitation energy for the electronic transition $o\to k$, $f_{o\to k}$ its oscillator strength, and M the number of the excited states involved. The result of computing Eq.(4) (see also [3]) takes the form

$$C_3^{A-S} = \frac{g_o\omega_s}{8}\sum_{k=1}^{M}\frac{f_{o\to k}}{\omega_k(\omega_k+\omega_s)} \tag{6}$$

Recalling the expression for oscillator strength

$$f_{o\to k} = \frac{2\omega_k}{3}\left(\left|Q^x_{o\to k}\right|^2+\left|Q^y_{o\to k}\right|^2+\left|Q^z_{o\to k}\right|^2\right) \tag{7}$$

where the transition moments between the N-electron states $|\psi_0>$ $|\psi_k>$ are defined as

$$Q_{o\to k} = <\psi_o|H_N^{(x)}|\psi_k>$$

$$H_N^{(x)} = \sum_{i=1}^{N} h_x(i)\,,\quad h_x = \hat{x}\,, \tag{8}$$

one arrives at the desired sum-over-state formula

$$C_3^{A-S} = \frac{g_o\omega_s}{12}\sum_{k=1}^{M}(\omega_k+\omega_s)^{-1}\left(\left|Q^x_{0\to k}\right|^2+\right.$$

$$\left.+\left|Q^y_{0\to k}\right|^2+\left|Q^z_{0\to k}\right|^2\right), \tag{9}$$

In practice, there is no point in an explicit summation as above. A more appropriate is the next procedure which is familiar from the ordinary perturbation technique (PT). First, one introduces the «correction» $|\psi^x(\omega)>$ to the initial ground state $|\psi^o>$. This correction satisfies the inhomogeneus equation

$$(H_N - E_o + \omega)\,|\psi^x(\omega)> = (E^{(x)} - H_N^x)\,|\psi_o>\,, \tag{10}$$

H_N being the N-electron unperturbed Hamiltonian of the molecule $E^{(x)} = <\psi_o|\,H_N^{(x)}\,|\psi_o>$. Then, owing to the evident spectral resolution

$$|\psi^x(\omega)> = \sum_{k=1}^{M}(\omega_k+\omega)^{-1}\,Q^x_{0\to k}\,|\psi_k> \tag{11}$$

one easily gets the equivalence of Eq. (9) to the following expression

$$C_3^{A-S} = \frac{g_o\omega_s}{12}\,[\,<\psi_o|H_N^{(x)}|\psi^x(\omega_s)> +$$

$$+<\psi_o|H_N^{(y)}|\psi^y(\omega_s)> + <\psi_o|H_N^{(z)}|\psi^z(\omega_s)>\,] \tag{12}$$

From such a form of the surface Van der Waals constant, many useful approaches proceed allowing for electron correlation via the configuration interaction. While our major aim is to present the full-CI results, so we restrict the consideration to that formally most accurate approach (within the finite-dimensional electronic models supplied by finite-size atomic orbital bases).

3. Full - CI computations

Pursuing the full-CI description of the molecular electronic shells we will resort to a pure

matrix formulation of this method [12,13], which was termed «wavefunction operator method». It may be displayed in term of the spinless n-electron operator $X = X(1...n)$ which emerges to be the operator counterpart (that is, the wave-function operator) of $2n$-electron vector state $\psi_0>$ (for simplicity, we consider the even-electron system, so n is integer). Then $2n$-electron Shrödinger equation

$$(H_{2n} - E_0)\,|\psi_0> = 0 \qquad (13)$$

is tantamount to the following n-electron operator equation

$$H_n X + XH_n + \hat{K}(X) - E_0 X = 0 \qquad (14)$$

where $\hat{K}$ is a superoperator acting on the n-electron entities analogously to Roothan's exchange operator for the one-electron entities.

This fact makes feasible a matrix algorithm for computing Eqs. (9), (12) within the previous full-CI technique from Ref. [13]. All one need to do is to solve the nonhomogeneous equation

$$H_n X^{(x)}(\omega) + X^{(x)}(\omega) H_n + \hat{K}\left(X^{(x)}(\omega)\right) + \omega X^{(x)} = \\ = E_0^{(x)} X - H_n^{(x)} X - X H_n^{(x)} \qquad (15)$$

for the given frequency $\omega = \omega_s$. Here, $X^{(x)}(w)$ is the operator counterpart of the correction $|\psi^x(\omega)>$ in Eq.(10). One can apply any of the known computational linear-algebraic schemes (after a relevant reformulation) solve the linear system in Eq. (15) to find $X^{(x)}(\omega_s)$. In so doing, an experience of the treatment of the analogous one-electron equations appearing in the density matrix formalism [14] is also of value too. Given the n-electron matrices $X^{(x)}(\omega_s)$, $X^{(y)}(\omega_s)$ and $X^{(z)}(\omega_s)$, the wanted quantity can be calculated in terms of the one-electron matrix traces, viz.

$$C_3^{A-S} = \frac{g_o \omega_s}{12} \mathrm{Tr}(h_x \tau^{(x)}(\omega_s) + \\ + h_y \tau^{(y)}(\omega_s) + h_z \tau^{(z)}(\omega_s)) \qquad (16)$$

where the spinless one-electron transition density matrix (at the state vector language, arising from $|\psi> <\psi^x|$)

$$\tau^{(x)}(\omega_s) = n\,\mathrm{Tr}_{(2...n)}\left[X^{(x)}(\omega_s) X + X X^{(x)}(\omega_s)\right] \qquad (17)$$

is computed by the same technique as for the one-electron matrix elements in [13].

In the further semiempirical implementations of this algorithm, we use the same parameterization scheme as in the our previous calculations in ref. [10]. In case of π-systems we take the nonzero resonance integral $\beta_{cc} = -2.274$ eV, and the repulsion integrals $\gamma_{\mu\nu}$ are estimated by Ohno formula and the one-center value $\gamma_{cc} = 11.13$ eV.

4. Evaluations for the conjugated molecule

Proceed now to the semiempirical computations of the Van der Waals constants taking several typical metals and semiconductors for which the phenomenological constants g_o and ω_s in Eq. (3) are known from Ref. [3,15]. These g and ω values are listed in Table 1. As to admolecules, we are interested first of all in the unsaturated hydrocarbons since their electric properties at the full-CI level have been studied earlier in Refs. [10,11,16]. Among such systems, aromatic molecules, linear polyenes, and cumulenes are of special interest due to the notable distinction between the Hartree-Fock (MO) values and the full-CI ones for the average π-electron polarizability α (see Table 2). To this set, we also added nonatetraenyl cation (a polymethene system) as being highly polarizabile, while in the case of charged systems, a pure electrostatic effect is evidently predominant over the dispersion interaction. Thus, the allowance for π-electron correlation effects is very important when describing π-system susceptibilities and the corresponding dispersion interactions to be closely related to the former.

Table 1. Phenomenological parameters of the dielectric function g(iω) in Eq.(3) for some substances

	Mg	Al	Ge	Graphite	Diamond	LiF	NaF
ω_s, eV	7.1	10.6	12.1	14.2	23.3	17.4	21.8
g_0	1.0	1.0	0.88	0.73	0.70	0.32	0.27

Table 2. Influence of electron correlation upon π-electron polarizability (in Å^3) for *trans*-polyenes

Molecule	MO		Full-CI
	CHF[a)]	VHF[b)]	
Hexatriene	10.53	8.32	5.60
Octatetraene	18.06	15.58	9.15
Decapentaene	27.04	22.70	13.25

[a)]CHF is the customary coupled HF perturbation theory.
[b)]VHF is the variational HF perturbation theory involving all the single excited configurations. These results are taken from Ref.[17]

Table 3. π-Contribution to Van der Waals components C_3^{A-S} (in eV · Å^3)

	Molecule	Surface						
		I	II	III	IV	V	VI	VII
		Mg	Al	Ge	Graphite	Diamond	LiF	NaF
1	Hexatriene	2.0	2.3	2.1	1.8	2.0	0.8	0.7
2	Octatetraene	3.1	3.5	3.2	2.8	2.9	1.3	1.1
3	Decapentaene	4.3	4.8	4.4	3.8	4.0	1.7	1.5
4	Nonatetraenyl cation	6.8	7.7	6.7	5.6	5.8	2.6	2.2
5	CH_2=C=C=C=CH_2	3.4	2.8	2.5	2.2	2.4	1.0	0.9
6	Benzene	1.6	1.9	1.7	1.5	1.7	0.7	0.6
7	Naphtalene	3.0	3.5	3.3	2.9	3.1	1.3	1.2

The results of calculation of the π-contribution to C_3^{A-S} are collected in Table 3. These data may be juxtaposed with that given by noble gas atoms having close polarizability values. So, for the benzene molecules our result is $\alpha^{\pi} = 3.6$ Å^3 that is about the value for Xe atom, α (Xe) = 4.0 Å^3, the corresponding values of C_3^{A-S} (in eV·Å^3) for Al surface being 1.85 and 3.0, respectively (the second number is taken from ref [18]). It is interesting to note that the Van der Waals interaction with graphite and diamond being almost the same, is similar to that with such metals as Mg, and only the insulators LiF and NaF give evidently lesser values.

Of course, to estimate the total dispersion constant, all electron shells should be taken into account. In order to hold within the π-electron approximation, an additive approach to the σ-shell can be applied. For this, one may exploit certain values, α_{CH} and α_{CC} as the simplest fitting parameters giving correspondently the average polarizabilities of the localized σ-bonds C—H and C—C, so that the total average polarizability is

$$\bar{\alpha} = \alpha^{\pi} + \alpha^{\sigma} \qquad (18)$$

$$\alpha^{\sigma} = N_{CH}\alpha_{CH} + N_{CC}\alpha_{CC} \qquad (19)$$

N_{CH}, N_{CC} being the numbers of C—H and C—C bonds, respectively. Putting α_{CH} = 0.80 Å^3, α_{CC} = 0.25 Å^3 one finds the overall dipole polarizability α to be in a resonable agreement with experimental values from Refs. [10,19] (see Table 4).

Therefore, we expect that a use of the additive scheme such as this gives rise to the adequate estimations of the full C_3^{A-S} values. The ensuing additive contribution to the latter owing to the σ-bonds is calculated in terms of the next addends

$$\frac{g_0\omega_s}{8}\left[N_{CH}\,\alpha_{CH}\,\omega_{CH}(\omega_s+\omega_{CH})^{-1} + N_{CC}\,\alpha_{CC}\,\omega_{CC}(\omega_s+\omega_{CC})^{-1}\right] \qquad (20)$$

where ω_{CH} and ω_{CC} are the mean excitation energies of the localized two-electron bonds C—H and C—C. For simplicity, we let $\omega_{CH} = \omega_{CC} = \omega_{\sigma}$ reminding the close electronegativity of the carbon 2*sp* AO and the hydrogeneous 1*s* AO [20]. Then the σ-contribution (20) is calculated by the expression

Table 4. The estimated and experimental values of the average polarizability (in Å^3)

System*	α_{σ}	$\alpha_{\sigma} + \alpha_{\pi}$	α_{exp}
1	7.65	13.25	12.7
2	9.75	18.90	—
3	11.85	25.10	—
4	10.30	40.71	—
5	4.20	10.49	—
6	6.30	9.90	9.9
7	9.15	16.41	16.6

*The numeration of the molecular systems is the same as in Table 3.

Table 5. The overall Van der Waals Constants C_3^{A-S} (in eV · Å^3) including σ-contribution

System*	Surface						
	I	II	III	IV	V	VI	VII
1	5.8	6.1	6.7	6.2	6.4	2.6	2.4
2	7.9	9.4	8.8	7.7	8.5	3.6	3.3
3	10.2	12.0	11.1	9.8	10.7	4.5	4.1
4	12.1	14.3	12.9	11.1	12.0	5.1	4.5
5	4.5	5.3	4.9	4.3	4.8	2.0	1.8
6	4.7	5.7	5.3	4.7	5.2	2.2	2.0
7	7.5	9.1	8.5	7.5	8.3	3.5	3.2

*)The numeration of the molecular systems (and the surface species) is the same as in Table 3.

$$\left[C_3^{A-S}\right]^{\sigma} = g_{\sigma}(\omega_{\sigma}^{-1} + \omega_s^{-1})^{-1}\alpha^{\sigma}/8 \qquad (21)$$

putting ω = 9 eV for the computations realized. The final results are summarized in table 5.

The excited states of admolecules are of special interest due their influence on photoadsorption effects. In this context, the computation of C_3^{A-S} for low-lying ππ*-excited states has been performed. Among the molecules above treated, the excitation effect is the most apparent for the nonatetraenyl cation and the isoelectronic cumulene system (systems 4 and 5 from table 3). In case of system 4, the first singlet excited state is of B symmetry, having (within full-CI) the excitation energy $\omega_* = 2.41$ eV and the large transition moment $Q_x = 2.58$ Å. The analogous data for system 5 are 5.12 eV and 1.67 Å. With the such low-lying excited state, the ground state gives a very important contribution to the dispersion constant $C_3^{A^*-S}$ for the excited states property since this contribution comprises (see Eq. (9))

$$\frac{g_0}{8}(\omega_*^{-1} - \omega_s^{-1})^{-1}\,\alpha^{[1]} \qquad (22)$$

where

$$\alpha^{[1]} = 2\,Q_*^2/3\omega_* \qquad (23)$$

is the one-term contribution to the average dipole polarizability (the Drude-like formula). Owing to the difference of the rather close reciprocal frequencies in Eq.(12) and the major value of $\alpha^{[1]}$ for the quasilinear system 4 and the linear system 5, the appreciable contribution (50%) to the whole effect of the excitation arises from the ground state alone. The full-CI data for these excited B_2 states are displayed in Table 6, where the corresponding results for the excited B_{2u} state of naphthalene are added for comparison.

Table 6. π-contribution to C_3^{A-S} (in eV · Å^3) for the lowest $^1B_2$ (or $^1B_{2u}$) excited states of some conjugated molecules

System*	Surface						
	I	II	III	IV	V	VI	VII
Decapentaene	20.8	20.3	17.8	14.6	14.3	6.5	5.5
Nonatetraenyl cation	17.3	12.5	10.6	8.5	7.9	3.7	3.1
Naphthalene	5.7	6.0	5.4	4.6	4.8	2.1	1.8

*)The numeration of the surface species is the same as in Table 3.

5. Conclusion

An attempt has been made here to make quantitatively understandable some features of the dispersion interaction of the conjugated systems with the surface. While our demonstrations are of the semiempirical type, the same approach within full-CI method can be applied to ab initio description of the molecular electronic structure (for the moderate-sized systems) if using the algorithm given in [13]. Moreover, the Van der Waals constants presented above at the full-CI level provide the most dependable bases for checking the approximated and yet more available methods such as coupled and variational Hartree-Fock methods (both restricted and unrestricted ones). But this item is under study now.

Acknowledgements

This research was made possible in part by Grant No. U2M000 from the International Science Foundation and the Ukrainian Fundamental Science Foundation.

References

1. M.W.Cole, D.R.Frankl, D.L.Goodstein, *Rev. Mod. Phys.*, **53**, 199 (1981).
2. A.Zangwille, Physics at Surface, Cambridge University Press, Cambridge, New York (1988).
3. G.Muhhopodhyay, J.Mahanty, *Solid.State Commun.*, **16**, 597 (1975).
4. G.Vidali, M.V.Cole, *Surface.Sci.*, **110**, 10 (1981).
5. X.P.Jiang, F.Toigo, M.W.Cole, *Surface.Sci.*, **145**, 281 (1984).

6. P.W.Flower, J.M.Hutsou, *Surface Sci.*, **165**, 165 (1986).
7. W.Rich, P.Wormer, *J.Chem.Phys.*, **88**, 5704 (1988).
8. M.Dupuis, A.Farazdel, S.P.Karna, S.A.Maluender, in: Modern Technigüe in Computational Chemistry, MOTECC-90, ed. by E.Clementi, Leiden, ESCOM (1990), p.277.
9. J.E.Rice, N.C.Handy, *J.Chem.Phys.*, **94**, 4959 (1991).
10. Yu.F.Pedash, V.V.Ivanov, A.V.Luzanov, *Theor. Eksp. Khim.*, **25**, 659 (1989).
11. R.Rumasesha, I.D.L.Albert, *Chem.Phys.Lett.*, **154**, 659 (1989).
12. A.V.Luzanov, *Theor.Eksp.Khim.*, **25**, 3 (1989).
13. A.V.Luzanov, A.L.Wulfov, V.O.Krouglov, *Chem. Phys. Lett.*, **197**, 614(1992).
14. M.M.Mestechkin in: Self-Consistent Field Theory and Application, ed. by R.Carbo and M.Klobykowski, Elsevier (1990), p.312.
15. N.H.March, M.Parrinello, Collective Effects in Solids and Liquids, Adam Hilder Ltd., Bristol (1982).
16. A.V.Luzanov, Yu.F.Pedash, V.V.Ivanov, in: Reseach Reports in Physics. Condensed Matter. Electron-Electron Correlation Effects in Low-Dimensional Conductors and Semiconductors, Springer Verlag, Heidelberg, New York, 93.
17. Yu.F.Pedash, V.F.Pedash, A.V.Luzanov, *Zhur.Strukt.Khim*, **27**, 164 (1986).
18. R.J.Schwarz, Le Roy, *Surface Sci.*, **L141**, 166 (1986).
19. K.Fukui, H.Kato, T.Yonezava, *Bull.Chem.Soc.Jap.*, **33**, 1198 (1960).

К полуэмпирическим расчетам ван-дер-ваальсового взамодействия между сложными молекулами и поверхностью в рамках многоэлектронной схемы

А.В.Лузанов, В.В.Иванов

Расчитаны ван-дер-ваальсовы константы C_3^{A-S}, которые описывают дисперсонное взаимодействие сопряженной молекулы A с поверхностью (S) металлов или полупроводников. Для расчетов использовалась феноменологическая диэлектрическая функция соответствующего материала, исследование π-оболочек базировалось на методе полного конфигурационного взаимодействия. Предложенный подход требует одноразового решения уравнения теории возмущений. Вклад σ-оболочки оценен по аддитивной схеме через соответствующую динамическую поляризуемость. Приведены результаты расчетов для малых полиенов, кумуленов, бензола и нафталина, а также C_3^{A-S} для некоторых возбужденных состояний этих молекул.

Functional Materials **2**, No.1 (1995)

Internal chain dynamics in polymer-like distearyldimethylammonium hydroxide (DSDMA OH) and their interactions with surfaces

Michael Thies, Henrich.H. Paradies, David Shaun F. Clansy*

Markische Fachhochscule Biotechnology and Physical Chemistry,
D-58580 Iserlohn, P.O.Box 2061, Germany

*Witco Corporation, Safety, Health, and Environmental Affairs,
One American Lane, Greenwich, Connecticut, 068131-2559, USA

A detailed physical analysis of date obtained from static light (LS) and dynamic light scattering (QLS) experiments with polymer-like DSDMA OH micelles has been undertaken, supported by small-angle X-ray scattering (SAXS) measurements.

Докладний фізичний аналіз даних, одержаних в експериментах по статичному (LC) та динамічному (QLS) розсіянню світла на полімероподібних міцелах DSDMA OH, підкріплений результатами вимірювань малокутового розсіяння рентгенівського проміння (SAXS).

1. Introduction

It is well known that surfactant molecules self-aggregate into assemblies in aqueous solutions above the critical micelle concentration (CMC). Below the CMC the surfactants are in a monomeric state, above the CMC and at low micellar (volume fraction) concentrations, the aggregates are generally rotund, spherical micelles [1]. In some cationic surfactant systems and non-ionic or anionic systems as well as mixtures of cationic and anionic systems, long wormlike micelles form at higher concentrations and/or upon additions of salt or acid [2–5]. Solution properties of di-(*n*-alkyl)dimethyl-ammonium surfactants with different counterions have been investigated mainly for *n*-alkyl residues of C_{12} [6,7]. Brady et al. [8] and others studied the more water soluble didodecyldimethylammonium salts in the presence of various anions with respect to solubility, CMC, particularly emphazing the counterion specifity of doubl-echained cationic surfactants. However, there is little information available on the solution properties of distearyldimethylammonium (DSDMA) chloride in aqueous solutions [9]. Furthermore, there are no experimental date available on the DSDMA hydroxide in aqueous solutions which is believed to be an intermediate within the microbial biodegradation and metabolism of DSDMA halides [10]. DSDMA OH reveals a fairly unusual pattern in aqueous solution: at low molarity of salt it forms vesicles, at high salt as well as high surfactant concentration in forms threadlike micelles. Since the theory of the vesicle or spherical-to-wormlike micelle transition including the theory of the rheological behavior of wormilke micellar solution presently lack predictive powers, we believe it is important to establish convincing date of this system undergoing spherical (vesicular) to wormlike micelle transition for DSDMA OH. We studied in detail the conformation of DSDMA OH by means of dynamic light (QLS) and static light scattering (LS), including small-angle X-ray scattering (SAXS), because its importance of DSDMA Cl including its various applications as fabric softners etc., and its counterpart DSDMA OH within the microbial transformation which is dependent on the surfactant concentration (monomers vs. micelles) as well as on salt. Furthermore, we explored the adhesion of DSDMA

OH on solid surfaces by means of X-ray reflectivity and QLS in order to compare the solution structures of DSDMA OH, e.g. wormlike micelles vs. ordered Langmuir-Blodgett structures. The solid surfaces applied in this study are rutile (TiO_2) and kaolinite ($Al_2Si_2O_5(OH)_4$), respectively.

2. Theory

The scaling theory developed by de Gennes has been applied in describing the static properties of DSDMA OH as flexible polymer chains within the semidilute regime in terms of the correlation length, ζ [11]. The theory teaches that the osmotic pressure, π, in the semidilute regime is a function of ζ only, which is dependent on polymer concentration, C, but independent of molecular weight M, so relating $\pi \propto M^{\circ} c^{9/4}$ for semidilute solutions of polymers in good solvents.

It is appropriate to review the physical behavior of polymers in solution to compare to dilute and semi-dilute concentrations of DSDMA OH (0.005–0.05 M) in H_2O (0.1–0.25 M NaCl). This comparison is particularly relevant for polymers in good solvents when the polymer chains are expanded due to excluded volume effects. At very dilute solutions, the radius of gyration, R_g, and the polymerization index, N, of a coil are related through equation (1) [12,13]:

$$R_g \approx N^{\nu} \tag{1}$$

with $\nu = 0.6$. More recent determinations led to an exponent of 0.588 [13]. In the semi-dilute system where φ equals φ^* ($\varphi = 10^3 c_2 V_2$ where V_2 is the molal volume and c_2 the molar concentration of the solute, and φ^* is the crossover volume fraction of the solute), the thermodynamic properties are no longer dependent on N. The screening length, ζ, is the relevant parameter which is related to the average distance between nearest chain contacts:

$$\zeta = \varphi^{-0.77} \tag{2}$$

visualizing the micelle in semi-dilute solutions as a polymer having a mesh size of ζ which decreases in the good solvent limit. At the crossover volume fraction, φ^*, the correlation length, ζ, which is almost equal to the radius of gyration is related to the intensity of scattered light as:

$$I_s = \varphi^2 \zeta^3 = \varphi^{-0.31} \tag{3}$$

for semi-dilute solution versus dilute solution:

$$\frac{1}{I_s} = \frac{1}{AP(q)} + B \tag{4}$$

where I_s is the intensity of the scattered light, $q=(4\pi n/\lambda)\sin\varphi$ (n is the refractive index of the solution, λ the wavelength of the incident light, θ the scattering angle), and A and B are constants dependent on the weighted average molecular weight and on the concentration of the polymer. The function $P(q)^{-1}$ is related to the structure factor:

$$\frac{1}{P(q)} = \frac{1 + q^2\left(R^{2/3}\right) + Cq^4}{P(0)} \tag{5}$$

The factor C is a constant which depends on molecular weight, polydispersity, and structure. A plot of $P(q)^{-1}$ vs q^2 can reveal an upward curvature at small q-vectors, and subsequently a downward curvature at high c_2 in the case where the polydispersity index $\frac{M_w}{M_n}$ increases [14]. For dilute solutions of flexible chains with $qR_g << 5$ the reduced first cumulants are described in equation (6):

$$\frac{\Gamma_1}{q^2} = D(1 + C^1 q^2 R_g^2) \tag{6}$$

where D is the z-average diffusion coefficient $< D >_z$ at concentration c_2, and C' is equal to 2/15 or 13/75 [15]. For $qR_g \leq 1$, the q^2 term can be neglected so $\frac{\Gamma_1}{q^2}$ does not show any q-dependence. Extrapolation of $< D >_z$ to zero concentration reduces to the self-diffusion coefficient according to:

$$D_0 = \frac{k_B \cdot T}{6\pi n_0 \cdot R_H} \tag{7}$$

If the particle is non-spherical, then R_H is referred to as the apparent hydrodynamic radius. The autocorrelation function for relatively small particles undergoing Brownian diffusion can be described as:

$$g^{(1)}(\tau) = e^{-q^2 D_0 \tau} \tag{8}$$

For non-spherical particles, particularly considering the flexibility of long chain macromolecules, internal relaxation processes as well as rotational diffusion contribute to the line width of the scattered light. For a Gaussian coil, Pecora [16] developed an expression similar to equation (8) for the light scattering first-order correlation function:

$$q^{(1)}(\tau) = S_0(x)e^{-q^2D_0\tau} + S_2(x)e^{\frac{-q^2D_0+\frac{2}{\tau_1}}{\tau}} + \ldots \quad (9)$$

with $x \approx \frac{q^2}{R_g^2}$, τ_1 is the relaxation time of the first normal mode of the Gaussian coil, and the S_s are dynamic form factors [16]. Maeda and Fujime [17], and Harris [18] developed a theoretical description of dynamic light scattering from very long, very flexible rod-like macromolecules. The model expresses the elastic constants as the inverse of the Kuhn statistical length segment, γ, which is related to the persistence length by:

$$\gamma = \frac{1}{2l} \quad (10)$$

The first order correlation function can be expressed as a series of exponential analogues of equation (9). For the Gaussian coil limit ($\gamma L >> 1$), with L the length of the macromolecule, equation (11) can be obtained:

$$\tau_n = \frac{<R^2>}{3D_0\pi^2n^2} = \frac{2R_g^2}{D_0\pi^2n^2} \quad (11)$$

with $<R^2> = \frac{L^2}{\gamma L}$, which is the mean squared end-to end distance of the particle.

The apparent diffusion coefficient obtained by dynamic light scattering is defined as:

$$D_{app} = \frac{k_bT}{f^0} \cdot \frac{H(q)}{S(q)} = \frac{\bar{\Gamma}_1}{q^2} \quad (12)$$

with $k_s \cdot T$ the thermal energy, f^0 the friction factor at infinite dilution of the colloidal particle, $H(q)$ accounts for the hydrodynamic interactions between the particles, and $S(q)$ is the partial solution structure factor. For $q \to 0$, D_{app} is identified as the self-diffusion coefficient, D_m, and for $q \to \infty$ and $S(q \to \infty) = 1$, D_{app} is identified as the self-diffusion coefficient, D_{self} [19].

For DSDMA OH solutions above the CMC, micelle-micelle interactions are predominant so counterion diffusion, D_1, is much larger than D_0^{DSDMA} of these micelles. At the CMC, the mutual diffusion coefficient, D_m, of these micelle is constant; so micelle-micelle as indicated by the subscripts 22 correlations predominate:

$$D_m = D_0^{DSDMA} \cdot \frac{H_{22}}{S_{22}} = \frac{D_0^{DSDMA}(1 - k_h\phi)}{1 - k_d\phi} = D_0^{DSDMA}(1 + k_d\phi) \quad (13)$$

For a hard-sphere model, k_h ~6.45 and k_d~1.56 [20-21]. Due to the low CMC and the fast reaction rate regime of this system, the autocorrelation function of the scattered intensity represents only the micelle dynamics, and ϕ is the volume fraction of the micelles above the CMC.

In the limit of non-interacting particles, the translation diffusion coefficient D_{app}, which has been derived directly from the time-dependent part of the correlation function, coincides with the translational diffusion coefficient of the particle, D_0^{DSDMA}. For dilute solutions, D_{app} can me expressed according to equation (14):

$$D_{app} = D_0^{DSDMA}(1 + K \cdot c_2 + \ldots) = D_0^{DSDMA}(1 + [K_t + K_h] \cdot \phi) \quad (14)$$

where the coefficient K_t is the thermodynamic perturbation coefficient and proportional to the well-known second virial coefficient, K_h is the hydrodynamic perturbation coefficient, which has been evaluated by Batchelor [20] and Felderhof [21]. For spheric particles, D_0^{DSDMA} related to the Stokes' radius R_h by equation (9).

3. Results and Discussion

A. Surfactant concentration dependency of DSDMA OH at 25° C in water.

Let us represent the light scattering results in the form:

$$\frac{K(C - C_0)}{R_0 - R_0^0} = \frac{1}{M_2}[(1 + \frac{16\pi^2n_0^2}{3\lambda^2}R_g^2 \sin^2\frac{\theta}{2} + \ldots) + 2A_2(C - C_0) + \ldots] \quad (15)$$

where λ is the wavelength of light (632.8 nm), and n_0 is the refractive index of the NaOH solutions, R_g is the radius of gyration of the DSDMA OH particle in solution, and $C_0 = CMC_{\text{DSDMA OH}}$.

Assuming the DSDMA OH solution (5 mM) at salt concentrations between 0.0–0.15 NaOH behaves, in the first approximation, as ideal considering the low second virial coefficient, the angular dependence of the light scattering, and Debye-plot represent the radius of gyration and the reciprocal of micelle (vesicle) molecular weight (M_2) as function of DSDMA OH concentration (1–5 mM). We then can suppose that spherical particles having a radius of gyration of 135 Å would be formed at the CMC, and they associate with one another to form these particles which are vesicles up to concentrations of DSDMA OH

of 5 mM. In the concentration range between 1 mM to approximately 50 mM of DSDMA OH ($CMC = 1.05 \cdot 10^{-4}$), the radius of gyration, R_g, the second virial coefficient A_2, and weight-averaged molecular weight are obtained having values of $R = 135$ Å, $A_2 = 3.5 \cdot 10^{-2}$ mL · mol · g^{-2}, and $MW = 3.5 \cdot 10^6$. These values are consistent with those obtained from small-angle X-ray scattering experiments. However, by increasing the surfactant concentration above 5 mM (6–50 mM), a considerable increase of the radius of gyration occurs to $R_g = 815$ Å, weight-average molecular weight of $3.7 \cdot 10^6$, and $A_2 = 4.6 \cdot 10^5$ mL · mol · g^{-2}. Furthermore, increasing the DSDMA OH concentration in H_2O beyond 50 mM, the average molecular weight was determined to be 36.500, and from apparent diffusion coefficient we calculate a hydrodynamic radius of 25.0 Å. The apparent radius of gyration was found to be 19.5 Å, as determined by SAXS, resulting in a hydrodynamic sphere for DSDMA OH, having a radius of 24.7 Å. The «dry» hydrodynamic radius for DSDMA OH was calculated to be 22.83 Å, applying a partial specific volume of $v_2 = 0.8195$ mL · g^{-1}.

Considering now the intermediate concentration range more closely, the physical properties of DSDMA OH in the concentration range of 6–50 mM indicate that the DSDMA OH micelles are bulky, highly extended structures. The determined value of $R_g = 815$ Å agrees with the calculated Gaussian coil quantity of 805 Å. Similar values have been determined for DSDMA OH solutions (0.05 M) in the presence of 0.25 M NaOH or 0,25 M NaCl.

B. Effects on light scattering of DSDMA OH solutions by varying NaOH concentration (0.1–0.25 M).

Log-log plots of the scattered intensity and DSDMA OH concentrations (0.005–0.05 M) in 0.1 M and 0.25 M NaOH, both in water, at scattered wave factors of $q = 6.0 \cdot 10^{10}$, $q = 3.5 \cdot 10^{10}$, and $q = 0$, show that the maximum of the scattered intensity is shifted toward lower surfactant concentration when q decreases. In addition, the dissymmetry coefficient Z_{45} ($= \frac{R_{45}}{R_{135}}$) decreases with increasing DSDMA OH concentrations between 0.005–0.05 M under the same salt concentration. Below 5 mM, Z_{45} is about 1.15, but above 5 mM DSDMA OH, large values are observed in the presence of 0.1 M NaOH or 0.25 M NaOH, and decreasing by increasing the surfactant concentration. Furthermore, $\frac{1}{I_s}$ increases linearly with q^2 what is also observed for the most dilute solution of DSDMA OH of 0.005 M. The crossover between dilute and semi-dilute solutions of DSDMA OH, as seen in the log-log plots, is related to the strength of the maximum of intensity. Indeed, for long thin chains, $qR_q < 1$ is not obeyed over the whole scattering range of q values, since they are not accessible experimentally. Therefore, for a fixed q value, the maximum I_s appears at the crossover concentration where $q\zeta = 1$. To overcome this difficulty, I_s was extrapolated to $q = 0$ for determining the overlapping of chains. The slope was determined to be –0.37 vs. 0.31 as predicted by DesCloizeaux (equation 2) [22]. The experimental data for the semi-dilute range of DSDMA OH yield a slope of –0.33 ($C_{DSDMAOH} = 0.005$ M). The decrease of the scattered intensity, I_s, upon increasing DSDMA OH concentration in the range studied can be attributed to the decrease in correlation length ζ according to equation (11), which is also supported by the q^2 dependence of I_s. Applying equation (6) we calculate a radius of gyration of $R_q = 819$ Å. Taking virial effects into consideration, with $B_2 = 5.4 \cdot 10^{-5}$ mL · $mol \cdot g^{-2}$, the extrapolated radius of gyration becomes $R = 816$ Å. The analysis of the system comprising 50 mM DSDMA OH in 0.25 M NaOH in H_2O yields a radius of gyration of 800 Å.

The DSDMA OH micelles do not show significant polydispersity, and there are no changes of the characteristic length ζ of this system as long the narrow DSDMA OH concentration range is fixed. However, another explanation can well be a interpenetration of the DSDMA OH micelles resulting in a new characteristic length, ζ, which is independent of the micelle length, rather than polydispersity. So ζ is independent of the DSDMA OH micelle length with no overlapping of micelle size with DSDMA OH concentration, and the correlation length can be identified with R_g.

1. Low DSDMA OH concentrations [$c = 2.0 \cdot 10^{-3}$ *M, 1.86 c*;* $c_s = 0.55 - 0.75$ *M NaOH*].

Fig.1 shows a plot of Γ vs. q^2 where Γ is the average decay rate (see equations 6&7) for differ-

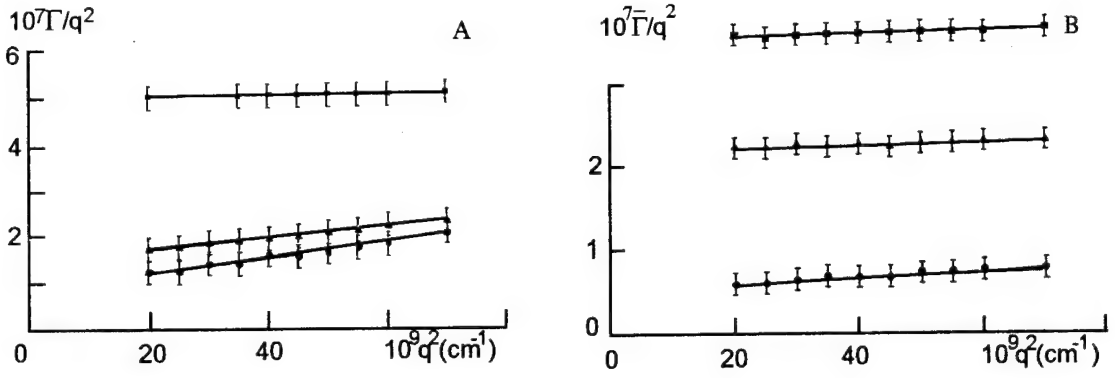

Fig.1. Variation of $\frac{\bar{\Gamma}}{q^2}\left(cm^2 \cdot s^{-1}\right)$ for DSDMA OH solution in H_2O - 0.55 M NaOH at different surfactant concentrations: (A) $C_{DSDMAOH} = 2$ mM (•), 5 μM (Δ), 20 μM (×);

(B) ιν H_2O-0.75 M NaOH at different surfactant concentrations: $C_{DSDMAOH} = 2\,mM$, 5 mM, 20 mM. The scattering vector is expressed in cm^{-1}.

ent DSDMA OH concentrations. The values of the average diffusion coefficients obtained by the cumulants method as a function of angle increases due to contributions of the internal modes for DSDMA OH concentration of $c = 2.0 \cdot 10^{-3}$ M. The values of the self-diffusion coefficients can be obtained from the intercepts of Fig.1 and the particle hydrodynamic radius R_h can be calculated according to equation (9). Within experimental error the DSDMA OH concentration dependence on the translational diffusion coefficient is seen in a log-log plot of the cooperative diffusion coefficient vs. concentration of DSDMA OH (Fig.2). The interesting finding is the concentration dependence of DSDMA OH on D, which is the z-average diffusion coefficient at concentration C. The decrease of D with a decrease in concentration of DSDMA OH in the range of 2 – 30 mM DSDMA OH in the presence of 0.5 – 0.75 M NaOH is associated with a decrease of ζ according to:

$$D \sim \Phi^{0.77} \sim \frac{k_b T}{\eta_0 \zeta} \qquad (16)$$

which is in agreement with our intensity measurements. Considering DSDMA OH micelles as flexible long-chain macromolecules in solution, as indicated by the findings shown above, internal relaxation processes need to be taken into account. These processes include random motions of segments of the chains as well as rotational diffusion which also contributes to the line width of the scattered intensity [26]. Analyzing the decay spectra according to equations (9), (11) for a Gaussian coil at selected angles following the notations of Pecora and Perico et al. [16,24], we were able to determine the first internal mode, τ_1, with reasonable precision at angles greater than 60°. This is because $q \cdot R_g = 1$ at $q = 51°$. At smaller angles, only one peak is obtained representing the translational diffusion coefficient terms. By increasing the magnitude of the scattering vector length, a second peak appears at a faster decay time and hence smaller in apparent size. The proximity of the image peak to the minor peak causes a perturbation on the peak position of the minor component of the time scale. For elimination of this drawback we divided the correlation

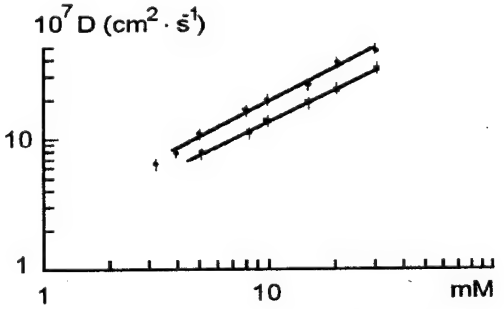

Fig.2. Decay time distribution function at different angles obtained through the Laplace inversions With CONTIN. The quantity $\Gamma A(\tau)$ has been plotted to yield an equal area represention. The unsmoothed results are represented showing the separation between translational diffusional constribution and the peak containing the constribution from internal modes for DSDMA OH.

function by $\exp(-qDt)$ to yield a «normalized» correlation function. By applying the correct limiting value for D as obtained through Fig.1, the contribution from the internal modes can be retained only by considering a single coil [25]. According to equation (9), the position of the fast moving peak on the scale corresponds then to both the diffusional and internal mode contributions of $g^{(1)}(t)$. At small scattering angles, e.g. $qR_g<1$, the translation diffusion coefficient is the only contribution to $g^{(1)}$, so the correlation function decays approximately as a single exponential. However, when qR_q becomes larger with increasing angle ($qR_q = 1.82 - 2.10$), the internal normal modes will contribute to the correlation function, so it becomes multi-exponential. The increase in the average diffusion coefficient, $<D>_z$, with scattering angle, also shows an increase in the relative variance, namely from 0.6–1.02, in the angular range of 30100°. Furthermore, when the DSDMA OH concentration increases, the variance $<v>$ of the correlation function decreases. This is in accord with the view that a progressive interpenetration of the flexible chains (micelles) occurs which indicates that the diffusion coefficient becomes independent of the internal characteristics of the micelle, but only dependent on the average distances between closest chain contact.

The experimental data have been prosecuted by applying a double exponential expression with a fixed Dvalue which is related to the slow relaxation rate, Γ_s, according to equation (17):

$$G^{(2)}(t) = 1 + \beta\left[A_s \cdot e^{-\Gamma_s t} + A_F \cdot e^{-\Gamma_F t} + C\right]^2 \qquad (17)$$

with $G^{(2)}(t)$ the measured correlation function, β is a constant which accounts for the deviations from ideal correlation, and C is the base line. The variables Γ_s and Γ_f are the relaxation rates of the slow and fast components, respectively, with Γ_s reflecting the translational mode, and Γ_f combines the fast internal modes and the diffusive component. This satisfies equation (9) so that $\Gamma_f - \Gamma_s = \frac{2}{\tau_1}$. The diffusion coefficient determined was fixed to $4.11 \cdot 10^{-6}\ \mathrm{cm}^{-2} \cdot \mathrm{s}^{-2}$ as measured at small angles. Fig.3 shows angular dependence of the fast mode amplitude for $c = 0.005$M DSDMA OH. The average τ_1 value calculated according to equation (17) fit the $G^{(2)}(t)$ measured correlation function, and was found to be 311 μs. This obtained value can be compared with the one computed from he first normal mode τ_1 for a free-draining coil according to Rouse and Zimm [26,27].

Now considering different interpretations of $<D>_z$, τ_1, τ_2, and R_h, e.g. if a Gaussian coil has o be long and very flexible. Following the Fujima notation for flexible macromolecules, $\gamma \cdot L >> 1$ with varying degrees of flexibility, the flexibility can be expressed in terms of the product of the particle length, $\gamma \cdot L$, where γ is the inverse Kuhn segment length, $1/\gamma = 2l$ with l the persistence length, and L is the length of the macromolecule in solution. Taking $n = 6020$ as the apparent aggregation number for DSDMA OH, for a spherical micelle the radius of the hydrocarbon core, R_{Hc} would be:

$$R_{HC} = \left(\frac{V_{HC}}{4\pi}\right)^{1/3} = 12.77\ \text{Å} \qquad (18)$$

with

$$V_C = n[27.4 + 26.9(n_C - 1)] = 485 \cdot n \qquad (19)$$

where $n_c = 18$, the number of carbons in the chains. For a cylinder of the same radius we calculate:

$$\pi r_{HC}^2 \cdot L(n) = 485 \cdot n \qquad (20)$$

which furnishes us with a value of $L(6020) = 2498.9$ Å. If $\gamma \cdot L = 10$, for a Gaussian coil where minimum flexibility is assumed, then the statistical segment length of $l' = \frac{L}{\gamma L} = 249.9$ Å is obtained with $n' = \frac{L}{l'} = 10$. The radius of gyration of such Gaussian coil is calculated according to:

$$R_g = \frac{n' l^2}{6} \qquad (21)$$

and would be 322.6 Å. This is much more smaller value than the 810 Å obtained for DSDMA OH, indicating that a Gaussian coil is not consistent with the experimental data obtained. The limit $\gamma \cdot L >> 1$ corresponds to a completely flexible coil, and would agree with equation (10) for the Rouse-Zimm model. We find a γL value of 9.9 (10) which indicates that the coil is not in the extreme limit of flexibiliby. If we introduce this values into he Fujima model [28] we calculate $\tau_1 = 596$ μs. This is much lower than the value of 311 μs obtained experimentally. One explanation for this discrepancy is that we are dealing with a semi-dilute solution so the overall rotational motion, which is related to τ_1, is suppressed. The τ_1

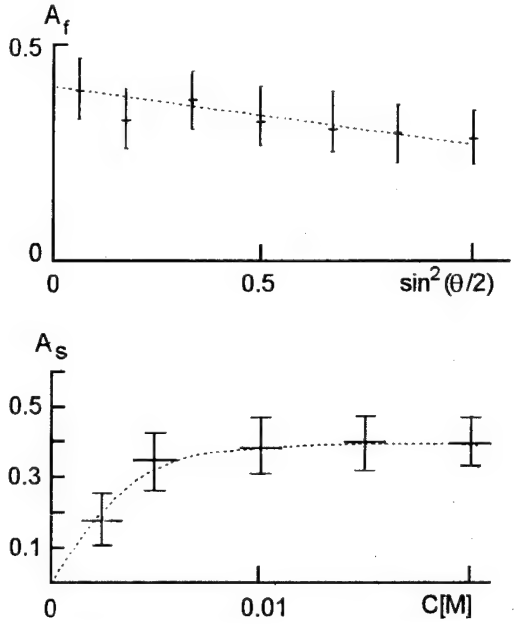

Fig.3. Relative amplitudes of the fast components as a function of the scattering angle (A) at $c = 0.005\ M$ DSDMA OH, and concentration of DSDMA OH (B), slow component.

value observed can also be related to a combination of τ_1 and τ_2 which, for a flexible rod, is of the order of $\tau_2 = 100$ μs. In addition, the τ_1 measured can be a combination of τ_1 and higher terms on the time scale which was not measured experimentally. However, the best qualitative description of the findings in this particular salt region (0.55 – 0.75 M NaCl) in the concentration range of DSDMA OH ($2.0 \cdot 10^{-3}$ M to $1.0 \cdot 10^{-2}$ M, 1.86 C^*–3.72 C^*) is that of a semi-dilute polymer solution, comprised of polymeric chains which are not at the extreme limit of flexibility, but revealing some stiffness of the hydrocarbon chains.

D. Concentration Dependence of DSDMA OH

The correlation functions with increasing concentration of DSDMA OH at 25 °C in absence of salt are shown in Fig.3. The single-modal distribution is seen at $C = 0.02$ M of DSDMA OH and at lower concentrations, also. However, by increasing the surfactant concentration to 0.05 M, a bimodal distribution is seen. Above 0.08 M DSDMA OH, gelation began which became stiff upon increasing DSDMA OH concentration up to 0.1 M. The same effect can be achieved by adding 0.02 M NaCl to a 0.05 M DSDMA OH solution (25 °C). Fig.4 depicts the angular dependence of the fast and slow peaks for $c = 0.05$ M DSDMA OH in the presence of 0.02 M NaCl which is almost identical in the presence of 0.01 M NaCl. Obviously the fast component is dependent on q^2 which is in accordance with a diffusive behavior. However, the slow component is independent of the scattering vector, q. This can be reconciled in view of a structural relaxation process of a stabilized polymeric network. The diffusive q^2 dependent fast mode seems to be temperature independent, when measured in the range of 25–35 °C, which is not the case for the slow component. Since gelation appears at $c_2 = 0.08$ M which is above c_2^* and corresponds to $2.7 \cdot 10^{-3}$ M surfactant, one can interpret the diffusive mode with increasing DSDMA OH concentration as a net of entanglements of extended flexible micellar aggregates. This reasoning follows the interpretation by Candau et al. [29] and Imae et al. [30] for solutions of cationic surfactants at high concentrations. The concentration dependence of the dynamic correlation length from the fast mode conforms to the Stokes–Einstein equation (see equation (9)). In

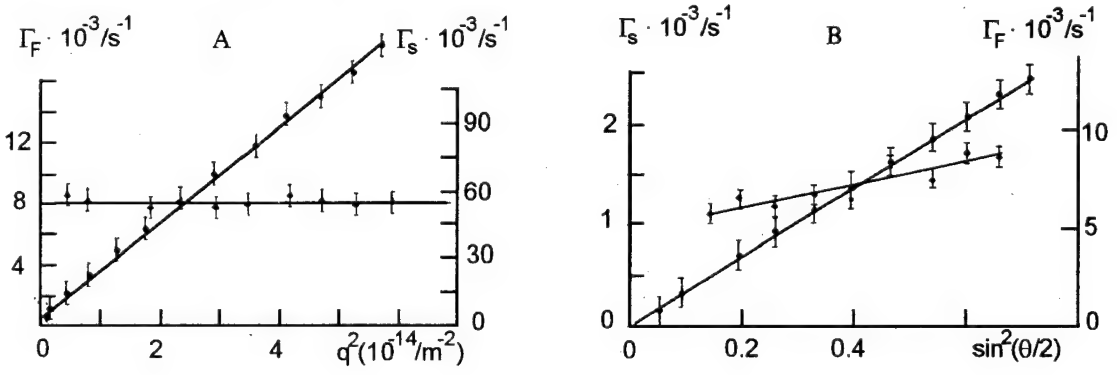

Fig.4. Angular dependence of the fast (•) (A) and the slow peaks (×) for 20 mM DSDMA OH in H_2O 0.02 M NaCl (25°C) or 0.02 M NaOH (B).

the range 2535 °C and 0.02 M salt at $c_2 = 0.08$ M DSDMA OH, the correlation length, ζ, was found to be temperature independent. The concentration exponent was found to be –0.66, which is smaller than the predicted value for long flexible chains in semidilute solutions of 0.77 [11]. The average dynamic correlation length (ζ) is of the order of 677 Å, whereas the persistence length is calculated to be 329 Å. Thus, according to equation (3), the semi-dilute solution of DSDMA OH can be visualized as a polymeric net with a mesh size of approximately 650-700 Å, which decreases as the polymer volume fraction, Φ, increases. The crossover volume fraction, Φ^*, (or c^* in terms of concentration) and the length, ζ, can be identified with R_g. The results are consistent with those obtained by LS.

E. DSDMA OH concentration between 0.08 M *and* 0.15 M

We observed a drastic decrease of the apparent aggregation number of DSDMA OH at 25 °C at surfactant concentrations above 0.08 M, and the presence of 1.5 M NaOH or 1.5 M NaCl in H_2O. The addition of NaOH does not change the picture, nor is there any precipitation. The high salt concentration experiments reveal that the Debye length, λ_D, can be approximated by the addition of salt, and interactions between the DSDMA OH micelles are most likely strongly screened. This is further substantiated by the concentration dependence of the translational diffusion coefficient upon surfactant concentration at different NaCl concentrations (1.0 to 2.0 M NaCl) (Fig.5). The slope of the line in Fig. 5 at 1.0 M NaCl (25 °C) is almost zero, indicating an approximately balance between repulsive and attractive forces. The extrapolated value of the apparent diffusion coefficient in this concentration range of DSDMA OH at 25 °C was found to be (5.82±0.35) 10^{-7} $cm^2 \cdot s^{-1}$. This corresponds to a hydrodynamic radius of $R_h = 24.95$ Å, and an actual frictional ratio of 1.11 assuming a partial specific volume of 0.819 $mL \cdot g^{-1}$ as measured by densimetric techniques. The value determined from theoretical calculations is 0.8188 $mL \cdot g^{-1}$.

The DSDMA OH micelles under these particular ionic conditions are reasonable well described by a hard-sphere model with k_S~7.9 and $k_D = 1.45$ after fitting the experimental obtained diffusivity data.

4. Adsorption of DSDMA OH on solids

There have been only few studies of polyelectrolyte adsorption at charged solid/solution interfaces using well-defined systems. For DSDMA OH or Cl^- there are no experimental data available. Obvious features to be considered in the absorption of DSDMA OH are the charge on the cationic surfactant, the charge on the substrate surface, and the conformation of DSDMA OH within the aqueous environment as seen in the preceding section. At high ionic strength, these charge effects are screened out due to micellization of DSDMA OH, and the system behaves essentially as neutral polymers or micelles. Decreasing ionic strength and following the conditions as found for DSDMA OH is akin to increasing the solvency. This opposes strong adsorption because of the build-up of strong intra- and intermolecular repulsions of segments of DSDMA OH in loops or segment tails. Furthermore, strong hydrophobic contribution to the adsorption free energy in addition to the electrostatic attraction/repulsion has to be considered also. Preliminary results for the adsorption processes as well as for the conformation of DSDMA OH on rutile, TiO_2, and kaolinite, $Al_2Si_2O_5(OH)_4$ are obtained at 25 °C.

A. Inelastic Light Scattering.

As a function of DSDMA OH concentration, ionic strength varied between by 0.005–0.1 M NaCl as a function of particle concentration (0.01–0.005 %) of rutile or kaolinite, respectively. The hydrodynamic thickness was determined in each experiment. The thickness has been calculated as the difference in the radii of the bare and

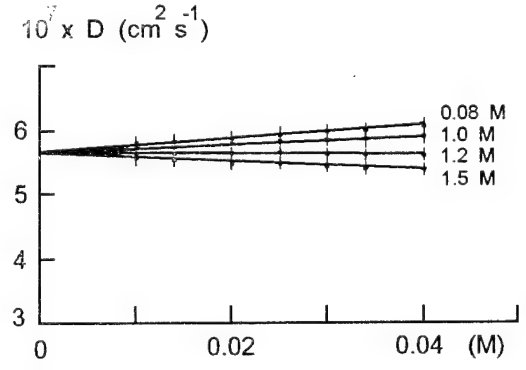

Fig.5. Apparent diffusion coefficient (D_{app}) for DSDMA OH as a function of DSDMA OH concentration (c = 0.08-0.015 M), and NaOH concentration (1.0 M - 1.5 M) at 298 K.

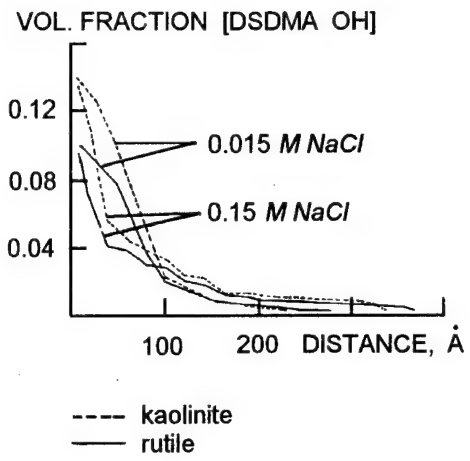

Fig.6. Segment volume fraction profiles for DSDMA OH on rutile or kaolinite at different ionic strengths (20°C). The surface excess, $\Gamma_{DSDMAOH}$, resulting from adsorption on surface sites equal the total number of surfactant chains comprised in one layer of thickness; R_0; $R_0 = N^{1/2}.a.$; $\Gamma_{DSDMA} = \frac{N^{-1/2}}{a^3} = \frac{1}{a^3}\Phi$, and a is the ideal chain radius.

covered inorganic particles through equation (7). Applying the different conditions as disclosed in the preceding section for DSDMA OH, we can compare the determined hydrodynamic radii directly with the values obtained in solution. Within the concentration range of DSDMA OH of $C_2 = (20\text{-}50) \cdot 10^{-3}$ M, equivalent $7.44\,C_2^* - 18.6\,C_2^*$ where $C_2^* = \frac{3M_r}{4\pi R_g^2 N_A}$, we determined a hydrodynamic radius of $R_h \approx 200.0$ Å which is a strong indication of segments occurring in extended tails which are highly hydrated. There is apparently no difference between the two substrates used in the adsorption studies. For the negatively charged surface, there is an initial increase in the thickness of DSDMA OH on increasing DSDMA OH concentration up to 0.01 M reaching a plateau of $R_h \approx 2.050$ Å. Increasing the ionic strength to 0.8–0.1 M NaCl, the determined hydrodynamic thickness is of the order of $\approx 50 - 60$ Å. This would tend to favor the formation of an extended layer at low ionic strength of DSDMA OH, but it seems to be offset at high ionic strength due to formation of «micellar» aggregates at the surface, or by the coil concentration due to the reduction in the intrachain repulsion of DSDMA OH coils. Furthermore, the transition of DSDMA OH of long flexible entangled micelles to spherical micelles of diameter of 60 Å is reversible by changing the surfactant or salt concentration which is seen on the solid surfaces also. The only difference of the behavior of DSDMA OH on these inorganic surfaces is the pH dependent decrease of the CMC on either hydrophilic (as shown here) and the hydrophobic surfaces.

B. X-ray reflectivity Measurement.

Very preliminary results are obtained for DSDMA OH an kaolinite surface as substrate. The $I(h)$ data are analyzed according to equation (26):

$$I(h) = \frac{A}{h^2}\left|\int_0^\infty e^{ihz}\rho(z)dz\right|^2 + B \qquad (26)$$

with $h = 4\pi/\lambda \sin\theta/2$, $\lambda = 1.54$ Å, θ – scattering angle, A is a constant related to the bare koalinite radius and the adsorbed amount of DSDMA OH, and B a constant (incoherent background) [31]. $\rho(z)$ has been evaluated as described in [32]. The $\rho(z)$ for DSDMA OH on kaolinite particles under conditions of $c_2 = 25 \cdot 10^{-3}$ M ($\hat{=} 7.40\,c_2^*$) or at salt concentrations of $c_S = 0.40 - 0.51$ M NaCl) shows profiles reflecting a hydrated flat conformation with $\rho(z)$ falling rapidly to a value of 210.0 Å. This can also be interpreted as evidence for entangled tails of DSDMA OH (Fig.6). Furthermore, the $\rho(z)$ profiles for DSDMA OH demonstrate a similar adsorption behavior as determined by QLS. The shape profiles suggest strongly upon changing the ionic strength (or the DSDMA OH concentration) that on the kaolinite surface the entanglement ("loop") of DSDMA OH is seen within narrow c_2 and ionic strength, respectively. Increasing the ionic strength from 0.8 to 1.1 M, the $\rho(z)$ decreases to values of approx. 60–70 Å. Again, the intersegmental and electrostatic repultions that occur in the entanglement are suppressed at higher ionic strength. The larger adsorbed amounts with increasing ionic strength or c_2 (DSDMA OH) is also consistent with these findings. Additional information of DSDMA OH orientation on hydrated and dehydrated surfaces are obtained from Landmuir-Blodgett films of DSDMA OH at 1.2 M NaCl (25 °C). For films of five and more layers we were able to distinguish peaks that are (001) Bragg peaks corresponding to a unit cell spacing of 54.8 Å. Furthermore, the conclusion that the C_{18} chains are nearly perpendicular to the surface of the kaolinite follows the fact that

$D = 54.8$ to -56.5 Å (dependent on the degree of hydration) is close to the estimated length of the molecule, 50.451.8 Å including the hydroxyl which is located at the outer surface, approx. ~48.049.0 Å. This finding is supported by surface IR-measurements revealing that the chains of C_{18} are perpendicular to the surface, and are also in extended conformation. However, upon drying a different pattern is to be seen which is reversible upon addition of H_2O. One possible explanation is that the sorbed DSDMA OH move apart upon drying due to the repulsive interactions of the polar cationic head groups which are less well shielded as water being removed. In the wet stage, the CH_2 chain form an aggregate structure due to favorable hydrophobic interaction, dependent on c_2, T, ionic strength and the nature of the substrate also. Steric interactions between DSDMA residues also occur when particles have been an absorbed layer depending on the conformation of the adsorbed molecules and substrate. Repulsive effects can be in part arise from a loss of configurational entropy of flexible segments on the approach of another surface, particularly using fabrics, or a metal surface, metal oxides. As a result, the volume available for the absorbed flexible chains on the surface becomes restricted leading to a loss of configurational entropy. This effect is referred to as the volume restriction effect.

4. Conclusion

The DSDMA OH is highly soluble in water forming spherical vesicles of size $R_h = 300$ Å and does not flocculate upon addition of salt. The DSDMA OH vesicles revert to micelles with increasing surfactant concentration having an aggregation number of approximately 60. The same aggregation number for the hydroxide can be obtained by raising the salt concentration to 1.0–2.0 M NaCl keeping the surfactant concentration constant. In the overlapping range with respect to DSDMA OH and salt concentrations, the appropriate hydrodynamic description is that of thread-like micelles. In dilute DSDMA OH and in the presence of 0.01 M NaCl solutions, the first normal mode of the chains (τ_1-value) supports the free-draining Zimm model when compared to theoretical calculations. At semi-dilute surfactant concentrations and low salt concentrations, the decay time distribution is bimodal with two well separated components on the inelastic time scale. The faster q^2 dependent component is due to cooperative motions of a transient network being formed through the interchain entanglements. The slow q independent component is of large amplitude and reflects the disruption/coalescence kinetics of the micellar aggregates which are characterized by a strong positive concentration dependence of the obtained relaxation rate. The relaxation time decreases with increasing concentrations of salt (NaCl) and DSDMA OH. The result obtained for DSDMA OH can be interpreted according to theories of solutions of long flexible polymer chains within the semi-dilute concentration range where the DSDMA OH polymer coils overlap by forming a network of mesh size $\zeta = 815$ Å. This has been found for DSDMA OH in the concentration range of $c_2 = (20 - 50)\cdot 10^{-3}$ M ($7.44\, c_2^* - 18.6\, c_2^*$) or at low surfactant concentrations ($2.0 \cdot 10^{-3}$ M, $7.44 \cdot c_2^*$) and salt concentrations $c_s = 0.55 - 0.75$ M NaOH or NaCl. Above DSDMA OH concentrations of 0.08 M, the aggregation number decreased to 61, leaving micelles of hydrodynamic radius of 25.0 Å which are stable at high salt concentrations. The transition of DSDMA OH vesicles to long flexible entangled micelles to spherical micelles of diameter 50 Å is reversible by changing the surfactant or salt concentration. These results strongly support a model of long flexible entangled DSDMA OH micelles in aqueous solutions as an important intermediate in microbial transformation [33].

The results obtained for DSDMA OH in solution can be compared to studies on solids, e.g. rutile and kaolinite, revealing a lowering of the CMC upon sorption imparting a less hydrophilic surface of the substrates studied. However, the different conformations of DSDMA OH upon adsorption to the substrates can be detected referring to entanglements at medium ionic strength and the semidilute regime, and compact micellar arrangements at high salt (1.0 M NaCl) and high DSDMA OH concentrations.

Acknowledgment: H.H.Paradies and M.Thies would like to acknowledge the support of the BRITE-EURAM-Program #4088 and U.Hinze for valuable discussions.

References

1. J.Appell, G.Porte, *Europhys. Lett.*, **12**, 185 (1990).
2. S.J.Candau, F.Merikhi, G.Walton, P.J.Lemarechal, *J.Phys.* (Paris), **51**, 977 (1990).
3. H.Rehage, H.Hoffmann, *J. Phys. Chem.*, **92**, 4217 (1988).
4. M.E.Cates, *J. Phys. Chem.*, **94**, 371 (1990); T.Imae, S.Ikeda, *J. Phys. Chem.*, **90**, 5216 (1986).

5. H.H.Paradies, S.F.Clancy, J.G.Fuller, manuscript in preparation, 1994.
6. Y.Talmon, D.F.Evans, B.W.Ninham, *Science*, **221**, 1047 (1983).
7. S.Hashimodo, J.K.Thomas, D.F.Evans, et al. *J.Colloid Interface Sci.*, **95**, 594 (1983).
8. J.F.Brady, D.F.Evans, G.G.Warr, et al., *J.Phys.Chem.*, **90**, 1853 (1986).
9. H.H.Paradies, *Angew.Chem.*, **94**, 793 (1982); H.H.Paradies, *Angew.Chem.Supplement*, 1670-1981 (1982); R.G.Laughlin, R.L.Munyon, Y.-C.Fu, J.T.Enige, *J.Phys.Chem.*, **95**, 3852 (1991); R.G.Laughlin, R.L.Munyon, Y.-C.Fu, A.Fehl, *J.Phys.Chem.*, **94**, 2546 (1990); H.H.Paradies, *J.Phys.Chem.*, **90**, 5956 (1986); H.H.Paradies, *Medicinale*, **14**, 1 (1984).
10. S.F.Clancy, P.H.Steiger, D.A.Tanner, at al., *J.Phys.Chem.*, **98**, (1994) in press.
11. P.G.DeGennes, *Scaling Concepts in Polymer Physics*, Cornell University Press, Ithaca, N.Y. (1979).
12. S.J.Candau, E.Hirsch, R.Zana, *J. Colloid Interface Sci.*, **105**, 521 (1985).
13. J.Prost, F.Rondelez, *Nature, Supplement*, **350**, 11 (1991); J. P.Flory, *Principles of Polymer Chemistry*, Cornell University Press, Ithaca, N..Y. (1953).
14. C.Quivolan, *Chimii Macromoleculaire II*, Chapter III, p.117, Hermann, Paris (1972).
15. W.Burchard, M.Schmidt, W.H.Stockmeyer, *Macromolecules*, **13**, 580 (1980).
16. R.Pecora, *J.Phys.Chem.*, **45**, 1562 (1965).
17. T.Maeda, S.Fujime, *Macromolecules*, **14**, 809 (1981).
18. RA.Harris, J.EHearst, *J.Phys.Chem.*, **44**, 2595 (1966).
19. K.S.Schmitz, *Introduction to Dynamic Light Scattering by Macromolecules*, Academic Press, Inc., Boston, San Diego, New York, 205–249 (1990).
20. G.K.Batchelor, *J.Fluid Mech.*, **131**, 155 (1983).
21. B.U.Felderhof, *J.Phys.Chem.*, **11**, 929 (1978).
22. J.Des Cloizeaux, *J.Phys.Chem.*, **36**, 281 (1975).
23. S.W.Provencher, *Makromol.Chem.*, **180**, 201 (1979); S.W.Provencher, J.Hendrix, L.Detiayer, *J.Phys.Chem.*, **69**, 4273 (1970).
24. A.Flamberg, R.Pecora, *J.Phys.Chem.*, **88**, 3026 (1984).
25. T.Nicolai, W.Brown, R.M.Johnson, MIMacromolecules, **22**, 2795 (1989).
26. P.E.Rouse, *J.Phys.Chem.*, **21**, 1272 (1955).
27. B.H.Zimm, *J.Phys.Chem.*, **24**, 269 (1956).
28. S.Fujima, M.Maruyama, *Macromolecules*, **6**, 237 (1973).
29. S.J.Candau, E.Hirsch, R.Zana, M.Adam, *J.Colloid Interface Sci.*, **122**, 430 (1982).
30. T.imae, R.Kamiya, S.Ikeda, *J.Colloid Interface Sci.*, **108**, 215 (1985).
31. J.Als Nielsen, *Physica*, **1497**, 376-(1974).
32. T.Cosgrove, T.L.Crowley, B.Vincent, et al., *Faraday Symp.Chem.Soc.* , **16**, 101 (1981).
33. S.F.Clancy, D.A.Tanner, M.Thies, H.H.Paradies, San Francisco, CA, 203'rd National Meeting of the American Chemical Society, **32(1)**, 907 (1992); S.F.Clancy, D.A.Tanner, Extended Abstracts Division of Environmental Chemistry, Atlanta, GA, 201'st National Meeting of the American Chemical Society, **31(1)**, 117 (1991); S.F.Clancy, D.A.Tanner, M.Thies, H.H.Paradies, submitted to *Science* (1994).

Динамика внутренних цепей в полимероподобных гидроксиде дистеарилдиметиламмония (DSDMA OH) и их взаимодействие с поверхностями

Михаэль Тиз, Генрих Г.Парадиз, Дэвид Шон Ф.Кланси

Подробный физический анализ данных, полученных при экспериментах по статическому (LS) и динамическому светорассеянию (QLS) на полимероподобных мицеллах DSDMA OH, подкрепленный результатами измерений малоуглового рентгеновского рассеяния (SAXS).

Functional Materials **2**, No.1 (1995)

Ion exchange processes on synthetic carbons

A.M.Puziy, T.M.Mironyuk, N.T.Kartel and I.P.Khanasyuk

Institute for Sorption and Problems of Endoecology,
32/34 Palladin Ave., 252142 Kiev, Ukraine

The process of copper adsorption on synthetic oxidized carbons with various structure of matrix is investigated. The carbons involved have been obtained by carbonization of styrene-divinylbenzene precursor at various temperatures (400-1100 °)C with subsequent oxidation by nitric acid. The structure of carbon matrix was studied using electrical resistance measurements and ESR method. It has been shown that ion exchange properties of synthetic oxidized carbons depend heavily on the structure of carbon matrix. Three mechanisms of copper adsorption are recognized depending on quantity of spin electrons in carbon matrix and its electrical resistance.

Вивчено процес адсорбції іонів міді на синтетичному окисленому вугіллі з різними властивостями вуглецевої матриці. Зразки вугілля одержано карбонізацією стирол-дивінілбензольного співполімера до різних температур (400 - 1100 °С) з наступним окисленням азотною кислотою. Структура вуглецевої матриці була вивчена по електропровідності та методом ЕПР. Показано, що іонообмінні властивості синтетичного окисленого вугілля сильно залежать від структури вуглецевої матриці. Встановлено три різних механізми адсорбції іонов міді в залежності від кількості неспарених електронів у матриці та її електричного опору.

Introduction

Active carbons find a widespread use in various processes for their unique properties (thermal, chemical and radiation stability, low swell, high adsorptive capacity) [1]. In presence of oxygen (air), active carbons acquire positive charge and can exchange anions in water solutions. Unlike active carbons, the oxidized carbons have the ability to exchange cations due to presence of surface functional groups [2]. Ion exchange behaviour of such adsorbents depends on the properties of matrix to where surface functional groups are attached. This paper deals with the peculiarities of ion exchange on synthetic carbons having various structure of matrix.

Experimental

Synthetic active carbons were prepared by carbonization of porous styrene-divinylbenzene precursor (10% DVB) at various temperatures ranging from 400 °C to 1100 °C [3]. Then carbons were oxidized with boiling 20% nitric acid during 5 hours and washed with water. Resistance was measured on powdered carbons using alternative current (10 KHz) and constant pressure. ESR signal was measured in air at 3 cm radiation using SEPR-03 apparatus (St.Petersburg).

Results and discussion

Resistance of active carbons depends critically on the treatment temperature (Fig.1). As the temperature increases, the resistance drops sharply within the 600-700 °C range. What this means is a structural transformation occurs when copolymer is pyrolysed. Conductance of carbons is due mainly to π-electrons displacement over the polyaromatic chain through the conjugated bonds.Low-temperature carbons though contain conductive domains, however, these are separated from each other by insulating layers of uncompletely carbonized hydrocarbons. These compounds burn away further as temperature increases. As this takes place, the structure of carbon matrix is ordered, the graphite-like domains come directly into contact to form unified conjugated system of electrons. Because of this, the sharp fall in resistivity at 600-700 °C is ob-

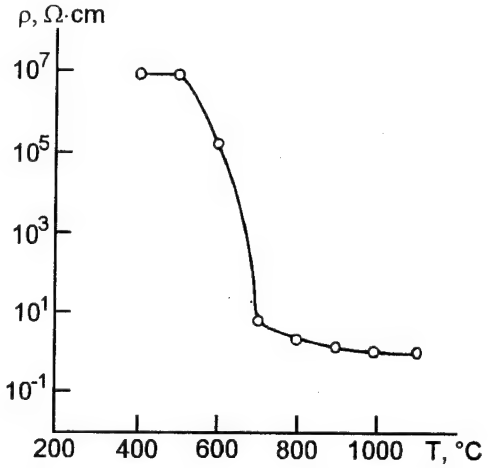

Fig.1. Dependence of resistance on temperature heat treatment of styrene divinylbenzene copolimer.

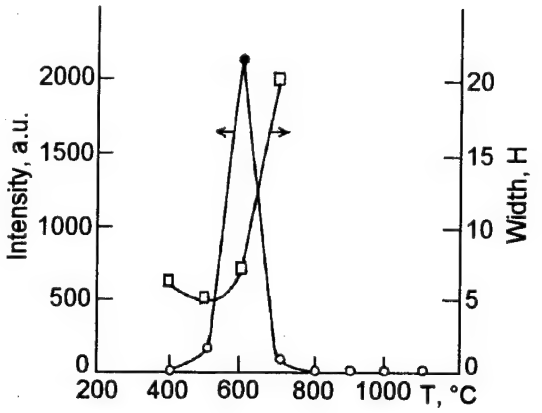

Fig.2. Dependence of ESR spectra parameters (intensity and width) on the heat treatment temperature of styrene- divinylbenzene copolimer.

served. This hypothetical scheme is supported by ESR measurements (Fig.2). At the carbonization of styrene-divinylbenzene copolymer, ESR signal at first increases indicating the breaking of bonds to yield the unpaired electron. Further increasing of temperature cause the spin electrons to decrease by recombination of carbon fragments to large condensed aromatic domains. Above 700-800 °C, carbon matrix is so conductive that ESR signal disappears, probably because of broadening the signal.

This is indirectly supported by changes in catalytic properties of active carbons in red-ox reaction. In such systems, the catalytic activity depends heavily on the presence of virtually delocalized π-electrons in carbon crystallites which can move freely through system of conjugated bonds and makes carbons an active catalyst [4]. With the rise of temperature, the reactions of hydrogen peroxide decomposition and cumene oxidation show an increase in velocity (Fig.3). This action is to account for the increase of electron donative ability (namely electron transfer from carbon surface to the substrate molecules) of carbons due to enhancement of conjugated area as the heat treatment temperature increases.

Being oxidized in the same conditions, synthetic carbons have different total ion exchange capacity and distribution of surface functional groups (Table). This fact is caused by distinctions in reactivity of carbons towards nitric acid. The ability of carbons to react with nitric acid gradually decreases as the temperature of heat treatment increases. Low-temperature carbons are chemically similar to aromatic compounds whereas high temperature carbons are similar to glassy carbon. Despite the steady decrease in total exchange capacity as temperature is increased,

Table. Distribution of surface functional groups on synthetic active carbons having various temperature heat treatment.

Temperature	Total	Strong acid	Weak acid	Phenolic
400	3.65	-	-	-
500	2.5	1.1	0.7	0.7
600	2.3	1.0	0.7	0.6
700	2.2	0.9	0.7	0.6
800	2.0	0.8	0.7	0.5
900	1.95	-	-	-
1000	1.6	0.6	0.7	0.3
1100	1.55	-	0.7	-

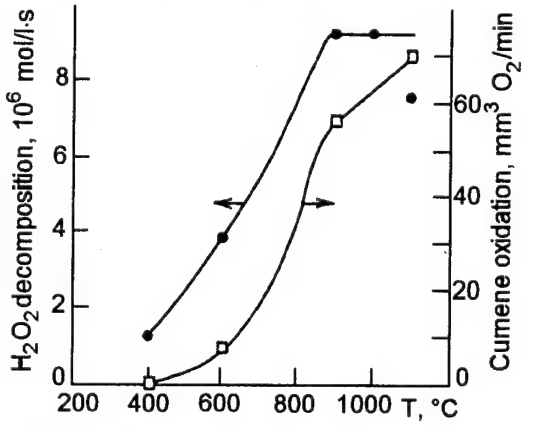

Fig.3. Dependence of catalytic activity in H_2O_2 decomposition and cumene oxidation on the heat treatment temperature of styrene-divinylbenzene copolimer.

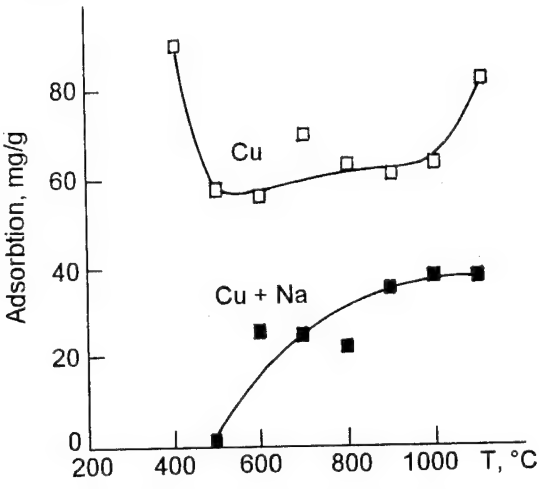

Fig.4. Dependence of cooper adsorption without and in presence of large amount os sodium ions (1:100) on the heat treatment temperature of styrene-divinylbenzene copolimer.

the adsorption of copper decreases only in early stage of carbonization (Fig.4). Then the adsorption increases and, for high temperature carbons, exceeds the total exchange capacity (Fig.5). Temperature dependence of ESR signal from adsorbed copper (Fig.6) has analogous run up to 700 °C. Thereafter, ESR signal decreases heavily probably due to reduction of Cu(II) to Cu(I). The data obtained indicate the changes in mechanism of copper adsorption on oxidized carbons having various structure. Three stages of mechanism of copper adsorption may be recognized:

I. 400-500 °C. Adsorption of copper is due to ion exchange on surface functional groups attached to non-conductive carbon matrix. At this stage, the ion exchange mechanism like to that on cation exchange resins is observed.

II. 500-700 °C. Despite decreasing of the total exchange capacity, the increasing copper adsorption is due to changes in quality of surface functional groups attached to conductive carbon matrix.One conceivable reason for this increasing is formation of complex with charge transfer from carbon surface to adsorbed copper.

III. 700-1100 °C. Further increasing of copper adsorption is due to full electron transfer from carbon surface to adsorbedcopper yielding Cu(I).

Conclusions

Ion exchange properties of synthetic carbons depends heavily on structure of carbon matrix,

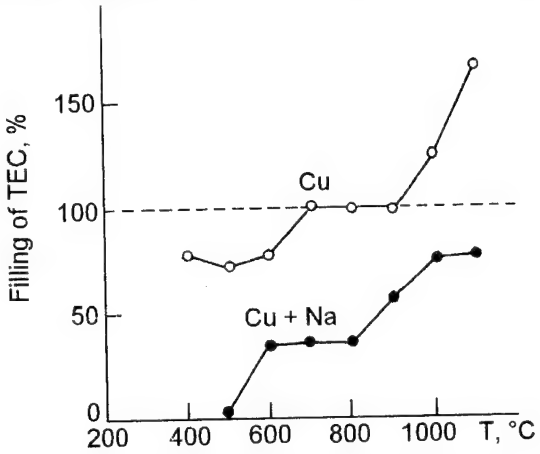

Fig.5. Dependence of filling of total exchange capacity on the heat treatment temperature of styrene-divinylbenzene copolimer.

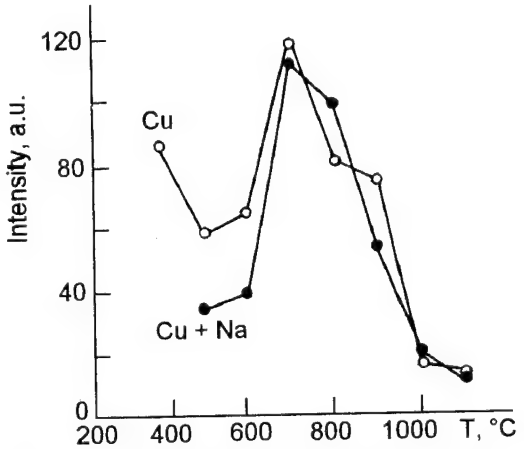

Fig.6. Dependence of ESR signal from adsorbed cooper on the heat treatment temperature of styrene-divinylbenzene copolimer.

particularly on electron conductivity. Three stages of cations exchanges of copper is recognized depending on quantity of spin electrons in carbon matrix and its electrical resistance.

References

1. B.McEnamey, T.J.Mays, P.D.Causton, *Langmuir*, **3**, 695 (1987).
2. B.R.Puri, Chemistry and Physics of Carbon., N.Y. (1970), p.191.
3. N.T.Kartel, A.M.Puziy and V.V.Strelko, *Porous Structure of Synthetic Active Carbons. Characterization of Porous Solids (COPS II), Amsterdam-Oxford-N.Y.-Tokyo: Elsevier,* (1991).
4. S.V.Mikhalovskii, Yu.P.Zaitsev, A.M.Puziy, Ist. European Congress on Catalysis EUROPACAT-1, Montpelier, France, Book of Abstracts, **1**, 263 (1993)

Ионообменные процессы на синтетических углях

А.М.Пузий, Т.И.Миронюк, Н.Т.Картель, И.П.Ханасюк

Исследован процесс адсорбции ионов меди на синтетических окисленных углях с различными свойствами углеродной матрицы. Образцы углей получали карбонизацией стирол-дивинилбензольного сополимера до различных температур (400-1100 °С) с последующим окислением азотной кислотой. Структура углеродной матрицы изучена по электропроводности и методом ЭПР. Показано, что ионообменные свойства синтетических окисленных углей сильно зависят от свойств углеродной матрицы. Установлены три различных механизма адсорбции ионов меди в зависимости от количества неспаренных электронов в матрице и ее электрического сопротивления.

Functional Materials **2**, No 1 (1995)

Enamine-metal complexes immobilized on the silica surface

V.V. Antoschuk, A.A.Golub and A.B. Lusenko

T.Shevchenko Kiev University, 60 Vladimirskaya St., 252001 Kiev, Ukraine

A number of Schiff bases immobilized on the silica surface has been synthesized. The individuality of compounds obtained has been proved with the help of physical and physico-chemical methods. The adsorbtion properties of obtained carriers with respect to Cu^{2+}, Co^{2+}, Ni^{2+}, Zn^{2+} and VO^{2+} have been studied. The structure and composition of forming complexes have been researched with different spectroscopic methods. It has been shown that, for copper and cobalt, pseudo-tetrahedral surroundings are primarily realized with immobilized ligands. Square-pyramidal structures are observed for VO^{2+} and nickel is adsorbed in square-planar positions.

Синтезовано ряд іммобілізованих на поверхні аеросилу основ Шиффа. За допомогою фізичних та фізико-хімічних методів доведено індивідуальність отриманих сполук. Вивчено сорбційну здатність отриманих носіїв по відношенню до катіонів Cu^{2+}, Co^{2+}, Ni^{2+}, Zn^{2+} та VO^{2+}. Спектроскопічними методами досліджено будову та склад комплексів, що утворюються. Показано, що для міді та кобальту, з іммобілізованими лігандами, реалізується переважно псевдотетраедричне оточення. Для ванадилу спостерігаються квадратно-пірамідальні структури, а нікель сорбується в площинно-квадратні позиції.

Studies involving the immobilization of organic compounds and chelating groups became an ongoing area of active research. Much attention has been devoted to structural and spectroscopic studies of immobilized compounds. Schiff base complexes are of interest as model compounds for the understanding the processes of adsorbtion. Major topics of the investigation have included Schiff bases immobilization on the silica surfaces, investigation of their adsorbtion properties and structure of complexes formed.

In this contribution we report on our studies involving the synthesis and investigation of immobilized ligands and complexes thereof with metal ions. Some immobilized Schiff bases were synthesized represented on Fig.1. A general preparation method for the immobilized ligands is described below.

Information about the structure of the products prepared be several synthetic methods was obtained from IR spectroscopy, electronic absorption spectroscopy, electron paramagnetic resonance spectroscopy, elemental and thermogravimetric analyses.

The IR spectra of all immobilized ligands and complexes were recorded in the solid phase as thin films between KBr discs on the UR-10, UR-20 spectrometers.

UV spectra were obtained with Specord M-40 as diffusion reflectance ones.

ESR spectra of solid samples are recorded at room temperature on the PS.100 X spectrometer.

All starting materials and solvents were obtained from commercial sources and used with further purification (recrystallization of aldehydes and ketones, drying and cleaning of organic solvents for the synthesis). Immobilized amines were prepared according to standard method by reacting silica gel with γ-aminopropyltriethoxysilane or N-β-aminoethyl-γ-aminopropyltriethoxysilane. All Schiff bases were made by stirring 10 g of γ-aminopropyl silica gel (γ-APA) or N-β-aminoethyl-γ-aminopropyl silica gel (AE-γ-APA) with 100 ml of the appropriate ketone or aldehyde solution in the mixture of benzene and 2-propanol 5:1). In all cases, coloured product was separated from the reaction mixture by filtration washed with benzene, 2-propanol, and dried under vacuum at 40-60 °C.

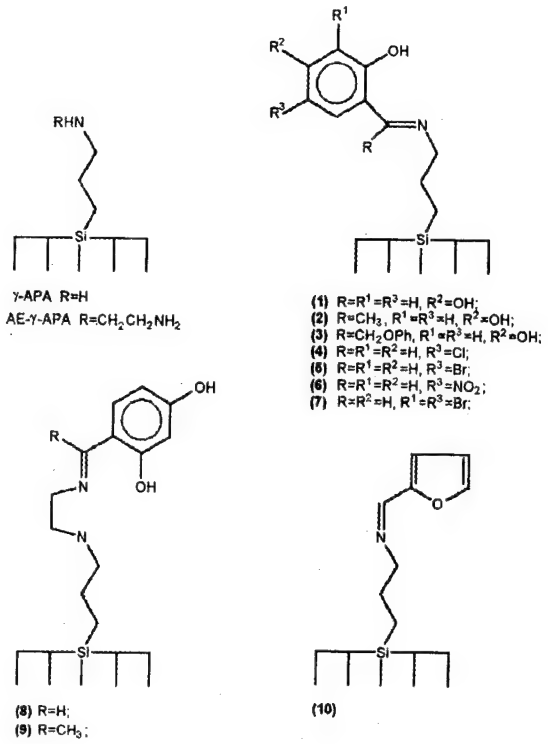

Fig. 1. Immobilized ligands and symbols for designation thereof.

All products are stable to benzene and methanol extraction and to hydrolysis by water. In agreement with the thermogravimetric analysis, the immobilized Schiff bases are stable to 140-170 °C. For the species, are observed two thermoeffects at 150-200 °C, 560-590 °C which correspond with step-to-step destruction immobilized groups.

The sorption capacities of the immobilized ligands for Cu^{2+}, Co^{2+}, Ni^{2+}, VO^{2+} and Zn^{2+} was determined. In each case, 0.5 g of silica gel containing the immobilized groups was equilibrated with 50 ml of metal solution (with different concentration) for 1 hour with intermixing. The solid extractant along with the metal ion adsorbed were separated from the solution by filtration. The residual metal ions were titrated according to standard EDTA methods.

The adsorbtion capacity of these modified silica gels may be different under various experimental conditions. In this work, the capacities range from about 0.1-0.7 mmol per gram (minimum for Ni^{2+} cations and maximum for Cu^{2+}). The results are represented on Fig.2-3.

IR spectra of the immobilized groups were taken in the range 1300-3600 cm^{-1}. The spectra show bands at 1640 and 3300-3400 cm^{-1} due to ν(C=N), ν_{as}(N—H) and ν_s(N—H) (residual amino-groups) respectively [1]. As a result of the coordination, the band ν(C=N) is shifted to 1610-

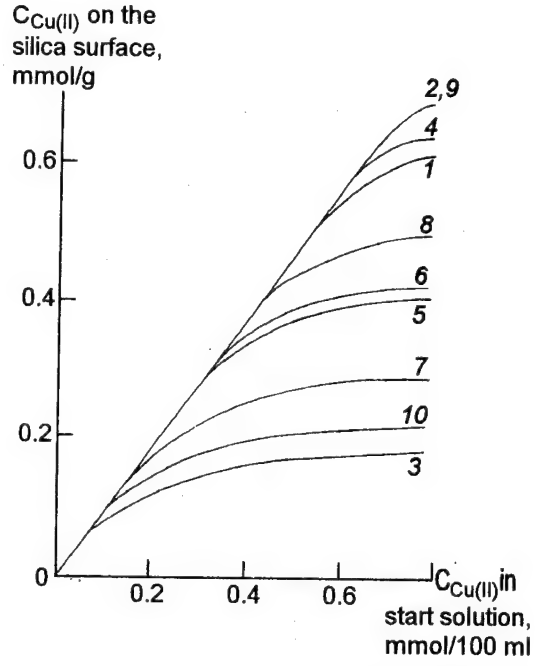

Fig. 2. Extraction of Cu(II) by various immobilized groups.

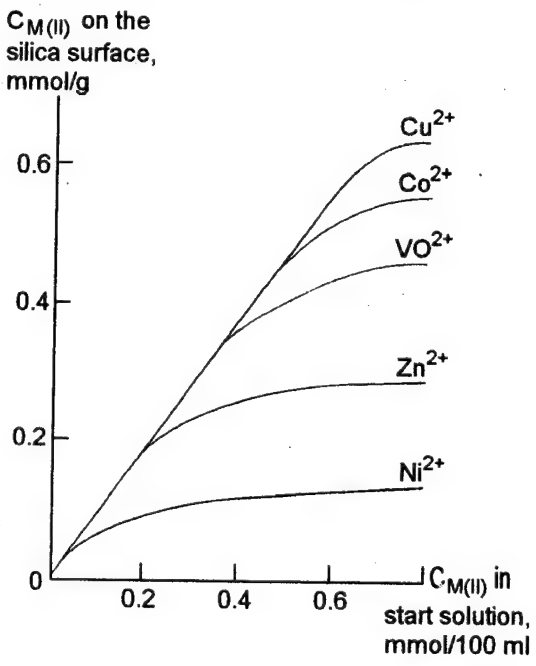

Fig. 3. Extraction of M(II) by the immobilized group 4.

Table 1. Concentrations of immobilized ligands and their bands in the diffuse reflectance spectra.

Ligand	$C_{lig.}$	Bands in the UV-spectra					
γ-APA	0.55	-	-	-	-	-	-
AE-γ-APA	0.36	-	-	-	-	-	-
1	0.45	42000	39800	31800	27400	-	19800
2	0.35	42800	39900	32000	27000	-	20000
3	0.25	-	39000	32000	-	-	20000
4	0.45	42300	34400	30000	-	23800^{+}	18600
5	0.35	43600	39500	35800	30200	23900	19500
6	0.40	-	37800	-	28600	25000	19800
7	0.38	42000	38000	34900	29700	23600	18600^{+}
8	0.35	42500	39900	32200	27000	-	19800^{+}
9	0.35	43000	39900	32000	27200	-	-
10	0.35	-	37200	31500	-	23000^{+}	-

1630 cm^{-1}. This shift depends on the concentration of immobilized metal. The weak bands of the residual amino-groups shift by 30-60 cm^{-1} with metal concentration increase ($C_{Me(II)}$:$C_{lig.}$ > 1:2). These residual amino-groups are responsible for the additional adsorbtion that is observed for Cu^{2+} and Co^{2+}.

The bands between 2800 and 3000 cm^{-1} are the various symmetric and asymmetric CH stretching frequencies associated with the groups which are bonded to the silica surface [1].

The immobilized ligands and complexes show some electronic absorption $\pi \rightarrow \pi^*$ and $\sigma \rightarrow \pi^*$ within the C=N and phenoxy group (Table 1). All the bands show a shift from the free ligand values by 300-500 cm^{-1} due to the complex formation.

The electronic spectra of the immobilized complexes of Cu^{2+} show a broad *d-d* transition in the visible region at 11000-12500 cm^{-1} — distorted tetrahedral structure [2].

For Co^{2+} complexes with immobilized Schiff bases, three bands are observed at 15000 cm^{-1}, consistent with supposition of tetrahedral struc-

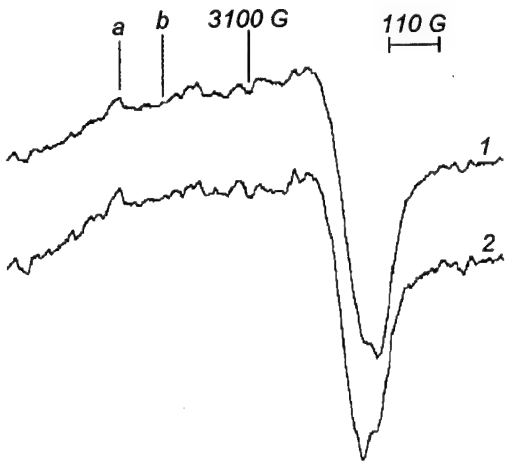

Fig. 4. ESR spectra of immobilized complexes Cu^{2+} with 3, 1 — $C_{Me(II)}$:$C_{lig.}$=1:2; 2 — $C_{Me(II)}$:$C_{lig.}$≈1:1. a) signal of complex (I), $g_{\perp}$= 2.033, $g_{\parallel}$=2.265; b) signal of complex (II), $g_{\perp}$=2.018, $g_{\parallel}$=2.215.

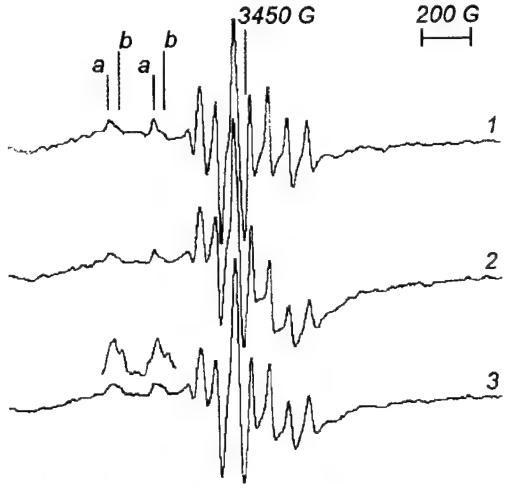

Fig. 5. ESR spectra of immobilized complexes VO^{2+} with 1, 1 — $C_{Me(II)}$:$C_{lig.}$=1:3; 2 — $C_{Me(II)}$:$C_{lig.}$=1:2.5; 3—$C_{Me(II)}$:$C_{lig.}$≈1:2. a) signal of complex 1:2, $g_{\perp}$= 1.977, $g_{\parallel}$=1.949; b) signal of complex 1:1, $g_{\perp}$≈1.977, $g_{\parallel}$=1.937.

ture (for all ligands,with exception of 7,8). For 7 and 8, two additional bands are observed at 15000 and 20000 cm^{-1} (for the $C_{Me(II)}$:$C_{lig.}$ ratio 1:1 and grater) which are correlative to octahedral structure [1,2].

All complexes of Co^{2+} do not change their colour in the air in the presence of moisture. That testifies to the presence of metal cations in rigid position and impossibility of reconstruction of coordination polyhedron.

Besides, in the UV spectra of complexes Cu^{2+} with 4, 10 and Co^{2+} with 7, 8 at small metal concentrations ($C_{Me(II)}$:$C_{lig.}$ ≤ 1:3), a band of free ligand is observed (marked as "+" in Table 1).

The positions of weak bands in the spectrum of Ni^{2+} complexes at 25000, 19000 cm^{-1} (for all ligands) are consistent with square-planar structure [2].

The electronic spectra of the VO^{2+} Schiff base complexes exhibit a single band at 17000 cm^{-1} with additional inflections at 14000 and 20000 cm^{-1}. These spectra are consistent with a five-coordinate, squarepyramidal structure.

The ESR spectra for Cu^{2+} and VO^{2+} at room temperature showed two different structural possibilities for immobilized complexes (Fig.4-5). Under low concentration of VO^{2+}, the square-pyramidal structure is realized with $C_{Me(II)}$:$C_{lig.}$ ratio 1:2; when amount of metal rises the bands of the square-pyramidal structure with the ratio $C_{Me(II)}$:$C_{lig.}$ 1:1 appear in the spectrum. For copper complexes having distorted tetrahedral environment, the similar changes with ratio $C_{Me(II)}$:$C_{lig.}$ are observed in the ESR spectra.

References

1. L.A.Kazycina, N.B.Kupletskaya, Appliance UV-, NMR- and massspectroscopy in organic chemistry, Moscow Univ., Moscow (1979), p.240.
2. R.S. Drago, Physical Methods in Chemistry, W.B.Saunders Company, Philadelphia-London-Toronto (1977).

Енамин-металлические комплексы, иммобилизованные на поверхности кремнезема

В.В.Антощук, А.А.Голуб, А.В.Лысенко

Синтезирован ряд иммобилизованных на поверхности аэросила оснований Шиффа. С помощью физических и физико-химических методов доказана индивидуальность полученных соединений. Изучены сорбционные свойства полученных носителей по отношению к катионам Cu^{2+}, Co^{2+}, Ni^{2+}, Zn^{2+} и VO^{2+} . Спектрометрическими методами исследованы строение и состав образующихся комплексов. Показано, что для меди и кобальта, с иммобилизованными лигандами, реализуется преимущественно псевдотетраэдрическое окружение. Для ванадила наблюдаются квадратно-пирамидальные структуры, а никель сорбируется в плоско-квадратные позиции.

Functional Materials **2**, No 1 (1995)

Dielectric behavior of hydrated pyrogenic silica and titania/silica

V.I.Zarko and V.M.Gun'ko

Institute for Surface Chemistry, National Academy of Sciences of Ukraine,
31 Nauki Ave., 252022 Kiev, Ukraine

The water sorption on the surface of pyrogenic silica and titania/silica is discussed. The occurence of TiO_2/SiO_2 interphase boundary is shown to cause a significant change in the water sorption processes on the pyrogenic titania/silica surface.

Розглянуто сорбцію молекул води на поверхні пірогенного кремнезему та титанокремнезему. Показано, що поява міжфазної межі TiO_2/SiO_2 суттєво змінює процеси сорбції води на поверхні пірогенного титанокремнезему, відповідальними за які є титаносилоксанові містки Ti–O–Si.

1. Introduction

The properties of water absorbed on metal oxide surfaces are different from those of bulk water [1–4]. Characteristic changes are observed in layer of 10 nm [5]. Titania–silica (TS) surfaces are more heterogeneous in respect of water absorption than silica. This is the result of the formation of individual TiO_2 phase and Ti–O–Si or Ti–O(H)–Si bridges in the interface regions [5–8].

The Ti–O–Si bridge content in TS increases with the n_{TiO_2} value growth and it is maximum at $n_{TiO_2} \approx$ 20 wt.% [9]. This value is close to maximum solubility of titania into silica matrix [10]. The adsorption capacity value for TS is not explained through additive adsorption of water on the SiO_2 and TiO_2 phases [11]. The aim of this work is the investigation of water adsorbed on the silica and titania–silica surfaces and determination of interface influence on characteristic properties of such systems.

2. Experimental

Materials. Pyrogenic silica Aerosil (A-300, ($300\ m^2 \cdot g^{-1}$) 99.9%) was obtained from PU «Chlorovinil» (Kalush, Ukraine). The samples were heated during an hour at T = 470 K for removal of residual HCl.

Pyrogenic titania/silica (with 99.5% purity) has been studied; the samples used contained 9 (TS_9), 14 (TS_{14}), 20 (TS_{20}), 22 (TS_{22}), 29 (TS_{29}), and 36 (TS_{36}) wt.% of titania with specific surface area (S) of 215, 137, 70, 250, 60 and 90 $m^2 \cdot g^{-1}$ correspondingly.

DS method. Water adsorption measurements were performed at room temperature with mean error near ±0.01 g/g. Dielectric characteristics were measured in the 3–10 MHz frequency range. A choice of this region is conditioned by neglecting of Maxwell–Wagner effects [12]. The measurements of $\varepsilon' = \Phi(T)$ and $\varepsilon'' = \Psi(T)$ were taken by thermochamber with programmed temperature changes. Heating rate was equal 0.05 K/s at $\delta T = \pm 5$ %.

3. Results

The activation energy of Debye type polarization (E_p) may be obtained from spectra of dielectric losses. The E_p values are calculated usually from shift of the temperature maximum $\varepsilon''(T)$ for different frequencies (Fig. 1). The E_p value increases at C_{H_2O} rising; e.g., at C_{H_2O} = 0.05 g/g, E_p is 13 kJ/mol and at C_{H_2O} = 0.45 g/g, E_p is 21 kJ/mol for low-temperature peak. This may be interpreted as a result of hydrogen bond number increase for each molecule in adsorption complex

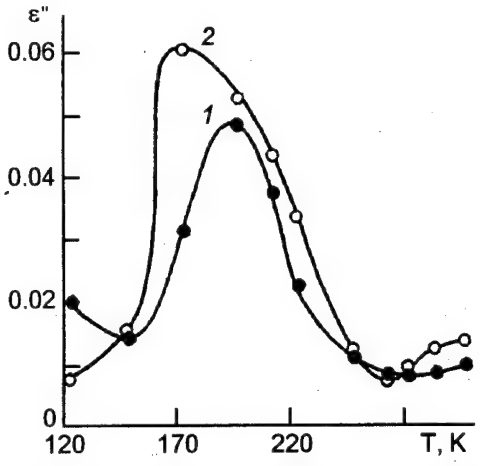

Fig.1. Dependence of the ε'' values on temperature at f = 9 (1), 3 (2) MHz and C_{H_2O} = 0.05 g/g.

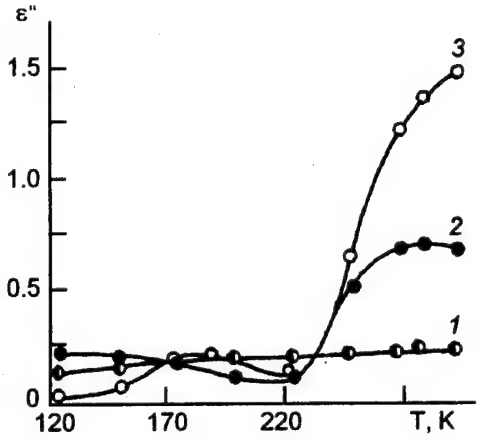

Fig.2. Dielectric losses of pyrogenic silica dependencies on temperature at the C_{H_2O} for 0.10 (1), 0.25 (2), 0.45 (3).

at C_{H_2O} = 0.45 g/g. The E_p value is 46±15 kJ/mol for the high-temperature peak at C_{H_2O} = 0.25 g/g.

Relaxation time of adsorbed water polarization (τ_{rp}) on Aerosil surfaces is nearly 10^{-8} s [13], i.e., it lies between those for τ_l (liquid bulk water) and τ_i (ice). However, for silica gel, τ_{rp} (10^{-9}- 10^{-10} s) is less than for Aerosil owing to spatial filling of the gel pores and higher sizes of adsorbed water clusters. The τ_{rp} value growth relative to τ_l is due to orientation and polarization actions of oxide surfaces hindering any motions of molecules adsorbed. For example, in Aerosil hydrogel the random mobility of water molecules differs from bulk water. The mean-square value of scattering atom displacements $\langle x^2 \rangle$ (obtained by analysis of angular dependence for noncoherent quasi-elastic scattering of slow neutrons) [11] is $6 \cdot 10^{-4}$ nm^2 for dehydrated Aerosil. At C_{H_2O} = 0.006 g/g, the $\langle x^2 \rangle$ value increases to $0.9–1.0 \cdot 10^{-3}$ nm^2, and at C_{H_2O} = 0.02 g/g, it amounts $1.3 \cdot 10^{-3}$ nm^2. For bulk water, $\langle x^2 \rangle$ is $1.5 \cdot 10^{-3}$ nm^2 at the same conditions.

As C_{H_2O} grows, the ε''(T) maximum shifts to lower temperatures at first, but then it returns to the region of 170–190 K (Fig. 2). The ε''(T) intensity changes are as small as from 0.05 to 0.20 at C_{H_2O} increase and at $T \leq 200$ K. This effect may be interpreted as small changes number of water molecules directly bound to the surfaces, i.e., water cluster sizes increase, but the most part of molecules in these clusters are ice-shaped at $T \leq 220$ K.

All samples containing 0.1–0.45 g/g of water have a relaxation maximum at 0° C which may be caused by water molecules bound in great clusters, i.e., not directly contacting the silica surfaces.

For the ε'' = Ψ(T) function, two temperature regions may be separated: I, at $T \leq 220$ K and II, at T = 240-320 K. Internally frozen adsorbed clusters are characteristic for the second region, and the ε'' intensity depends on C_{H_2O} strongly (at room temperature this dependence is linear) [15]. In the first region, freezing-out of molecules directly bound to the silica surfaces (type I) occurs in the first region. The E_p value dependence on C_{H_2O} is non-linear: at first, E_p decreases with C_{H_2O} growth but then it increases, i.e., number of molecules directly bound to the surface depends on C_{H_2O} and cluster sizes non-linearly. Apparently, at first, the number of molecules directly bound to the surface changes very little, i.e., the

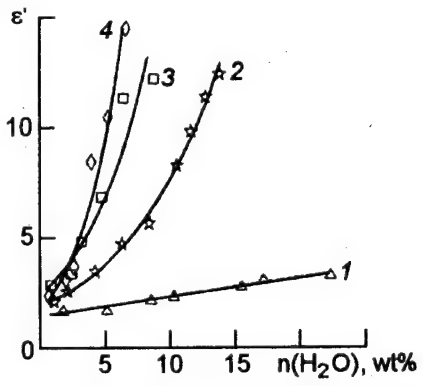

Fig.3. Dependence ε'' = f(n_{H_2O}) for the samples SiO_2 (1), TS_9 (2), TS_{14} (3), TS_{20} (4); frequency is equal 3 MHz.

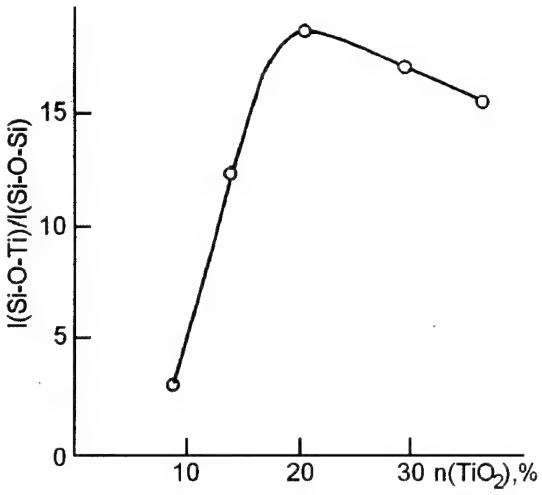

Fig.4. Dependencies of the Si-O-Ti bridge content on n_{TiO_2} in TS.

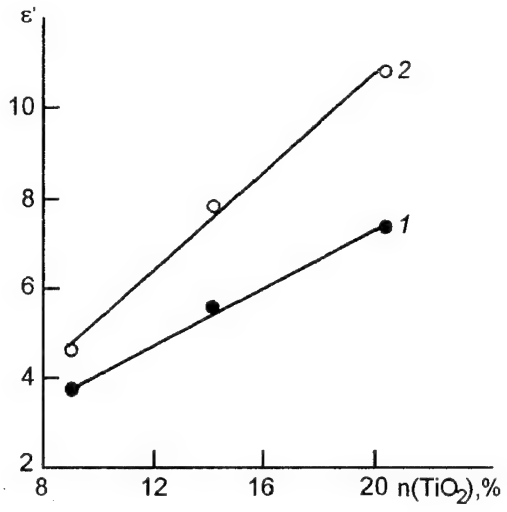

Fig.5. Dependece ε'' on n_{TiO_2} for TS at water content of 4 (1) and 6 (2) wt.%.

clusters increase at the expense of superstructure. The E_p value decrease may be caused by mobility limitation of water type I at freezing-out of water type II in cluster superstructure. Water clusters can coalesce at further growth of C_{H_2O} (according to ε''(T) and ε''(C_{H_2O}) this transition occurs in the range $0.25 \le C_{H_2O} \le 0.45$ g/g), and amount of type I water increases that leads to the E_p value rising. Hexagon "windows" on Aerosil surface (which has structure similar to face (111) of β-crystobalite) have only three Si atoms with OH groups which are active sites for water adsorption [8]. There is some critical size (R_c) of water clusters, and its excess leads to coalescence of separated clusters. At $C_{H_2O} \approx 0.25$–0.30 g/g, the R_c value corresponds to 20–30 molecules in a cluster.

Dielectric permittivity (ε') of TS depends on the n_{H_2O} value more strongly than for silica (Fig. 3, curves 2-4). The character of the function ε' = $f(n_{H_2O})$ (kink up) allows us to explain the data obtained within the scope the layered model [16] according to which, in the first layers, the molecules adsorbed on the most active sites have lower orientational mobility in external electric field than ones in the second layers, which give higher contribution to orientational polarization of adsorbate. It increases through TiO_2 phase influence and, as a result, the ε' value grows. The ε' value for dehydrated pyrogenic silica and TS are nearly equal [17]. The ε' values changes nearly linearly with the Si–O–Ti bridge content (Fig. 4), i.e., we can assume that these sites are the most important for water adsorption. They lead to fast rise of great clusters of water adsorbed on TS as the n_{H_2O} value grows. The peculiar form of the function ε' = $f(n_{H_2O})$, which is observed for TS_{14} and TS_{20} (Fig. 3, curves 3, 4) (at such n_{TiO_2} values, individual titania phase forms into TS), attests that continuous water layer forms on TiO_2 phase.

Dielectric permittivity is proportional to the n_{TiO_2} and Si–O–Ti bridge amounts (Fig. 5). The ε'' value dependence on temperature (Fig. 6) for TS_9 differs from one for pyrogenic silica and the ε'' values of TS in the 220–300 K range are well above that for silica. However, the n_{H_2O} value for TS_9 is higher than for silica by 2–3 wt.% only, i.e., this difference of the ε'' values can not be explained only by water content on the SiO_2 and TS_9 surfaces. This may be caused by a difference between adsorbed water clusters sizes for this ox-

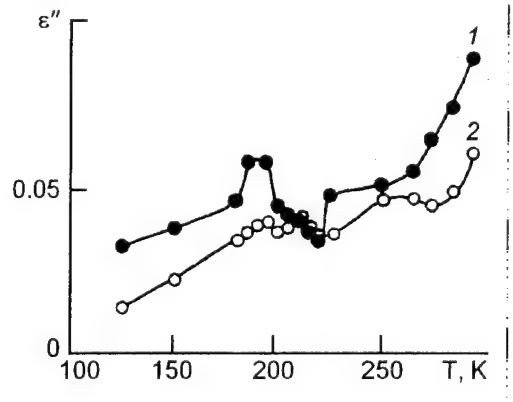

Fig.6. Dependence ε'' on temperature for TS_9 at frequencies of 3.2 (1) and 9.4 (2) MHz.

ides. As the temperature drops from 300 to 220 K, such change in the ε″ values is characteristic for a surface containing great water clusters, but it is observed for pure SiO_2 only at $n_{H_2O} \geq 25$ wt.%. At least two relaxation maxima are observed for TS_9 in the 160–220 K range in which one maximum is exhibited for silica, i.e., on the TS surfaces, several types of water adsorption sites exist, e.g.

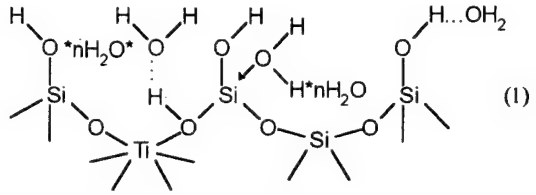

(1)

Calculation of the activation energy of polarization (E_P) may be performed through a relaxation maximum shift at two different frequencies (f) [16]

$$E_p \approx const \cdot \frac{\ln(\Delta f)}{\Delta T_{max}}. \qquad (2)$$

The E_p value according to eq.(2) for TS_9 is 28 kJ/mol (220–300 K) and 21 kJ/mol (160–220 K). An estimation of the E_p value may be made via a maximum of ε″ measured on a certain frequency

$$(f_{max} \cdot 2\pi)^{-1} = \tau \approx (h/kT) \exp\left(\frac{\Delta F}{RT}\right). \qquad (3)$$

Where ΔF is free energy of activation, and as we measure temperature dependence but not frequency one that

$$\Delta F \approx E_a = RT_{max} \ln\left(\frac{T_{max}}{T_0}\right). \qquad (4)$$

An estimation of activation energies for three DS peaks of TS_9 according to eq.(4) gives following values: 18, 21 and 25 kJ/mol.

4. Theoretical simulations

Theoretical investigations were carried out in cluster approach by the AM1 method [18] for SiO_2 and NDDO [19] for TiO_2/SiO_2. The Aerosil surface fragments were modeled through the clusters $(O_3^*SiO)_3SiOH$ (I) and $(O_3^*SiO)_2Si(OH)OSi(O_2^*)OSi(OH)(OSiO_3^*)_2$ (II), where O* is monovalent oxygen pseudoatom [8]. Adsorbed water clusters contained from 1 to 12 molecules. The following motions of molecules were simulated:

a) rotation of one molecule which had donor-acceptor bond with Si atom in the ≡SiOH group and different number of hydrogen bonds with other molecules

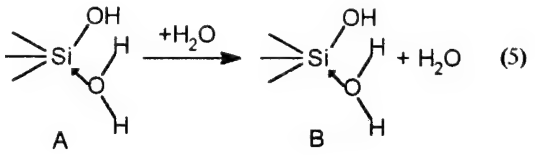

(5)

b) rotation of molecules from different surface layers with variable number of hydrogen bonds

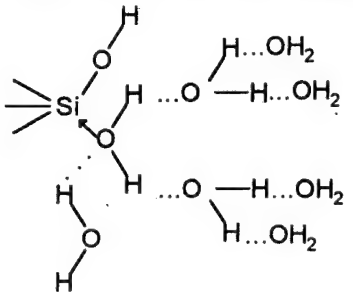

(6)

c) diffusion of molecules which had donor-acceptor bond or hydrogen bond (or physically adsorbed). The calculation were carried out with account for the vibrational-rotational relaxation of molecule surroundings and without it by adiabatic (ARC) and dynamic reaction coordinate (DRC) methods [20]. In the latter case, the start points had the structures obtained by ARC method and corresponding to different rotations or transition states of diffusion jumps between neighboring sites.

Minimum activation energy of water molecule rotations is observed at soft concurrent reorientation of surroundings Table 1 that corresponds to slow rotations of molecules in liquid states. Maximum activation energy is obtained at "rigid" surroundings that is close to ice characteristics (for ice, $E_{rot}^{\neq} \approx 55$ kJ/mol [4]). At weak response of surroundings, the rotation barrier is maximum (42 kJ/mol) for a molecule with donor-acceptor bond $Si \leftarrow OH_2$.

This value approaches to the E_{dp} maximum characterizing the depolarization of adsorption complexes which remain after heating (Fig. 6), i.e., strongest complexes.

Activation energy of surface diffusion (E_D) was calculated for water molecule "jump" between neighboring sites with ≡SiOH groups (≈ 0.7 nm):

Table 1. Energetic parameters of adsorption comlexes

N Cluster	*N*=*n*+1	Bond type of rotated molecule, (number of bonds)	$-\frac{\Delta E_l}{n+1}$	$E^{\neq}$	$E^{\neq}$	(surr.relax.)
I	1	DAC (2)	39	13	7	
II	1	DAC (2)	55	36	-	1375** (ΔE_{H^+})
I	2	DAC (3)	42	24	18	
I	3	DAC (3)	40	42	-	
I	5	DAC (4)	33	69	17	
I	8	HB (3)	37	26	-	
I	9	DAC (4)	35	41	-	
I	10	HB (1)	36	8		
I	9	DAC (4)	45	59*	31*	F=7.2·10^5 V/m
I	9	DAC (4)	40		29*	F=3.6·10^5 V/m
II	9	DAC	36			1109 (ΔE_{H^+})
I	1	HB	13-15			
I	2	HB	30			
I	2		24			
I $OH^-...H_3^+O$	7		15			
I	7		33			
I	4		30			
I	6		29			
I	12		32			

Notes. *The $E^{\neq}$ values were obtained without field, but after polarization. **Proton detachment energy.

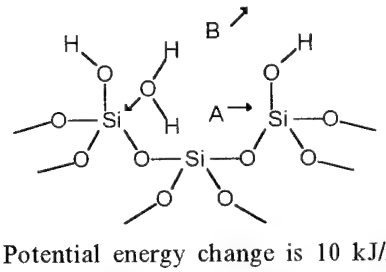

(7)

Potential energy change is 10 kJ/mol, if the molecule resides between ≡SiOH groups in (7A). Time of one jump between these groups with kinetic energy of molecule corresponding to $T \approx 330$ K is about 10^{-2} s at the mean velocity of molecule motion along surface 3.6 m/s. The E_D value is equal 30 kJ/mol at molecule removal on 0.7 nm from the ≡SiOH group (7B), i.e., it is 25 kJ/mol less than energy of initial complex formation; that is caused by the conservation of attraction between solid and molecule under the diffusion along the surface.

For titania surface fragments, clusters including from three to six hexahedrons $TiO_{6/3}$ with anatase structure were calculated. The TiO_2/SiO_2 surface models contained from one to three $TiO_{6/3}$ hexahedrons and 7–10 $SiO_{4/2}$ tetrahedrons. The H_3^*SiO and OH groups were used on the cluster boundaries. The TiO_2 and TiO_2/SiO_2 clusters contained the Ti–O(H)–Me (Me = Ti, Si) bridges and terminal OH groups.

The $E_r^{\neq}$ value for TS is minimum (for molecules bound directly to a surface) in hydrogen complexes of only one molecule

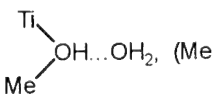

(8)

and it is about 10 kJ/mol. In the case if these molecules interact with other water molecules, the $E_r^{\neq}$ value increase to 25 kJ/mol. For donor-ac-

ceptor complexes (DAC) Ti←OH_2, the $E_r^{\neq}$ value is higher (≈ 40 kJ/mol, i.e., it is nearly equal to the $E_r^{\neq}$ value for DAC on a silica surface [4]). With growing number of water molecules in a complex, when the first adsorbed molecule forms DAC, the $E_r^{\neq}$ value rises to 55–60 kJ/mol. If a molecule surrounding in DAC is assumed to be fully rigid that the $E_r^{\neq}$ value is equal 85 kJ/mol. However, the probability of Ti←OH_2 DAC formation on pyrogenic TS surfaces is small as the Ti atoms at a surface form hexahedron structures $TiO_{6/3}$.

From a comparison of experimental data with theoretical simulation results we can conclude that the most formation probability exists of following type complexes:

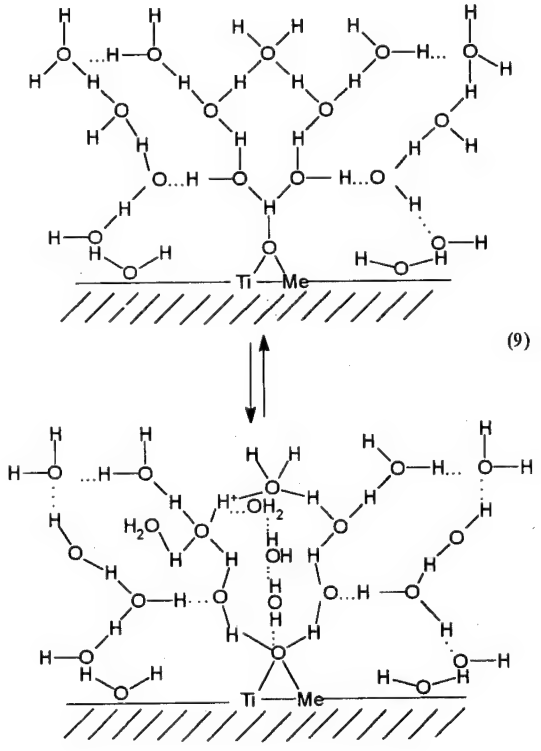

where Me is Ti or Si. Therefore, a number of water molecules in DAC on TS surfaces is lower than on pure silica on which DAC are the most preferential, i.e., the most probable formation of water superclusters occurs on the TS interface sites (**B**-centers) which form easily ion pairs at solvation. However, thermodynamic stabilization of ion pairs requires a participation in this process many water molecules on every center (n >10 in (7)) [21].

5. Conclusion

The relaxation time τ_{rp}(DS) decreases with rising of water quantity in adsorbed clusters owing to increased dissipation rate of vibration-rotation energy.

Analyzis of the experimental results favors the view that the most probable sites for water molecule adsorption are the TiO_2/SiO_2 phase boundary region, and water molecules adsorbed on the Ti–O(H)–Si bridges loss less degrees of freedom than at donor-acceptor complex Me←OH_2 formation. This effect has influence on a lowering of activation barriers of polarization and depolarization of water clusters adsorbed on mixed oxide surfaces.

References

1. A.W. Adamson, Physical Chemistry of Surfaces, Wiley, New York (1976).
2. R.K.Iler, The Chemistry of Silica, Wiley, New York (1976).
3. M.J.Jaycock and G.Parfitt, Chemistry of Interface, Ellis Horwood, Chichester (1981).
4. G.N.Zatsepina, Physical Properties and Structure of Water, [in Russian], Nauka, Moskow (1987).
5. G.Nimtz, W.Z.Weiss, *Z.Phys.*, **B67**, 483 (1987).
6. V.F.Kiselev, O.V.Krylov, Electronic Phenomena in Adsorption and Catalysis on Semiconductors and Dielectrics, [in Russian], Nauka, Moskow (1979).
7. Sorbents on the Basis of Silica Gel in Radio-Chemistry, [in Russian], ed. B.N.Laskorin, Atomizdat, Moskow (1977).
8. A.A.Chuiko, Yu.I.Gorlov, Surface Chemistry of Silica, Surface Structure, Active Sites, Sorption Mechanisms, [in Russian], Naukova Dumka, Kiev (1992).
9. M.Heggie, R.Jones, *Izv. AN USSR, Fiz. Ser.*, **51**, 1634 (1987).
10. P.Ruelle, Ho Nam-Tran, M.Buchman and U.M.Kesselring, *J. Mol. Struct. Theochem.*, **109**, 177 (1984).
11. A.A.Tumanov, V.I.Zarko, G.M.Kozub and A.A.Chuiko *Poverkhn.*, **N 5**, 115 (1993).
12. T.Morimoto, T.Iwaki, *J.Chem.Soc., Faraday Trans.1*, **83**, 943 (1987).
13. L.G.Grechko, V.I.Zarko, V.V.Motrich, *React. Kinet. Catal.Lett.*, **50**, 183 (1993).
14. T.Sakamoto, H.Nakamura, H.Hedaira and A.Wada, *J.Phys.Chem.*, **93**, 357 (1989).
15. V.I.Zarko, O.V.Gul'ko, *React. Kinet. Catal.Lett.*, **50** (1993).
16. T.L. Chelidze, A.N.Derevyanko, O.D.Kurilenko, Electrical Spectroscopy of Heterogenous Systems, [in Russian], Naukova Dumka, Kiev (1977).
17. V.I.Zarko, A.V.Gette, G.M.Kozub et al., *Izv. AN USSR, Neorgan. Mater.*, **19**, 239 (1983).
18. M.J.S.Dewar, E.G.Zoebisch, E.F.Healy and J.J.P.Stewart, *J. Am. Chem. Soc.*, **107**, 3902 (1985).
19. A.G.Grebenyuk, V.A.Zaets, Yu.I.Gorlov, in Exten.Abstr.Int.Conf. *"Oxide Surf. Chem. and Reaction Mechanisms"*, [in Russian], Kiev (1992). P.197.
20. V.M.Gun'ko, *React. Kinet. Catal.Lett.*, **50**, 97 (1993).
21. V.M.Gun'ko, *Zh. Fiz. Khim.*, **65**, 398 (1991).

Диэлектрические исследования гидратированного пирогенного кремнезема и титанокремнезема

В.И.Зарко, В.М.Гунько

Рассмотрена сорбция молекул воды на поверхности пирогенного кремнезема и титанокремнезема. Показано, что появление межфазной границы TiO_2/SiO_2 приводит к существенному изменению процессов сорбции воды на поверхности пирогенного титанокремнезема, ответственными за которые являются титаносилоксановые мостики Ti–O–Si.

Functional Materials **2**, No.1 (1995)

The influence of the thin film with 2*D* surface zone in an adsorbate on the potential barrier in the external electric field

L.G.Il'chenko and A.A.Savon

Institute of Surface Chemistry, National Academy of Science of Ukraine,
31 Nauki Ave., 252028 Kiev, Ukraine

External field penetration effect in the thin films of a metal (semimetal or degenerate semiconductor) with a size quantized electron spectrum have been calculated in the framework of nonlocal electrostatics. On the basis of these results we determined the influence of the thin adsorption coating with 2*D* surface zone in the adsorbate on the potential barrier in the case of the field emission from the semi-infinite metals.

З використанням теоретичних методів нелокальної електростатики знайдено вираз для потенціалу проникнення зовнішнього електричного поля в тонкі плівки металів (напівметалів або вироджених напівпровідників) з розмірно-квантованим спектром електронів. Одержані результати застосовано для визначення впливу тонких адсорбційних покриттів з 2*D* поверхневою зоною в плівці адсорбату на форму потенціального бар'єру при автоелектронній емісії.

The emission characteristics of metallic cathodes are determined by the bulk properties of the metal (the electronic structure) and the surface state of the metal (the adsorbate layers). In [1–3] it is shown that, for the calculation of the potential barrier $\Phi(x, F)$ in the external electric field F for electrons tunnelling from the metal, the good approximation is the following:

$$\Phi^M(x,F) = \chi^M + \varphi^M_{VAC}(x,F)$$

$$\varphi^M_{VAC}(x,F) = -\frac{e^2}{4(x+x_0)} - eF(x+x_1) \qquad (1)$$

where χ is the affinity energy of the bulk metal, x is the value of the image plane displacement for the calculation of the image force potential $V_M(x)$, x_1 is the contribution from the field penetration effect. All these values are determined by the electronic structure of metal. In the framework of the Thomas-Fermi approximation (TFA) we obtain:

$$\chi = -\frac{e^2\kappa}{2};\ x_0 = \frac{3}{4}\kappa^{-1};\ x_1 = \kappa^{-1},$$

where κ^{-1} is radius of screening by free carriers in the TFA. Taking into account the quantum nature of conduction electrons in metal within the framework of the Random-Phase approximation (RPA) for the dielectric function of metal $\varepsilon(\vec{k})$, and the many-body correlations between the electrons give the possibility of a classification of metals according to their electronic properties. In RPA, χ, x_0 and x_1 are obtained in the integral form.

It is known that the adsorption of atoms on a cathode surface influences essentially its current characteristics. The work function of the metal varies with the coating degree θ. The collective properties of the electrons in the film of adsorbate begin to play a significant role for the coats $\theta > \theta_c$ [4,5]. In this case, the spectrum of electrons becomes quasi-two-dimensional (*Q*2*D*). The *Q*2*D* layer on the metal surface changes the barrier in the external field *F*. At the same time, in addition to the conventional emission of electrons from the metal, the emission from the *Q*2*D* layer (2*D* zone) appears.

On the basis of the Green functions of the nonlocal Poisson equation in an unsymmetric system of three media with a spatial dispersion [6], we have calculated the potential electrostatic charge near the metal surface with a metal coating (adsorbate) in the external electric field *F*.

Let us consider the interaction of a charge e with surface of a semi-infinite metal taking into account the screening effects induced by free conduction electrons. The dielectric function of metal in the region $x \le L$ we choose in TFA

$$\varepsilon_N(k,q) = 1 + \frac{\kappa^2}{k^2+q^2}, \quad \kappa^2 = \frac{6\pi e^2 n}{E_F}, \qquad (2)$$

where n is electron concentration and E is the Fermi energy.

Let us suppose that the spectrum of the free carriers in the metal film of the thikness L (in region $-L \le x \le 0$) is size-quantized (SQ). The dielectric function $\varepsilon_N(\vec{k})$ of SQ film can be written in the form (RPA) [1,7]

$$\varepsilon_N(k,q) = 1 + \frac{\kappa_N^2(q)}{k^2+q^2}, \qquad (3)$$

In the electric quantum limit, when electrons fill one level in the adsorbate layer, the polarisation operator $\kappa_N^2(q)$ has the form

$$\kappa_N^2(q) = \frac{4}{a_0^* L} Re\{1 - (1 - (2k_F/q)^2)^{1/2}\}, \qquad (4)$$

where $k_F = \sqrt{2\pi n L}$ is the Fermi pulse of electrons in the $Q2D$ zone, $a_0^* = \frac{h}{m^* e^2}$ is the effective Bohr radius, m^* is effective mass of electrons, $n = \frac{N_A}{L}$ is the bulk concentration of electrons in $Q2D$ zone, N_A is two-dimensional concentration of adatoms in the adsorbate layer. Note that, in TFA, $\kappa_N^2(q) = \kappa_N^2 = const.$

For a total case of unsymmetric system of three media with spatial dispersion, in [6] Poisson equation were found, which determine uniquely the electrostatic energy of the Green function of the nonlocal charge $V_i^0(x)$ (the potential of image forces) in the inhomoneous system for $F = 0$.

As it was shown in [6], the account for the spatial dispersion effects in the media with different screening properties provides finiteness and continuity of $V_i^0(x)$ at the interfaces $x = -L$ (semi-infinite metal/SQ film) and $x = 0$ (SQ film/vacuum/,and the common (vacuum) counting level of the potential of forces.

In the total case for the unsymmetric system of three media, we obtained the field Green function of the nonlocal Poisson equation which determines the field component $\Delta V_i(x,F)$ of the total electrostatical potential for $F \neq 0$

$$\Delta V_i(x,F) = V_i^0(x) + \Delta V_i(x,F) \qquad (5)$$

We found a strict solution of the nonlocal Poisson equation taking into account the finite bounds of the normal component of the electrostatic induction vector at the interface $x = -L$ and $x = 0$ in the external electric field F.

The external field penetration effect ($F = const.$) in the thin metal film (with SQ spectrum of the electrons) on the metal surface (TFA) is described by the following expressions:

$$\Delta V_1(|x|,F) = -eF \frac{e^{-|x+L|\kappa_N}}{\kappa_N sh(L\kappa_N) + \kappa ch(L\kappa_N)} \qquad (6)$$

(in metal region, $x \le L$);

$$\Delta V_2(|x|,F) = -\frac{eF}{\kappa_N} \frac{\kappa sh(|x+L|\kappa_N) + \kappa_N ch(|x+L|\kappa_N)}{\kappa_N sh(L\kappa_N) + \kappa ch(L\kappa_N)} \qquad (7)$$

(inside the film $-L \le x \le 0$);

$$\Delta V_3(x,F) = -eF\left(x + \frac{1}{\kappa_N}\frac{\kappa + \kappa_N cth(L\kappa_N)}{\kappa_N + \kappa cth(L\kappa_N)}\right) \qquad (8)$$

(in vacuum, $x \ge 0$).

Fig.1 shows the field penetration effect in the thin (superthin) metal film for $L = 3.3$ Å,, $m^* = 0.08\,m$ (m is the mass of free electron) on the semi-infinite metal with different concentrations of bulk electrons $n = 10^{21}\,cm^{-3}$ (curve 1), $n = 10^{22}\,cm^{-3}$ (curve 2) and $n = 10^{23}\,cm^{-3}$ (curve 3).

Fig.2 demonstrates the contribution of the field penetration effect into the potential value at the interface $Q2D$/vacuum ($x = 0$) for different concentrations of electrons in the semi-infinite

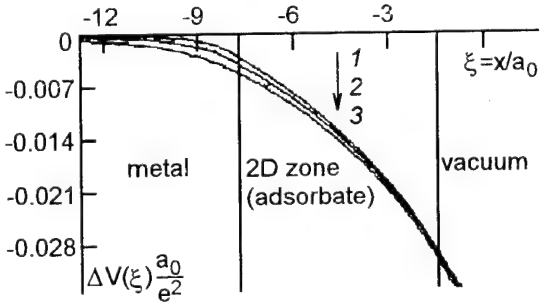

Fig.1 Dimensionless potential energy $\Delta v(\zeta) = \Delta V(x)\frac{a_0}{e^2}$ in the thin metal film as a function of $\zeta = x/a_0$ for $L = 3.3$ Å, $m^* = 0.08\,m$, $F = 8 \cdot 10^7$ on the semi-infinite metal for $n = 10^{21}\,cm^{-3}$ (curve 1), $n = 10^{22}\,cm^{-3}$ (curve 2), $n = 10^{23}\,cm^{-3}$ (curve 3).

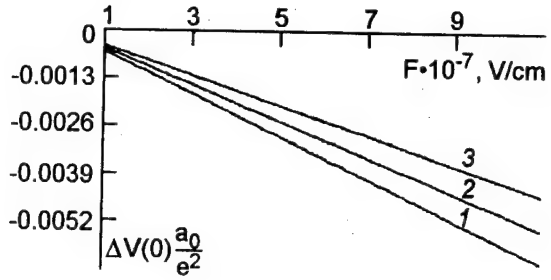

Fig.2 Dimensionless potential energy $\Delta v(\zeta) = \Delta V(x)\frac{a_0}{e^2}$ in the thin metal film as a function of F into potential value at the interface $Q2D$/vacuum for $L = 3.3$ Å,, $m^* = 0.08\,m$ and $n = 10^{21}$ cm^{-3} (curve 1), $n = 10^{22}$ cm^{-3} (curve 2), $n = 10^{23}$ cm^{-3} (curve 3).

bulk of a metal $n=10^{21}$cm^{-3} (curve 1), $n = 10^{22}$cm^{-3} (curve 2) and $n = 10^{23}$cm^{-3} (curve 3).

It is seen that the effect of field penetration in the metal film is defined by the electronic structure of the semi-infinite metal for the superthin metal film, for $\theta > \theta_c$.

For the thickness $L >> a_0^*$ in (6)–(8), we obtain the field penetration effect in the form

$$\Delta V_2(|x|,F) = -\frac{eF}{\kappa_N}\exp(-|x|\kappa_N); \qquad (9)$$

(inside the film, $x \le 0$)

$$\Delta V_3(x,F) = -eF(x + \frac{1}{\kappa_N}) \qquad (10)$$

(in vacuum, $x \ge 0$)

As it can be seen, the equations (9) and (10) describe the field penetration effect in a semi-infinite metal [3] we replace $\kappa_N \to \kappa$.

The potential barrier $\Phi(x,F)$ for the electrons tunneling through the $Q2D$ layer from the semi-infinite metal into vacuum can be written in the form

$$\begin{aligned}\Phi(|x|,F) &= \chi + \varphi_{2D}(|x|,F) + \varphi_{VAC}(x,F)\\ \varphi_{2D}(|x|,F) &= V^0_{2D}(|x|,F) + \Delta V_2(|x|,F)\\ \varphi_{VAC}(x,F) &= V^0_{VAC}(x) + \Delta V_3(x,F)\end{aligned} \qquad (11)$$

The potential barrier $\Phi_{2d}(X,f)$ for the electrons tunneling from the $Q2D$ zone into vacuum is given by the expression

$$\Phi_{2D}(x,F) = \chi_{2D} + \varphi_{VAC}(x,F). \qquad (12)$$

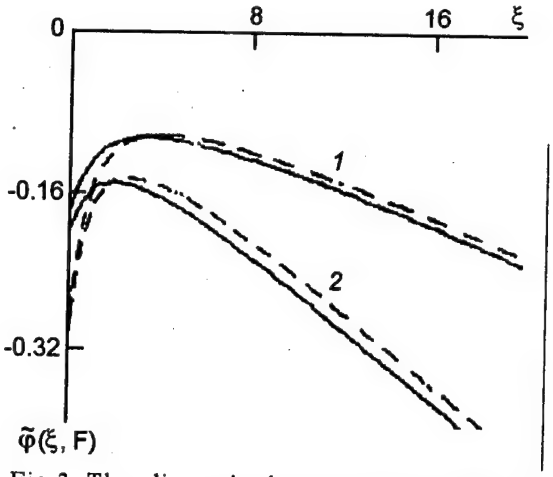

Fig.3 The dimensionless potential barrier $\bar{\varphi}(\zeta,F) = \frac{\varphi_{VAC}(x,F)a_0}{e^2}$ on distances $\zeta = \frac{x}{a_0}$ in vacuum in the external electric field $F = 5\cdot10^7$ V/cm (curve 1) and $F = 10^8$ V/cm (curve 2) near the $Q2D$ layer for $L = 3.3$ Å, and $n = 10^{21}$ cm^{-3}. The dependence for the potential barrier $\bar{\varphi}^M_{VAC}(\zeta,F) = \frac{\varphi^M_{VAC}(x,F)a_0}{e^2}$ in the absence of a metal coat is shown by dashed lines.

Here, $V^0_{2D}(|x|)$ is the potential of the image forces in Q2D layer, $V^0_{VAC}(x)$ is the potential of the image force in vacuum. In the case of TFA when $L >> a_0^*$, we obtain $V^0_{VAC}(x)$ in analytical form

$$\begin{aligned}V^*_{VAC}(x) = -\frac{e^2}{4x}\Big\{1 + \frac{1}{(\kappa_n x)^2} + \\ \pi\big[H_0(2\kappa_N x) - N_0(2\kappa_N x)\big] - \\ \frac{\pi}{\kappa_N x}\big[H_1(2\kappa_N x) - N_1(2\kappa_N x)\big]\end{aligned} \qquad (13)$$

where $H_\nu(z)$ and $N_\nu(z)$ are Struve and Neumann functions. χ_{2D} and $V^0_{2D}(x)$ in TFA (as well as in RPA) are determined in the integral form.

The potential barrier for emission of electrons from $Q2D$ zone is

$$\Phi_{2D}(x,F) = \chi_{2D} + V_{VAC}(x) - eF(x + \kappa_N^{-1}) \qquad (14)$$

where $\chi_{2D} = V^0_{2D}(-L/2) + \Delta V_2(-L/2)$ is the affinity energy.

Dependences of the dimensionless potential barrier $\bar{\varphi}(\zeta,F) = \frac{\varphi_{VAC}(x,F)a_0}{e^2}$ on distances $\zeta = \frac{x}{a_0}$ in vacuum in the external electric field $F=5\cdot10^7$ V/cm (curve 1) and $F=10^8$ V/cm (curve 2)

near the $Q2D$ layer ($L = 3.3A$) and $a_0^* = a_0^\sigma$, $L > a_0^\sigma$ on the metal ($n=10^{12}$ cm^{-3}) are plotted in Fig.3. The dependences of the potential barrier $\bar{\varphi}^{M}_{A\sigma}(\zeta,F) = \frac{\varphi^{M}_{A\sigma}(x,F)a_0}{e^2}$ in the absence of metal coat are shown by dashed lines.

It is seen that, with increasing effective screening radius in the $Q2D$ zone of the adsorbate, the influence of the metal substrate (its electronic structure) on the formation the potential barrier in the external electric field $\Delta V_i(x,F)$ increases.

Increasing of the surface degree coating $\theta > \theta_c$ contributes to the filling of higher levels in the layer. It can lead to the appearance of oscillations in dependence of the emission current $j_N(F)$ from the SQ metallic coat.

It should be noted that, in the framework of a nonlocal electrostatic the method presented for the determination of the potential barrier form in an external electric field F can be used for the calculation of current-voltage characteristics of metal emitters with dielectric coats, dipoles coats, etc.

References

1. A.M.Gabovich, L.G.Il'chenko, E.A.Pashitskii, Yu.A.Romanov, *Surface Sci.*, **94**, 179 (1980).
2. V.G.Litovchenko, Yu.V.Kryuchenko, L.G.Il'chenko, *J. Micromech. Microeng.*, **3**, 74 (1993).
3. L.G.Il'chenko, Yu.V.Kryuchenko, in: 7th Int. Vac. Microelectr. Conf., France (1994), p.53.
4. A.G.Naumovetz, Sov. Sci. Rev. Sec. A: Physics, **5**, 443 (1984).
5. N.D.Lang, *Phys. Rev. Ser.* **B.4**, 4234 (1971).
6. L.G.Il'chenko, *Surface Sci.*, **121**, 375 (1982).
7. L.G.Il'chenko, E.A.Pashiitskii, Yu.A.Romanov, *Surface Sci.*, **243**, 334 (1991).

Влияние тонких пленок с 2*D* поверхностной зоной в адсорбате на потенциальный барьер во внешнем магнитном поле

С.Г.Ильченко, А.А.Савон

С применением теоретических методов нелокальной электростатики получено выражение для потенциала проникновения внешнего электрического поля в тонкие пленки металлов (полуметаллов или вырожденных полупроводников), спектр электронов в которых размерноквантован. Полученные результаты применены для определения влияния адсорбционных покрытий с 2*D* поверхностной зоной в слое адсорбата на форму потенциального барьера при автоэлектронной эмиссии

Functional Materials **2**, No.1 (1995)

Electrochemical microscopy: conductometric measurements

V.I.Strikha and I.E.Konovalov

T.Shevchenko Kiev University, 64 Vladimirskaya St., 252017 Kiev, Ukraine

The application of electrochemical microscopy in association with conductometry for evaluation of thickness of biosensor membrane (enzyme-albumin one cross-linked with glutaraldehyde) in aqueous substrate solution is presented. It turned out that the reactive component of tip current is the most sensitive for the position of the tip inside the membrane.

Кондуктометричні виміри за допомогою електрохімічного мікроскопу були використані для знаходження товщини мембрани біосенсора на основі альбуміну безпосередньо у робочому розчині (калійфосфатний буфер). Це дало змогу врахувати розбухання мембрани. Виміри на змінному струмі дозволяють легко визначити положення межі електроліт-мембрана.

Introduction

The development of electrochemical microscopy technique gave one more powerful instrument for an investigator in the field of processes in the polymer films. Due to small tip size, the local determination of vast number of the object parameters became possible. The specific difficulty of biosensors is their swelling in substrate solution where the sensor, operates. Because of this swelling, even the determination of film thickness causes difficulties. But for local measurements in biosensors one must know reliably at least the position of film-solution interface, and therefore, the film thickness. It has been known that the position of such interface could be easily defined by means of electrochemical microscopy if the conditions of charge transfer inside the film differ from that outside of it. Such measurements in so-called feedback mode were described in [1–3]. There was no charge transfer if electrode was outside of the film. However, there was mechanism of charge transfer involving mediator (a species, which can get charge at one electrode and them release their charge at the other) inside the film while the liquid (aqueous solution of 40 mM $NaClO_4$ as a supporting electrolyte, for example), which the film was placed in, was almost insulating. The position of film-liquid interface could be defined by dipping of sharp tip in the film and measuring the current through this tip at applied voltage. It is quite clear that such method of attack in the case of biosensors which can operate at aqueous conditions and use no mediator is not convenient. The variation of tip current between inside and outside the membrane ought to be small, because the last swells significantly and, thus, mostly consists of solution. It turned out, however, that applying of ac voltage can make this measurements more precise.

Experimental

1. Electronic circuit

The schematic diagram of electronic circuit used for the experiments presented in this paper is shown in Fig.1. Sinusoidally varying alternating voltage at a frequency of 799 Hz comes from the

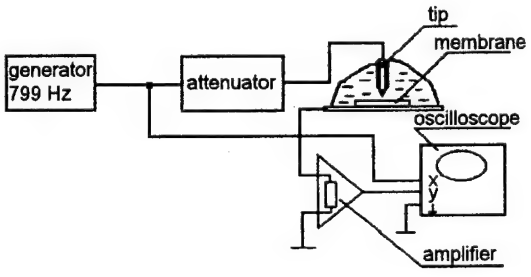

Fig.1. Electronic circuit for conductometric measurements.

oscilator through the variable attenuator to the tip electrode. The tip current is measured in the substrate circuit using bandpass amplifier. The amplified signal comes to the measurement unit, where its amplitude and phase with respect to the the reference signal from the oscillator are measured. The variable attenuator allows to change amplified voltage in order to minimize it for each specific sample and tip. By this means, one can avoid the unwanted changes of the tip due to faradaic processes, and besides, that allows to measure really differential values.

2. Tip driver

The experiments were performed using magnetoelectric driver schematically shown in Fig.2. This principle can provide wide range of motions, unlike the customary piezoelectric one. This is very important for the measurements in the relatively thick films (biosensor membranes could be as thick as 100 μ and more). The deformation of the elastic suspension is caused by electromagnetic force exerted on the coil with current in the magnetic field. Such driver has almost linear current-distance dependence.

3. Electrochemical cell

Electrochemical cell consists of biosensor membrane on the substrate electrode and the tip electrode. It operates in aqueous potassium phosphate buffer solution (pH 8.0). The membrane is enzyme–albumin one cross-linked with glutaraldehyde, containing glucose oxidase as an enzyme. The technique of its fabrication was described in [4]. We used silver plate as substrate electrode. The membrane on it was about 5 mm in diameter. The tip was sharpened by electrochemical etching of 110 μm diameter tungsten rod in saturated aqueous solution of NaOH at 24 V root mean square ac. After etching and washing, tip was insulated with molten paraffin as described in [2]. The degree of the tip insulation was checked by dipping it into conductive liquid and measuring the resistance between the tip and the liquid. Then the very end of a completely insulated tip was exposed by touching a hard surface using electrochemical microscope. The tip was then placed over the membrane in buffer solution and measurements were carried out.

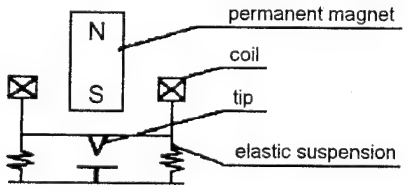

Fig.2. Magnetoelectric tip driver.

Results and discussion

Fig.3 shows typical distance dependences of the values of active and reactive tip current components. They were obtained for the voltage amplitude of 85 mV on the tip. The distance is measured from the start position of the tip outside the membrane. The point $d = 24$ μ corresponds to the beginning of penetration of solution-membrane interface by the tip. At $d = 44$ μ, the direct contact between tip and substrate occurs. There are 4 main areas of curves: 1) $d = 0$–24 μ; tip current does not change, because the edge is outside the membrane. 2) $d = 24$–32 μ; the reactive component of tip current increases due to penetration of stripped edge through the interface between membrane and solution. The immersed area of the tip is increased and causes reactive component of the current to fall. 3) $d = 32$–40 μ; the stripped edge is entirely inside the membrane, so conditions on its surface vary to only a small extent. The reactive component is almost a constant. 4) $d = 40$–44 μ; still unexplained decay of reactive current. It may be connected with processes on the substrate electrode. The active current decreases almost uniformly across the thickness of the membrane. It may be associated with unhomogenity of the membrane or unhomogeneous swelling of it.

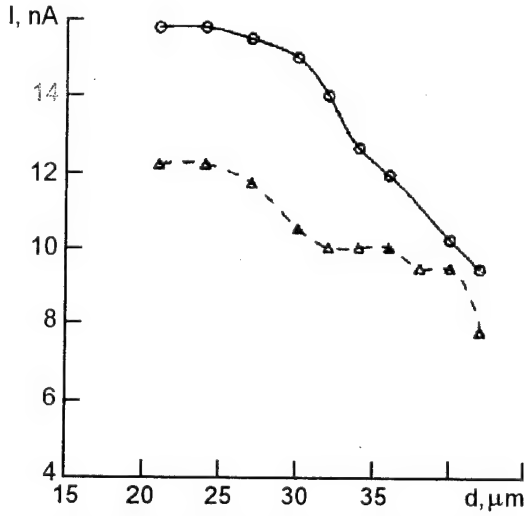

Fig.3. Active (circles) and reactive (triangles) tip current components vs. distance. Point at $d = 44$ μ corresponds to the direct contact between substrate and tip.

A fall in reactive current when measured inside the film could be explained by the difference in the value of dielectric constant inside the film.

One can easily notice that the reactive component of tip current is the most sensitive for substance around the tip. That is why it can be used for evaluation of film thickness. In our case, it is about 20 μm thick. The accuracy of these measurements could be improved by more careful exposing of the tip so that it could remain very sharp. This must decrease the portions 2) and 4) of reactive current — distance dependence.

References

1. D.O.Wipf, A.J.Bard, *J.Elecrochem.Soc.*, **138**, 469 (1991).
2. M.V.Mirkin, F.-R.F.Fan, A.J.Bard, *J.Elecrochem. Soc.*, **328**, 47 (1992).
3. M.V.Mirkin, F.-R.F.Fan, A.J.Bard, *Science*, **257**, 364 (1992).
4. A.P.Soldatkin, A.K.Sandrovsky, A.A.Shulga et al., *Zh.analit.khimii*, **45**, 1405 (1990).

Электрохимический микроскоп: кондуктометрические измерения.

В.И.Стриха, И.Е.Коновалов

Кондуктометрические измерения с помощью электрохимического микроскопа были использованы для определения толщины мембраны биосенсора на основе альбумина непосредственно в рабочем растворе (калийфосфатный буфер). Это позволило учесть разбухание мембраны. Измерения на переменном токе позволяют легко определить положение границы электролит-мембрана.

Functional Materials **2**, No.1 (1995)

Ion exchange processes on the surface of graphite during intercalation under action of magnesium perchlorate

S.B.Lyubchik and V.V.Shapranov

Institute of Physical Organic & Coal Chemistry, National Academy of Sciences of Ukraine, 70 R.Luxemburg St., 340114 Donetsk, Ukraine

The process of graphite exfoliation in the system graphite-magnesium perchlorate is shown to be occur, in the strictly defined temperature range (400—440 °C), according to a new proposed mechanism involving the graphite intercalation products as instable intermediates only.

Показано, що процес розшарування графіту в системі графіт—перхлорат магнію в певному температурному інтервалі (400—440 °C) проходить за специфічним механізмом, в якому інтеркаляційні сполуки беруть участь тільки як нестійкі проміжні продукти.

Processes of thermally initiated syntheses of acceptor type graphite intercalation compounds (**GICs**) and exfoliated graphite (**EG**) are usually studied and considered to be independent processes by virtue of essentially different temperature conditions for **GICs** and **EG** formation [1]. That is, for **EG** obtaining, the initial graphite must be at first transformed into **GICs** and after that, thermolysis of the latter must be carried out. This variant has been studied for various graphite (**G**) — oxidative reagent (**R**) systems where **R** = = HNO_3, H_2SO_4 — Cr (VI), H_2O_2 — H_2SO_4, SO_3, N_2O_5, $FeCl_3$, etc. [2—5] and implemented to produce EG on industrial scale [6].

We wish to report about the discovery of graphite (**G**) — oxidative reagent (**R**) systems for which thermally initiated processes of **GICs** and **EG** syntheses can proceed simultaneously. Such systems are powder graphite — $M^{2+}A_2^-$ mixtures, where M^{2+} is an alkali or alkali-earth metal and A^- is an anion of oxygen—containing Bronsted acid (NO_3^-,ClO_4^-, etc.). The behaviour of such mixtures within a certain range of temperature is similar: graphite gets exfoliated very rapidly to yield **EG** as a single solid carbon product. Outside of this temperature range, no reactions of salt with graphite are observed. It is only the nature of the reactant **R** that defines numerical values of the temperature range and the exfoliation degree estimated by K_V (i.e. exfoliation coefficient).

Experimental dependences of K_V on temperature and salt concentration for powder graphite — $M^{2+}A_2^-$ mixtures are shown in Fig.1.

While studying the thermally initiated processes for graphite-oxidant systems in order to identify the mechanism of **GICs** and **EG** formation and reagents properties which are responsible for their thermal behaviour, we carried out detailed thermal analytical and kinetic investigations on the decomposition of magnesium perchlorate and its mixtures with graphite in temperature range of 150—500 °C using the techniques of isothermal kinetics, differential thermal analysis (DTA), and thermogravimetric analysis (DTG).

An acceleration of the thermolysis reaction for mixtures is observed (Fig.2). The main peaks of decomposition shift to low temperature region.

According to DTA data, there are two main non-additivity areas for the decomposition of **G**—$Mg(ClO_4)_2$ mixtures in comparison with decomposition of individual salt (Fig.3):

1. In the temperature region of 250—380 °C, all the main reactions of graphite interaction with salt occur.

We suggest that the active species which oxidize the graphite and the anions that intercalate result from salt decomposition. Their lifetime is sufficient to interact with graphite following **GIC** formation.

For the reaction of graphite with anhydrous $Mg(ClO_4)_2$, the mechanism of **GIC** formation is

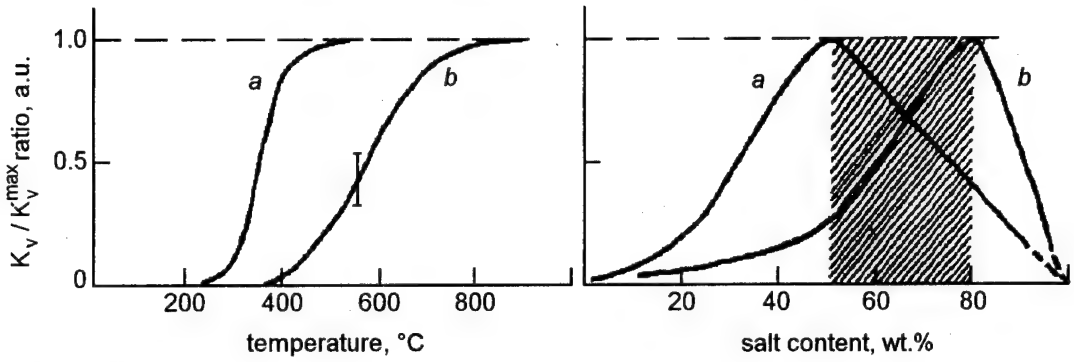

Fig.1. Effects of temperature and salt content on the K_V/K_V^{max} ratio for G—$Zn(NO_3)_2$ (*a*) and G—$Mg(NO_3)_2$ (*b*) mixtures.

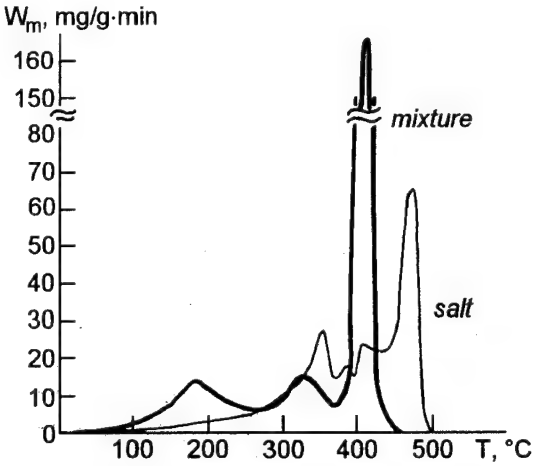

Fig.2. Temperature dependences of mass loss rate (W_m) for magnesium perchlorate (*a*) and its mixture with graphite.

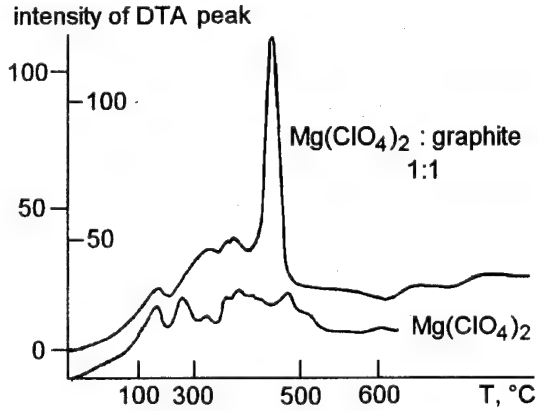

Fig.3. Data of differential thermal analysis for thermolysis of $Mg(ClO_4)_2$ and its mixture with graphite.

proposed which involves a chloronium cation as an oxidant of graphite layers and chlorooxygen-containing anions, e.g. ClO_x^-, which are able to intercalate. It is postulated that this is due to the formation of a melt in which the decomposition of $Mg(ClO_4)_2$ leads to ClO_3^+ according to an autoionization equilibrium of the type (1) [7].

$$ClO_4^- \rightleftharpoons ClO_3^+ + O_2^- \qquad (1)$$

Thus, although total melting of the reactants is evidently not a prerequisite for reaction, partial melting at the magnesium perclorate and graphite interface probably does occur and it affects the **GICs** formation. This fact is not excluded by DTA evidence.

Defects in the natural graphite act as acceptors of active oxygen and lead to oxygen-containing functional groups that shift the equilibrium (1) to the right. An indirect proof of such supposition is burnout of a portion of graphite to CO and CO_2, which is in linear dependence on $Mg(ClO_4)_2$ content (Fig.4).

These intermediate products of **G**—$Mg(ClO_4)_2$ system thermolysis reacts with graphite in a melt or gaseous phase according to the scheme:

$$C_n + ClO_3^+ \longrightarrow C_n^+ + ClO_3 \qquad (2)$$

$$C_n^+ + ClO_4^- \longrightarrow C_n^+ClO_4^- \qquad (3)$$

2. In the temperature region of 400—440 °C, a thermal expansion effect is observed and **EG** is formed. The DTA data indicate a powerful exothermic peak. This peak is to be attributed to the decomposition of the mixture components with irreversible exfoliation.

According to preliminary studies, the rate of **GIC** formation from graphite is lower or equal to

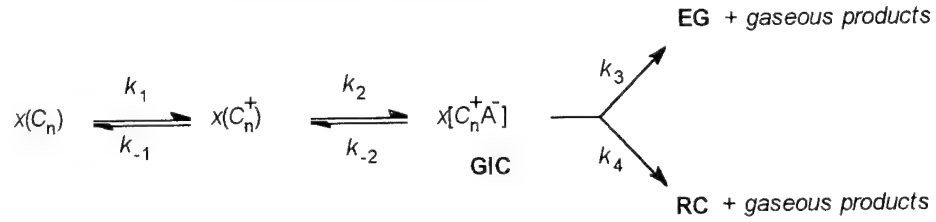

The kinetic model includes the following steps:

1 — an oxidation of graphite polyarene layer to the macrocation C_n^+ or radical cation $C_n^{+\cdot}$;
2 — **GIC** formation as intermediate;
3 — exfoliation of **GIC** resulting in **EG** formation;
4 — decomposition of **GIC** to residue compounds **RC** without exfoliation ($k_3 >> k_4$).

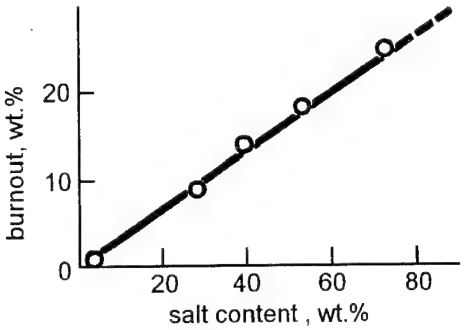

Fig.4. Plot of graphite burn out *versus* magnesium perchlorate content for "**G**—$Mg(ClO_4)_2$" mixture (from TG data).

its conversion rate to **EG** for thermolysis of **G**—$Mg(ClO_4)_2$ mixtures at 300—400 °C. So, it is suggested that an exfoliation in these systems proceeds according to early described scheme of direct oxidative conversion of graphite to **EG** (DOC-process) with **EG** formation in graphite reactions with oxidants without obtaining and isolation of specified **GIC** (**GIC** appears as a very unstable intermediate only) [8].

Conclusion

1. **G**—$Mg(ClO_4)_2$ system does belong to binary systems in which the components being inert themselves are able to interact under strictly defined temperature conditions.

2. A novel mechanism of **EG** formation, different from early known one, is assumed for the system under investigation, in which intercalation compounds exist in the form of an unstable intermediate only.

3. The possibility of a new way for formation of acceptor graphite intercalation compounds has been shown for powder mixtures of graphite with alcaline-earth metal perchlorates by a purely thermal process (instead of the usual chemical or electrochemical oxidation assistance) when active species which are able to interact with graphite appear as a result of initial salt decomposition.

4. Exceptionally high values of $K\mathcal{V}^{max} \approx 350$—400 cm^3/g for investigated **G**—$Mg(ClO_4)_2$ system are assumed to have application in practice in the range areas where **GIC**s are used now for obtaining **EG**.

References

1. D.D.L.Chung, *J.Mater.Sci.*, **22**, 190 (1987).
2. W.Rudorf, *Adv.Inorg.Chem.Radiochem.*, **1**, 223 (1959).
3. Pat.0085121 Ep (1983).
4. Pat.51-5997 Jp (1976).
5. H.Thiele, *Z.Anorg.Allg.Chem.*, **207**, 340 (1932).
6. B.Setton, *Synth.Met.*, **23**, 467 (1988).
7. M.Markowitz, A.Boryta, *J.Phys.CHem.*, **69**, 1114 (1965).
8. S.B.Lyubchik, V.A.Kucherenko, A.P.Yaroshenko, *Mol.Cryst.Liq.Cryst.*, **244**, 107 (1994).

Ионообменные процессы на поверхности графита при интеркаляции под действием перхлората магния

С.Б.Любчик, В.В.Шапранов

Показано, что процесс расслоения графита в системе графит—перхлорат магния в определенном температурном интервале (400—440 °C) проходит по специфическому механизму, включающему интеркаляционные соединения лишь в качестве нестойких промежуточных продуктов.

Functional Materials **2**, No.1 (1995)

Effect of anthraquinone dye molecules aggregation on the spectral properties of the Langmuir-Blodgett mono- and multilayers

Yu.P.Piryatinsky, V.N.Yashchuk and O.V.Yatsun

Institute of Physics, National Academy of Sciences of Ukraine,
46 Nauki Ave., 252650 Kiev, Ukraine

The spectral properties of the anthraquinone dye (AD) Langmuir-Blodgett (LB) layers have been studied. It follows from the analysis of absorption and reflection spectra that there are dimers which are the structural elements of the layers under investigation. At temperature decreasing to 4.2 K, an "excimer-like" fluorescence appears in radiation spectra of the AD LB layers. The relative importance of the excimer, prodimer, and dimer states in the Langmuir film of dye is discussed. At low temperatures, an intensive band appears in the reflection spectra of the multilayer LB films, which is to be associated with the J-aggregates existence. The properties of the J-band in the AD LB layers is discussed.

Досліджено спектральні властивості шарів Ленгмюра-Блоджетт (ЛБ) антрахінонового барвника (АБ). Із аналізу спектрів поглинання і відбиття випливає, що структурними елементами ЛБ плівок є димери. При зниженні температури до 4,2 К у спектрах флуоресценції ЛБ шарів АБ проявляється "ексимероподібне" випромінювання. Обговорюється місце ексимерних, переддимерних та димерних станів у ленгмюрівській плівці барвника. При низьких температурах у спектрах відбиття багатошарових ЛБ плівок виникає інтенсивна смуга, що пов'язується з існуванням J-агрегатів. Обговорюються властивості J-смуги у ЛБ шарах АБ.

The recent comprehensive studies have shown that the molecularly ordered Langmuir-Blodgett (LB) mono- and multilayers exhibit very interesting linear and nonlinear optic properties which may have a widespread use [1]. These highly ordered molecular structures are of paramount interest due to the perspectives of their use in the molecular electronics as the basic functional elements for new generations of electronic devices [1,2]. The initial stage in the solution of this problem consists in the study of the structural and electronic properties of LB layers.

In this work, the absorption, reflection, and time-resolved fluorescence spectra at 300, 77, and 4.2 K were studied for Langmuir films consisting of an anthraquinone dye (AD) molecules.

To obtain the multilayer structures, the Langmuir-Blodgett and Langmuir-Schaeffer methods were used. The monolayers were transferred from the water surface at the pressure of 13 din/cm. The absorption and reflection spectra were measured at normal light incidence on the film plane. To study the kinetics and spectra of the time-resolved fluorescence, a stroboscopic recording system was used having nanosecond resolution. The fluorescence was excited by nitrogen laser LGI-21. The time-resolved fluorescence spectra were recorded in the maximum of the laser pulse through the SPM-2 monochromator.

Absorption and reflection spectra of LB films

In [3], the spectral-luminescent characteristics of the AD solution were investigated. It was established that it is anthraquinone group incorporating the intramolecular hydrogen bond, which is the chromophore determining the optical properties of the molecules under question in the considered spectral range. Therewith, the dipole moment of the optical transition is directed along the short axis of that group. A characteristic feature of the AD spatial configuration is that one of amide groups contained in the molecule may

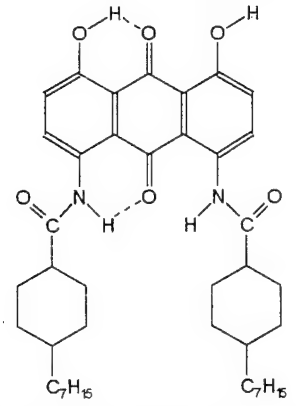

Fig.1. Anthraquinone dye (AD) molecular structure.

form the intramolecular hydrogen bond with the oxygen atom of the anthraquinone group. This results in the planar position of the anthraquinone group and one of amide systems. Another amide group may rotate around the single bond taking up the conformation corresponding to the potential energy minimum. In Fig.1, the hydrogen bonds mentioned are shown by dashed lines.

When passing from the AD solutions (Fig.2, curve 1) to the LB films, in the absorption spectra of the latter measured at 300 K (Fig.2, curves 2 to 4), a significant long-wave shift is observed (curves 3 and 4 are the absorption spectra of X- and Z-type monolayers, respectively; curve 2, that of twelve-layer X-type film). In the LB layers absorption spectra, the bands having maxima at 623; 577, and 535 nm can be distinguished. The comparison of the absorption and reflection spectra taken at 300 and 4.2 K shows that the above-mentioned bands are doubled. Their splitting makes itself evident more distinctly in Fig.3, where the absorption spectrum (curve 1) and reflection one (curve 2) of LB layers at 4.2 K are shown. Such spectral features are known [4] to be characteristic for the physical dimers, namely for such ones in which the transition moments of molecules constituing the dimer are not parallel but positioned at a certain angle to each another. It is just the case when, at the dimer formation, the splitting of the first excited level of monomer into two levels [4]:

$$E_{\pm} = E_1 + E_2 + W \pm \beta,$$

where β is the energy of the resonance molecular interaction in the dimer; W, the energy of Coulombian interaction between distributed charges of the first excited molecule having energy E_1^*, and the unexcited second one with energy E_2.

At the consideration of AD molecules [3], their optical properties in the spectral area under question were shown to be determined mainly by the anthraquinone groups; in those, the first electron transition is polarized along the short axis of the π-electron system. Therefore, the dimers in the LB films being studied are likely to be the AD molecules pairs, in which the mutual disposition of molecules is determined by the anthraquinone groups orientation.

The temperature lowering to 4.2 K causes an additional splitting of bands in adsorption and reflection spectra (Fig.3). The absorption spectrum of the X- and Z-type monomolecular film consists of three bands groups with gravity centers at 623; 574, and 532 nm, in which the cyclic vibration with $\nu \approx 1400$ cm^{-1} is manifested. Each of the band is splitted. The additional maxima are

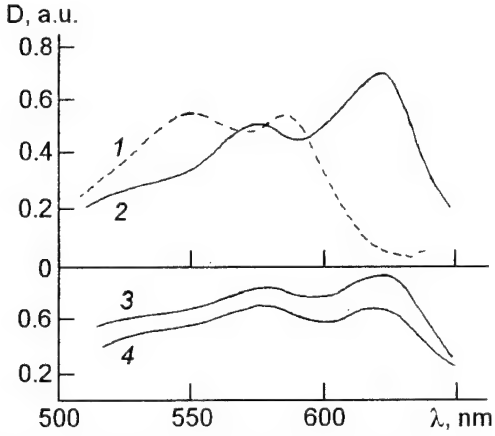

Fig.2. Absorption spectra of the AD solution in dioxane (C=10^{-4} M) (curve 1) and of LB films: 12-layer (curve 2) and monolayers of X- and Z-type (curves 3,4 respectively) at T=300 K.

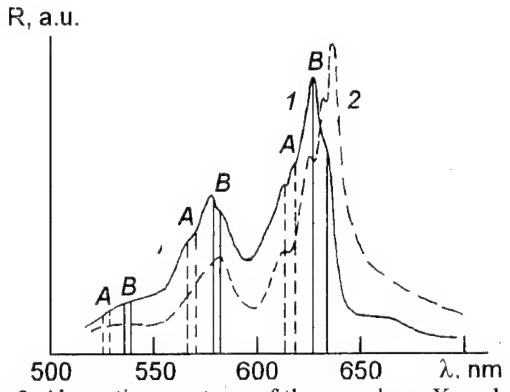

Fig.3. Absorption spectrum of the monolayer X- and Z-type film (curve 1) and reflection spectrum of the multylayer LB film at T=4.2 K.

defined particularly clearly within the first band group: at 633; 629; 618, and 614 nm. In general, the whole absorption spectrum can be divided, conventionally, into A and B series of doublet bands. In Fig.3, they are displayed by vertical solid and dashed lines; the splitting value, 2β, is approximately 380 cm^{-1} between the series and near to 100 cm^{-1} within a series. When the number of layers increased (the structures constitued of 3; 6, and 12 layers were investigated), in the reflection spectrum at 4.2 K, a significant intensity increase and a weak long-wave shift were observed for the band having 638 nm maximum.

The double splitting of the absorption bands of LB films at low temperatures can be assotiated with the arise of two dimer types for which the stable configurations exist at different Θ angles between the vectors of transition moments in the π-electron systems of molecules forming the dimer. According to [4]

$$\Theta \approx \arccos[(M^2-\beta R^3)M^2/3]^{1/2}$$

where R is the distance between the centers of dipoles; M, the transition dipole moment for the molecule.

The above-mentioned absorption spectrum bands in the range λ<635 nm at 4.2 K (Fig.3, curve 1) can be related to the reflection spectra bands having maxima whether coincident with those of absorption bands or shifted slightly to the short-wave range.

The most intensive band of reflection spectra having the maximum at 638 nm has yet no analogues in the absorption spectra. It follows from this fact that, in LB layers, some structures exist which do not show up by absorption but manifest themselves in the reflected light. Such structures, in our opinion, may present single-dimensioned chain-like formations arising in the films due to hydrogen bonds between the neighbouring amide groups. In this case, when the electric field vector of the impinging electromagnetic wave is parallel to the chain direction, the reflection ($R_\parallel$) and absorption ($\kappa_\parallel$) coefficients have maximum values, and vise versa. Yet the electromagnetic wave having electric field vector perpendicular to the chain direction "lights over" the absorption band with $\kappa_\parallel$ at the measuring of AD transmission spectra because the absorption is very weak; therefore, this latter band does not reveal in the absorption spectra. In the same time, the intensive reflection band ($R_\parallel$) is recorded without any distorsions.

Fluorescence of mono- and multilayer LB films

In Fig.4, the fluorescence spectra of AD solution (curve 1) as well as those of mono- (curve 2) and multilayer LB films of AD (curve 3 for 3; 6, and 12 layers; curve 4 for 32 layers) at 300 K are shown. In the fluorescence spectra of X- and Z-type monomolecular layers which coincident with each other (curve 2), the bands at 635 nm (15750 cm^{-1}) and 697 nm (14350 cm^{-1}) can be recognized, $\Delta\nu\approx$1400 cm^{-1}. The comparison with the corresponding absorption spectra (see Fig.2) makes evident a significant overlapping between the short-wave fluorescence band (635 nm) and the long-wave one of the absorption spectrum (632 nm, corresponding to 0-0). This fact, as well as the mirror symmetry of the absorption and fluorescence spectra and the manifestation of a common cycle frequency $\Delta\nu\approx$1400 cm^{-1} indicate that, at 300 K, the same centers, namely AD dimers, absorb and emit in the AD layers. At 4.2 K, an essential change of the film emission spectral composition occurs (Fig.4, curve 5). The fluorescence spectrum of AD layers is, in this case, a broad band having "the gravity center" near to 700 nm, with maxima at 695 and 732 nm standing out on its background. When the films are heated to 300 K, the intensity of the long-wave emission with a structureless spectrum decreases significantly. Yet, the absorption spectra do not change essentially at the transition from 300 to 4.2 K and back. This indicates that, at low temperatures, the transition of initially excited centers to excited states of lower energy takes place. From the appearance of the spectrum and its important shift in relation to the absorption one, a supposition can be made that those states are of excimer nature. It should be noted that similar spectral features have been observed for tetracene dimers dispersed in a polymer matrix [5]. Those authors

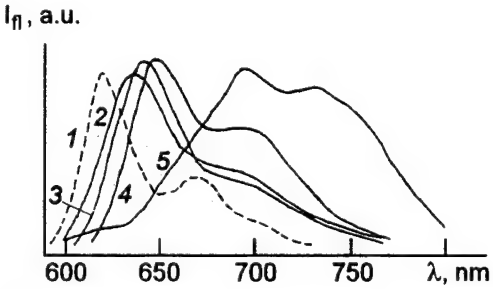

Fig.4. Fluorescence spectra of the AD solution (curve 1), mono- (curve 2) and multilayer LB films (curve 3 for 3,6, and 12 layers, curve 4 for 32 layers) at T=300 K and of monolayer film at T=4.2 K.

concluded that, at low temperatures, dimeric states may arise in tetracene pairs after an excitation of one tetracene molecule, such states corresponding to the potential energy minimum of such a pair. The part played by low temperature is that, in such a case, the dimers of that type do not destruct because of the heat motion. Similar to the case of AD LB layers, in the "excimer-like" spectra of tetracene pairs, a weakly-expressed structure was observed assigned to the formation of variously configurated excimer.

In our opinion, the excimer-like states are responsive for the low-temperature fluorescence in the AD films, too. At the formation of the AD layers, a certain number of the pre-excimer pair may form initially. When the temperature decreases, the spatial rapprochement of molecules constituting a pair becomes possible due to the thermal contraction or a phase transition. As a result of such an evolution, the excimer arises, which absorbs energy as a single molecule but emits similar to a dimer. In a film, there is some distribution of excimer configurations having their own emission frequencies, which manifests itself as the unresolved spectrum of low-temperature fluorescence. The long-wave background (λ>650 nm) in the low-temperature absorption and reflection spectra of LB films (Fig.3) indicates the existence of prodimer state where the molecules in a pair are approached more closely each other then in an excimer. This fact shows that prodimer centers become active, at low temperatures, already in the ground state. In such a case, the prodimer states may serve as the traps for the excitation energy of single molecules and excitons and transform that energy to long-wave spectral range.

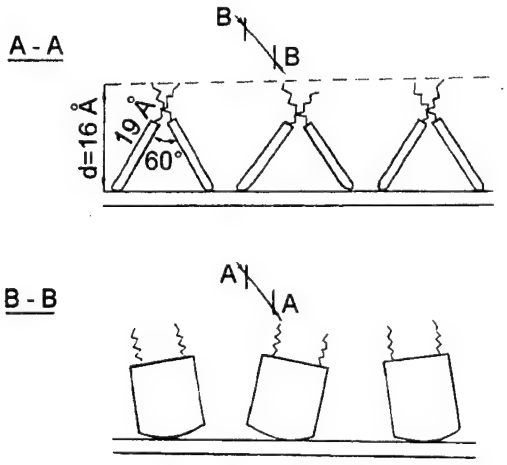

Fig.5. Scheme of the AD molecules distribution in the monolayer presented as the layer section by two perpendicular planes.

Proposed structure of LB film

The investigation results of the AD LB films spectral properties indicate that AD molecules form in those layers excimer, prodimer, and dimer states. Excimers manifest themselves in the fluorescence spectra at liquid helium temperatures while prodimer states are active already in the absorption and reflection spectra. The dipole moments of transition to the lowest excited states for the AD molecules constituting dimers are positioned at an angle Θ different of 180 °. For anthracene dimers, the Θ angle was shown [6,7] to be close to 60 °. If we admit the same Θ value for AD dimers and take into account the AD molecule length d=19 Å [8], we can suppose the scheme of the AD molecules disposition in the layer; that scheme is presented in Fig.5 as the section of the layer by two mutually perpendicular planes. It follows from Fig.5,*a* that the LB monolayer thickness (d) must be equal to 16 Å. This estimation is consistent with the double AD layer thickness d=29 Å given in [8]. For the monolayer d=14.5 Å, counting not the interpenetration of the layers. As is seen from Fig.5,*b*, the long axes of AD molecules are disposed at an angle to each other, what results in the formation of another type dimers in the layer.

Let us consider the nature of the band having maximum at 638 nm in the reflection spectrum taken at 4.2 K. Attention must be drawn to its spectral features. This band appears at low temperatures only; at 300 K, the reflection spectra do not contain it. When the multilayer thickness increases, the intensity of that band becomes considerably higher. So, if the LB film consists of 3 layers, the intensity of the band under question and that of nearest to it, the most intense reflection band at 633 nm are equal. In the film of 12 layers, the intensity of the 638 nm increases significantly, the 633 nm reflection band being recognizable on the background of the former as a slight shoulder. In the band under discussion, the excitation of the strong polarizability $\Delta\alpha$ was observed, which, for the 20-layer LB film of AD, exceeds the monolayer $\Delta\alpha$ by three decimal orders [8]. It should be noted that the above-mentioned properties of the reflection band with maximum at 638 nm (high intensity; a large long-wave shift and small half-width; the temperature-dependent intensity; anomally great values of the

non-linear interaction parameters) are characteristic for the low-dimensional coherent structures, called J-aggregates. There is a high probability that the AD J-aggregates arise in LB films, perhaps involving the hydrogen bonds between amide groups of the dye molecules.

The J-aggregation, indeed, has been revealed and studied [9-11] in the LB films of an anthropyrimidine (AP) dye having molecular structure similar to that of AD. The excitation of anomally high polarizability of the aggregates was observed ($\Delta\alpha \approx 6 \cdot 10^{-21}$ cm^3 [11]). This has been assigned to the electron excitation delocalization on an aggregate consisting of 6 to 8 molecules [10]. The temperature dependence of the aggregate J-band intensity and half-width can be explained similar to the above-mentioned prodimer states formation in LB films of AD, or, alternatively, in terms of the concept of the heat-localized exciton excitation in an associate [12]. According to that concept, not all aggregated molecules but the coherently bounded ones contribute to the aggregate spectral characteristics; the number of such molecules depends on temperature [10]. The J-band amplification with the growing number of AD LB layers can be associated with the increase of molecular interaction between the aggregate piles belonging to neighbouring monolayers. In this case, the two-dimensional J-aggregate must be considered where the interaction between linear piles plays a substantial part. It is shown [13] that such interaction extends the possibilities of J-aggregates formation. Thus, the J-aggregate structure becomes associated to the linear molecular piles interacting between themselves. Perhaps the molecules in the piles are disposed not fully equivalently but at certain angles (see Fig.5) which causes splitting in the reflection and absorption spectra.

References

1. L.M.Blinov, *Usp.Fiz.Nauk*, **155**, 443 (1988).
2. N.G.Rambidi, V.M.Zamalin, *Poverkhnost'*, No.8, 5 (1986).
3. Yu.P.Piryatinsky, V.N.Yashchuk, S.G.Yudin, S.P.Palto, *Ukr.Fiz.Zhurn.*, **37**, 395 (1992).
4. M.Poupe, Ch.Swenberg, Electronic Processes in Organic Crystals, Oxford Univ.Press (1982) Vol.1.
5. M.Ianone, G.W.Scott, *Chem.Phys.Lett.*, **171**, 569 (1990).
6. J.Ferguson, A.W.-H.Mau, J.M.Morris, *Austral. J. Chem.*, **26**, 91 (1979).
7. T.T.Nakashima, H.W.Offen, *J.Chem.Phys.*, **48**, 4817 (1968).
8. L.M.Blinov, S.P.Palto, S.G.Yudin, *Opt. i Spektr.*, **64**, 579 (1988).
9. Yu.P.Piryatinsky, O.V.Yatsun et al., *Ukr.Fiz.Zhurn.*, **38**, 1697 (1993).
10. Yu.P.Piryatinsky, O.V.Yatsun, *Ukr.Fiz.Zhurn.*, **39**, 1049 (1994).
11. Yu.P.Piryatinsky, O.V.Yatsun et al., *Ukr.Fiz.Zhurn.* (to be publ.).
12. H.Fidder, J.Knoster, A.Wiersma, *Chem.Phys.Lett.*, **171**, 529 (1990).
13. V.M.Rosenbaum, M.L.Dekhtyar, *Ukr.Fiz.Zhurn.*, **38**, 1296 (1993).

Влияние агрегации молекул антрахинонового красителя на спектральные свойства моно- и мультислоев Лэнгмюра-Блоджетт

Ю.П.Пирятинский, В.Н.Ящук, О.В.Яцун

Исследованы спектральные свойства слоев Лэнгмюра-Блоджетт (ЛБ) антрахинонового красителя (АК). Из анализа спектров поглощения и отражения следует, что структурными элементами исследуемых слоев являются димеры. При понижении температуры до 4,2 К проявляется "эксимероподобная" флуоресценция. Обсуждается место эксимерных, преддимерных и димерных состояний в лэнгмюровской пленке красителя. При низких температурах в спектрах отражения многослойных ЛБ пленок проявляется интенсивная полоса, которая связывается с существованием J-агрегатов. Обсуждаются свойства J-полосы в ЛБ слоях АК.

Functional Materials **2**, No.1

Heavy metals ion adsorption on the sorbents containing lignine

A.M.Yatsenko and V.M.Shmandiy

Kharkov Polytechnical University, Kremenchug Division, Kremenchug, Ukraine

The paper deals with the process of heavy metal ions (chromium, nickel, iron, copper, lead, etc.) trapping in industrial wastewaters. A method is proposed to obtain a sorbent on the basis of hydrolysed lignine production wastes and high-concentrated spent sulphuric acid products. The sorption capacity of the material obtained is studied as a function of temperature, reaction duration, and reagents concentrations; optimum values are established for those parameters. It is worth to note that the industrial wastes use for sorbent preparation allows to reduce significantly the production cost of the latter as compared to traditional materials.

Робота присвячена дослідженням процесу уловлювання іонів важких металів (хром, нікель, залізо, мідь, свинець та ін.) у стічних водах промислових підприємств. Запропоновано технологію отримання сорбента на основі відходів виробництва гідролізного лігніну та висококонцентрованих відпрацьованих сірчанокислотних відходів. Проведено дослідження сорбційної ємності отриманого матеріалу в залежності від температури, часу реакції, концентрації реагентів та встановлено оптимальні значення цих параметрів. Відмічено, що за рахунок використання промислових відходів для одержання сорбента помітно знижено собівартість останнього у порівнянні з традиційними матеріалами.

Ions of the heavy metals — chrome, nickel, copper, lead, iron, etc., — are characterized by high toxicity and, if brought into the environment, cause its pollution. The main sources of the heavy metal ions are the galvanic processes on the machine works and the sections for the surface preparation of several metals before various treatments. The machine works wastewaters content the above-mentioned ions in considerable quantities, and, for their removal, the waters are cleaned by several techniques.

The traditional methods of wastewater treatment are based on the pre-precipitation of heavy metal ions in form of hydroxydes with subsequent final cleaning by the biochemical, sorption, or ion-exchange methods [1]. The sorption wastewater treatment is based on the interaction of ions with the sorbent active centers. In this case, the bonding energy corresponds to that of hydrogen bond, or energy of weak chemical co-ordination bond (like to that of heavy metal complex compounds).

It is noted [1] that the activated carbons and other similar sorbents adsorb the heavy metal ions only slightly and, therefore, these sorbents have no practical use in the wastewater treatment processes. However, in [2], it is noted that it is possible to use the fresh-obtained hydrolysed lignine (HL) to remove the chrome ions from water. These authors believe that the HL contains the active centers capable to hold the chrome ions firmly enough. It is noted also [2] that the HL is a natural polymer containing chemically active aromatic groups.

One of disadvantages of the sorbent mentioned consists in the dependence its sorption characteristics on the obtaining and storage conditions.

We have developed the method of sorbent production from the hydrolysis industry wastes in form of the HL and the high-concentrated spent sulphuric-acid product (SSA). The method consist in the mixing of the HL and SSA at 70-90 °C for 10 to 15 min. Subsequently, the reaction mixture was neutralized by the 20 per cent aqueous ammonia solution; this was resulted in a solid product with 25 to 35 % moisture, which has used

Table 1. Sorption capacity of the sorbents on the hydrolysis lignine base.

Sorbent type	Sorbed ion amount, mg-eq./g of sorbent			
	chrome	nickel	copper	iron
Initial hydrolysis lignine	0.11	0.15	0.12	0.16
Sorbent obtained at the HL/SSA ratio (w/w)				
1:0.4	0.36	0.42	0.33	0.46
1:0.8	0.63	0.60	0.57	0.71
1:1.2	0.98	0.92	0.84	0.93
1:1.6	1.08	1.02	0.95	0.99
Sorbent modified by lignosulphonates, HL:SSA=1:1.2	1.36	1.18	1.15	1.44

Note: temperature of treatment 85 °C, reaction time 12 min. Lignosuphonates amount 2 % relative to HL mass.

as the sorbent for heavy metal ions. The experimental results are given in the Table 1.

The increase of the HL:SSA ratio enhances the sorption capacity of the product obtained (see Table 1). However, it seems unpractical to raise the SSA amount more then by 1.2 times as related to HL, because, at the further increase, the absorbed ion amount change only unsignificantly. If the reaction temperature exceeds 90 °C the sorption capacity of the product drops by 1.5-2.5 times. The lignosulphonates introduced into the sorbent obtaining process enhance the sorption capacity by 20 to 30 %.

The results obtained can be explained as follows. The unmodified HL contains a small number of the active centers interacting with the heavy metal ions, and that fact is responsive for the low sorption capacity of the product. The addition of the sulphuric acid solution with 60 to 80 per cent concentration favours the increase of the active centers amount due to the sulphuric acid reaction with the aromatic fragments of the HL polymer chain. Accordingly, the amount of the heavy metal ions adsorbed increases considerably. Perhaps, the introduction of the technical grade lignosulphates into the sorbent preparation process also enhances the active centers amount increasing, what results in a further increase of the mass of ion adsorbed.

Thus, the activation of the natural polymer sorbents surface by means of chemical reagents gives the hydrophilic character to that surface, i.e. enhances the surface wetting, what, in turn, assists considerably the heavy metal ions interaction with the sorbent surface and forms the additional active centers which build up the sorption capacityof the products. The use of the production wastes in the sorbent preparation allows to reduce significantly its price and substantially eliminate the use of the costly ion-exchange resins in the processes of the heavy metal ions removing from wastewaters.

The further investigations are desirable to search the products capable to increase the sorption capacity of the sorbent.

References

1. S.V.Yakovlev, Ya.A.Karelin, Yu.M.Laskov, Yu.V.Voronov, Drainage Systems of Industrial Works [in Russian], Ed. by S.V.Yakovlev, Stroyizdat, Moscow (1990).
2. V.A.Kosenko, V.I.Rudenko, V.E.Romanenko, et al., In: Chemistry and Chemical Technology Problems [in Russian], Osnova, Kharkov (1991), 94th issue.

Процесс адсорбции ионов тяжелых металлов на лигнинсодержащих сорбентах

А.М.Яценко, В.М.Шмандий

Работа посвящена исследованиям процесса улавливания ионов тяжелых металлов (хром, никель, железо, медь, свинец и др.) в сточных водах промышленных предприятий. Предложена технология получения сорбента на основе отходов производства гидролизного лигнина и высококонцентрированных отработанных сернокислотных отходов. Проведены исследования сорбционной емкости полученного материала в зависимости от температуры, времени реакции, концентрации реагентов и установлены оптимальные значения этих параметров. Отмечено, что за счет использования промышленных отходов для получения сорбента заметно снижается себестоимость последнего по сравнению с традиционными материалами.

Functional Materials **2**, No.1 (1995)

Biomolecules interactions with the surface of mineral particles

V.V.Dudnik

Institute for Surface Chemistry, National Academy of Sciences of Ukraine,
31 Nauki Ave., 252650, Kiev, Ukraine

A new mechanism is proposed for the regulation of the disperse particles selective aggregation by living microorganisms at the change of the non-uniform charge distribution in the cell membrane. The possibility of creation of membranes having selectivity in terms of particle size and surface characteristics is pointed out.

У роботі запропоновано новий механізм регуляції селективної агрегації дисперних часток живими мікроорганізмами при зміні неоднорідного розподілу заряду у клітинній мембрані та вказано на можливість формування мембран з селективністю за розмірами та характеристиками поверхні часток.

At present, much attention is given to the study of the biological objects (e.g. microorganisms, macromolecules) interaction with various mineral particles. The importance of these investigations is due to the possibilities of widespread use of various effects in biological processe as well as in medicine.

There is a great number of publications dealing with the selective aggregation of metals by some species of microorganisms, both in the sol form [1,2] and in solutions [3,4].

Several hypotheses are known explaining using various approaches. The authors of [5] suppose that the living cells produce an unhomogene electromagnetic field and the selectivity is due to the particles polarization. Thus, in water medium, the metallic particles move to the area of the maximum electrical field intensity (i.e. toward a cell) while the dielectric ones displace toward the minimum field strength, i.e. away from the cell. The estimations given in [6] have shown, however, that such a mechanism is hardly realizable because of great energy required. In [7], theory is developed describing the microorganisms interaction with disperse particles in the stage of the capture and transfer of a particle toward a cell. According to that work, the selectivity in the capture stage is due to the drift in a concentration gradient of metabolism products (selective diffusiophoresis), and in the transfer one — by the different charge redistribution on a cell (flip-flop, lateral diffusion) and on a particle (metallic and dielectric). However, is was pointed out [8] that the selective diffusiophoresis is possible at the electrolyte concentration not exceeding 10^{-5} mol/dm^3 what was inconsistent with the experimental conditions [1,7]. The second mechanism does not discriminate the intact cell and the inactivated one. Besides, the calculation of the energy on the basis of the disjoining pressure values Π_{max} given in [7] using the circular zones approximation [9] gives the U_{max} values $\approx 10\ kT$ for metallic particles ($U_{max} \approx 100\ kT$ for dielectric ones); hence, the coagulation time should have order of several days (for dielectric particles, several months), in contrast to several dozens of minutes in experiment [1,7]. Later, the same authors have proposed the neutralizational coagulation mechanism [8,10] for the discharging of the gold particles by polysaccharides being released in vital processes of a cell; however, such a high selectivity degree was not proved just for polysaccharides, and, moreover, in mixed gold-and-rock suspensions, the discharged gold particles should be coagulated with the neighbouring rock ones. In [11] and [12], a protein residing on the cell membrane and specially sorbing the gold is believed to response for the selectivity; however, the widespread variety of functional groups on the cell surface may assure the chemical bond-

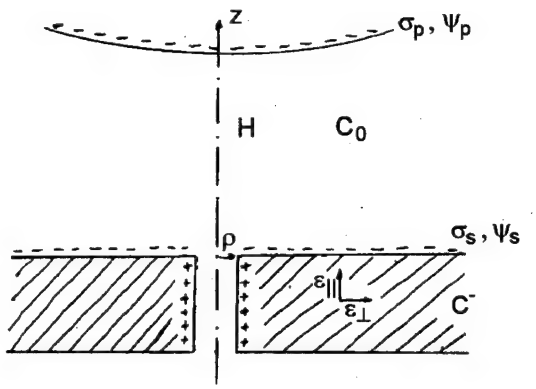

Fig.1. Membrane charge forming model.

ing not only of gold, but of any particle which is attained membrane. The authors of [12] and [13] say about the effect of cell surface unhomogeneity on the coagulation of metallic particles on a cell, but do not discuss any models.

The estimated values of the coagulation time from the experimental data [1,7] allow to admit, reasonably enough, that the particle transfer to a cell is due to the Brownian diffusion. As to the causes of of the selectivity, each of hypotheses mentioned contains some contradictions. Besides, all the hypotheses take not into account an unusual fact, namely, the adsorption and coagulation of negatively charged metal particles intensifies when electronegativity of a living cell increases.

In our work, an attempt is made to explain the selective coagulation from the fact that charges are distributed non-uniformly through-out the cell membrane, and various areas bear the opposite-sign charges; the mechanism of such areas originating and development being not discussed at the moment.

Let us consider at first the charge and potential distribution in the membrane. Assume that a charge is formed, first, as a result of ion adsorption by the surface, and second, is consequence of cell living activity processes inside the membrane. Let admit that the first factor is associated to the charge (and potential) of an inactivied cell ($\sigma^{d<ied>}$) and the second one to the those of an intact cell ($\sigma^{l<ive>}$) (see Fig.1). Moreover, let suppose that, inside of a membrane, charges exist which move along its surface only (lateral diffusion).

The potential distribution in the membrane ($l<ayer>$) can be found from the known system of equations Laplace

$$\Delta\varepsilon\Phi^l = -4\pi e^2 / kT \cdot \sum z_i C_i \qquad (1)$$

and Focker-Planck equations

$$j_i = -D_i \nabla C_i - D_i z_i C_i \nabla\Phi^l \qquad (2)$$

where ε is the dielectric constant; e, the electron charge; k, Boltzmann constant; T, absolute temperature; z_i, C_i, the electrovalency and concentration of i-th kind of ions, respectively; Φ, dimensionless potential; $(e/kT)\cdot\Phi$, the dimensioned potential).

Let the potential be represented as the sum of two items

$$\Phi^l = \Phi_1^l(z) + \Phi_2^l(\rho) \qquad (3)$$

where $\Phi_1^l(z)$ is the potential of the uniformly charged surface; $\Phi_2^l(\rho)$, that of non-uniformly charged area. It should by noted that, in contrast to the preceding work [14], each component of the surface charge is associated to the certain mechanism of its forming.

Since ions are moving along the membrane, C_i depends on ρ, and, taking into account that, in a quasi-steady state, $j_i = 0$, we have

$$C_i^l = C_{C_i}^l \exp(-z_i\Phi_2^l(\rho)) \qquad (4)$$

where C_{Ci} is the ion concentration in the membrane away from a non-uniformly charged area.

Accounting for the anisotropy of the membrane, we must distinguish its dielectric constant values along the surface ($\varepsilon_\parallel$) and normal to that ($\varepsilon_\perp$). To simplificate the mathematical expression let assume only singly charged ions to be presented in the membrane (C^-, z=-1). Then, from Eq.(1)–(4), in the Debye approximation, we obtain

$$\varepsilon_\parallel \frac{\partial^2\Phi_1^l(z)}{\partial z^2} + \varepsilon_\perp \frac{I}{\rho}\cdot\frac{\partial}{\partial\rho}\left(\rho\frac{\partial\Phi(\rho)}{\partial\rho}\right) = = \frac{4\pi e^2}{kT}\cdot C_0\cdot(I+\Phi_2^l(\rho)) \qquad (5)$$

wherefrom, by dividing up to two equations

$$\frac{\partial^2\Phi_1^l(z)}{\partial z^2} = \kappa_\parallel^2 \qquad (6)$$

$$\frac{I}{\rho}\cdot\frac{\partial}{\partial\rho}\left(\rho\frac{\partial\Phi_2^l(\rho)}{\partial\rho}\right) = \kappa_\perp^l\,\Phi_2^l(\rho) \qquad (7)$$

we can, without difficulties, obtain the solutions for each

$$\Phi_1^l(z) = (\kappa_\parallel z)^2/2 + A_1^l(\kappa_\parallel z) + B_1^l \qquad (8)$$

$$\Phi_2^l(\rho) = A_2^l K_0(\kappa_\perp\rho) + B_2^l I_0(\kappa_\perp\rho) \qquad (9)$$

(10)

where $\kappa_{\|,\perp}^{-1}=\left(\frac{\varepsilon_{\|,\perp}kT}{4\pi e^2 C_0}\right)^{1/2}$ is the Debye shielding radius, $K_0(\kappa_\perp \rho)$; $I_0(\kappa_\perp \rho)$, the modified Besselian functions of zero order. Imposing the boundary conditions

$$\Phi_1^l(0) = \Phi_1^l(-l) = \Phi_0 \tag{10}$$

$$\Phi_2^l(\kappa_\perp a) = \Phi_u \tag{11}$$

we obtain ultimately

$$\Phi_1^l(z) = (\kappa_\| z)^2/2 + (\kappa_\|^2 lz)/2 + \Phi_0 \tag{12}$$

$$\Phi_2^l(\rho) = \Phi_u \begin{cases} K_0(\kappa_\perp \rho)/K_0(\kappa_\perp a), & \rho \geq a \\ I_0(\kappa_\perp \rho)/I_0(\kappa_\perp a), & \rho \geq a \end{cases} \tag{13}$$

Now, let us describe the potential distribution in the bulk electrolyte (*m<edium>*). Similar to the above scheme, expressing the potential as the superposition of two items in the Debye approximation, we obtain equations

$$\frac{\partial^2 \Phi_1^l(z)}{\partial z^2} = \kappa^2 \tag{14}$$

$$\frac{I}{\rho}\cdot\frac{\partial}{\partial\rho}\left(\rho\frac{\partial\Phi_2^l(\rho,z)}{\partial\rho}\right)+\frac{\partial^2\Phi_2^l(\rho,z)}{\partial z^2} = \kappa^2\,\Phi_2^l(\rho,z) \tag{15}$$

the solutions of which have the form

$$\Phi_1^m(z) = A_1^m \exp(-\kappa z) + B_1^l \exp(\kappa z) \tag{16}$$

$$\Phi_2^m(\rho,z) = \left[A_2^m \exp(-z\sqrt{\kappa^2-\kappa_s^2}) + B_2^m \exp(z\sqrt{\kappa^2-\kappa_s^2})\right] \times \left[K_0(\kappa_\perp \rho) + C_2^m I_0(\kappa_\perp \rho)\right] \tag{17}$$

The unknown constants κ_s, $A_{1,2}^m$, $B_{1,2}^m$, C_2^m can be determined from the conditions of continuity for the Φ_1 and Φ_2 potentials and convergence in the infinity. Ultimately, from Eq.(12), (13), (16), and (17), we obtain

$$\Phi_1^m(z) = \Phi_0 \exp(-\kappa z) \tag{18}$$

$$\Phi_2^m(\rho,z) = \Phi_u \exp(-z\sqrt{\kappa^2-\kappa_s^2}) \times \begin{cases} K_0(\kappa_\perp \rho)/K_0(\kappa_\perp a), & \rho \geq a \\ I_0(\kappa_\perp \rho)/I_0(\kappa_\perp a), & \rho \geq a \end{cases} \tag{19}$$

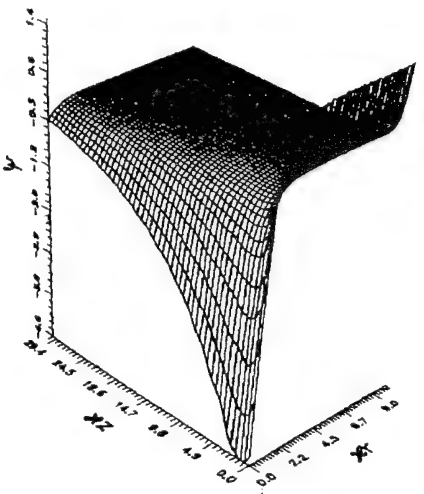

Fig.2. Non-uniform potential distribution at the membrane surface.

Moreover, since the charge and potential distributions in the membrane are subject to the integral electro-neutrality, we can write an additional relationship

$$\sigma_d + elC_c^l = -e\Phi_0 C_0 \kappa^{-1} \tag{20}$$

wherefrom

$$C_c^l = -\left(\Phi_0 + \frac{\sigma_d \kappa}{eC_0}\right)\cdot\frac{C_0}{\kappa l} \tag{21}$$

Assuming that, for an inactivated cell, $C_c^l = 0$, and having denoted

$$\Phi_0^d = -\frac{\sigma_d \kappa}{eC_0} \tag{22}$$

we obtain, after some simple rearrangements,

$$\frac{\kappa_\perp^2}{\kappa^2} = \frac{\varepsilon}{\varepsilon_\perp}\cdot\frac{C_c^l}{C_c} = \frac{\varepsilon}{\varepsilon_\perp}\cdot\frac{I}{\kappa l}\cdot(\Phi_0^d - \Phi_0) \tag{23}$$

Unfortunately, the precise determination of the $\frac{\varepsilon I}{\varepsilon_\perp \kappa l}$ value is very difficult, since, for thin surface layers, the dielectric conctant $\varepsilon_\perp$ can differ fron bulk one ε. We admitted $\frac{\varepsilon I}{\varepsilon_\perp \kappa l} \approx 1$ ($\kappa^{-1} \approx 30$ Å, $l \approx 100$ Å, $\varepsilon \approx 80$, $\varepsilon_\perp \approx 24$). As is seen from Eq.(19) and (23), if the living cell potential, Φ_0, becomes more electronegative, the bulk shielding radius in the non-uniform charge area, $\left(\kappa\sqrt{1-(\Phi_0^d - \Phi_0)}\right)^{-1}$, decreases, and, hence, the potential becomes more long-range acting.

Fig.2 shows the potential distribution in the bulk electrolyte (z) and along the surface (ρ). It is seen that, in the non-uniform charge area, at $\Phi_0<0$, $\Phi_u>0$, some "channels" exist along which a negatively charged particle can attain the living cell. The cell may provide for selective sorption of several particle forms and sizes by regulation of the Φ_u value.

The model proposed can serve as an important supplement to the theory linking transmembran potential and the bioenergetic processes [13,15], since, on its basis, one can find a natural explanation for the selective heterocoagulation of disperse particles on living cells as well as its relation to the membrane processes. Moreover, a possibility arises for the creating of membranes containing builded-in charge structures which assure the selectivity in terms of the particle sizes and surface characteristics.

References

1. F.D.Ovcharenko, N.V.Pertsov, Z.R.Ulberg et al., In: Physico-Chemical Mechanics and Lyophilness of Disperse Systems [in Russian], Naukova dumka, Kiev (1985), p.96.
2. G.G.Mineev, *Geokhimia*, No.4, 577 (1976).
3. S.A.Marakushev, T.L.Balezina, A.N.Kovalevskaya, *Doklady AN SSSR*, **300**, 1211 (1988).
4. Z.R.Ulberg, V.I.Karamushka, T.G.Gruzina et al., *Kolloidnyi Zhurnal*, **51**, 172 (1989).
5. H.L.Pohl, Interaction between Electromagnetic Field and Cell, Plenum Press, N.Y.;L. (1985), p.437.
6. V.N.Shilov, I.A.Razilov, V.P.Estrela-Llopis, *Kolloidnyi Zhurnal*, **49**, 98 (1987).
7. F.D.Ovcharenko, V.R.Estrela-Llopis, A.I.Gavrilyuk, A.S.Dukhin, In: Physico-Chemical Mechanics and Lyophilness of Disperse Systems [in Russian], Naukova dumka, Kiev (1985), p.3.
8. F.D.Ovcharenko, V.R.Estrela-Llopis, I.N.Yurkova, Proc. 5th Conf. on Colloid Chem., Budapest (1990), p.85.
9. B.V.Deryagin, V.N.Churayev, V.M.Miller, Surface Forces [in Russian], Nauka, Moscow (1985), 400 p.p.
10. V.R.Estrela-Llopis, I.N.Yurkova, In: Physico-Chemical Mechanics and Lyophilness of Disperse Systems [in Russian], Naukova dumka, Kiev (1985), p.15.
11. Z.R.Ulberg, V.I.Karamushka, T.G.Gruzina et al., *Biotekhnologia*, No.1, 109 (1986).
12. V.I.Karamushka, Z.R.Ulberg, T.G.Gruzina et al., *Prikladnaya biokhimia i mikrobiologia*, **27**, 119 (1991).
13. F.D.Ovcharenko, Z.R.Ulberg, A.S.Dukhin et al., *Uspekhi sovremennoy biologii*, **111**, 286 (1991).
14. V.V.Dudnik, *Kolloidnyi Zhurnal*, **54**, 38 (1992).
15. A.V.Markin, Yu.A.Chizmadzhev, Induced Ionic Transport [in Russian], Nauka, Moscow (1974), 252 p.p.

Взаимодействие биомолекул с поверхностью минеральных частиц

В.В.Дудник

В работе предложен новый механизм регуляции избирательной агрегации дисперных частиц живыми микроорганизмами при изменении неоднородного распределения заряда в клеточной мембране и указана возможность формирования мембран с селективностью по размерам и характеристикам поверхности частиц.

Functional Materials **2**, No.1 (1995)

Water desorption processes research on the actual surface of stainless steel

Yu.F.Stefanov

Research and Education Center "Physics, mechanics and technology of unhomogeneous systems", T.Shevchenko Kiev University, 64 Vladimirskaya St., 252017, Kiev, Ukraine

The nature of the water displacement desorption stimulated by the contact of oxygen with the high-vacuum chamber walls is investigated. It is shown that, on the stainless steel actual surface, in the high vacuum, three types of water adsorption centers exist characterized by the desorption activation energy values of 0.2; 0.4; and 0.9 eV. The two first types of adsorption centers can be the surface hydroxyls as well as the surface oxygen having lone electron pair, which interact with a water molecule by one or two hydrogen bonds, respectively. The third adsorption center type is responsive for the associative water desorption from two hydroxyls. The mechanism of the oxygen-stimulated displacement desorption of water is proposed and substantiated.

Досліджено природу ефекту витискувальної десорбції води, стимульованої контактом кисню зі стінками високовакуумної камери з нержавіючої сталі. Показано, що на реальній поверхні нержавіючої сталі у високому вакуумі для молекул води існують три типи адсорбційних центрів, які характеризуються енергіями активації десорбції 0,2; 0,4; 0,9 еВ і подано їх інтерпретацію. Перші два типи адсорбційних центрів можуть бути поверхневими гідроксилами, а також поверхневим киснем, що має неподілену електронну пару, які взаємодіють з молекулами води однією та двома водневими зв'язками, відповідно. Третій тип адсорбційних центрів забезпечує асоціативну десорбцію води з двох гідроксилів. Запропоновано та обгрунтовано механізм витискувальної десорбції води, стимульованої киснем.

Recently, the water desorption investigations on the transitional metals surfaces are topical, since these processes are of great importance in the catalysis, corrosion, electrochemistry, and vacuum techniques areas [1]. Among the transitional metals and their alloys, the stainless steel 12X18H10T is of particular interest being the main construction material in the vacuum devices area.

Water desorption processes on the stainless steel surface are still almost unresearched, though there are just these which determine the water vapour background level in the high vacuum equipment, which always is desirable to reduce to minimum because of the water activity. Besides, the secondary effects are revealed associated to the release of the water molecules in a high-vacuum chamber due to oxygen action [2] which influence significantly on the reliability of the adsorbtion-desorption research performed by the mass-spectrometry method. These effects are the "false peak" of water associated to the design features of mass-spectrometer ion source [3] and the effect of water displacement desorption from the high-vacuum chamber walls stimulated by the oxygen [4,5]. The latter effect is of particularly interest since it is not an instrumental artifact, in contrast to the "water false peak" [3]. The first attempt to study the nature of the oxygen-stimulated displacement desorption of water is made by us in [4]. However, in that work, the nature of the revealed adsorption centers on the stainless steel actual surface and, on this basis, the mechanism explaining the water displacement desorption effect were based on the rather intuitive assumptions.

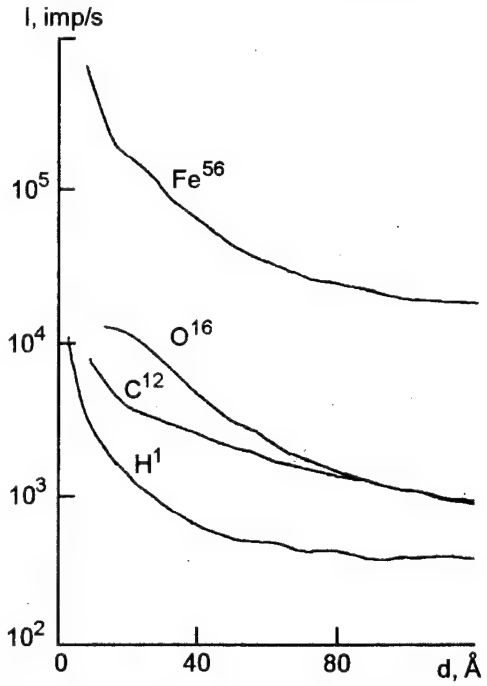

Fig.1. Iron, oxygen, carbon, and hydrogen distributions profiles in the thickness of the surface layer for the stainless steel 12X18H10T actual surface obtained after surface machining and exposure to air at ambient temperature for 48 h.

The aim of the present work is to research the oxygen stimulated displacement desorption of water.

Characteristics of specimens and experimental methods used

In our experiments, the stainless steel 12X18H10T was used, its correspondance to the GOST 5632-72 requirements from the viewpoint of the elemental composition was proved by X-ray spectroscopy.

The desorption features of stainless steel actual surface were studied, i.e. those of the machined surface exposed to air at the ambient temperature, as well as of specially oxidized one in the dried air at the atmospheric pressure and temperature 473 K for 15 h.

The surface composition of the specimens was analysed by secondary-ion mass-spectroscopy method using the ion probe IMS-4F; the H, C, and O impurities distribution profiles in depth of the surface layer were obtained. The analysis results are presented on the Figs.1 and 2 where is shown that the actual surface, as well as the specially oxidized one, is enriched by the hydrogen, carbon and oxygen.

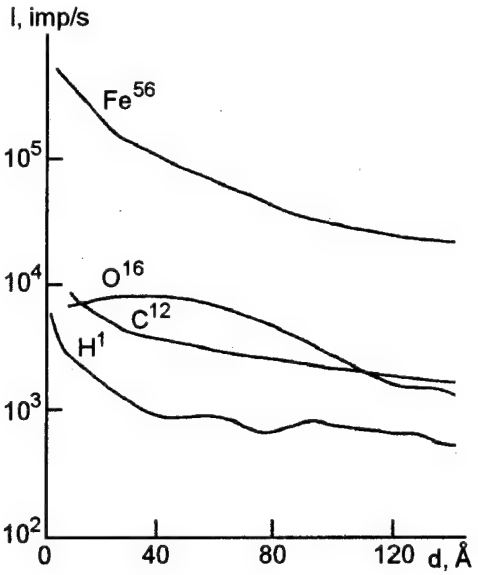

Fig.2. Iron, oxygen, carbon, and hydrogen distributions profiles in the thickness of the surface layer for the stainless steel 12X18H10T after the special oxidation in dried air at T=473 K for for 15 h.

To study the water desorption processes on the stainless steel surface, the unique procedures were applied consisting in that the walls of high-vacuum chambers were used as the specimens.

For the kinetics investigation of the water molecules desorption on the stainless steel surface in the high vacuum, a chamber made from 12X18H10T steel of 0.8 dm^3 volume was used, attached directly to the MX-7304 mass-spectrometer and being pumped out, through a stop value, to the residual pressure of 10^{-8} Torr. The chamber and the ion source of the mass-spectrometer were provided with the thermostated heating system. The water and hydrogen thermal desorption curves were taken after the chamber pump-out closing at constant temperatures in the 293-493 K range through 10 K intervals. All the curves obtained flatten out at saturation, what indicated their nature is associated with desorption. The stabilization of the surface under research in terms of the adsorption centers quantity was achieved by the long-time (not less than 8 hours) high-vacuum exposure of the chamber walls at 493 K, what assured a good results reproducibility.

The identical initial conditions of the filling of the adsorption centers by the OH particles involving in the associative desorption of water molecules, were assured, at various temperatures, each time before the desorption curve was taken, by the achieving of the equilibrium adsorption-

desorption state in which the velocities of molecules being desorbed and of those being outpumped were equal to each other. In this case, the mentioned adsorption centers were admitted to be completely filled, since, at the saturation of the stainless steel surface with the hydrogen and oxygen, it is just the associative desorption process which is the limiting stage in the water molecules formation. The desorption rate of the molecules under study was determined as the slope of the corresponding desorption kinetics curve in the time range 20-60 s after the pump-out closing, where the curve can be adequately approximated by a straight line. The activation energy was estimated from the Arrhenius' relationships by the linear regression method.

To investigate the displacement desorption in the oxygen medium, another chamber was used made from 12X18H10T material, too, but 1.0 dm^3 in volume, which has been pumped out to a high vacuum by a diffusion pump provided with the liquid nitrogen trap to the 10^{-6} Torr residual pressure, and was connected, on one side, to the mass-spectrometer ion source through a diaphragm with 50 μm orifice, and on the other side, to a sampler being purged with the dry oxygen. The sampler was a measured volume which can be closed by two stop valves, one on the chamber side and other on the side of gas line assuring the purging of the sampler by the dried oxygen, the humidity of the latter being controlled by means of Baikal 3M hydrometer. The water displacement desorption curves were taken at fixed chambers temperatures in the 293-493 K range through 10 K intervals after the admission of the chamber with the dry oxygen to 10^{-2} Torr pressure and molecular flowing to the mass-spectrometer ion source. Therewith, the admission of a gas sample has been carried out at the closed high-vacuum valve after the adsorption-desorption equilibrium has been previously attained, which is characterized by a constant water vapour background level. The sample admission were so chosen that, over an appreciable length of time (order of 20 min), the pressure drop due to pumping by the magnet-discharghing pump through the mass-spectrometer ion source can be neglected. In this case, the water release kinetics curves (from 5 min after the beginning of the sample admission to ion source and on) can be satisfactorily approximated by straight lines, and the water releasing rate has been determined from the slope of these lines related to horizontal axis. The water release so measured has nothing to do with the "false peak" arising from the ion source design and work. That was proved by the experiments dealing with the water release kinetics at a fixed (ambient) temperature of the chamber under study and varying (in the range of 293-473 K) temperatures of the ion source; these investigations had shown that, in all cases, the saturation stage of the kinetics curve is achieved substantially within 5 min after the beginning of the oxygen admitting to ion source. The stabilization of the chamber walls from the viewpoint of the adsorption centers amount and the assuring of identical initial conditions of filling by OH particles involving in the associative water molecules desorption, were achieved similar to experiments on the thermal desorption of water in a high vacuum.

It should be noted that both high-vacuum chambers under study as well as satellite specimens for the elemental analysis were made from a common piece of the 12X18H10T steel.

Results and discussion

The data characterizing the water molecules desorption kinetics in high vacuum on the stainless steel actual surface, as represented in the form of the Arrhenius' relationships, have the appearance of a broken line consisting of three linear portions characterized by the activation energy values of 0.18±0.05 eV at $293<T<333$ K; 0.38±0.05 eV at 333<T<393 K, and 0.9±0.1 eV at 393<T<493 K and corresponding to the water desorption from the adsorption centers of three types. In fact, the experimental procedure used for the water thermal desorption study realizes the mode of the multiple water molecules interactions with the high-vacuum chamber walls and, consequently, with all types of adsorption centers existing on the stainless steel surface. Thus, at first, the water molecules are associatively desorbed from the primary adsorption centers according to the following scheme:

$$OH(ad) + OH(ad) \rightarrow H_2O(gas) + O(ad)$$

After the landing of these water molecules on the other (secondary) adsorption centers, they will be registered as if they are desorbed from the latters, their true origin being "forgotten". Therefore, in our case, the increase of the water vapour partial pressure in a unit time registered by a measuring device can be presented as

$$dP/dT = W(V_1 + V_2 + V_3)/kT \qquad (1)$$

where $V_1 = CN_1\exp(-E_1/kT)$, $V_2 = CN_2\exp(-E_2/kT)$ is the water molecules quantities in a unit time registered from the secondary adsorption centers N_1 and N_2, respectively; V_3, the water molecules quantity in a unit of time registered from primary adsorption

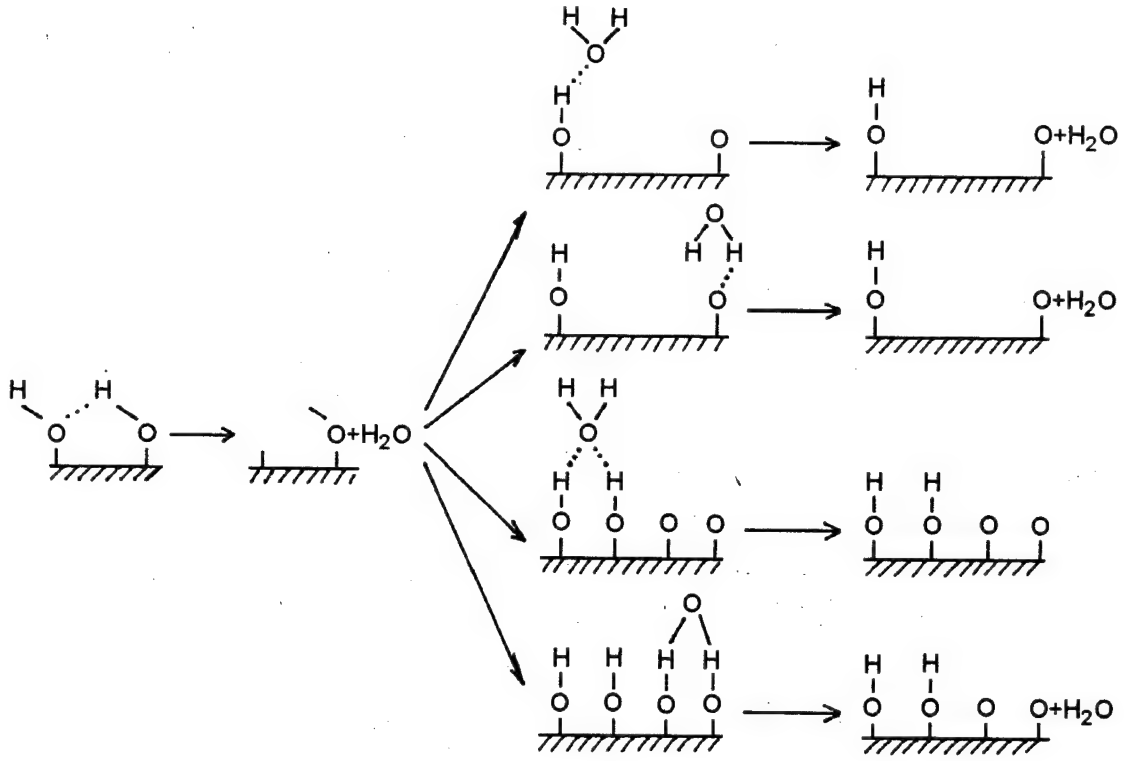

Fig.3. Model of the water molecules desorption from the stainless steel actual surface in high vacuum.

centers; W, the chamber volume; k, the Boltzmann constant; T, the chamber walls surface temperature; C, the factor at the exponential term; E, the desorption activation energy. The first linear portion (293 K<T<333 K) of the Arrhenius' curve corresponds to the case when

$$V_1 = CN_1\exp(-E/kT) >> V_2 + V_3,$$

the second one (333 K<T<393 K) — to

$$V_2 = CN_2\exp(-E/kT) >> V_1 + V_3,$$

while the third (393 K<T<493 K) — to

$$V_3 = CN_3\exp(-E/kT) >> V_1 + V_2,$$

where N_0 is the quantity of the primary adsorption centers.

Thus, on the actual surface of the stainless steel, three types of adsorptions centers are experimentally found, corresponding to the water molecules desorption activation energy values of approximately 0.2; 0.4; and 0.9 eV. Since the stainless steel actual surface is saturated with the oxygen and hydrogen and, consequently, with surface hydroxyls, it can be supposed that the desorption activation energy value of 0.2 eV corresponds to the desorption of the water molecules which interact with the adsorption centers formin with those one hydrogen bond; 0.4 eV — two hydrogen bonds and 0.9 eV energy corresponds to the associative desorption with the formation of one water molecule from two hydroxyls. The first two types of the (secondary) adsorption centers can by the surface hydroxyls as well as oxygen atoms having a lone electron pair necessary for the hydrogen bond formation. The model of the water desorption from the stainless steel actual surface in a high vacuum is presented on the Fig.3.

The Arrhenius' relationships obtained in experiments dealing with the water thermal desorption on the specially oxidized surface of the stainless steel, have, too, the broken line appearance consisting of the three linear portions characterized by the desorption activation energy values of 0.19±0.05 eV at 293K<T<383 K; 0.39±0.05 eV at 383K<T<433 K; and 1.0±0.1 eV at 433K<T<493 K. Hence, in comparison to the case of the stainless steel actual surface, the elevation of the first temperature range upper limit by 50 K and that of second one by 40 K is observed for the oxidized surface, what supports the proposed model of the water desorption processes on the stainless steel surface in high vacuum. Indeed, the stainless steel oxidation results in an increasing quantity of the secondary adsorption centers N_1 and N_2, associated to the surface oxygen, what

should, according to Eq.(1), cause the broadening of the temperature range in which the contribution of the water molecules desorbed from the secondary adsorption centers prevails.

The experinemtal data relating to the water displacement desorption stimulated by the oxygen, as presented in the form of the Arrhenius' relationships, have the appearance of a broken line consisting of two portions; these correspond to the activation energy values of 0.42±0.05 eV (at 363K<T<393 K) and 0.8±0.1 eV (at 393K<T<453 K). The low temperature range at T<363 K remained unresearched because of poor sensitivity.

Besides, as is seen from Table 1, the water release from the chamber walls is accompanied by the activated adsorption of the oxygen, and the water liberation rate is correlated with the rate of the oxygen partial pressure dropping. Hence, the water evolving is associated with the oxygen chemisorption.

When comparing the experimental results related to the oxygen-stimulated water release and those of the thermal water desorption in high vacuum, the surprising similarity can be noted in the behaviour of the Arrhenius' curves describing two these processes, at first glance so distinct. Only a small difference in the desorption activation energy is observed, which amounts to 0.1 eV.

From the aforesaid, an assumption can be made as to desorptive nature of the oxygen-stimulated water release, and the mechanism explaining it can be proposed. The principle of the oxygen-stimulated displacement water desorption is that the oxygen adsorbed on the metal surface

Table 1. Temperature dependence of the relative changing rate of the oxygen and water partial pressure at the dry oxygen admission into a stainless steel vacuum chamber.

T, K	Actual surface		Specially oxydized surface	
	$-dP/dt$ O_2 (arb. units)	dP/dt H_2O (arb. units)	$-dP/dt$ O_2 (arb.units)	dP/dt H_2O (arb. units)
403	1.4	0.052	-	-
413	2.2	0.100	-	-
423	2.8	0.529	-	-
433	4.0	0.279	-	-
443	6.2	0.529	0.9	0.047
453	7.2	0.814	1.7	0.090
473	-	-	2.9	0.414

adjacent to a hydroxyls pair forming a water molecule brings a perturbation into the metal surface — hydroxyl pair system, what results in the decrease of the associative water desorption activation energy by a value of 0.1 eV order. This causes a breaking of the adsorption-desorption equilibrium in the measuring chamber and an increase of the water partial pressure. This supposition is supported by a theoretical work [6] where authors, assuming the Ni(111) surface simulated by means of the two-layer cluster Ni_{10} model, have performed the calculation of the water molecule interaction with the pure Ni(111) surface and with Ni(111) surface presaturated with the adsorbed oxygen. It is shown that, in Ni/H_2O system, the bonding energy of water molecule with the metal surface is higher by a value of 0.1 eV order then in the $Ni+O/H_2O$ system.

Taking into account that, in experiments on the water displacement desorption, the oxygen partial pressure in the measuring chamber has the order of 10^{-2} Torr, it can be assumed that the oxygen chemisorption is not the limiting stage in the water displacement desorption process. Before the oxygen is admitted to the measuring chamber, the velocity of the water molecules desorbed from primary adsorption centers is $V_3 = CN_0N_0\exp(-E_3/kT)$ (see Eq.(1)).

Then, according to the proposed mechanism of the water displacement desorption, in the conditions of oxygen contact with the chamber surface, the velocity of the desorbed water molecules $V_{3'} = CN_0N_0\exp(-E_{3'}/kT)$ where $E_3 - E_{3'} = 0.1$ eV.

The increase of the desorbed water molecules velocity associated with the displacement desorption effect

$$V_3 - V_{3'} = CN_0N_0\exp(-E_3/kT)\{1 - \exp[-(E_3 - E_{3'})/kT]\} \approx \approx CN_0N_0\exp(-E_3/kT) \quad (2)$$

since, at T<473 K, $\exp[-(E_3 - E_{3'})/kT] << 1$.

Thus, at the oxygen admission in the measuring chamber, the rate of the water molecules release from the chamber walls is defined by the Eq.(2). However, similar to the case of the thermal water desorption, at the temperature lower than critical one (393 K for the stainless steel actual surface), the water molecules are registered as those desorbed from the secondary adsorption centers of 1st and 2nd type, corresponding to the desorption activation energy values of 0.2 and 0.4 eV, respectively.

An alternative mechanism of the oxygen-stimulated water release based on a catalytic interaction of the hydrogen with oxygen on the stainless steel surface resulting in the water for-

mation, is, in our opinion, unlikely. In fact, according to modern views [7], the catalytic hydrogen oxydation reaction goes through the intermediate stage of the hydroxyl formation. However, there is no information in the literature confirming the hydroxyl formation on metal surfaces in the course of the oxygen chemisorption. So, in [8], during the research of the oxygen interaction with the polycrystallic nickel surface presaturated with hydrogen, the surface hydroxyls formation was not found.

Conclusions

1. On the actual surface of the stainless steel, in a high vacuum, three types of the adsorption centers for water molecules, characterized by desorption activation energy values of 0.2; 0.4; 0.9 eV, are identified and interpreted. The activation energy of 0.2 eV corresponds to the desorption of water molecules bonded to the surface hydroxyls and oxygen by one hydrogen bond; 0.4 eV — by two bonds, and 0.9 eV corresponds to the associative desorption of water forming from two hydroxyls.

2. The mechanism of the oxygen-stimulated water displacement desorption is proposed and substantiated. Its principle consist in that the oxygen, being in contact with the high-vacuum chamber walls, chemisorbs itself on their surface. Therewith, when oxygen is chemisorbed on the metal surface in the vicinity of a hydroxyls pair forming a water molecule, a disturbation is brought in the metal surface — hydroxyl pair system, resulting in a lowering of the activation energy of the water associative desorption by a value of 0.1 eV. The minimization of the oxygen-stimulated displacement water desorption is associated with the decrease of the oxygen chemisorption rate and is achievable by the stainless steel surface oxidation.

References

1. P.A.Tiel, T.E.Madey, *Surf.Sci.Repts.*, Nos.6-7, 211 (1987).
2. J.J.Quinn, R.V.Elliot, *Vacuum*, **27**, 473 (1977).
3. J.Kiiely, P.Flinn, B.Sun, Proc. 19th Reliab. Phys. Symp., N.Y., (1983) p.270.
4. G.Ya.Pikus, I.M.Protas, Yu.F.Stefanov, *Zhurn.Fiz.Khim.*, No.11, 3089 (1989).
5. G.Ya.Pikus, I.M.Protas, Yu.F.Stefanov, *Poverkhnost'*, No.8, 107 (1992).
6. S.K.Saha, N.C.Debnath, *Chem.Phys.Lett.*, **121**, 490 (1985).
7. M.Hock, J.Kuppers, *Surf.Sci.*, **188**, 575 (1987).
8. A.Benninghoven, P.Beekmann, K.H.Miller, M.Schemmer, *Surf.Sci.*, **89**, 701 (1979).

Исследование десорбционных процессов воды на реальной поверхности нержавеющей стали

Ю.Ф.Стефанов

Исследована природа эффекта вытеснительной десорбции воды, стимулированной контактом кислорода со стенками высоковакуумной камеры из нержавеющей стали. Показано, что на реальной поверхности нержавеющей стали в высоком вакууме для молекул воды существует три типа адсорбционных центров, характеризующихся энергиями активации десорбции 0,2; 0,4; 0,9 эВ и дана их интерпретация. Первые два типа адсорбционных центров могут быть поверхностными гидроксилами, а также поверхностным кислородом, имеющим неподеленную электронную пару, которые взаимодействуют с молекулами воды одной и двумя водородными связями, соответственно. Третий тип адсорбционных центров обеспечивает ассоциативную десорбцию воды из двух гидроксилов. Предложен и обоснован механизм вытеснительной десорбции воды, стимулированной кислородом.

Functional Materials **2**, No.1 (1995)

The porous structure features of metal-oxide type vacuum condensates

G.M.Kochetov, G.G.Didikin and B.M.Emel'yanov

Kiev State University of Architecture and Building,
31 Vozdukhoflotsky Ave., 252037 Kiev, Ukraine

The structure of porous vacuum condensates of Fe–Al_2O_3 and Co–Al_2O_3 systems has been investigated using large-angle and small-angle X-ray scattering, gas adsorption and microhardness measurements. These two-phase compositions have been established to consist of the porous metallic matrix and the oxide phase dispers particles distributed uniformly therein. The porosity characteristics have been studied as dependent on the condensate composition. The chemical nature of the matrix metal is noted two influence the structure parameters and sorption properties of metal-oxide compositions.

Методами рентгенографії на великих та малих кутах, газової адсорбції, вимірювання мікротвердості досліджено структуру пористих вакуумних конденсатів систем Fe–Al_2O_3 і Co–Al_2O_3. Встановлено, що ці двофазні композиції складаються з пористої металічної матриці і рівномірно розподілених в ній дисперсних часток оксидної фази. Вивчено характеристики пористості в залежності від складу конденсату. Відмічено вплив хімічної природи матричного металу на структурні параметри та сорбційні властивості металооксидних композицій.

The leading branches of modern industry have an urgent need for refractory high-strength materials characterized by chemical resistance, low density, specified heat and electrical conductivity values, as well as by special magnetic and optical properties.

The electron beam technology allows to obtain the metal-ceramic composite materials with specified properties and working characteristics [1]. In this connection, much interest is given to investigations of porous compositions containing a metal and alumina obtained by the electron-beam evaporation with subsequent condensation in vacuum. Such condensates can be used as the refractory protective coatings, heat-insulating materials, selective filters and sorbents.

Results of the structure investigations of Ni–Al_2O_3 vacuum condensates are considered in detail in [2–6]. The literature data about the metal-oxide systems based on iron and cobalt are meagre enough and relate only to compositions obtained by traditional powder metallurgy methods.

In this work, the results of study of the vacuum condensates Fe–Al_2O_3 and Co–Al_2O_3 structure and porosity are presented; also, data are compared obtained for systems having matrices based on various metals of iron triade and prepared in the identical conditions.

Materials and techniques

As the initial materials for condensates preparation, the iron and cobalt ingots were used prepared by induction melting in vacuum with subsequent electron-beam remelting, and alumina bars made of the analytical grade material (p.a.) by presssing and sintering at 1700°C. The metal and alumina evaporation was performed by two independent sources in the vacuum of $1.33 \cdot 10^{-3}$ Pa. The mixed vapour flow condensation occurred on a carbon steel (St.3). The evaporators and support arrangement allowed to obtain about 1 mm thick condensates with alumina content varying in the 0–30% (by mass) range.

The X-ray phase analysis of the condensates was perfomed by means of DRON-3 diffractometer in the filtered copper radiation. The lattice constants were determined basing on gravity cen-

Table 1. Lattice constants (a±0.00008), pores concentrations (C±0.3) and oxygen sorption values (g±1) as functions of alumina content (m) in Fe–Al_2O_3 condensates

m, % by mass	a, nm	C, %	g, mg/g
0.8	0.28669	5.1	99
2.3	0.28673	10.4	102
5.9	0.28697	19.0	119
14.2	0.28759	22.7	138
21.3	0.28793	25.1	149
28.3	0.28821	27.4	149

Table 2. Concentration dependences of crystalline structure, total porosity and oxygen sorption for Co–Al_2O_3 condensates

m, % by mass	Lattice type	C, %	g, mg/g
0.7	HCP	9.0	82
2.4	HCP	13.2	89
5.1	HCP	15.8	91
10.2	FCC	23.9	105
20.4	FCC	26.4	140
30.8	FCC	29.8	137

ters of the diffraction maxima registered in the precision region.

The condensates were studied by the small-angle X-ray scattering using the CRM unit in FeK_α radiation. The measurements were made on the specimens of less than 80 μm thickness by the "transmission" technique in the angular range 3.5–2 deg, with the slot-collimated primary beam. The scattering intensity was registered by the pulses counting over a specified time interval (exceeding 100 s), discretely, at the step size from 20″ to 5′. The RMS error of the intensity measurements did not exceed 3%. To evaluate the experimental data characterizing the angular dependence of the X-ray scattering, the method described in [7] was used. Calculations were performed using formulas [5] allowing to obtain, without preliminary introducing the collimational correction, the size distribution of structure microinhomogeneities (small pores and disperse oxide particles).

Sorption tests of the compositions obtained were performed by the static method at 20°C. The sorption capacity value was established as the difference between the mass of an adsorbent sample after oxygen sorption at atmospheric pressure and that of vacuum-degassed one. The total porosity of condensates was determined by the hydrostatic weighing method. The microhardness was measured on the PMT instrument at 50 g indentor loading.

Results

Fe–Al_2O_3 system

The condensates of compositions presented in Table 1 were investigated. The X-ray phase analysis of these condensates had given following results: the diffraction patterns of all the samples studied show only reflections corresponding to the α modification of iron. No other phases have been revealed. The absence of alumina reflections evidences its amorphous state in the condensates (in terms of X-ray method). The results of the lattice constant measurements show that, for all the samples studied, it exceeds somewhat the reference value for the pure α–Fe; therewith, the lattice constant increases when the oxide phase content in the condensate rises. It follows from the data presented in Table 1 that the condensate porosity grows with the alumina concentration increase. In Fig.1, the microinhomogeneities size distribution is shown. In the samples studied, submicropores of 36 nm radius are prevailing. On the $f(R)$–R curve for the Fe–14.2% Al_2O_3 sample, an additional maximum arises which increases with the alumina content growth. The results of the microhardnness measurements are presented in Fig.2, those for sorption capacity – in Table 1.

Co–Al_2O_3 system

The specific feature of this condensate system is that the crystalline modification of metal matrix depends on the alumina concentration. The phase composition study has shown that, in the range of oxide phase concentrations from 0 to 10% (by mass), the diffraction pattern of the α-cobalt HCP lattice is characteristic for those condensates. At higher aluminium oxide contents, the FCC modification of the β-cobalt is realized. No other phases have been found. Data presented in Table 2 indicate that the condensate porosity increases with Al_2O_3 concentration growing. The small-angle scattering measurements have shown that, in the initial samples, the submicropores of about 40 nm radius and disperse oxide particles having radius about 25 nm prevail. The concentration dependence of the condensates microhardness is shown in Fig.2, the sorption measurements results are presented in Table 2.

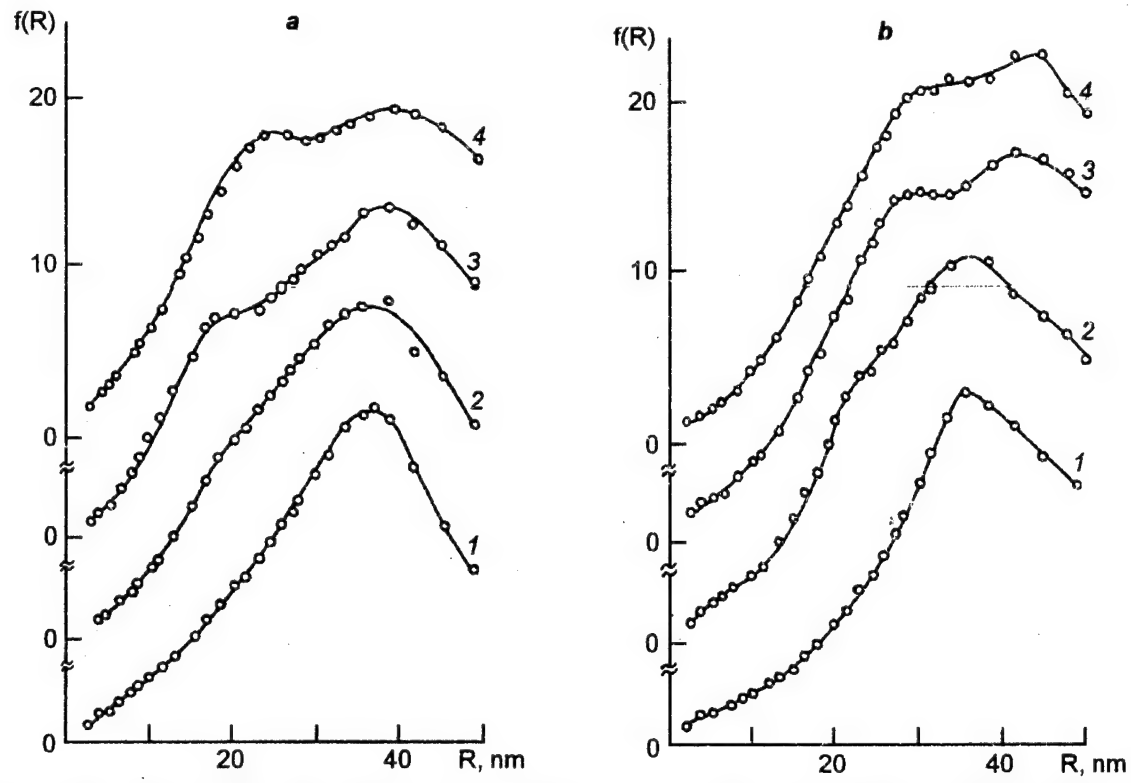

Fig.1. Microinhomogeneities size distribution in Fe–Al_2O_3 (a) and Co–Al_2O_3 (b) condensates containing respectively 0.8 and 0.6 (1), 5.8 and 5.0 (2), 14.2 and 10.2 (3), 28.3 and 30.8 (4) per cent of Al_2O_3 (by mass).

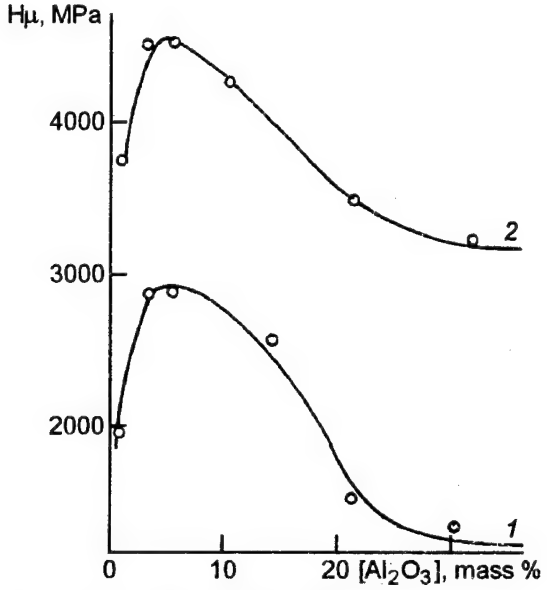

Fig.2. Concentration dependences of the microhardness for Fe–Al_2O_3 (1) and Co–Al_2O_3 (2) condensates.

Discussion

The specific character of the metal-oxide compositions obtaining by the electron-beam evaporation method consist in that processes of the mixed vapour flow condensation onto the support and of formation of the deposited layer thereon occur in the non-equilibrium conditions. Therefore, the condensates studied are complex heterogeneous systems characterized by high concentrations of various structural imperfections (from point-type defects to macropores) and physico-chemical properties different from those of similar massive samples. Studies of Me–Al_2O_3 binary systems based on the iron triade elements have shown a great similarity of their structural characteristics. So, all the objects studied consist of the porous metallic matrix and alumina particles of average size about 40 nm distributed uniformly therein. In the whole concentration range studied, the absence of interaction is established between phases forming the condensate. Besides, for all three systems, the lattice constant and the condensate porosity increase regularly with the rise of the second phase content. The increase of the lattice constant is associated obviously with the metallic matrix doping by aluminium atoms arising as a result of the partial dissociation of oxide in the course of the electron-beam evaporation. The microhardness measurements of the condensates studied (Fe–Al_2O_3, Co–Al_2O_3, Ni–Al_2O_3) have shown that the increase of the Al_2O_3 content up to 3–4% by mass causes

the microhardness growth. The relationship observed is associated obviously with that small alumina admixtures result in the fine-grain condensate structure formation [2]: the small crystallite sizes and disperse alumina particles promote the microhardness rise of condensates wherein pores are arranged mainly on the grain interfaces. The further increase of the disperse oxide particles amount causes a microhardness lowering due to open pores formation over the whole condensate volume, increase of those sizes and concentration.

The combined analysis of the sorption data and structural parameters given in this work allows to suggest that all the compositions studied have rather developed specific surfaces due to high micropores concentrations. Thus, the use of the electron-beam technology makes possible to obtain effective sorbents characterized by high sorption capacity and prespecified structural features.

Along with the similarity mentioned above, we have found some distinctions in the characteristics studied of the porous structure of binary condensates on the basis of iron friade metals. Namely, the submicropores size and total condensate porosity increase with the rising ordinal number of the matrix metal. These distinctions are in agreement with the commonly accepted temperature model of the vacuum condensate structure [1]: the porous structure features of compositions deposited under identical conditions depend on the melting temperature of matrix metal, moreover, the size and amount of pores form according to the diffusion mechanism, is proportional to the diffusional activity of metal increasing over the Fe–Co–Ni series [8].

The results of sorption tests presented in this work show that the sorption properties of the compositions studied are due not only to structure characteristics, but also the condensate chemical composition. It seems impossible to explain this fact only by the oxygen physical adsorption process. It is our opinion that, in parallel with the physical adsorption, the oxygen chemisorption occurs. Since iron possesses a higher chemical affinity to oxygen than cobalt, the oxygen chemisorption by Fe–Al_2O_3 condensate must be more active, what is confirmed by experimental data.

A specific effect of the alumina disperse particles on the crystalline structure of the cobalt-based condensates is to be noted: when the oxide phase content increases, the high-temperature FCC lattice of the cobalt matrix becomes more stable, what is in agreement with the literature data for similar massive compositions [9].

The structure characteristics variations of binary metal-oxide type systems as functions of oxide phase concentration and conditions of the condensate obtaining were considered in publications [3–6].

From the comparison of the structure characteristics of the condensates based on iron triade metals, the conclusion can be made about the sensitivity of the porosity and physico-chemical properties determined thereby to the metal matrix nature.

Conclusions

1. Porous composite materials have been obtained by the electron-beam evaporation of a metal (iron or cobalt) and alumina out of two independentsources and subsequent condensation of the mixed vapour flow onto a heated support.

2. Alumina in two-phase condensates is found to be in fine-dispersed state. The composition total porosity and the crystal lattice constant of the metallic matrix increase with rising alumina content. The submicropores size distribution in the condensates has been established.

3. The comparison of structure characteristics of Fe–Al_2O_3, Co–Al_2O_3 and Ni–Al_2O_3 condensates obtained under identical conditions, shows that the submicropores size and total metallic matrix porosity increase regularly from iron to nickel.

4. A correlation has been revealed between condensate structure, microhardness and sorption properties. The investigation results allow to determine the optimum compositions of metal-oxide type porous materials intended to use as the selective sorbents.

References

1. B.A.Movchan, I.S.Malashenko, Refractory Coatings Deposited in Vacuum [in Russian], Naukova Dumka, Kiev (1983).
2. B.A.Movchan, N.I.Grechnyuk, V.O.Mushegian, *Fiz.Khim.Obr.Mater.*, No.6, 92 (1984).
3. G.M.Kochetov, G.I.Batalin, *Izv.AN SSSR, Neorg.Mater.*, **21**, 150 (1985).
4. G.I.Batalin, G.M.Kochetov, *Izv.AN SSSR, Neorg.Mater*, **22**, 431 (1986).
5. G.M.Kochetov, G.I.Batalin, V.O.Mushegian, *Fiz.Khim.Obr.Mater.*, No.1, 104 (1987).
6. G.M.Kochetov, G.I.Batalin, N.I.Grechanyuk, *Izv.AN SSSR, Neorg.Mater.*, **29**, 882 (1988).
7. G.M.Plavnik, *Kristallografia*, No.3, 447 (1980).
8. L.S.Palatnik, P.G.Cheremskoy, M.Ya.Fuks, Pores in Films [in Russian], Energoizdat, Moscow (1982).
9. V.B.Brik, Diffusion and Phase Transitions in Metals and Alloys [in Russian], Naukova Dumka, Kiev (1985).

Особенности пористой структуры металлоксидных вакуумных конденсатов

Г.М.Кочетов, Г.Г.Дидикин, Б.М.Емельянов

Методами рентгенографии на больших и малых углах, газовой адсорбции, измерения микротвердости исследована структура пористых вакуумных конденсатов систем $Fe–Al_2O_3$ и $Co–Al_2O_3$. Установлено, что эти двухфазные композиции состоят из пористой металлической матрицы и равномерно распределенных в ней дисперсных частиц оксидной фазы. Изучены характеристики пористости в зависимости от состава конденсата. Отмечено влияние химической природы матричного металла на структурные параметры и сорбционные свойства металлоксидных композиций.

Functional Materials 2, No.1 (1995)

Study of surface chemistry of the active titanium dioxide used in sorption and catalysis processes

V.P.Koryukova, E.V.Shabanov and G.L.Kamalov

A.V.Bogatsky Physico-Chemical Institute, National Academy of Sciences of Ukraine, 86 Chernomorskaya Doroga, 270080 Odessa, Ukraine

The influence of the preparing conditions and the composition of the heterogeneous system TiO_2 — aqueous solution (gas) on the surface groups composition of crystalline hydrated titanium dioxide (pigment industry) was studied. The nature, polyfunctionality and lability of the sorption and catalytic centers are explained on a base of the hydrolytical model of the SO_4-inclusions transformations on the titania surface.

Вивчено вплив умов одержання та складу гетерогенної системи TiO_2 — водний розчин (газ) на склад поверхневих груп кристалічного гідратованого діоксиду титану (виробництво пігментів). Природа, поліфункціональність та лабільність активних центрів сорбції і каталізу модифікацій TiO_2 інтерпретована на базі гідролітичної моделі трансформації SO_4-включень на поверхні.

The wide variety of surface groups of the active titanium dioxide and their transformations in the function medium cause the ambiguity of theoretical notions about the nature of adsorption and catalysis active centers.

Among the heterogeneous photocatalytic systems on the basis of titanium dioxide, those prepared by thermal hydrolysis of sulphuric acid solutions containing titanium (THT) are believed to be most effective [1]. In contrast to other synthesis techniques, the thermo-hydrolytic method of obtaining, in a solution, of the crystalline hydrated titanium dioxide (anatase) ensures the reproducibility of the solid phase composition and properties and the stability thereof during storage and heat treatment [2]. The THT products are characterized by the high crystallinity degree, developed surface and a pronouced structure imperfection, which causes the variety of active center types [3]. This fact determines significant potential of THT as the base for selective sorbents and photocatalysts [4—7].

The marked composition non-stoichiometry characteristic for THT is represented by various types of structure defects. Among those, disruptions of the anatase lattice regularity are predominant, including dope-type ones due to the incomplete hydrolysis of acid residues and controlling the TiO_2 semiconducting properties. Heterogeneous cations poorly coordinated on the surface, including those substituting titanium (statistically distributed Si, Fe, Al) or occluded during crystallization (Cu, Co, Ni), create the high uncompensated charge areas causing formation of additional hydroxyl groups with increased acidity due to the water dissociative adsorption. The presence of such proton-donor centers, along with numerous forms of oxygen-hydrogenic groups bonded to titanium, determines the pronounced polyfunctionality of the titanium dioxide technical grades. Admixtures, distorting the electron-energy structure of the wide-zone semiconductor, cause the Fermi quasi-level shift under lighting. The unhydrolyzed acid residues, i.e. sulphate groups having a high mobility and forming a solid solution in the anatase do organize the structure of the hydrate sphere on the THT interphase surface and, via the crystal lattice, effect inductively the chemisorbed water molecules, thus changing the surface energy pattern and acid-base properties [2,3]. The sulphate presence in the bridge-like coordination [10] brings about changes manifesting theirself, especially, in the value of the specific surface of the hydrated anatase which is anomalously great for crystalline modifications, as well as in the absence of olation

and oxolation processes ("ageing") during storage and heat treatment. Of substantial importance are distinctions between technical-grade and regular anatase preparations concerning the structural cavities dimensions and transport channels system permeability, which define the mass transfer conditions in sorption and catalysis processes. The predominance of micropores which cannot be measured using traditional methods is responsive for the scatter of the specific surface values depending of the sorbate nature. In all cases, however, these values are underrated as compared with the true size of the active surface accessible for small molecules or ions [3].

The aim of this work is to study the specific chemical and structural features of the hydrated titanium dioxide (anatase) obtained by thermal hydrolysis of sulphuric acid solutions of titanium (IV), including polymetallic ones.

Experimental

Samples used in this work were obtained in our laboratory by thermal hydrolysis of solutions produced by means the sulphuric-acid stripping of ilmenite concentrate during titanium pigment production, as well as the purified solutions; the industrial intermediate products (technical grade and special purity grade) were also employed. The laboratory preparations were obtained according to the optimized version of the thermal hydrolysis method [8] which ensured the chemical, phase and dispersion homogeneity and a high crystallinity degree (anatase 93—97 %, rutile 3—5 %) without the specific surface reduction (not less than 120 m^2/g). The possibility of matrix standardization enables more correct determination the specific chemical features of the sample surface.

Results of the THT attestation by the low-temperature nitrogen adsorption method are as follows (mmol/g):NH_3, 1.38; HCl, 0.27; and CO_2, 0.38 (after NH_3 preadsorption) at the atmospheric pressure and 3.2, 1.0, and 0.38, respectively, at the surface saturation by sorbates. The mild dehydration conditions (100°C) excluding the destruction of the active hydrate structures chemisorbed on the surface have assured the maximum approximation to the interphase surface state in heterogeneous systems TiO_2—gas and TiO_2—solution. Due to high strength of chemical bonds, the air-dried samples and those dehydrated at the temperature of the physically sorbed water elimination restore the surface structure by chemisorption of water vapour from the ambient air.

In Tables 1,2 and in Fig.1-3, characteristics of preparations studied are presented.

Fig.1 and 2 illustrate the results of the acidimetric determination of the fluoride-substitutable surface functional groups compensating the coor-

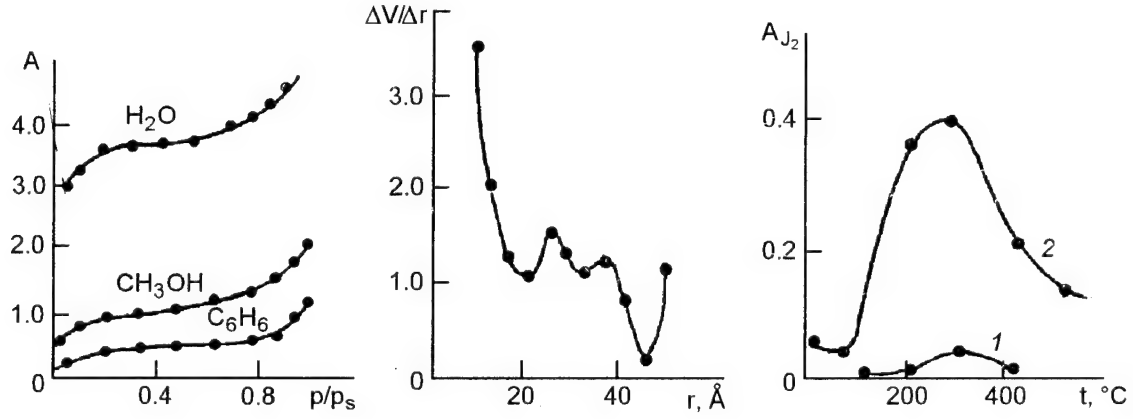

Fig.1. Variation of the samples surface hydroxylation degree depending on the pre-hydrolysis mixture composition (*a*) and on the contact time (τ, hours) with modifying agent (*b*)

Sample No.	1	2	3	4	5	6
TiO_2, g/dm^3	100	100	100	100	50	20
Fe/TiO_2, %	-	-	0.45	0.45	0.45	0.45
Anatase nuclei, %	1.0	1.0	1.0	0.5	0.5	0.5

Table 1. Characteristics of samples. Σ is the Cu, Co, Ni, Cr, Mn, Cd and Pb total content.

No.	Composition, % by mass							Specific surface, m^2/g (BET method)	Density, g/cm^3	Particle size, μm	ΣOH, pH 11, mequiv/g
	10^3				TiO_2	SO_3	H_2O				
	Si	Fe	Al	Σ							
1**	0.1	0.1	0.1	0.1	69.80	3.86	26.34	90	2.45	1-10	1.0
2	10	3	1	5	77.70	7.18	15.12	166	2.61	0.2-10	3.2
3	10	5	1	5	77.90	4.61	17.49	159	2.62	4-6	3.4
4	10	1	1	5	76.50	4.79	18.71	132	2.57	4-6	3.4
5*	2	0.1	0.1	2.3	77.4	7.10	15.50	-	2.65	4.6	3.6

* Cu, Cr, Mn, Cd $5 \cdot 10^{-4}$%; Ni, Co, Pb $1 \cdot 10^{-4}$%.
** Special purity grade. The crystallinity degree: Nos.1,2 - 50%; 3,4,5 - 96 to 100%.

Table 2. Chemical composition and sorption characteristics of samples No.1,2 and 3 in the ion-exchange cycle. H_2O^c is the water eliminable up to 150°C; H_2O^p, that eliminable in the temperature range 150–500°C.

Characteristic of samples	No.1	No.2	No.3
Composition, mass %:			
TiO_2	79.0	81.1	78.6
H_2O	16.6	18.7	17.9
SO_3	4.4	0.2	3.5
Formula:			
$TiO_{1.8}(SO_3)_{0.056}(H_2O)^p_{0.370}(H_2O)^c_{0.565}$	No.1		
$TiO_{1.8}(SO_3)_{0.0025}(H_2O)^p_{0.256}(H_2O)^c_{0.781}(Na)_{0.041}$		No.2	
$TiO_{1.8}(SO_3)_{0.044}(H_2O)^p_{0.379}(H_2O)^c_{0.633}$			No.3
Specific surface, m^2	110.0	213.1	191.4
OH groups content (pK ~ 3.5), mequiv/g	0.36	0.40	0.37
Na content, equiv/g	-	1.40	-
Na content after water washing, mequiv/g	-	0.40	-
Catalytic activity in relation to that of the initial sample, increase by, times:			
H_2O_2 decomposition	-	4	-
H_2O photoreduction	-	10	-

dinational unsaturation of the surface ions [9] and the variation range of the TiO_2 active surface state as depending on the thermal hydrolysis conditions (under reaction medium parameter variation).

The appearance of the sorption isotherms for molecules (Fig.3) and alkali metal ions as the pH function (Fig.2) reflects the polyfunctionality and "sieve" properties of anatase.

In Table 2, the chemical analysis of ion-exchange products and characteristics are presented for samples obtained under step-by-step control of the ion-exchange cycle, i.e. of initial THT (No.1), of that treated by sodium chloride solution up to saturation (No.2), and of the latter "regenerated" by the acid washing.

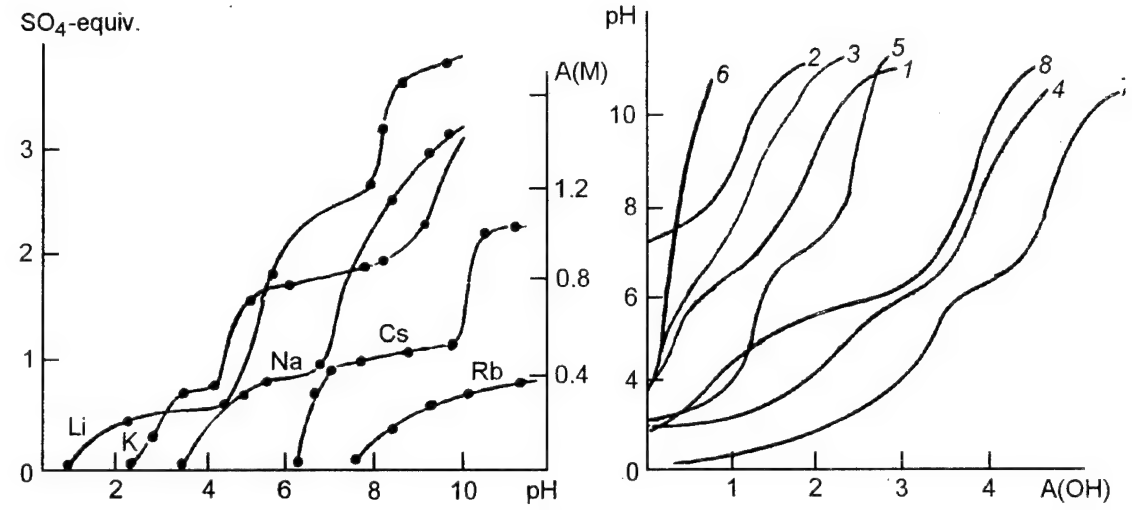

Fig.2. Isotherms of alkali metal ions sorption (a) and of pH-neutralization. Isomolar series, 0.04 mmol/g: 1 to 7 - NaOH + NaCl; 8 - $Ba(OH)_2$ + $BaCl_2$. Nos. 1.8 - THT; No.2 - THT neutralized to pH 11; No.3 - THT neutralized to pH 11, water-washed; No.4 - "regenerated" No.2; Nos.2,3,4 - suspension in 0.02 mM HCl; Nos.5,6 - THT thermally treated at 400 and 500°C, respectively; No.7 - THT highly doped by Fe(III).

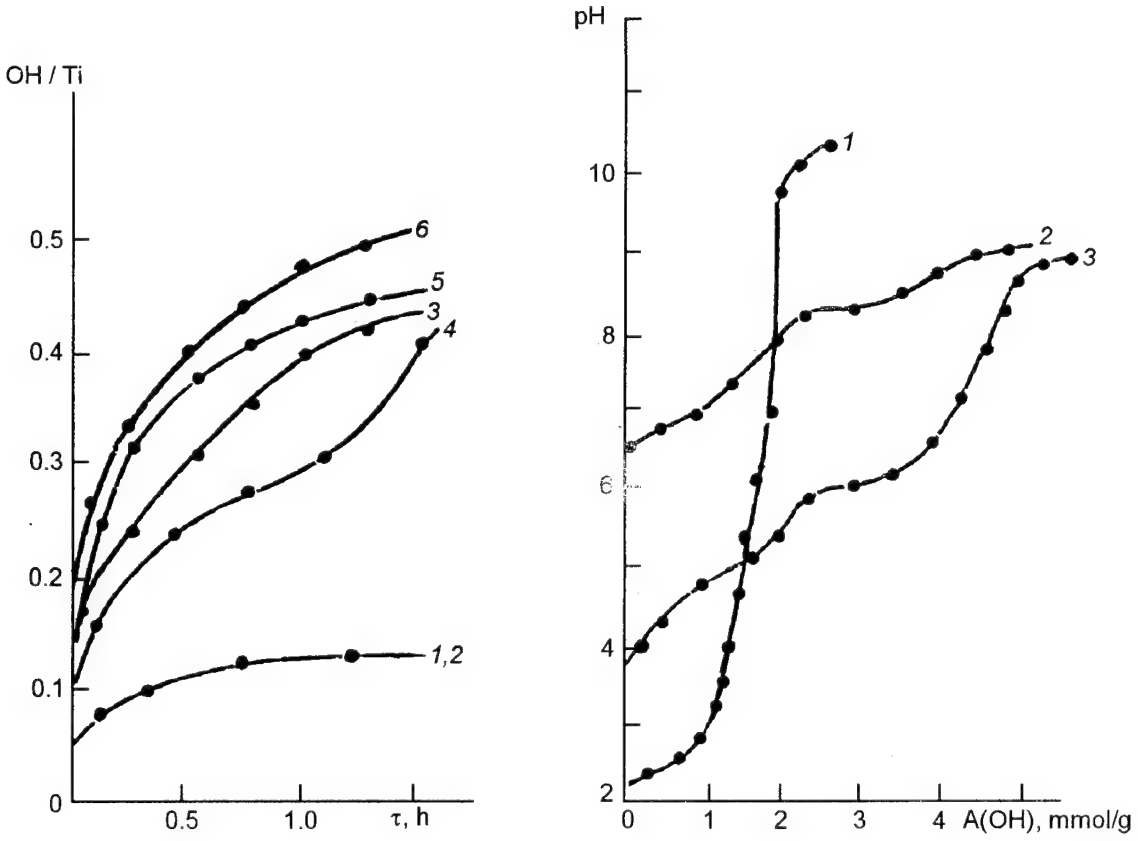

Fig.3. Molecules adsorption isotherms for THT (1) and THT + NH_3 (2). $\Delta V/\Delta r$ - pore radius distribution; A - sorption value, mmol/g.

Discussion

The comparison of results obtained in the course of study of thermohydrolytic anatase modifications by sorption methods as well as of data concerning pH-alkalimetry and acidimetry of fluor-substitutable hydroxyls leads to the following conclusions about the nature of active groups which may act as the sorption, proton exchange, and catalysis centers. The total amount of the ammonia-adsorbing acid centers corresponds to the data of the alkalimetry at high pH values which accounts for various acid center types. The number of *ab initio* reactive centers coincides with results of the acidimetry of hydroxyls substituted by fluoride ion as well as with the maximum value of the alkali metal ion sorption (of sodium which is adsorbed without by-processes).

The CO_2 adsorption by THT sample treated by the NH_3 preadsorption depends not on the relative pressure. The values of CO_2 and I_2 sorption (0.38 mmol/g) by dehydrated "salt" anatase forms from solutions in CCl_4 are the same, while the initial "hydrogen" THT form does not sorb iodine. Since the "salt" forms differ from "hydrogen" one by that they contain, in interlayer cavities of the anatase lattice, instead of sulphate bridges, hydrolysis products thereof, it can be supposed that there are just centers induced by a cation at pH values exceeding the isoelectric point which are responsive for CO_2 and I_2 adsorption. After $-SO_4$ admixture elimination under anhydrous conditions (calcination at 500 °C), the samples remain inert in relation to I_2. These transformations effect only slightly the adsorption of sterically unlimited water molecules. Therefore, the results of CO_2 and I_2 adsorption do not characterize the initial anatase sample, but its ammonium derivative. The value of HCl sorption on samples treated by the ammonia preadsorption amounts to one-half of the ammonia consumption (1.6 mequiv/g) and characterizes the total number of surface groups of non-acid and basic types present on the surface initially and induced by the incorporated ammonium ion. These centers can be suggested to be presented mainly by amphoteric hydroxyls, pair to the acid OH groups in the interlayer space, as well as by more basic hydroxyls being formed in the process of THT interaction with alkalies.

Isoterms of sorption and those of pH-neutralization of the THT acid groups (Fig.2) are characterized by the pronounced polyfunctionality and values multiplicity on the sections where the proton-donor groups amount depends stepwise on the suspension pH. The structure reveals a "memory" in relation to the defect being eliminated (sulphogroup) incorporated earlier in the course of the anatase crystallization during the thermohydrolysis of the sulphate titanium complexes. The number and strength of acid groups is controlled by the conditions of the subsequent thermohydrolysate treatment.

The sorbat nature influence reveals itself clearly (Fig.2,3) caused by the combination of the THT ultramicroporous surface sieve effect and of chemical factors limiting the nature of the surface complex. The complex form of the alkali metal sorption isotherms is explained by the superposition, onto the exchange stoichiometry, of conjugated dehydration and rehydration reactions as well as of interphase surface transformations induced by the sorbate (differentiated due to distinctions in the sorbate effects on hydrate water structure and nearest OH groups, ion size and basicity).

The relationship between the alkali metal ion sorption value and ion size under variation of the suspension pH (as the most intensive factor in the system) and the jump-like capacity increase at pH exceeding 7 allow, in agreement with the pH-alkalimetry data, to suggest that the cation-exchange centers are just the hydroxonium ions of interlayer hydroxyl-hydrate structures being formed in the process of anatase samples interaction with the reaction medium. These structures are decomposed by a mineral acid or alkali excess, but are regenerated after a longterm water washing. Such a suggestion is not in contradiction to data published [11] characterizing the hydroxonium groups bonded with titanium-oxygen surface groups as most strong acid centers; moreover, the replacement of the hydroxyl group proton by the fluoride ion results in the loss of cation-exchange function due to the destruction of the three-spin configuration.

The active anatase polyfunctionality, taking into account the clearly revealed multiplicity of the sorption value to the sulphate residue content in the initial THT sample, indicates the presence of a genetic association between corresponding functional groups acting as the sorption centers.

The water molecules compensating the coordinative unsaturation of the surface titanium ions are able, as a result of the dissociative chemisorption, to form additional hydroxyl groups of two types (Ti–OH and –O(H)–); the number thereof correspond stoichiometrically to the sulphogroups desorption (OH/SO_4 for the surface sulphogroups and $2OH/SO_4$ for the bridge-type ones).

The dynamics of the active anatase surface formation in an electolyte solution is showed illustratively in Fig.2. The sulphate admixture elimination at the sample contact with the electrolyte, pH exceeding the isoelectric point, is accompanied by a substantial decrease of its acid capacity. Under the Na-modified sample "regeneration" conditions by the acid treatment (titration of the THT suspension in HCl), the initial acid capacity does not recover and is determined by the $2OH/SO_4$ stoihiometry. The water washing of such a sample from the excessive acid leads to a sharp increase of its surface acid properties: the dissociation pK diminishes by 4 units, and amount of the proton-donor centers having pK ~ 6 becomes corresponding to the initial sample total alkali and ammonia capacity.

Comparison of the components ratio in the samples (see Table 2), with account for the temperature limits of the chemisorption and physical sorption of water, shows that, as a result of the contact with sodium chloride solution, the desorption of sulphate inclusions occurs, the relative water molecules number being changed in equivalence with the sulphate groups content, The sodium sorption value corresponds to the doubled number of sulphogroups being regenerated in the sample and to the number of the structural hydroxyls as determined by PMR experiment [3]. The specific surface of the sample increases twofold due to the modification. Therewith, a sharp increase of the THT catalytic activity in the hydrogen peroxide decomposition and water photodecomposition processes is observed.

Studying the anatase contact with the potassium fluoride solution at pH>8, it is possible to trace the time evolution of the hydroxyl-hydrate bridge structures formation. First, the surface hydroxyl-containing groups are displaced into solution by the fluoride. Then, after 16 hours of a quasi-equilibrium, the jump-like doubling of the number of hydroxyls evolved occurs. Comparison of the pH-alkalimetric titration curves for samples taken in the first and seconds quasi-equilibrium states of the heterogeneous THT-aqueous KF system (Fig.1) illustrates clearly the time evolution of the formation of proton-donor centers with pK 4,5 at pH exceeding the TiO_2 isoelectric point, i.e. that ensuring the anionic admixtures desorption from the solid phase. The ultrasonic treatment of the anatase sample suspension modified by KF for 24 h results in the break of bridge-type linkages which reveals as the specific surface doubling and crystal aggregates destruction. A prolonged contact of the phases is accompanied by anatase corrosion due to the fluor-titanium complexes formation; therewith, first of all, the most reactive part of the active surface in the interlayer space becomes lost. Therefore, such preparations loss their sorption and catalytic activity. The samples corresponding to various portions of the "fluoration" kinetic curve differ substantially in the functional activity in sorption and photocatalytic systems.

A critical value of the residual sulphate bridges content in anatase (about 0.2 %) seems to exist, below of which, the deterioration of crystal aggregates occurs, which manifests itself as the specific surface increase (by two times) and rise of the powder dispersity. The action of monobasic mineral acids solutions can cause their peptization. The sulphate bridges presence appears to be a necessary condition for the preservation of the layer-like structure character of active anatase with all its functional advantages ensuing therefrom.

Exceeding the 400 °C temperature limit causes a sharp drop of the acid centers number, therefore, that value seems to be considered as the upper limit of the THT active centers thermal stability.

It can be suggested from the foregoing that, due to high mobility of sulphate inclusions, in THT aqueous suspensions at pH exceeding the isoelectric point, a new interlayer surface composition arises in which hydroxyl-hydrate bridge-like structures become predominant ones. Combination of the wedging effect of ions (SO_4^{2-}, alkali metals) with increasing number of interlayer channels, being formed due to the sulphate bridges hydrolysis and containing the most active proton-donor centers, is favourable for the reacting particles transportation, causes a radical change in the surface electron-energy state and, as a consequence, the mass transfer intensification in the sorption and photocatalytic systems. Numerous experimental facts point to a substantial change of the TiO_2 surface nature influenced by structural defects. We can suggest obviously that the state of the surface active centers is a resulting effective function of several variables determined by the synthesis conditions and function medium. Therefore, the sample pre-history must be taken into account, i.e. the initial surface state and its transformation dynamics influenced by intrinsic or induced structure defects.

References

1. Energy Resources through Photochemistry and Catalysis, Academic Press, New York – London – Paris (1983).
2. E.F.Belen'kiy, I.V.Riskin, Chemistry and Technology of Pigments [in Russian], Khimia, Leningrad (1974).

3. V.P.Koryukova, L.I.Koval'chuk, E.V.Shabanov, *Neorganicheskie Materialy*, **16**, 1684 (1980).
4. V.P.Koryukova, N.P.Kirichenko, E.V.Shabanov, G.L.Kamalov, in: Abstr.of XIII All-Union Sem.on Chemistry and Technology of Inorganic Sorbents [in Russian], Minsk (1991), p.37.
5. V.P.Koryukova, E.V.Shabanov, L.I.Ilchenko et al., in: Abstr.of Intern.Confer.on Photochemistry [in Russian], Kiev (1992), p.123.
6. G.L.Kamalov, V.P.Koryukova et al., Ibid, p.144.
7. V.P.Koryukova, L.I.Koval'chuk, A.M.Andrianov, *Khimia i Tekhnologia Vody*, **9**, 373 (1987).
8. V.P.Koryukova, E.V.Shabanov, A.M.Andrianov, *Zh.Prikl.Khimii*, **53**, 9 (1980).
9. L.I.Biryuk, Ya.G.Goroshchenko, E.L.Khandros, *Ukr.Khim.Zh.*, **39**, 504 (1973).
10. Ya.G.Goroshchenko, L.I.Biryuk, *Ukr.Khim.Zh.*, **34**, 54 (1968).
11. Hydrated Oxides of IV and V Group Elements, ed. by Yu.V.Egorov [in Russian], Nauka, Moscow (1986).

Изучение химии поверхности активного диоксида титана, используемого в процессах сорбции и катализа

В.П.Корюкова, Е.В.Шабанов, Г.Л.Камалов

Изучено влияние условий получения и состава гетерогенной системы TiO_2 - водный раствор (газ) на состав поверхностных групп кристаллического гидратированного диоксида титана (производство пигментов). Природа, полифункциональность и лабильность активных центров сорбции и катализа производных TiO_2 объяснена на основе гидролитической модели превращений SO_4 - включений на поверхности.

Functional Materials **2**, No. 1 (1995)

Influence of hydrogen on reconstruction diamond (111) (2 × 1) surface by the ESR

N.V.Tokiy, D.L.Savina and V.V.Tokiy

Donbass State Academy of Architecture and Constructions,
339023, Makeyevka, Ukraine

The hyperfine interaction parameters for a ^{13}C nucleus positioned on the (111) surface of diamond have been examined and scrutinized. Within the limits of the tight-binding theory, the cluster calculation have been performed for the models with the reconstruction (2 × 1) of the monoatomically pure (111) diamond surface as well as of that containing hydrogen atoms. Comparison of the experimental and theoretical data on the ESR of the surface paramagnetic centers in diamond is made.

Проаналізовані параметри надтонкої взаємодії на ядрі вуглецю ^{13}C, розміщеного на поверхні (111) алмазу. У рамках теорії сильного зв'язку проведені кластерні розрахунки моделей з реконструкцією (2 × 1) алмазної поверхні (111) моноатомно чистої та з атомами водню. Проведено порівняння експериментальних та теоретичних даних по ЕПР поверхневих парамагнітних центрів у алмазі.

1. Introduction

Recently, investigation of diamond surface (111) has aroused a great attention of researchers. Fairly detailed statements and interpretations, concerning the fact of the growing interest, can be found a number of papers, [1,2] are being a good example. Disposition of atoms close to the diamond (111) surface presents both theoretical and practical interest. At the same time, using conventional surface science techniques (Auger electron spectroscopy, X-ray photoelectron spectroscopy, low energy electron diffraction and other standard surface analytical tools) a success is only achieved in the establishment of symmetry of superstructures caused by rearrangements of the close- to-surface atoms. The experimental data on the displacement values near the ideal monoatomically pure surface remain still unavailable. The problem concerning the so-called real surface, i.e. the surface which is not isolated from the environment (gas, liquid and solids of a different composition) presents even a more complicated aspect. Moreover, we have no accurate data on the atomic configuration of such a surface [3].

2. Hyperfine interaction on ^{13}C in diamond

ESR is one of the most powerful tools for microscopic identification of the surface paramagnetic centers in diamond, particularly when the nuclei on which the unpaired spin resides have naturally magnetic isotope.

Electron spin resonance is observed for electrons in variety of situations. The one which will concern to us is unpaired electron localized in orbitals at defect sites in solids. Such electrons are far from being free but are rather described by wave functions localized in a region of the discrete crystal lattice. The paramagnetism of these electrons reflects the interaction of electrons with the lattice and we will express this interaction in terms of the "Spin Hamiltonian". For the defects in diamond, the most common presentation of the spin Hamiltonian is one of the form [4]

$$H_{spin} = \sum_{i,k=1}^{3} \beta H_i g_{ik} S_k + \sum_{i,k=1}^{3} S_i D_{ik} S_k + \sum_{i,k=1}^{3} S_i A_{ik} I_k \qquad (1)$$

The first term is the Zeeman splitting of spin states in external magnetic field H_i. The g_{ik} reflects the anisotropy of the local environment.

The second term is the interaction of the electron spin with the crystal field produced by the surroundings of the paramagnetic centre. This term exists only if the effective spin $S>1/2$. The last term presents the unpaired spin ($S=1/2$) interaction with magnetic nuclei ^{13}C($I=1/2$ is the nuclear magnetic moment of ^{13}C). The components of the hyperfine interaction tensor A_{ik} are written as

$$A_{ik} = gg_N\mu\mu_N [< \Phi | (3x_ix_k/x^5 - \delta_{ik}/x^3) | \Phi > + + \delta_{ik}8\pi | \Phi(0) |^2/3], \quad (2)$$

where Φ is the electronic defect wave function, g and g_N are the electronic and nuclear g factors, respectively, and μ and μ_N are the electronic and nuclear magnetons. The x vectors are measured from the magnetic nuclear ^{13}C. For axially symmetric systems, the diagonal components of A_{ik} have a nondegenerate and twofold degenerate eigenvalues, conventionally written as $A_\parallel$ (nondegenerate) and $A_\perp$ (twofold degenerate). If we assume that the defect wave function can be written in the form of the sum of $2s$- and $2p$-orbitals of each atom of carbon ^{12}C and separately of carbon ^{13}C, we shall have:

$$\Phi = \sum_j^{N-1} (C_s^j | 2s^j > + \sum_{k=1}^{3} C_{p_k}^j | 2p_k^j >) + + {}^{13}C_s | 2s > + \sum_{k=1}^{3} {}^{13}C_{p_k} | 2p_k >, \quad (3)$$

where N-1 is the number of carbon atoms ^{12}C in the system; k runs along the value of the three coordinate axes. Then, the diagonal components of A_{ik} can be written as

$$A_\parallel = a + 2b \quad (4)$$

$$A_\perp = a - b, \quad (5)$$

where

$$3a = 8\pi gg_N\mu\mu_N | 2s(0) |^2 (^{13}C_s)^2 \quad (6)$$

and

$$b = 0.4\, gg_N\mu\mu_N <2p | r^{-3} | 2p> \sum_{k=1}^{3} \left(^{13}C_{p_k}\right)^2. \quad (7)$$

Often (4), (5) when taking into account (6), (7), are written as:

$$A_\parallel = \rho_s A^* + 2\rho_p B^*, \quad (8)$$

$$A_\perp = \rho_s A^* - \rho_p B^*, \quad (9)$$

where: $A^* = 8\pi gg_N\mu\mu_N | 2s(0) |^2/3$ and $B^* = 0.4gg_N\mu\mu_N <2p | r^{-3} | 2p>$ are constants of the hyperfine interaction for the free carbon atom ^{13}C which usually cannot be identified experimentally but can be calculated with a sufficient accuracy from the wave functions of that free ^{13}C atom. In this work, we have used $A^*=1130$ G and $B^*=33$ G [5]. $\rho_s=(^{13}C_s)^2$ is the probability of the unpaired electron residence on the $2s$ orbital of the carbon ^{13}C. $\rho_p = \sum_{k=1}^{3} \left(^{13}C_{p_k}\right)^2$ is the probability of the unpaired electron residence on the $2p$ orbital of the carbon ^{13}C.

3. ESR of the surface of diamond

The experimental data on ESR of the diamond surface are few in number, see, for example, the review [3]. Among them, there are practically no reports dealing with the magnetic nuclei of carbon ^{13}C which are a real probe of the microstructure of the diamond surface. Only in [6,7] one of the authors of the present work has scrutinized the peculiarities of the paramagnetic resonance on the surface centers of diamond and identified the HFI parameters of the unpaired electron on the carbon ^{13}C nucleus ($A_\parallel = 238$ G and $A_\perp = 120$ G).

4. Cluster calculation

In this work, the consideration is based on the simulation of the C(111) diamond surface by a cluster of 22 carbon atoms with C_3 symmetry. The system is interpreted as a large molecule.

The group, in the shape of a hemisphere, includes a central nodal point (0,0,0) plus its first three (1,1,1), nine second (2,2,2), six third (3,1,1) and three forth (4,0,0) nearest neighbours in a diamond lattice. We have modelled a C (111) surface consisting of a single central carbon ^{13}C having a dangling bond perpendicular to the surface and surrounded by six secondary carbon atoms, each having a surface-normal dangling bond (variant I) or four having a C—H bond and two having a dangling bond perpendicular to the surface (variant II).

We use the tight-binding theory [8,9]. In this theory of sp-bonded systems, the electronic eigenstates are written in terms of a basis set consisting of a single s state and three p states on each atom.

The corresponding one-electron eigenvalues and eigenfunctions are then obtained by diagonalizing an $N\times N$ Hamiltonian matrix based upon these N orbitals.

In this work, the basis system is limited by sp^3- hybridized orbitals made of one s-orbital and three p_x-, p_y- and p_z- orbitals of the valence shell

of each atom. These are *2s*- and *2p*- atom wave functions of carbon. It is assumed that these orbitals are orthogonal on different atoms. However, the hybridized orbitals are not eigenfunctions of the quantum-mechanical system under question. Since the Hamiltonian matrix elements among different hybrids are not equal to zero, we utilize parameters consisting of Herman-Skillman term [10] values for diagonal terms ε_s=-17.52 eV, e_s= -8.97 eVand the formula

$$V_{ll'm}=\eta_{ll'm}\hbar^2/(md^2) \qquad (10)$$

for the interaction between nearest neighbouring orbitals. The first two subscripts indicate the orbital coupled and the last indicates the component of angular momentum around the internuclear axis. The coefficients are $\eta_{ss\sigma}$=-1.40, $\eta_{sp\sigma}$=1.84, $\eta_{pp\sigma}$=3.24 and $\eta_{pp\pi}$=-0.81 from [8].

To find the eigenfunctions and eigenvalues of the system energy, it is necessary to diagonalize the symmetrical matrix $\mathbf{H}_{\mu\nu}$. The single electron orbitals in our cluster can be expressed as

$$\Phi_\alpha=\sum_{\nu}^{N} c_{\nu\alpha}\,|\,h_\nu>, \qquad (11)$$

where (h_ν) — basis hybridized orbitals, and index ν runs along all the hybridized orbitals on each atom and on all atoms; N — the number of the basis functions; $c_{\nu\alpha}$ — the solution of the single-electron equations for the cluster:

$$\sum_{\nu}^{N}\left(\mathbf{H}_{\mu\nu}-\delta_{\mu\nu}E_\alpha\right)c_{\nu\alpha}=0, \quad \alpha=1,2,...N, \qquad (12)$$

where E_α — the single-electron eigenvalue of the cluster energy, $H_{\mu\nu}$ — the matrix elements between the hybridized orbitals. The wave function of the unpaired electron localized on the carbon ^{13}C, in which the coefficients are the solutions of the equation system (12), is given as (3).

5. Results and discussions

By diagonalising the Hamiltonian matrix and by finding c_ν coefficients of the wave function (3), using the formula (8) and (9), we can find $A_\parallel$ and $A_\perp$. The interaction results calculation of the hyperfine parameter $A_{iso} = A^*(^{13}C_s)^2$ on the surface nucleus of carbon ^{13}C for the cluster model of C(111) surface are shown in Fig. 1.

These lines show ρ_s and A_{iso} vs displacement (r) of elevated (line Ib) and downcast (line Ia) ^{13}C from their ideal value on the surface not containing (line II) and containing hydrogen.

The isotropic hyperfine interaction constant $A_{iso}=(A_\parallel + 2A_\perp)/3$, determined by the experimentally measured $A_\parallel$ and $A_\perp$ from [6], is shown in the shape of a dashed line. These experimental data have been obtained from the ESR spectrum of powdered natural diamond with a particle size of 1 μm at room temperature. Analysis of the figure 1 shows that, at a room temperature, which is used at the ESR experiments, the (111) surface is hardly reconstructed on (2 × 1). The experimental data agree beat of all with our calculations [7] of relaxation of the surface layer into depth of crystal on 4.5 pm (line III in the Fig. 1).

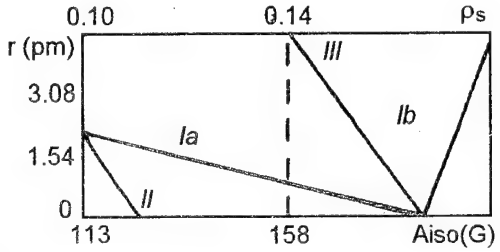

Fig. 1.

References

1. H.Seki, Taro Yamada, T.J.Chuang et. al., *Diamond and Related Materials*, **2**, 567 (1993).
2. K.Larsson, S.Lunell and J.O.Carlsson, *Diamond and Related Materials*, **2**, 949 (1993).
3. A.B.Roycin, B.M.Mayexsky, *Uspekhi Fizicheskikh Nauk*, **159**, 297 (1989).
4. J.H.N. Loubser and J.a.van WYK, *Rep.Prog.Phys.*, **41**, 1201 (1978).
5. P.W.Atkins, M.S.R.Symons, The structure of Inorganic Radicals, Amsterdam, Elsevier (1967).
6. D.L.Savina, V.V.Tokiy, N.D.Samsonenko, Abstract booklet of Second International Symposium on Diamond Films 3-5 May 1994 and NATO Advanced Workshop on Wide Bandgap Electronic Materials (Diamond, Aluminum Nitride, Boron Nitride) 4-6 May, 157 (1994).
7. V.V.Tokiy, N.D.Samsonenko, D.L.Savina, Diamond Films-93: 4-th Europian Conf. on Diam. Diamond-like and Related Mater., Albufeira, Algarve, Portugal, 12.019, (1993).
8. W.A.Harrison, Electronic Structure and the Properties of Solids, Freeman, San-Francisco, 1980, reprinted by Dover, New York, (1989).
9. W.A.Harrison, *Phys.Rev.*, **B 41**, 6008 (1990).
10. F.Herman, S.Shillman, Atomic Structure Calculations, Prentice Hall Englewood Cliffs, New York (1963).

Влияние водорода на реконструкцию (2 × 1) поверхности (111) алмаза по данным электронного спинового (парамагнитного) резонанса

Н.В.Токий, Д.Л.Савина, В.В.Токий

Проанализированы параметры сверхтонкого взаимодействия на ядре углерода ^{13}C, расположенного на поверхности (111) алмаза. В рамках теории сильной связи проведены кластерные вычисления моделей реконструкции (2 × 1) алмазной поверхности (111) моноатомно чистой и с атомами водорода. Проведено сравнение теоретических и экспериментальных данных по ЭПР поверхностных парамагнитных центров в алмазе.

Functional Materials **2**, No.1 (1995)

Study of phase transition parameters in components of the polychlorotrifluorethylene — vanadium dioxide system

P.A.Vozny, P.P.Gorbik, V.V.Levandovsky,
V.Nagorny, V.M.Ogenko and L.K.Yanchevsky

Institute for Surface Chemistry, National Academy of Sciences of Ukraine,
31 Nauki Ave., 252022 Kiev, Ukraine

Dependences of temperature and heat of phase transitions in components of the polychlorotrifluorethylene (PCTFE) — dispersed vanadium dioxide (VO_2) system on the VO_2 concentration have been studied. It is shown that VO_2 is an active regulator of the supermolecular PCTFE structure.An effect of the polymeric matrix on parameters of the metal-semiconductor phase transition (PTMS) in the filler has been found and studied. It is shown that areas of the polymeric matrix that are adjacent to filler particles make a significant contribution to variations of the PTMS temperature and heat in vanadium dioxide.

Вивчено залежності температури та теплоти фазових переходів у компонентах системи поліхлортрифторетилен (ПХТФЕ) — дисперсний діоксид ванадію від концентрації VO_2. Показано, що VO_2 є активним регулятором надмолекулярної структури ПХТФЕ. Виявлено і досліджено вплив полімерної матриці на параметри фазового переходу метал-напівпровідник (ФПМН) у наповнювачі. Показано, що суттєвий внесок у зміну температури та теплоти ФПМН в діоксиді ванадію вносять області полімерної матриці, які межують з частинками наповнювача.

Study of materials having new functional properties, including filled polymers, is of applied as well as of scientific interest [1,2]. In [3,4], new polymeric composite materials (PCM) were described containing polychlorotrifluorethylene (PCTFE) as the matrix and disperse vanadium dioxide (VO_2) possessing a metal-semiconductor type transition (PTMS) as the filler.

The PTMS in VO_2 is known to occur in the temperature region T ~ 340 K and to be accompanied by the reversible jump-like conductivity change by 3 to 5 orders of magnitude [5]. On the other hand, in the temperature region T ~ 485 K, the phase transition (melting) in PCTFE takes place. Experimental data [3,4] evidence to a rather strong interaction of components in the PCTFE + VO_2 system. It is known that the presence of such an interaction can influence substantially the phase transition parameters in the polymer matrix [2]. Therefore, of interest is to study the character and degree of the influence mentioned as well as the PTMS parameters behaviour for VO_2 included in the polymer matrix, as depending on the filler content in PCM.

The aim of this work is to study the features of phase transitions parameters in the PCTFE-dispersed VO_2 system in the range of components phase instabilities.

The PCM samples for the investigation were prepared by hot pressing method at 523 K under 200 MPa pressure; the melt was exposed for 20 min and cooled subsequently at the rate of 0.2 K/s in a device ensuring the reproducibility of the thermal and temporal forming conditions. Composition containing PCTFE and VO_2 at the content of the latter from 0.1 to 3.0 mass % every 0.5 % and from 55 to 95 % every 5 % were prepared from suspensions [6]. Specimens were made as cylinders of 7-20 mm diameter and 5-20 mm height, the butt planes were parallel to within ±0.01 mm. The B grade PCTFE [7] and disperse vanadium dioxide obtained by the solid phase synthesis method according to reaction $V_2O_3 + V_2O_5 \rightarrow 4VO_2$ [3,8] were used as the in-

itial materials. According to the granulometric analysis data, the VO_2 consisted by about 80 % by mass of 1-10 μm size particles.

The heat conductivity coefficient (λ) of PCM was measured by the dynamic method of monotone heating [9] at 0.05 K/s rate on the modernized IT-λ-400 unit in the continuous regime. The temperature difference on opposite butts of samples did not exceed 2 K. The specific heat capacity (C_p) was measured by means of a differential scanning calorimeter on the diathermic envelope [10]. The relative error of λ and C_p measured values did not exceed ±3 % and ±2.5 %, respectively. Acoustic properties — the ultrasound propagation velocity (U) and absorption coefficient (α) were determined according to procedure based on the combination of the pulse-phase and echo-pulse methods [11] on 5 and 7.5 MHz frequencies at 293 K. The relative error of U and α measurements was ±0.75 and ±5 %, respectively.

Fig.1 shows the experimental dependence of the PCM heat conductivity coefficient (1), as well as those of the polymer matrix melting heat (2) and melting temperature (3) on the filler concentration for the low filling ratios range. It is seen that the PCM heat conductivity increases with the VO_2 concentration rising up to 1.5 %, with subsequent drop in the 1.5-3 % concentration region. The experimental relationship $\lambda=f(C)$ is inconsistent with the calculated one (curve 1') obtained according to mixing formulas [12] under the assumption that there is no interaction between the polymeric binder and filler, what evidences an active influence of vanadium dioxide on the PCTFE supermolecular structure.Moreover, the introduction of VO_2 in an amount of $0 \le C \le 1.5$ % leads to a progressive diminishing of the polymer melting specific heat (S_m) and temperature (T_m) (the T_m value was taken as temperature corresponding to the melting peak maximum of the $C_p=f(T)$ curve, S_m was determined from the area value of peak mentioned). Therewith, the symbate variation of the ultrasound propagation velocity and of the acoustic wave absorption coefficient was also observed in specimens studied.

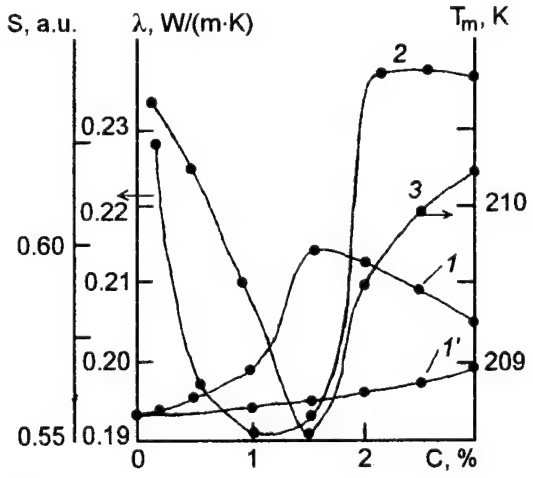

Fig. 1.

The experimental data presented together with the IR spectrometry results allow to the conclusion that the crystallinity degree of PCTFE varies substantially under the VO_2 influence in the low filling region of PCM. So, the decrease of the polymeric matrix melting temperature and heat at $0 < C \le 1.5$ % is possibly due to a decrease of the large crystallites number. The experimentally observed λ rise of PCM at the crystallinity degree drop may occur as a result of the molecular chains orientation in the polymer layers neigbouring to the filler [13].

Investigation of PCTFE + VO_2 system by the IR spectroscopy methods has revealed the presence of characteristic absorption bands (920-1080 and 1250-1349 cm^{-1}); the appearance thereof can be related to a chemical interaction of the vanadium dioxide surface layer with PCTFE macromolecules under the formation of bonds in complexes, most likely between vanadium and fluor [14]. Such an interaction is responsive for the increase of PCM structure-mechanical characteristics [3] as compared with those of initial VO_2 and PCTFE, as well as for the active filler influence on the composite properties (Fig.1).

Experimental dependences of the polymer matrix melting temperature and heat on the VO_2 concentration in the high filling range of PCM are presented on Fig.2,a. These data show that the T_m and S_m values are influenced substantially by the PCM composition. The rise of those characteristics in the $50 \le C \le 75$ % range can be associated with the increase of the PCTFE crystallinity degree which grows therewith from 50 to 68 % (as determined from the specific melting heat variation). The T_m and S_m drop at $C > 75$ % is due to the decrease of the polymer matrix crystallinity degree because of the crystallite size limitations associated with the polymer shortage.It should be noted that, in the high filling range, the fold crystallization mechanism may be replaced by the straight-chain one. A similar filler influence on polymer properties is known and described in [13].

Consideration of the PTMS temperature and heat (T_{ptms} and S_{ptms}, respectively) in the filler as

functions of the PCM composition indicates, however, the presence of an unusual phenomenon, i.e. the active influence of polymer matrix on the phase transition parameters in vanadium dioxide (Fig.2,b). As mentioned above, the PCTFE + VO_2 system is characterized by the strong enough interaction between polymer macromolecules in the boundary layer and filler; this interaction is due to chemical factors, besides physical ones. Therefore, it can be suggested that the structural transformations of the VO_2 particles in the course of PTMS occur under some polymer matrix influences, e.g. by means of elastic or electrical forces (note that the PTMS in VO_2 may take place due to the pressure or electrical field action [15]).

In fact, as the filler concentration grows, the volume of polymer being in the boundary layers neighbouring to VO_2 particles increases relatively, up to the overlap of such layers. Therewith, the elasticity module of composite and its apparent density increase, while the porosity reduces [3]. With the chemical bond between the VO_2 surface and polymer, distortion occurring in the filler particle at a structure reconstruction in the course of PTMS can pass to the whole matrix; the response of the latter will depend obviously on the composite filling degree. The elastic stresses arising thereat may, in turn, propagate over the whole volume of VO_2 particle and contribute to the change (increase) of thermodynamic characteristics of the filler and, therefore, of the composite as a whole, what is in fact observed in the concentration range $50<C\leq85$ % (Fig.2,b).

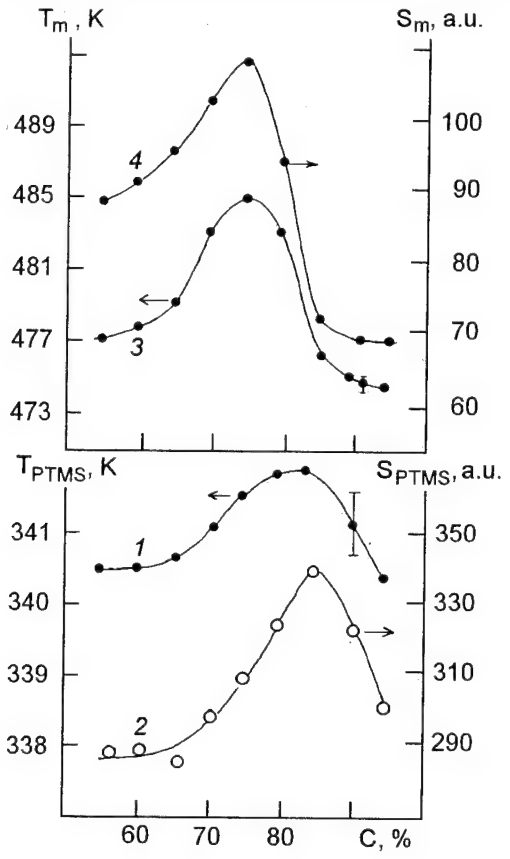

Fig. 2.

In our case, it is characteristic that the polymer matrix area adjoining the filler particle contributes substantially to the T_{ptms} and S_{ptms} changes for the metal-semiconductor phase transition it the composite. The presence of such areas is showed by us at the study of the ultrasound dissipation coefficient in the composite material by the two-frequency technique [3]. In the region of $C > 85$ %, a decrease in the PTMS heat and temperature in VO_2 is observed (Fig.2,b) which can be associated with the shortage in binder and reduction of the relative part of the VO_2 surface coated by the polymer. The latter instance causes the increase of macroporous volume and the sharp drop of the composite physico-mechanical characteristics.

Thus, this work has showed that the disperse vanadium dioxide is an active regulating agent for the PCTFE supermolecular structure. Also, the phenomenon of the polymeric matrix influence on paramerers of the metal-semiconductor phase transition in the filler of the PCTFE + VO_2 system is first revealed and investigated. The data obtained indicate a basic possibility to change the properties of the polymer matrix-functional filler type solid systems as compared to components conditioning those properties. The phenomenon observed is due, in our opinion, to the mutual overlapping of the polychlorotrifluorethylene layers adjoining the filler and to corresponding parameter change of the polymer matrix influence on the vanadium dioxide electronic structure.

Feferences

1. Yu.Tretyakov, Yu.G.Metlin, *Zh.Vsesoyuzn.Khim.Obshch. im.D.I.Mendeleeva*, **36**, 265 (1991).
2. Yu.DTretyakov, Ibid., **34**, 436 (1989).
3. P.A.Vozny, P.P.Gorbik, V.V.Dyakin et al., *Dokl.AN Ukrainy*, No.12, 36 (1991).
4. P.A.Vozny, L.V.Galushko, P.P.Gorbik et al., *Sverkhprovodimost'*, **5**, 1478 (1992).
5. A.A.Bugayev, B.P.Zakharchenya, F.A.Chudnovsky, Metal-semiconductor Phase Transition and Its Applications [in Russian], Nauka, Leningrad (1979).
6. Yu.A.Panshin, S.G.Malkevich, C.S.Dunayevskaya, Fluroplastics [in Russian], Khimia, Leningrad (1978).

7. Encyclopoedia of Polymers [in Russian], Sovetskaya Encyklopedia, Moscow (1977).
8. G.Brauer, Handbuch der präparativen anorganischen Chemie, Verdinand Enke Verlag, Stuttgart (1954).
9. E.S.Platunov, *Izv.Vuzov, Ser.Priborostroenie*, **4**, 90 (1961).
10. Yu.K.Godovsky, Thermophysical Methods of Polymers Investigation [in Russian], Khimia, Moscow (1976).
11. L.K.Yanchevsky, V.V.Levandovsky, in: Ultrasound and Thermodynamic Properties of Substances [in Russian], KGPI Publ., Kursk (1988), p.96.
12. G.N.Dul'nev, Yu.P.Zarichnyak, Heat Conductivity of Mixtures and Composite Materials [in Russian], Energia, Leningrad (1974).
13. Yu.S.Lipatov, Physico-Chemistry of Filled Polymers [in Russian], Naukova Dumka, Kiev (1967).
14. K.Nakomoto, Infrared and Raman Spectra of Inorganic and Coordination Compounds, 4 ed., New York, D.Wiley and Sons (1990).
15. I.S.Rez, Yu.M.Poplavko, Dielectrics: Main Properties, Applications in Electronics [in Russian], Radio i Svyaz', Moscow (1989).

Исследование параметров фазового перехода в компонентах системы полихлортрифторэтилен — диоксид ванадия

П.А.Возный, П.П.Горбик, В.В.Левандовский, В.А.Нагорный, В.М.Огенко, Л.К.Янчевский

Изучены зависимости температуры и теплоты фазовых переходов в компонентах системы полихлортрифторэтилен (ПХТФЭ) - дисперсный диоксид ванадия от концентрации VO_2. Показано, что VO_2 является активным регулятором надмолекулярной структуры ПХТФЭ. Обнаружено и исследовано влияние воздействия полимерной матрицы на параметры фазового перехода металл-полупроводник (ФПМП) в наполнителе. Показано, что существенный вклад в изменение температуры и теплоты ФПМП в диоксиде ванадия вносят области полимерной матрицы, граничащие с частицами наполнителя.

Functional Materials 2, No.1 (1995)

Letter to the Editor

Solid solutions of the $K(NO_3)_{1-x}(ClO_3)_x$ system and stable ferroelectric states

Yu.N.Velikhov, V.M.Ishchuk, V.L.Cherginets, V.D.Panikarskaya and T.S.Teplitskaya

Institute for Single Crystals, 60 Lenin Ave., 310001 Kharkov, Ukraine

Received 27 November 1994

The solid solutions of the $K(NO_3)_{1-x}(ClO_3)_x$ have been synthesized with $0 \le x \le 0.20$. The phase diagram has been constructed. The existence of the ferroelectric phase III of potassium nitrate in a wide temperatur range have been proved by the X-ray structure analysis.

Синтезовано тверді розчини системи $K(NO_3)_{1-x}(ClO_3)_x$ з $0 \le x \le 0.20$. Побудовано діаграму фазових станів. Методом рентгеноструктурного аналізу доказано існування сегнетоелектричної фази III нітрату калію в широкому інтервалі температур.

If potassium nitrate crystals were possessing the ferroelectric (FE) properties and, in consequence, nonlinear ones, they would be promising for use as electrooptic elements having a high bulk optical strength. Unfortunately, however, the FE state in potassium nitrate (so-called phase III) is realized only in a narrow temperature range near the Curie point (125—115 °C) and reveals only at the cooling of specimens [1—3]. A number of attempts was made to widenthe temperature range of the FE phase stability and to shift it towards the room temperature at least. For this purpose,the ionic substitutions in the cationic sublattice were accomplished either by Rb^+ [2,4] or by NH_4^+ ions [2,5,6]. In both cases some extension of the FE state realization was achieved, and the FE phase was revealed during specimens heating. The temperature range of the FE phase existence, however, remained narrow enough and did not descend lower than 40 °C.

The aim of this work was to obtain samples of the potassium nitrate basis in the FE state by the substitution of the NO_3^- anionic group by the ClO_3^- group, i.e. to obtain the FE solid solutions of the $K(NO_3)_{1-x}(ClO_3)_x$ family $0 \le x \le 0.20$. It is the isostructurality of anionic groups in both KNO_3 and $KClO_3$, which was the prerequisite for the choice of just this investigation direction.

Samples for experiments were obtained either by the melting of the compounds mixture or by combination of melting and solid state synthesis. X-ray structure investigations were performed on "Siemens" X-ray diffractometer D-500 using the Ni-filtered $CuK\alpha$ radiation. The phase transitions points of solid solutions under study were determined by differential calorimetry on the "Mettler" TA 3000 Differential Scanning Calorimetric System.

Fig.1 shows diffraction patterns of the solid solutions having $x = 0.05$; 0.10; 0.15 and 0.20. As it is seen from these results, there are no unreacted components in the compounds obtained. Also absent are the possible decomposition products ofinitial components. The crystallographic structure of the solid solutions with $x = 0.05$ is identical to that of potassium nitrate at the room temperature (so-called phase II). The X-ray diffraction pattern of the solid solution with $x = 0.10$ contains the reflections corresponding both to phase II and phase III of potassium nitrate.Reflections corresponding any other structures are absent. This indicates that at the room temperature the non-ferroelectric potassium nitrate phase II and ferroelectric one III are co-exis-

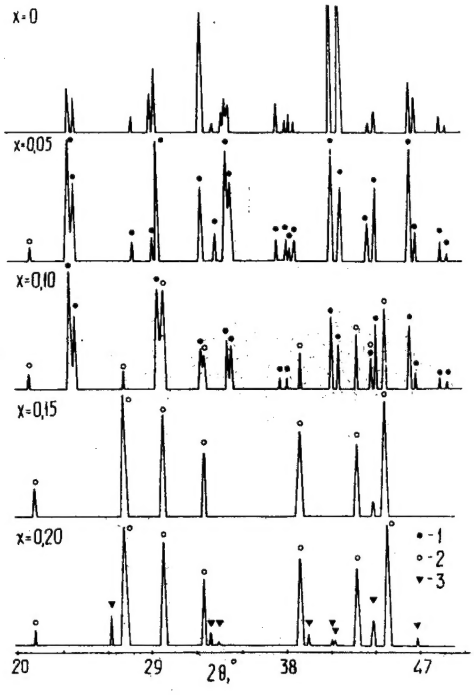

Fig.1. X-ray diffraction patterns of solid solutions of the $K(NO_3)_{1-x}(ClO_3)_x$ system. Reflexions are related to following structure modifications of potassium nitrate: I — phase II, II — phase III, III — phase IV (suppositively).

tent in the solid solution $K(NO_3)_{0.9}(ClO_3)_{0.1}$. On the X-ray pattern obtained from the solid solution with $x = 0.15$ only reflectes corresponding to the FE phase III of potassium nitrate are present. The mainset of the diffraction reflections from the solid solution with $x = 0.20$ corresponds also only to the FE phase III structure. Besides, however, week lines are present which, in our opining, are associated with the potassium nitrate phase IV stture. To answer this question more accurately, we intend to obtain and study solid solutions having $x > 0.20$.

Thus, the experimental data obtained allow to state unambiguously that in the synthesized solid solutions of the $K(NO_3)_{1-x}(ClO_3)_x$ with $x > 0.10$ the FE phase of potassium nitrate is realized at ambient temperature. The well-defined dielectric hysteresis loops correspond to this phase in solid-solutions menti- oned;the remanent polarization P_r has a value (9-10) $\mu C/cm^2$, which is close enough to the potassium nitrate polarization in the metastable phase III.

The temperature range of stability for each phase of solid solutions studied are presented on the phase state diagram (see Fig.2). The melting

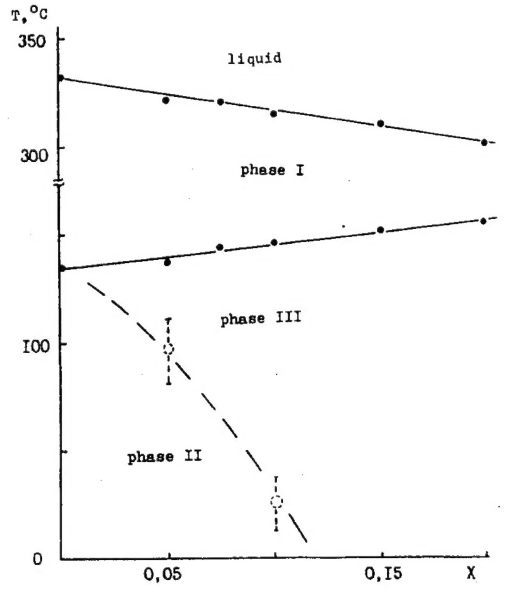

Fig.2. Phase diagram of $K(NO_3)_{1-x}(ClO_3)_x$ ($0 \le x \le 0.20$) solid solutions.

temperature of solid solutions decreases linearly as the potassium chlorate content raises: $(dT_{liq}/dx) = 1.7$ °C. The potassium chlorate content increase in the solid solutions results in a marked elevation of the temperature of phase transition into the paraelectric (PE) state (into the phase I of potassium nitrate). This phase transition is accompanied by a well-defined maximum on temperature dependence of dielectric constant. The transition point between FE phase III and nonferroelectric phase II is difficult to determine by the calorimetric method,since the temperature range of both phase coexistence is broad enough, and transition occurs in a gradual manner. It is hard to establish also using the temperature dependence of dielectric constant for reason mentioned above as well as because of small dielectric constant values. Therefore, on Fig.2 the line of the transition phase III — phase II is showed by a broken line. The boundary between these phases and temperature range of their coexistence are intended to be determined more precisely by X-ray method.

Thus,in this work the solid solutions $K(NO_3)_{1-x}(ClO_3)_x$ are shown to be synthesized which, at $x \ge 0.10$, have the structure of potassium nitrate phase III and possess the ferroelectric properties in a wide temperature range.

References

1. S.Sawada, S.Nomura, Y.Asao, *J.Phys.Soc.Japan*, **16**, 2486 (1961).

2. U.Kawabe, T.Yanagi, S.Sawada, *J.Phys.Soc.Japan*, **20**, 2059 (1965).
3. G.W.Taylor, B.J.Lechner, *J.Appl.Phys.*, **39**, 2372 (1968).
4. A.Ja.Danciger, *Izv AN SSSR, ser.Fiz.*, **26**, 1042 (1965).
5. T.Yanagi, S.Sawada, *J.Phys.Soc.Japan*, **18**, 1228 (1963).
6. T.Yanagi, *J.Phys.Soc.Japan*, **20**, 1351 (1965).

Твердые растворы системы $K(NO_3)_{1-x}(ClO_3)_x$ и стабильные сегнетоэлектрические состояния

Ю.Н.Велихов, В.Л.Чергинец, В.М.Ищук,
В.Д.Паникарская, Е.С.Теплицкая

Синтезированы твердые растворы системы $K(NO_3)_{1-x}(ClO_3)_x$ с $0 \le x \le 0.20$. Построена диаграмма фазовых состояний. Методом рентгеноструктурного анализа доказано существование сегнетоэлектрической фазы III нитрата калия в широком интервале температур.

Contents of Volume 2, issues 1–3:

Issues 1&2 will contain Transactions of the Ukrainian-USA Summer School on Chemistry and Physics of Surfaces CPS'94 (4-10 September 1994 Kiev, Ukraine).

Issue 3 – a Special Issue Devoted to Materials Science of Baromembranes for Ultra- and Nanofiltration.

Ordering information

To be sent to your supplier or to: Institute for Single Crystals
Editorial Office, 60, Lenin Ave., Kharkov 310001, Ukraine
Phone: +380 (572) 307 411, +380 (572) 307 960
Fax +380 (572) 320 273
E-mail: shcherbina@isc.kharkov.ua

The Journal will be issued quarterly and is published in English, Ukrainian or Russian.
Subscription rate for year (4 issues) USD 190.00
Price of separate issue: USD 50.00
Subscriptions are entered on a calendar year basis (January–December). Each issue can be ordered separately, too. Subscriptions and order are accepted on a prepaid basis only, and delivery will take place after receipt of paiment. For subscription or ordering, please send the corresponding sum to the account of the Institute for Single Crystals No. 001070802, in NPK-Bank, Kharkov, Ukraine, via Bank-correspondent Republic National Bank of New-York, Fifth Avenue at 40-th Street, New-York, accont No. 608206849.

A camera ready master copy is prepared by the Editorial Board of **Functional Materials** using the software and technical support of **LASERUSS** Scientific Publishing Group.

Editor of English text: V.Ya. Shnol

Translated by: V.Ya. Shnol

Computer Operators: V.Ya. Serebryanny, V.A. Tkachev, V.V. Shlakhturov, L.D. Patsenker

Proof–reader: E.G. Protsenko

Chief of the Editorial and Publishing Department: V.K. Galagan